







**Universiteit  
Antwerpen**

Faculty of Medicine and Health Sciences

# **Importin-8 and lysyl oxidase: human and murine insights into the pathogenesis of thoracic aortic aneurysm**

PhD thesis submitted for the degree of Doctor of Medical Sciences at the University of Antwerp to be defended by

**Ilse Van Gucht**

Supervisors:

Prof. Bart Loeys, Prof. Aline Verstraeten, Prof. Lut Van Laer

Antwerp, 2023

### **Members of the jury:**

Prof. Bart Loeys, *promotor*

Center of Medical Genetics, University of Antwerp and Antwerp University Hospital, Antwerp, Belgium

Prof. Aline Verstraeten, *promotor*

Center of Medical Genetics, University of Antwerp and Antwerp University Hospital, Antwerp, Belgium

Prof. Lut Van Laer, *promotor*

Center of Medical Genetics, University of Antwerp and Antwerp University Hospital, Antwerp, Belgium

Prof. Jonathan Baets, *chair*

Department of Neurology, Antwerp University Hospital, Antwerp, Belgium

Prof. An Van Berendoncks

Department of Cardiology, Antwerp University Hospital, Antwerp, Belgium

Prof. An Zwijsen

Department of Cardiovascular Sciences, KU Leuven, Leuven, Belgium

Dr. Ingrid Krapels

Carim – Cardiomyopathy, Maastricht UMS and Maastricht University, Maastricht, The Netherlands

Disclaimer

The author allows to consult and copy parts of this work for personal use. Further reproduction or transmission in any form or by any means, without the prior permission of the author is strictly forbidden



# TABLE OF CONTENTS

---

Summary.....	7
Samenvatting.....	11
Chapter 1 Introduction.....	17
Chapter 2 Aims of the thesis.....	59
Chapter 3 Novel <i>LOX</i> variants in five families with aortic/arterial aneurysm and dissection with variable connective tissue findings.....	61
Chapter 4 A human Importin- $\beta$ -related disorder: Syndromic thoracic aortic aneurysm caused by bi-allelic loss-of-function variants in <i>IPO8</i> .....	85
Chapter 5 Remarkable alleviation of ascending aortic aneurysm phenotype in 129/Sv <i>Ipo8</i> <sup>-/-</sup> mice as compared to their C57BL/6N <i>Ipo8</i> <sup>-/-</sup> counterparts.....	131
Chapter 6 Embryonic lethality in homozygous <i>Ipo8</i> <sup>-/-</sup> mice on a C57BL/6N genetic background.....	145
Chapter 7 Generation of one induced pluripotent stem cell (iPSC) line (BBANTWi011-A) from a patient carrying an <i>IPO8</i> bi-allelic loss-of-function variants.....	173
Chapter 8 General discussion.....	187
List of abbreviations.....	213
Curriculum vitae.....	219
Dankwoord.....	225

# SUMMARY

---

Thoracic aortic aneurysm (TAA) is a pathological dilatation of the thoracic aorta caused by vessel wall weakness. TAA is associated with a high mortality rate as it often leads to life-threatening aortic dissection or rupture (TAAD). Until now, pathogenic variants in more than 40 genes have been associated with TAAD development. Still, most TAAD patients (>70%) are missing a molecular genetic diagnosis. The hitherto discovered TAAD genes encode proteins involved in extracellular matrix (ECM) remodeling, vascular smooth muscle cell (VSMC) contraction and the transforming growth factor- $\beta$  (TGF- $\beta$ ) signaling pathway.

TAAD occurs as an isolated manifestation in most patients. However, in about 5% of cases, TAAD is part of the clinical profile of connective tissue disorders such as Marfan syndrome (MFS) or Loeys-Dietz syndrome (LDS). Although more rare, syndromic TAAD conditions are often used as a paradigm for TAAD in general as they are at the most severe end of the disease spectrum. Moreover, the most groundbreaking TAAD insights gained to date emerged from functional characterization of syndromic TAAD genes.

In this thesis, I aim to contribute to the elucidation of the etiology of syndromic TAAD by (1) identifying novel syndromic TAAD genes, (2) improving syndromic TAAD genotype-phenotype correlations, (3) delivering novel syndromic TAAD pre-clinical disease models, and (4) further unraveling the molecular processes underlying syndromic TAAD.

We describe the identification of pathogenic bi-allelic loss-of-function variants in a novel syndromic TAAD gene, i.e. *IPO8*, in LDS-resembling patients who are phenotypically characterized by severe early-onset TAA development, hypertelorism, motor developmental delay, pectus excavatum, joint laxity, hernia and hypotonia. *IPO8* encodes for the ubiquitously expressed transport-receptor Importin-8, which is a member of the importin- $\beta$  family and is involved in the translocation of cargoes such as

proteins, RNAs and ribonucleoprotein complexes from the cytosol into the nucleus in a RanGTP-dependent manner.

To allow further investigation of *IPO8*-related TAA, two pre-clinical models were created and validated. First, an *IPO8* patient-derived induced pluripotent stem cell (iPSC) line starting from peripheral blood mononuclear cells (PBMCs) was generated. A model which in the future can be differentiated into relevant aortic cell types such as vascular smooth muscle cells or endothelial cells. Second, we characterized a C57BL/6N *Ipo8* knock-out (*Ipo8*<sup>-/-</sup>) mouse model, recapitulating progressive early-onset TAA from 8-12 weeks onwards. Significant TAAs were observed in both sexes, but males presented with a more pronounced aneurysmal phenotype. Dissections were uniquely observed in males. Immunohistochemistry for pSmad2 and RT-qPCR for downstream targets of TGF-β signaling on *Ipo8*<sup>-/-</sup> aneurysmal aortic tissue revealed upregulation of the pathway.

Apart from the TAAD phenotype observed in adult animals, C57BL/6N *Ipo8*<sup>-/-</sup> mice also presented with embryonic lethality. Timed matings followed by morphological and histological embryo examination revealed embryonic death of 50% of *Ipo8*<sup>-/-</sup> mice between E13.5-E14.5 and birth. Macroscopic examination of pups reveals more common pale embryos due to lack of vasculature or decrease in cardiac output (45.2%) and hemorrhages (16.1%) in *Ipo8*<sup>-/-</sup> as compared to wild types, whereas microscopic examination reveals myocardial-endocardial edema (42.9%) and a decrease in left ventricular lumen (28.6%), increase in diameter of the pulmonary artery (42.9%) and decrease in aortic wall thickness in comparison with pulmonary artery (42.9%), providing a strong suspicion towards cardiovascular abnormalities as a cause of death.

To anticipate on possible genetic influences that could protect the C57BL/6N mice from developing TAAD, we backcrossed our *Ipo8* knock-out mouse model to another more TAAD susceptible, i.e. 129/Sv, genetic background. Somewhat unexpectedly, 129/Sv *Ipo8*<sup>-/-</sup> characterization did not reveal an earlier onset TAAD phenotype or higher

penetrance of embryonic lethality but demonstrated normal aortic dimensions throughout adulthood as well as normal genotype distributions at birth. With these results, we corroborate the importance of differences in genetic background on mouse phenotypical outcomes. Additionally, while asymptomatic, the 129/Sv *Ipo8*<sup>-/-</sup> model can still be of particular interest for the TAAD community in frame of the search for novel modifier genes and/or signatures.

Previously, it has been demonstrated that TAAD is characterized by reduced penetrance and variable phenotypic severity. Furthermore, my thesis contributed to the acquisition of better insight into the intra- and inter-familial variability of syndromic TAAD. Using next-generation TAAD gene panel sequencing we have identified five additional probands carrying pathogenic *LOX* variants. These probands, including the first *LOX* patient with spontaneous coronary artery dissection, had a heterogeneous TAAD phenotype combined with a spectrum of connective tissue manifestations. Although no connective tissue findings specific for *LOX* mutations were observed, a significant clinical overlap with other TAAD syndromes such as Marfan syndrome and Loeys-Dietz syndrome was observed, including splenic rupture and spontaneous pneumothorax.

In conclusion, my research contributes to the elucidation of the genetic and molecular landscape of patients with TAAD, by the identification of a novel syndromic TAAD gene. More specifically, it provides evidence for a link between *IPO8* deficiency and TGF- $\beta$  dysregulation causing early-onset TAA. I have broadened the phenotypical spectrum of pathogenic *LOX* variant carriers. Furthermore, it delivers novel syndromic TAAD pre-clinical disease models, i.e. *IPO8*-patient specific iPSCs and a characterized *Ipo8* knock-out mouse model. These models will be ideal for drug library screening and future preclinical application of TAAD drugs aiming to reduce TAAD associated morbidity and mortality.

## **SAMENVATTING**

---

Een thoracaal aorta-aneurysma (TAA) is een pathologische verwijding van de thoracale aorta als gevolg van een zwakke vaatwand. TAA gaat gepaard met een hoog sterftcijfer omdat het vaak leidt tot levensbedreigende aortadissecties of -rupturen (TAAD). Tot nu toe zijn pathogene varianten in meer dan 40 genen in verband gebracht met het ontstaan van TAAD. Toch ontbreekt bij de meeste TAAD-patiënten (>70%) een moleculair genetische diagnose. De reeds geïdentificeerde TAAD-genen coderen voor eiwitten die betrokken zijn bij remodellering van de extracellulaire matrix (ECM), contractie van vasculaire gladde spiercellen (VSMC) of signalisatie via de transforming growth factor- $\beta$  (TGF- $\beta$ ) pathway.

TAAD komt het vaakst voor als een geïsoleerde manifestatie. In ongeveer 5% van de gevallen maakt TAAD echter deel uit van het klinische profiel van bindweefselaandoeningen zoals het Marfan syndroom (MFS) of het Loeys-Dietz syndroom (LDS). Hoewel ze zeldzamer zijn, worden syndromale TAAD-aandoeningen vaak gebruikt als paradigma voor TAAD in het algemeen, omdat ze zich aan het meest ernstige eind van het ziektespectrum bevinden. Bovendien zijn de meest baanbrekende TAAD inzichten die tot op heden zijn verkregen voortgekomen uit functionele karakterisering van syndromale TAAD genen.

Met deze thesis wil ik bijdragen aan de opheldering van de etiologie van syndromale TAAD door (1) de identificatie van nieuwe syndromale TAAD genen, (2) de verbetering van syndromale TAAD genotype-fenotype correlaties, (3) de aanlevering van nieuwe syndromale TAAD preklinische ziektemodellen, en (4) de verdere ontrafeling van de moleculaire processen die ten grondslag liggen aan syndromale TAAD.

We beschrijven de identificatie van pathogene bi-allelische loss-of-function varianten in een nieuw syndromaal TAAD gen, namelijk *IPO8*, bij patiënten met een LDS-achtig fenotype dat wordt gekenmerkt door ernstige vroegtijdige TAA ontwikkeling, hypertelorisme, globale ontwikkelingsachterstand, pectus excavatum, gewrichtsluxatie,

hernia en hypotonie. *IPO8* komt wijdverspreid in het lichaam tot expressie en codeert voor een transport-receptor Importin-8 dat lid is van de importin- $\beta$  familie en betrokken is bij de translocatie van eiwitten, RNA's en ribonucleoproteïne complexen van het cytosol naar de kern op een RanGTP-afhankelijke manier.

Om verder onderzoek naar *IPO8*-gerelateerde TAA mogelijk te maken, werden twee preklinische modellen gecreëerd en gevalideerd. Ten eerste, werd een *IPO8*-patiënt-afgeleide geïnduceerde pluripotente stamcellijn (iPSC) uitgaande van perifere bloed mononucleaire cellen (PBMCs) gecreëerd, die in de toekomst kunnen worden gedifferentieerd in relevante aortaceltypes zoals vasculaire gladde spiercellen of endotheelcellen. Ten tweede hebben we een C57BL/6N *Ipo8* knock-out (*Ipo8*<sup>-/-</sup>) muismodel gekarakteriseerd, dat progressieve vroegtijdige TAA vanaf 8-12 weken vertoont. Significante TAAs werden waargenomen bij beide geslachten, maar mannetjes vertoonden een meer uitgesproken aneurysmatisch fenotype. Dissecties werden alleen bij mannetjes waargenomen. Immunohistochemie voor pSmad2 en RT-qPCR voor doelwitgenen van TGF- $\beta$  signalisatie pathway op *Ipo8*<sup>-/-</sup> aneurysmaal aortaweefsel toonde verhoogde activatie van de TGF- $\beta$  pathway aan.

Naast het TAAD fenotype bij volwassen dieren, vertoonden C57BL/6N *Ipo8*<sup>-/-</sup> muizen ook embryonale sterfte. Uit getimede paringen gevolgd door morfologisch en histologisch onderzoek bleek dat 50% van de *Ipo8*<sup>-/-</sup> embryo's stierf tussen E13,5-E14,5 en de geboorte. Bij macroscopisch onderzoek van de pups werd er bij *Ipo8*<sup>-/-</sup> embryo's vaker een bleek uiterlijk (45.2%), ten gevolge van een gebrek aan vasculatuur of gedaalde cardiac output, en bloedingen (16.1%) vastgesteld dan bij de wild type embryo's. Het microscopisch onderzoek toonde myocard-endocardiaal oedeem (42.9%), afname van het linker ventrikel lumen (28.6%), toename van de diameter van de longslagader (42.9%) en afname van de aortawanddikte in vergelijking met de longslagader (42.9%). Deze bevindingen doen sterk vermoeden dat cardiovasculaire afwijkingen de doodsoorzaak zijn.

Om te anticiperen op mogelijke genetische invloeden die de C57BL/6N muizen zouden kunnen beschermen tegen het ontwikkelen van TAAD, hebben wij ons *Ipo8* knock-out muismodel teruggekruid naar een andere meer vatbare genetische achtergrond, namelijk 129/Sv. Enigszins onverwacht kwam bij de karakterisatie van de 129/Sv *Ipo8*<sup>-/-</sup> muizen geen TAAD-fenotype of hogere penetrantie van embryonale letaliteit aan het licht, maar behielden de muizen normale aortadimensies gedurende de gehele volwassenheid, evenals normale genotypeverdelingen bij de geboorte. Met deze resultaten bevestigen wij het belang van de genetische achtergrond en zijn invloeden op het resulterende fenotype in muizen. Het 129/Sv *Ipo8*<sup>-/-</sup> model kan, hoewel asymptomatisch, nog steeds van bijzonder belang zijn voor de TAAD-gemeenschap in het kader van de zoektocht naar nieuwe modifierende genen.

Er werd reeds aangetoond dat TAAD gekenmerkt wordt door verminderde penetrantie en variabele fenotypische ernst. Verder heeft mijn thesis bijgedragen tot het verkrijgen van een beter inzicht in de intra- en interfamiliale variabiliteit van syndromale TAAD. Met behulp van next-generation TAAD gen sequencing hebben wij vijf bijkomende index patiënten geïdentificeerd die drager zijn van pathogene *LOX* varianten. Deze patiënten, waaronder ook de eerste *LOX* patiënt met spontane kransslagader dissectie, vertoonden een heterogeen TAAD fenotype, gecombineerd met een spectrum van bindweefsel manifestaties. Hoewel er voor *LOX*-mutaties geen specifieke bindweefsel afwijkingen werden waargenomen, werd een aanzienlijke klinische overlap met andere TAAD-syndromen zoals het Marfan-syndroom en het Loeys-Dietz-syndroom waargenomen, zoals bijvoorbeeld het voorkomen van miltruptuur en spontane pneumothorax.

Samenvattend kunnen we zeggen dat mijn onderzoek bijdraagt tot de opheldering van het genetische en moleculaire landschap van patiënten met TAAD, door de identificatie van nieuwe syndromale TAAD-genen. Meer specifiek levert mijn onderzoek het bewijs voor een verband tussen *IPO8*-deficiëntie, TGF- $\beta$  signalisatie ontregeling en vroegtijdige

TAA. Met mijn onderzoek heb ik ook het fenotypische spectrum van pathogene *LOX*-variantdragers verbreed. Verder levert deze thesis tevens nieuwe syndromale TAAD preklinische ziektemodellen op, namelijk *IPO8*-patiënt specifieke iPSCs en een gekarakteriseerd *ipo8* knock-out muismodel. Deze modellen zijn ideaal voor drug library screening en toekomstige preklinische toepassingen van TAAD geneesmiddelen gericht op het verminderen van TAAD geassocieerde morbiditeit en mortaliteit.



# CHAPTER 1: INTRODUCTION

---

## **Adapted from Chapter 12: Aortic and arterial diseases (aortopathies) in The Genomic and Molecular Cardiovascular Medicine**

Ilse Van Gucht,<sup>1</sup> Bart L. Loeys,<sup>1,2</sup> Aline Verstraeten<sup>1</sup>

<sup>1</sup>Cardiogenomics Research Group, University of Medical Genetics, University of Antwerp and Antwerp University Hospital, Antwerp, Belgium

<sup>2</sup>Department of Human Genetics, Radboud University Medical Center, Nijmegen, The Netherlands

Submitted for publication in The Genomic and Molecular Cardiovascular Medicine – Dr Kumar, Chapter 12: Aortic and arterial diseases (aortopathies).

## Abstract

---

Aortopathies or diseases of the aorta, are potentially life-threatening diseases, including thoracic and abdominal aortic aneurysm and associated dissection, accounting for 1-2% of all deaths in the Western population. More than 40 genes have been identified in TAA(D) development. These genes are involved in extracellular matrix (ECM) remodeling, VSMC contraction and TGF- $\beta$  signaling pathway. Recently, other TAA pathomechanisms such as inflammation, nitric oxide (NO) deficiency, oxidative stress response and mitochondrial dysfunction have been suggested. An important distinction between syndromic and non-syndromic TAAD (essentially vascular phenotype), as well as familial TAAD (FTAAD) and sporadic cases is made. TAA is a part of the clinical profile of several genetic diseases of which the most common disorders are Marfan syndrome (MFS) and Loeys-Dietz syndrome (LDS).

## 1. The aorta

---

The aorta is the largest artery in the human body fulfilling a critical function, delivering oxygen-rich blood to every cell throughout the body. Histologically, the aortic wall is composed of three distinct layers: the tunica intima, media, and adventitia [1, 2]. The tunica intima consists of endothelial cells that are arranged in a monolayer facing the lumen of the vessel supported by a basement membrane of collagen, functioning as a protective flexible barrier and sensing environmental changes [3]. Vascular smooth muscle cells (VSMCs) account for the bulk mass of the tunica media and, together with elastic fibers and a range of extracellular matrix proteins, maintain the structural integrity and biomechanical properties of the aortic wall. With respect to the VSMCs, cells of three distinct developmental lineages are involved. The aortic root is derived from secondary heart field-derived (SHF) VSMCs, whereas the ascending aorta and the aortic arch are neural crest derived, and the descending part originates from the paraxial mesoderm [4]. Finally, the outer layer, the adventitia, comprises collagen-producing fibroblasts [2, 5].

## 2. Aortic aneurysm

---

Pathological dilatation of the aorta, caused by vessel wall weakness, can occur at different sites along the aortic tree. Thoracic aortic aneurysm (TAA) often stays unnoticed until dissection or rupture occurs (TAAD). These life-threatening consequences are associated with a high mortality rate of almost 80% [6]. Every year, 1-2% of all deaths in Western populations are caused by aortic aneurysm/dissection, underscoring the disease impact on our societies [7].

Aortic aneurysm can be divided in thoracic aortic aneurysm (TAA) and abdominal aortic aneurysm (AAA), affecting the aorta above and below the diaphragm, respectively. AAAs and TAAs share pathophysiological characteristics, including VSMC loss and degradation of the elastic fibers, but differ with respect to their prevalence, degree of

heritability, and age of onset [8, 9]. AAAs are most common, affecting up to 5% (mostly males over 65 years) of the general population [10], whereas TAAs are estimated to occur in only 1% [11]. Despite their lower prevalence, TAA patients tend to have a more severe outcome [1]. Additionally, whereas about 20% of TAA patients report a positive family history (demonstrating the involvement of genetic factors), AAA is more often attributed to lifestyle-associated cardiovascular risk factors such as high blood pressure, smoking and elevated plasma cholesterol [7]. Up to now, more than 40 genes partaking a fundamental role in the development of aortic aneurysms have been discovered, providing a genetic diagnosis for less than 30% of individuals with familial TAA, leaving a major part of the genetic landscape of TAAD to be unraveled [12, 13]. For AAA, no monogenic causes have been pinpointed yet. A schematic representation of TAAD genes can be found in Figure 1.

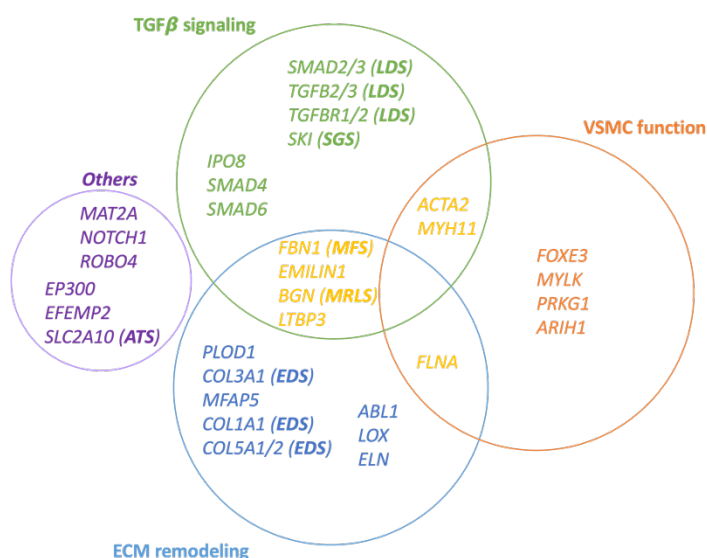


**Figure 1. Schematic representation of TAA genes**

TAAD can occur as an isolated condition or as a part of a clinical profile in which other organ systems are affected as well, also known as non-syndromic and syndromic TAAD, respectively [6]. An overview of the different genes causing syndromic and non-

syndromic TAAD with associated characteristics such as mode of inheritance, disease, and clinical features, is given in Table 1. The best studied and characterized syndromic aortopathies are Marfan syndrome and Loeys-Dietz syndrome [12].

**Table 1. Overview of genes associated with syndromic and non-syndromic TAAD**

Gene	Protein	Inheritance pattern	Disease	Cardiovascular features	Non-cardiovascular features	Reference
<b>ABL1</b>	Tyrosine-protein kinase, ABL1	AD	CHDSKM	Atrial and ventricular septal defect, ARD	Dysmorphic facial features, scoliosis, pectus excavatum, failure to thrive	[14]
<b>ACTA2</b>	Smooth muscle actin $\alpha$ -2 ( $\alpha$ SMA)	AD	Aortic aneurysm, familial thoracic 6 and multisystemic smooth muscle dysfunction (MSMDS)	TAD, TAA, BAV, stroke, premature CAD, PDA, pulmonary artery dilatation	Livedo reticularis, iris flocculi, Moya-Moya disease	[15]
<b>ARIH1</b>	Ariadne RBR E3-ubiquitin-protein ligase 1	AD	FTAA	Aortic and intracranial aneurysm	NA	[8, 16]
<b>BGN</b>	Biglycan	XL	Meester-Loeys syndrome	TAD, TAA, pulmonary artery aneurysm, IA, arterial tortuosity	Hypertelorism, pectus deformity, joint hypermobility, contractures and mild skeletal dysplasia	[17]
<b>COL1A1</b>	Collagen 1 $\alpha$ -1 chain	AD	EDS, arthrochalasia type	Arterial aneurysm, typically infrarenal	Osteoporosis, skin translucency	[11, 18]
<b>COL3A1</b>	Collagen 3 $\alpha$ -1 chain	AD	EDS, vascular type	AAA, arterial rupture without	Skin translucency, easy bruising, joint hypermobility and	[8, 11]

				aneurysm, TAD, MVP	luxation, intestinal rupture	
<b>COL5A1/2</b>	Collagen 5 $\alpha$ -1 chain/ Collagen 5 $\alpha$ -2 chain	AD	EDS classic type (I and II)	Spontaneous rupture of larger arteries and intracranial aneurysm, ARD	Joint luxations, hyperextensibility and atropic scarring	[19]
<b>EFEMP2/ FBLN4</b>	EGF-containing fibulin-like extracellular matrix protein 2 (aka fibulin4)	AR	Cutis Laxa type 1B	Arterial tortuosity, TAA, aortic/arterial stenosis	Arachnodactyly, hypertelorism, high-arched palate	[20]
<b>ELN</b>	Elastin	AD	Cutis laxa (GOF) - SVAS (LOF)	TAD occasionally (GOF), mitral and aortic valve regurgitation and BAV (GOF), pulmonary valvular and artery stenosis (LOF)	Loose redundant skin, emphysema (GOF)	[20]
<b>EMILIN1</b>	Elastin microfibril interfacier 1	AD	CTD and peripheral neuropathy	Ascending and descending aortic aneurysm	CTD, increased skin elasticity and peripheral neuropathy	[21]
<b>EP300</b>	EP300	AD	Rubinstein-Taybi syndrome	TAA	Intellectual disability, failure to thrive, microcephaly, broad thumbs and halluces, facial dysmorphisms	[22, 23]
<b>FBN1</b>	Fibrillin-1	AD	Marfan syndrome	Aortic root aneurysm and dissection, MVP	Joint laxity, skeletal overgrowth, lens displacement, myopia and striae	[24, 25]
<b>FLNA</b>	Filamin-A	XL	Periventricular nodular heterotopia	BAV, TAA, mitral valve disease, PDA	Seizures, joint hypermobility, periventricular	[8]

			and otopalato- digital syndrome,		nodular heterotopia, coagulopathy	
<b>FOXE3</b>	Forkhead box protein E3	AD	Aortic aneurysm, familial thoracic 11	TAA and TAD	NA	<b>[26]</b>
<b>LOX</b>	Lysyl oxidase	AD	Aortic aneurysm, familial thoracic 10	Aortic root aneurysm, BAV, TAA, TAD, coronary artery dissection	Joint hypermobility, skin striae	<b>[27]</b>
<b>LTBP3</b>	Latent transformin g growth factor $\beta$ binding protein 3 (LTBP-3)	AR	Dental anomalies and short stature syndrome	TAA, TAD (LOF)	Skeletal and dental abnormalities	<b>[28]</b>
<b>MAT2A</b>	S-adenosyl- methionine synthase isoform type-2 (METK2)	AD	FTAA	TAA, occasional BAV	NA	<b>[29]</b>
<b>MFAP5</b>	Microfibril- associated protein 5	AD	Aortic aneurysm, familial thoracic 9	ARD, TAA, TAD	NA	<b>[30]</b>
<b>MYH11</b>	Smooth muscle myosin heavy chain 11	AD	Aortic aneurysm, familial thoracic 4	PDA, TAA, TAD, PDA, carotid IA	NA	<b>[31]</b>
<b>MYLK</b>	Myosin light chain kinase	AD	FTAAD	TAA, acute aortic dissection	NA	<b>[32]</b>

<b>NOTCH1</b>	Notch1	AD	Aortic valve disease 1	Early calcified BAV, AVD and TAA	NA	[33]
<b>PLOD1</b>	Lysyl hydroxylase	AR	EDS, kyphoscoliotic type	Rare TAA, arterial rupture	Marfanoid features	[34]
<b>PRKG1</b>	Type 1 cGMP-dependent protein kinase	AD	Aortic aneurysm, familial thoracic 8	TAA, TAD, AAA, coronary artery aneurysm/dissection, aortic tortuosity, small vessel CVD	NA	[12]
<b>SKI</b>	Sloan Kettering proto-oncoprotein	AD	Shprintzen-Goldberg syndrome (SGS)	TAA	Skeletal muscle hypoplasia, craniosynostosis, intellectual disability	[35]
<b>SLC2A10</b>	Glucose transporter type 10	AR	Arterial tortuosity syndrome (ATS)	Arterial tortuosity, arterial aneurysm, pulmonary artery stenosis, ARD	High-arched palate, hypertelorism, arachnodactyly	[36]
<b>SMAD2</b>	Mothers against decapentaplegic drosophila homolog 2	AD	Loeys-Dietz syndrome type 6	Arterial aneurysm and dissections, AAA, ascending aortic aneurysm, vertebral carotid aneurysm and dissection, ARD	Marfanoid features	[37]
<b>SMAD3</b>	Mothers against decapentaplegic drosophila homolog 3	AD	Loeys-Dietz syndrome type 3	Arterial aneurysm, arterial tortuosity, TAA, TAD, ARD	Hypertelorism, bifid uvula, osteoarthritis	[38]
<b>SMAD4</b>	Mothers against decapentaplegic drosophila homolog 4	AD	Juvenile polyposis/hereditary hemorrhagic telangiectasia syndrome (JP/HHT)	ARD, TAA, TAD, AVM, IA	Marfanoid features	[8, 39]

<b>SMAD6</b>	Mothers against decapentaplegic drosophila homolog 6	AD	Aortic valve disease 2	BAV/TAA (LOF), CHD, mild to moderate valve stenosis, tetralogy of Fallot, coarctation of the aorta	NA	[40]
<b>ROBO4</b>	Roundabout guidance receptor 4	AD	Aortic valve disease 3	BAV/TAA	NA	[41]
<b>TGFB2</b>	Transforming growth factor $\beta$ 2	AD	Loeys-Dietz syndrome type 4	Arterial tortuosity, MVP, PDA, TAA, TAD, ARD	Hypertelorism, bifid uvula and club feet	[7]
<b>TGFB3</b>	Transforming growth factor $\beta$ 3	AD	Loeys-Dietz syndrome type 5	AAA, mitral valve disease, TAA, TAD, ARD	Cleft palate, bifid uvula, skeletal overgrowth, cervical spine instability and club feet	[42]
<b>TGFBR1</b>	TGF $\beta$ receptor I	AD	Loeys-Dietz syndrome type 1	Arterial tortuosity, PDA, widespread aortic and arterial aneurysms	Marfanoid features, hypertelorism, cleft palate, bifid uvula, craniosynostosis, club feet, dystrophic scarring, easy bruising	[43]
<b>TGFBR2</b>	TGF $\beta$ receptor II	AD	Loeys-Dietz syndrome type 2	Widespread aortic and arterial aneurysms, arterial tortuosity, PDA, TAA, TAD	Marfanoid features, hypertelorism, cleft palate, bifid uvula, craniosynostosis, club feet, dystrophic scarring, easy bruising	[43]

**Legend:** AR: autosomal recessive; AD: autosomal dominant; XL: X-linked; GOF: gain-of-function; LOS: loss-of-function; CHDSKM: congenital heart defects and skeletal malformations syndrome; TAA: thoracic aortic aneurysm; TAD: thoracic aortic dissection; FTAA: familial thoracic aortic aneurysm; AAA: abdominal aortic aneurysm; IA: intracranial aneurysm; MVP: mitral valve prolapse; ARD: aortic root dilatation; PDA: patent ductus arteriosus; CAD: coronary artery disease; AVM: arteriovenous malformation; ASD: atrial septum defect; VSD: ventricle septum

*defect; BAV: bicuspid aortic valve; CHD: congenital heart disease; AVD: aortic valve disease; CVD: cerebrovascular disease; SVAS: supraaortic stenosis*

### **3. Syndromic thoracic aortic disorders**

---

TAA is a hallmark of Marfan syndrome (MFS), Loeys-Dietz syndrome (LDS), Sphrintzen-Goldberg syndrome (SGS) and vascular Ehlers-Danlos syndrome (vEDS).

#### **3.1 Marfan syndrome**

MFS is a multisystemic connective tissue disorder affecting 1 in 5,000 people [44, 45]. MFS is inherited in an autosomal dominant manner and is associated with variable expressivity and severity. Affected organ systems include the cardiovascular (aortic root aneurysm and/or dissection and mitral valve prolapse), ocular (lens displacement) cutaneous (skin striae) and skeletal (joint laxity and vertebral column deformity) systems [46]. The cardiovascular manifestations are responsible for the associated high morbidity and mortality rate [11, 47, 48]. 95% of MFS cases have a pathogenic variant in the *FBN1* gene [49]. Over 3,000 different variants (*FBN1*-UMD database) have been discovered in more than 3,000 MFS patients. Whereas missense variants are most frequently observed (46%), other variant types such as nonsense (16%), frameshift (19%), splice altering (13%) and gene deletions are also commonly seen [25, 50, 51].

Several genotype-phenotype correlation studies have been performed revealing few strong associations [52, 53]. Pathogenic *FBN1* variants can be divided into two groups: (1) variants leading to a premature termination codon (PTC), causing *FBN1* haploinsufficiency; and (2) dominant-negative variants (mostly missense variants or in-frame insertions/deletions). In previous studies it has been suggested that PTC variants are associated with a more severe cardiovascular, skeletal and/or skin phenotype, but this is not confirmed in other studies [54-58]. The most convincing genotype-phenotype correlation is the strong enrichment of cysteine-affecting missense variants in ectopia lentis-presenting MFS patients [51, 58]. Cysteine-removing missense variants have been linked to an increased TAAD and mitral valve prolapse risk as compared to their

cysteine-creating counterparts [52]. Location of the variants matters too, with dominant negative pathogenic variants in exon 24-32 (called the neonatal region) typically resulting in a more severe phenotype [52, 58]. Meester et al recently demonstrated that the latter severe cardiovascular phenotype is not restricted to the neonatal region but can be extended to the exon 26-49 region. Additionally, it was shown that cysteine-involving variants at residues 611-921 and 1348-1429 lead to ectopia lentis in 100% of cases. The true value of these genotype-phenotype correlations is hampered by the clinical heterogeneity that is seen in MFS patients, even between individuals with an identical *FBN1* mutation or within one family. As such, genetic modifiers and/or environmental or non-genetic factors likely influence the phenotypical outcome of MFS patients. Franken et al evaluated if the aortic tortuosity index (ATI) is linked to the severity of the aortic phenotype in MFS patients. The ATI could reliably distinguish patients at higher risk for aortic rupture [59]. Another related non-genetic risk factor that is being suggested is the aortic length. For every one cm-increment in ascending aorta length, a five-fold increased risk for TAAD was observed [60, 61]. Abnormal flow patterns leading to aortic outflow aberrations as well as aortic micro-calcifications and increased amounts of fibrillin-1 fragments in the blood circulation have also been proposed to associate with a worse prognosis [62-65].

The *FBN1* gene encodes fibrillin-1, an extracellular glycoprotein, the major structural component of aortic microfibrils [1]. Historically, it was believed that structural deficiency due to fibrillin-1 deficiency was the main pathomechanistic driver of MFS. An *FBN1* knock-in C57Bl/6J mouse model (*Fbn1*<sup>1039G/+</sup>), however, pointed towards the involvement of the TGF- $\beta$  signaling pathway in MFS-related TAAD [66-68]. More precisely, within the aortic wall of the *Fbn1* mice and MFS patients an upregulation of the TGF- $\beta$  signaling was observed [69-71]. This discovery led to important new insights in the pathogenesis of MFS and TAAD in general and paved the way for novel therapeutic approaches [68, 72].

### 3.2 Loeys-Dietz syndrome

LDS is an autosomal dominant connective tissue disease affecting less than 1 in 50,000 individuals. Phenotypically, LDS patients resemble MFS patients, but they can be distinguished by the unique presence of the triad of aortic aneurysm with arterial tortuosity, hypertelorism and bifid uvula or cleft palate [73]. The aneurysms are more widespread and are more aggressive in nature as they tend to dissect at a smaller diameter and earlier age in comparison to what is observed in MFS patients [17, 74, 75]. So far, six LDS subtypes have been described, categorized according to the predisposing gene (*TGFBR1/2* (LDS1/2), *TGFB2/3* (LDS4/5), and *SMAD2/3* (LDS6/3)) [73]. The six LDS genes encode for receptors, ligands or intracellular downstream effectors of the TGF- $\beta$  pathway [11, 75-77].

No clear genotype-phenotype correlation for LDS has yet been established. Nonetheless, patients with a pathogenic variant in the *TGFBR1/TGFBR2* gene are generally more severely affected, experiencing dissections at smaller aortic diameters, as compared to those with a variant in the more recently discovered LDS genes [53, 78]. The disease genes can be ranked (in order of decreasing severity) as follows: *TGFBR1/2*, *SMAD3*, *TGFB2*, *SMAD2* and *TGFB3*, with a non-penetrance of up to 50% in individuals harboring *TGFB3* variants [75].

So far, all pathogenic variants in LDS genes encoding for components of the TGF- $\beta$  pathway exert a loss-of-function mechanism. As such, one would predict a resultant decrease in TGF- $\beta$  signaling. Paradoxically, an increase in TGF- $\beta$  signaling is observed in affected aortic walls of an LDS mouse model (*Tgfbr1*<sup>M318R/+</sup>) on a 129S6/SvEv genetic background and LDS patients [77].

The aggressive nature of aortic disease in LDS requires close and frequent imaging surveillance as well as prophylactic surgery at a lower aortic diameter threshold as compared to that in MFS [79].

### 3.3 Meester-Loeys syndrome

Meester-Loeys syndrome (MRLS) is an X-linked disease caused by pathogenic *BGN* variants [80]. *BGN* encodes for the extracellular matrix protein biglycan, which is a highly expressed small leucine-rich proteoglycan (SLRP) protein [81]. In addition to its structural role, biglycan regulates cytokine binding and pathway signaling, e.g., the TGF- $\beta$  pathway [82]. *BGN* variant harboring individuals present with LDS- and MFS-overlapping features such as early-onset TAA, hypertelorism, joint hypermobility and contractures, pectus deformity, dolichocephaly, skin striae and mild skeletal dysplasia. Distinctive manifestations for MRLS are brain ventricular dilatation, hypertrichosis (excessive hair growth), relative macrocephaly and gingival hypertrophy [17].

Meester et al reported five causal variants with a loss-of-function mechanism. In line with X-linked inheritance, males are more severely affected. Whereas all of them suffer from TAAs (sometimes already at a very young age), only 67% of female patients develop TAA of variable severity [17]. It has been suggested that biglycan is a regulator of the TGF- $\beta$  pathway. Increased TGF- $\beta$  signaling has been observed in the aortic wall of MRLS patients, as is seen in other TAA syndromes such as MFS and LDS. Remarkably, in contrast with LDS and MFS, biochemical analysis of the aortic tissue of the MRLS probands revealed normal elastic fibers and collagen content [17]. Male *Bgn*-deficient BALB/cA mice have been reported to suffer from aortic ruptures leading to sudden death, confirming a critical role for biglycan in the maintenance of the structural integrity of the aortic wall. Even more, structural investigation of the aortic wall uncovered no alterations in the collagen content but rather in the size of the collagen fibers [82].

### 3.4 Shprintzen-Goldberg syndrome

Shprintzen-Goldberg syndrome (SGS) is a rare autosomal dominant condition, caused by pathogenic variants in the *SKI* gene, encoding ski proto-oncogene [83]. SGS patients

typically display craniosynostosis and developmental delay with cognitive disability [84]. Whereas overlap with MFS and LDS is apparent as regards the skeletal symptoms (Marfanoid habitus, joint hypermobility & arachnodactyly), aortic dilatations are usually less penetrant, less severe and less progressive than in MFS or LDS [20, 85]. To date, most of the causal variants in *SKI* are missense variants or small in-frame deletions clustered in two distinct N-terminally located regions of the Ski protein: the R-SMAD binding domain (predominantly amino acids 31-35) [86] and the Dachshund-homology domain (p.(Thr180))[87], both described as mutational hotspots in SGS patients [86-88].

*SKI* is ubiquitously expressed throughout the body and particularly active during development [89]. It negatively regulates SMAD-dependent TGF- $\beta$  signaling [83, 90] by disrupting the formation of R-Smad3/Smad4 complexes and thereby translocation to the nucleus. Pathogenic variants prevent SKI from properly binding SMAD complexes, resulting in increased TGF- $\beta$  signaling activity [35].

### **3.5 Ehlers-Danlos syndrome**

Ehlers-Danlos syndrome (EDS) refers to a heterogeneous group of connective tissue disorders characterized by cutaneous (skin hyperextensibility), skeletal (joint hypermobility) and vascular/intestinal (arterial and bowel rupture) manifestations. It has an estimated prevalence of 1 in 5,000 to 1 in 25,000 [91, 92]. So far, 14 different EDS subtypes have been described, which are caused by pathogenic variants in 19 different genes and vary in mode of inheritance [18]. In this chapter, only the ones with aortic involvement are listed. In general, approximately 25% of EDS patients have concomitant aortic aneurysmal disease, most pronounced in vascular EDS (vEDS) patients [11]. vEDS is the most lethal form and is characterized by aortic or arterial dissecting disease, bowel perforations and uterine ruptures as well as skin translucency and easy bruising [12, 93, 94]. It follows an autosomal dominant inheritance pattern and is caused by pathogenic variants in *COL3A1* [74, 94]. Variants causing vEDS can be

divided into several subtypes, with missense variants affecting a glycine residue in the triple helix [Gly-X-Y]<sub>343</sub> repeat sequence being the most common subtype (1). Other variants cause haplo-insufficiency (2), affect splice-sites and/or result in in-frame deletions or insertions (3), or more rarely encompass non-glycine missense variants within the triple helix (4) or non-glycine missense variants in the N- or C-terminal part of the protein (5). A correlation exists between the type of *COL3A1* variant and the phenotypical outcome: *COL3A1* haplo-insufficient vEDS patients are less severely affected and have an older age of onset [95].

The cardiac-valvular EDS type is a rare type with a prevalence of 1 in a million people, characterized by heart valve problems, stretchy skin and joint hypermobility caused by recessive loss-of-function variants in *COL1A2* [96]. The classic type of EDS (cEDS) is the most common form, estimated to affect 1 in 20.000-40.000 individuals. In more than 90% of cases cEDS is caused by mutations in *COL5A1* and *COL5A2* and also but rarely by pathogenic variants in *COL1A1* (typically arginine for cysteine substitutions). Joint luxation, skin hyperextensibility and atrophic scarring are the major clinical hallmarks for cEDS diagnosis [20]. Furthermore, spontaneous rupture of large arteries and intracranial aneurysms have also been reported for cEDS [97, 98].

Other EDS subtypes that occasionally also present with aneurysmal disease are the kyphoscoliotic (kEDS) and arthrochalasia types caused by heterozygous variants in *PLOD1* and *COL1A1*, respectively [11]. kEDS patients are susceptible for ruptures of medium-sized arteries [19, 99]. *COL* genes encode collagen proteins, which are important components of connective tissue, providing strength and structure to organs and tissues throughout the body [100]. Pathogenic variants infer disorganization of the collagen fibers in the aortic wall, inducing vascular fragility leading to aortic/arterial dissection [93].

### **3.6 Osteogenesis imperfecta (OI)**

Osteogenesis imperfecta (OI) is a skeletal dysplasia with an estimated incidence of 1:15,000-1:20,000. It is most commonly inherited in an autosomal dominant manner, but recessive and X-linked inheritance has been observed as well. The hallmarks of OI are bone fragility, a high frequency of fractures, bone deformity and growth deficiency leading to short stature. Other clinical features are cardiac valvular insufficiency with regurgitation, blue sclerae, brittle teeth, hearing loss and reduced respiratory function [101, 102]. About 10 OI-patients with aortic dissections have been reported [103] and aortic measurements are described at the upper limit of normal (84). In approximately 90% of all cases, OI is caused by a triple helix glycine-affecting missense or haplo-insufficient pathogenic variant in *COL1A1* or *COL1A2*, encoding the  $\alpha 1(I)$  and  $\alpha 2(I)$  chains of type I collagen, respectively, which are main components of the ECM of bone, skin and aortic tissue [104, 105].

### **3.7 Arterial tortuosity syndrome**

Arterial tortuosity syndrome (ATS) is a very rare autosomal recessive connective tissue disorder with an estimated prevalence of less than 1 in 1,000,000 live births [106]. ATS patients present with generalized elongation and tortuosity of the aorta and mid-sized arteries and clinical features shared with other connective tissue disorders such as skin hyperextensibility, hernia, joint hypermobility, facial dysmorphism (high palate, elongated face, micrognathia, beaked nose, and down slanting palpebral fissures), arachnodactyly, pectus deformity and scoliosis [107]. Patients are also at increased risk for aneurysmal dilatation at any age throughout the whole arterial tree [108], but dissection seems rare. A unique feature found in the majority of ATS cases is the combination with arterial stenosis, including aortic stenosis (24% of ATS patients), pulmonary artery stenosis (57% of ATS patients) or stenosis in other arteries (15% of ATS patients) [106, 108].

ATS is caused by bi-allelic loss-of-function variants in the *SLC2A10* gene, encoding GLUT10, a facilitative glucose transporter present in the mitochondrial and endoplasmic reticulum membranes that is proposed to function as a dehydroxyascorbic acid (DAA) transporter [108]. Pathogenic variants in the *SLC2A10* gene lead to impaired DAA transport and instigate upregulation of the TGF- $\beta$  signaling pathway in the aortic wall, as well as altered ECM organization, cell energy balance and oxidative stress response [36, 109]. The variant spectrum of *SLC2A10* encompasses small intragenic deletions/insertions, missense, nonsense and splice-site variants [106, 110].

### **3.8 Lysyl oxidase (*LOX*) mediated aortic aneurysm**

*LOX* encodes one of the most vital ECM proteins: lysyl oxidase, a cuproenzyme that catalyzes crosslinking of the ECM components such as collagen and elastic fibers. The stability, elasticity and mechanical integrity of the aortic/arterial wall relies on proper fiber assembly. The clinical phenotype of *LOX* patients is ranging from individuals only having a cardiovascular phenotype not showing any connective tissue finding to individuals with a tall stature, flat feet and increased skin elasticity as well as inguinal hernia, joint hypermobility and arachnodactyly [27]. Several studies report on the identification of loss-of-function missense and nonsense *LOX* variants in patients presenting with arterial aneurysms, at the level of the aorta and/or throughout the rest of the body [27, 111].

### **3.9 *EFEMP2 (FBLN4)* autosomal recessive cutis laxa type 1B**

Autosomal recessive pathogenic variants in *EFEMP2* are typically missense or frameshift mutations manifesting in cutis laxa type 1B (ARCL1B), a disease with a highly variable phenotype ranging from perinatal lethality to limited vascular and craniofacial features. The most commonly seen characteristics are thoracic aortic aneurysm, arterial tortuosity, stenosis, joint laxity, extreme skin folds and arachnodactyly [112]. EGF containing fibulin extracellular matrix protein 2 (*EFEMP2*) (also called fibulin-4) plays a

crucial role in elastic fiber formation and collagen fibril assembly in tissue, and therefore aortic wall integrity maintenance [113].

### **3.10 Other syndromic TAA causes: *ABL1*, *ARIH1*, *EP300*, *FLNA*, *SMAD4* and *EMILIN1***

Variants in a few other genes have been linked to (variably penetrant) syndromic TAA. *ABL1* encodes for a tyrosine kinase with many diverse cell functions such as cell proliferation, differentiation or integration and apoptosis. Germline gain-of-function mutations in *ABL1* are associated with the congenital heart defects and skeletal malformations syndrome (CHDSKM), a rare autosomal dominant disorder with atrial and ventricular septum defect as well as aortic root dilatation, skeletal abnormalities, and failure to thrive [114].

*ARIH1* encodes Ari-1 which functions as an E3 ubiquitin-protein ligase which catalyzes ubiquitination. Rare pathogenic dominant variants in *ARIH1* have recently been identified in individuals with thoracic aortic aneurysm and cerebrovascular disease [115]. It is suggested that *ARIH1* mutations lead to loss of mechanosensing in VSMCs and therefore weaken the aortic wall leading to aortic aneurysms [116].

*EP300* encodes for E1A binding protein p300 which regulates transcription via chromatin remodeling and cell proliferation and differentiation. In 3% of Rubinstein-Taybi Syndrome 2 patients, the culprit gene is *EP300*. *EP300*-related disease has a broad phenotypic spectrum with cardiovascular features such as aortic aneurysms primarily affecting the ascending part of the aorta (circa 5% of all patients), mitral valve dysplasia, tetralogy of Fallot and atrial/ventricular septal defects are observed in 26% of *EP300* cases. Other non-cardiovascular features include high palate, hypertelorism and abnormal facial shape as well as postnatal growth retardation [23, 117].

Besides *BGN*, another X-linked gene, namely *FLNA*, which encodes for filamin A, is involved in the reorganization of the actin cytoskeleton which is crucial for maintenance of the cell shape and migration and cardiovascular remodeling. A wide spectrum of

connective tissue, skeletal, gastrointestinal and cardiovascular manifestations has been reported for *FLNA* patients [118]. The latter are typically associated with loss-of-function *FLNA* mutations. A pathognomonic (but not always present) feature of these LOF filaminopathies is periventricular nodular heterotopia (PVNH). 18.4% of PVNH patients develop thoracic aortic aneurysm or dilatation. Other structural cardiac anomalies such as patent ductus arteriosus and valvular abnormalities are present in 57.1% of PVNH patients [119]. In contrast, gain-of-function *FLNA* variants lead to phenotype in the spectrum of Melnick-Needle syndrome (MNS) and otopalatodigital syndromes (OPD) [120].

Patients with *SMAD4* mutations are associated with juvenile polyposis syndrome (JPS) and a combined JPS-hereditary hemorrhagic telangiectasia known as JPS-HHT and are at risk for thoracic aortic disease [39].

Pathogenic variants in another microfibril-associated protein, encoded by *EMILIN1*, were reported as well in TAA families. A proband carrying a heterozygous missense alteration with ascending and descending aortic aneurysms also presented with bilateral lower leg and foot sensorimotor peripheral neuropathy, arthropathy, and increased skin elasticity [21].

#### **4. BAV-related TAA**

---

Bicuspid aortic valve (BAV) denotes an aortic valve that has two leaflets instead of the normal three. Affecting 1-2% of the population (3:1 male preponderance), it is the most common congenital heart malformation [121, 122]. Importantly, it is enriched in LDS patients (up to 10%) [123] and BAV patients have a 9-fold increased risk for aortic dissection as compared to the general population [124]. BAV(/TAA) has an autosomal dominant inheritance pattern, with reduced penetrance and variable expressivity. The most important genes that have been linked to BAV/TAA patients are *NOTCH1*, *SMAD6*, *ROBO4* and *TBX20* [125-127]. Variants in *NOTCH1* have predominantly been associated

with sporadic and familial BAV along with valvular dysfunction, but a minor fraction of patients also present with TAA [128, 129]. NOTCH1 is an important player of the Notch signaling pathway, a highly conserved pathway involved in the development of the outflow tract [128]. Pathogenic variants in *SMAD6*, encoding an inhibitory protein of the bone morphogenetic protein (BMP) signaling pathway, explain about 1% of BAV/TAA patients [40]. Variants in *ROBO4*, a receptor for SLIT proteins, are a rare cause of BAV/TAA. They cause disease by affecting the aortic valve development and the endothelial barrier function in the aorta [41]. Finally, deleterious copy number variations (CNVs) and single nucleotide variants (SNVs) in *TBX20*, a transcription factor with a key role in heart development, explain roughly another 1% of BAV/TAA patients [125]. Despite extensive gene discovery efforts, still only up to 10% of BAV/TAA cases can be explained by pathogenic variants in the yet identified genes, warranting further research [123, 130].

## **5. Non-syndromic TAA(D)**

---

Non-syndromic TAA accounts for 95% of cases [131] and can be subdivided in familial (FTAA) and sporadic (STAA) forms. As compared to STAA, FTAA usually develops earlier in life and are characterized by accelerated aneurysm growth [16, 132].

FTAA inherits in an autosomal dominant manner with reduced penetrance [133]. *ACTA2* was the first discovered FTAA gene, explaining up to 14-21% of FTAA cases [131]. Along with TAA, *ACTA2* variant carrying individuals suffer from cerebral stroke, BAV, premature coronary artery disease and Moyamoya disease [134]. *ACTA2* encodes the VSMC-specific alpha-actin protein, which regulates actin filament polymerization. *ACTA2* deficiency leads to actin filament instability and, as a result, dysfunction of the actin-myosin contractile unit of VSMCs [135, 136]. *MYLK* encodes the VSMC-specific myosin light chain kinase, which regulates VSMC contraction [32]. Loss-of-function pathogenic variants in this gene have been described (<1% of cases) to cause aortic dissections, often in hypertensive patients without significant prior aortic dilatation [137], due to

impaired VSMC contractility [138]. *MYH11* (~2%) is another genetic cause of TAA, linked to the VSMC contractile apparatus. It encodes the thick filament component smooth muscle myosin heavy chain 11. Variants in this gene are predominantly found in patients that also present with patent ductus arteriosus [31]. Protein kinase cGMP dependent type 1 is a kinase encoded by *PRKG1*. It dephosphorylates regulatory light chains (RLCs), which controls VSMC relaxation. So far, only two specific gain-of-function pathogenic variants, p.(Arg177Gln) and p.(Gly370Ser), are known to cause TAAD [139]. *PRKG1* variant harboring individuals present with TAA at young age (15-51years), often in combination with arterial tortuosity and sometimes hypertension [140].

Besides the four previously mentioned VSMC-related disease genes, pathogenic variants in few ECM-related genes have been linked to FTAA with mild connective tissue findings. These genes are explaining only a restricted number of FTAA patients. First, loss-of-function variants in the *MFAP5* gene, encoding the microfibrillar associated protein 5 (MAPG2), have been observed in two families [30]. Variants in methionine adenosyltransferase 2- $\alpha$ , encoded by *MAT2A*, have been found in two TAA families with a reduced penetrance of thoracic aortic aneurysms and low risk for acute aortic dissection/rupture. *MAT2a* is involved in the synthesis of S-adenosylmethionine, which is a methyl donor group that participates in DNA, RNA and protein methylation [29]. *FOXE3* encodes forkhead box E3, a transcription factor that has most prominently been studied in the frame of eye lens development. Autosomal dominant variants in the forkhead domain have been suggested to cause acute aortic dissections [26], but replication of these findings has not been achieved yet, despite *FOXE3* screening in multiple diagnostic TAA labs. Pathogenic recessive variants in *LTBP3*, which were first linked to a skeletal and dental dysplasia phenotype, were subsequently also reported to predispose to TAA. Heterozygous *LTBP3* haplo-insufficient individuals are also predisposed for thoracic aortic aneurysm and dissection [28].

Genome wide association studies (GWAS) have successfully mapped thousands of loci associated with complex disease. Ashvetiya et al found genome wide associations between TAA and single nucleotide polymorphisms (SNPs) in distinct sets of genes (*CTNNA3*, *FRMD6* and *MBP*) [141]. Roychowdhury et al identified an additional TAA-associated locus in the intronic region of *TCF7L2*. Higher expression levels of *TCF7L2*, causing repression of the apoptosis inhibitor *BCL2*, lead to increased VSMCs apoptosis [142]. Besides SNPs, also common copy number variations (CNVs), in particular duplication of the 16p13.1 region including *MYH11*, have been linked to TAA [143].

## **6. Aortic aneurysmal disease-related mechanisms**

---

Functional characterization of the hitherto identified TAA genes revealed several implicated mechanisms, including ECM homeostasis, VSMC contraction, TGF- $\beta$  signaling, NO signaling pathway, mitochondrial dysfunction and inflammatory responses.

### **6.1 Extracellular matrix homeostasis**

Under normal physiological conditions, the aortic wall ECM provides tensile strength as well as recoil propensity. It is composed of a variety of proteins, including elastin, collagen, proteoglycans, laminin and fibronectin [1]. A series of TAA genes encode (associated) components of the ECM, including *FBN1*, *MFAP5*, *ELN*, *LOX*, *COL3A1*, *BGN* and *EFEMP2/FBLN4*, emphasizing the role of structural aortic weakness in TAA development [94]. Besides genetic clues, other observations further underscore an important contribution of ECM dysfunction. An increase in proteoglycans, particularly aggregates of aggrecan and versican, has been observed in aneurysmal aortic tissue samples. This increase can be explained by a reduced ADAMTS5-mediated cleavage and turnover of aggrecan and versican or an increased production of these proteoglycans [144]. Additionally, increased collagen deposition and elastic fiber fragmentation and degradation are two pathohistological hallmarks of TAA [3]. Abnormal arterial ECM

remodeling because of an imbalance in matrix metalloproteinases (MMPs) and tissue inhibitors of metalloproteinases (TIMPs) contribute to this process [5, 145]. *ELN* encodes for elastin, a major component of elastic fibers. Gain-of-function variants in this gene cause the autosomal dominant disorder, Cutis Laxa (ADCL), which has recently also been associated with aortic dilatation and rupture [1]. In addition, triplication of the *ELN* gene (7q11.23) has also been found to predispose to TAA [146].

## 6.2 VSMC contractile unit function

VSMCs are the most abundant cell type in the aortic media and play a vital role with their contractile properties/phenotype in regulating vascular diameter and vascular tone [1, 147]. Intermediate filaments (IFs) are a cytoskeletal system important in regulating the contraction/relaxation states of VSMCs and their interaction with the ECM. Connections between ECM and VSMCs are made by glycoproteins such as fibronectin, intermediate filaments (such as filamin-A) via specific integrin receptors expressed in VSMCs [148]. The contractile unit responsible for VSMCs contraction consists of regulatory proteins expressed by several smooth muscle cell-specific genes including *ACTA2*, *MYH11*, *MYLK* and *PRKG1* [15, 135]. The contractile apparatus consists of thin and thick filaments, with thin filaments comprising polymerized alpha-smooth muscle cell actin (alpha-SMA) encoded by *ACTA2* [3, 135] and thick filaments constructed by *MYH11*. The contraction mechanism itself is based on actomyosin cross-bridge cycling initiated by an increase in intracellular  $Ca^{2+}$  concentration levels. The increase in  $Ca^{2+}$  can originate from extracellular space or can be released from the sarcoplasmic reticulum (SR). This increase triggers the  $Ca^{2+}$ -dependent VSMC contraction via calmodulin, where  $Ca^{2+}$  binds and gets activated which in his turn, activates MYLK In the next step. MYLK regulates the phosphorylation of the RLCs, leading to a displacement of the myosin motor heads and enables with this cyclic binding to the actin filaments inducing force and VSMCs contraction. In non-active (non-phosphorylated) circumstances the RLCs prevent binding of the myosin motor heads to

actin by intramolecular interactions. The relaxation of VSMCs is mediated by type I cGMP-dependent protein kinase (PRKG1) [149-151]. Aberrant vascular remodeling or ECM stiffening is associated with a phenotypic transition of vascular smooth muscle cells from a contractile phenotype towards a synthetic phenotype. Pathologically, this phenotypic switch makes the vessel wall more vulnerable for hemodynamic changes and stress. This remodeling process is powered by the increase in extracellular protease production with an increase in MMPs production in VSMCs in TAAO patients [150, 152, 153]. In general, aortic VSMCs of TAAO patients are characterized by a decrease in actin-myosin filaments and an increase in matrix degrading enzymes [1].

### **6.3 TGF- $\beta$ signaling pathway**

The transforming growth factor- $\beta$  family encompasses a large number of various signaling pathways and defines numerous of receptors and ligands, such as activins, inhibins, TGF $\beta$ s, bone morphogenetic proteins (BMPs), growth and differentiation factors and SMAD proteins [71, 154]. In humans, three distinct TGF- $\beta$  ligands exist, namely TGF $\beta$ 1,  $\beta$ 2 and  $\beta$ 3 encoded by *TGF $\beta$ 1*, *2* and *3* respectively [154]. The transforming growth factor  $\beta$  (TGF- $\beta$ ) signaling pathway is involved in multiple diverse cellular processes including, cell proliferation, angiogenesis, apoptosis, wound healing, and cell differentiation [77]. Fibrillin-1 is a regulator of the TGF- $\beta$  homeostasis by regulating the bioavailability of TGF- $\beta$  ligands in the ECM [56].

In general, the TGF $\beta$  protein is secreted as an inactive (latent) precursor. Two precursor proteins dimerize by disulfide bridges forming a TGF $\beta$  dimer that is cleaved to obtain the small latent complex (SLC). This SLC is formed by the latency associated peptide (LAP) and the mature TGF $\beta$  peptide. The SLC covalently binds the latent TGF $\beta$  binding protein (LTBP) forming the large latent complex bound by fibrillin-1 to the ECM [56]. Upon release of mature TGF $\beta$  from the large latent complex, it binds its Type II TGF $\beta$  receptor unit (TGFBR2) followed by phosphorylation of the Type I TGF $\beta$  receptor unit

(TGFBR1/ALK5) and activates the downstream TGF- $\beta$  pathways [155, 156]. This downstream TGF- $\beta$  signaling pathway can be categorized in two types: the canonical and non-canonical signaling also known as the SMAD-dependent and SMAD-independent signaling, respectively [8].

In the canonical TGF- $\beta$  pathway, after the binding of one of the TGF- $\beta$  ligands to the heterodimeric TGF $\beta$  receptor complex consisting of TGFBR type 1 and TGFBR type 2, the activated type I receptor activates the receptor-regulated SMAD proteins (R-SMADs) including SMAD2 and SMAD3 by phosphorylation. The phosphorylated SMADs form a hetero-oligomeric complex with SMAD4, followed by shuttling into the nucleus. Once entered in the nucleus the complex acts as a transcription complex activating or repressing numerous downstream target genes [11, 157]. SKI and SMAD7 are inhibitors of the canonical TGF- $\beta$  signaling pathway. A negative feedback loop is induced by SKI through binding the pSMAD2/3-SMAD4 complex and blocking it from translocation towards the nucleus and thereby prevents the expression of downstream genes of the TGF- $\beta$  pathway [155]. On the other hand, the non-canonical pathway works through other kinases such as the mitogen-activated protein kinase (MAPK), extracellular signal-regulated kinase (ERK)1/2, p38 and Jun N-terminal kinase [91, 158]. A schematic representation of the TGF- $\beta$  pathway can be found in Figure 2.

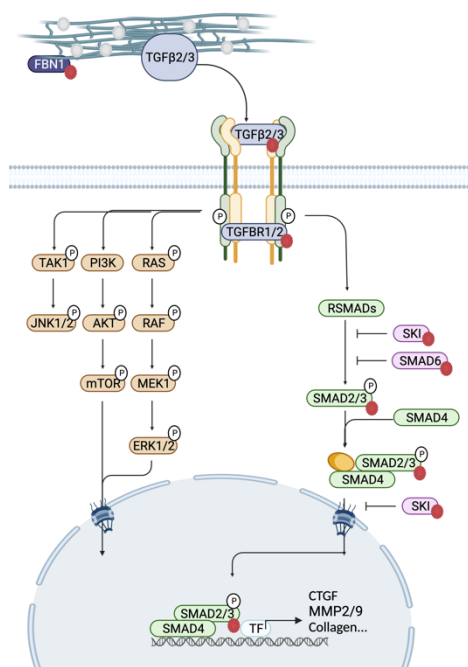


**Figure 2. Schematic representation of the TGF- $\beta$  signaling pathway**

Uncontrolled release of the TGF- $\beta$  ligands results in an upregulation of TGF- $\beta$  signaling and overexpression of downstream targets of the TGF- $\beta$  signaling pathway. This dysregulation is an important molecular signature of the TAA pathomechanisms in MFS patients [7, 159].

The precise role of the TGF- $\beta$  signaling is still a matter of debate as both activation and inhibition are reported to contribute to TAAD development [8, 69]. Interestingly, loss-of-function mutations in the LDS genes (*TGFB1/2*, *SMAD3*, *TGFB2/3*) result in a paradoxical increase in TGF- $\beta$  activity [43]. These findings were supported by increased levels of phosphorylated SMAD2 and ERK1/2 in the nuclei of aortic wall tissue from MFS and LDS patients [43]. Several explanations are considered for this counter-intuitive result. It was proposed that the malfunction of the Smad-dependent TGF- $\beta$  pathway components interrupts a certain auto-inhibitory feedback loop, that leads towards an unbalanced activation of components from the Smad-independent pathway [24]. More

recently, a difference in vulnerability for TGF- $\beta$  disturbance between vascular smooth muscles with a different embryonic origin (i. e. secondary heart field (SHF) and cardiac neural crest (CNC)-derived VSMCs) was proposed. Consequently, compensatory release of TGF $\beta$ 1 in the less vulnerable cardiac neural crest derived VSMCs is mediated [7, 155].

#### **6.4 NO-sGC-PRKG signaling in TAAD**

In addition, other pathways emerge as contributors to TAAD development, including endothelial dysfunction associated with nitric oxide (NO) deficiency. Under normal conditions, endothelial cells regulate VSMC contraction and relaxation, and inflammatory response through the release of NO produced by endothelial NO synthase (eNOS) followed by sGC-PRKG1 signaling [160]. Upon the release of e-NOS derived NO, sGC (soluble guanylate cyclase) is activated and catalyzes the production of cGMP, after which PRKG1 (protein kinase cGMP-dependent type 1) is activated. PRKG1 inhibits several processes leading towards the inhibition of VSMC contraction via intracellular Ca<sup>2+</sup> handling, actin filament regulation and myosin dynamics, and therefore vasodilatation. As such, the NO-sGC-PRKG1 pathway determines the phenotypic plasticity of VSMCs [161]. The uncoupling of eNOS and abnormal NO levels are associated with cardiovascular disease since they stimulate the generation of reactive oxygen species (ROS) that disrupt the endothelial function leading to decreased NO bioavailability and activation of highly reactive peroxynitrite (ONOO<sup>-</sup>), provoking ROS-induced cellular damage [162].

#### **6.5 VSMC mitochondrial dysfunction in TAAD**

A recent observation is the fact that VSMC mitochondrial dysfunction promotes aortic dilatation, aneurysms and possible dissection/ruptures. The mitochondrial transcription factor A (Tfam) controls replication, transcription, and stability of the mitochondrial DNA (mtDNA) [163]. A Tfam-deficient mouse model displayed

mitochondrial dysfunction, which was followed by aortic dilatation and aneurysm, medial degeneration and fatal dissections. Furthermore, it has been shown that aortas from MFS mice (*Fbn1*<sup>C1039G/+</sup>) present with decline in mitochondrial respiration, shift of their metabolism toward glycolysis, have a decreased mtDNA content and show inflammatory responses [164].

## 6.6 Inflammation in TAAD

In the past year, more attention is paid to the involvement of inflammatory pathways in TAAD development. Monocyte chemoattractant protein-1 (MCP-1), a key chemokine which regulates the migration and infiltration of macrophages/monocytes in aortic tissue has been associated with the amount of elastin fragmentation in the aorta, inflammation and aortic dilatation [165]. An increase in macrophage and T-cell infiltration was observed in the media of aortic tissue from MFS patients [166]. It is suggested that IL-1 $\beta$ , secreted by macrophages, is a strong proinflammatory cytokine since it has been found at 20-fold greater concentration in aortic tissue compared to a healthy control [167]. Besides IL-1 $\beta$ , IL-6 is also an important key player in aortic inflammation with increased IL-6 expression levels in aortic tissue from TAAD patients [168]. Additionally, both cytokines are mediators of increased *MMP2* and *MMP9* levels in aortic tissue, with increased *MMP2/9* expression levels as a known hallmark for TAAD [169]. In Figure 3 a schematic overview of the pathophysiology of TAAD is given.

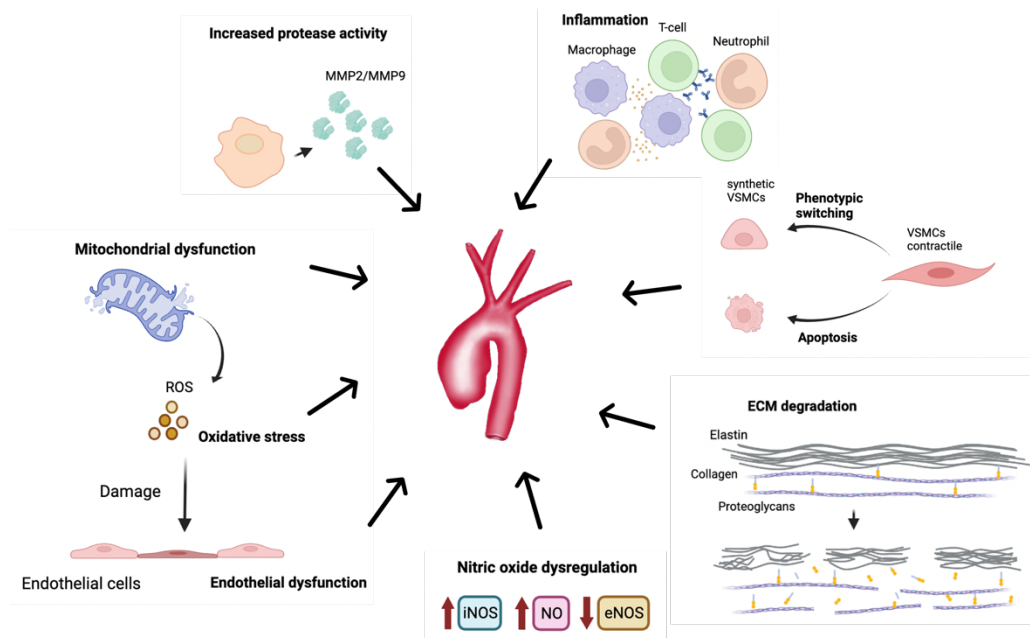


**Figure 3. Pathophysiology of TAAD.**

## 7. Molecular diagnostics

Targeted sequencing of known TAA-causing genes currently provides a genetic cause for 20-30% of all TAAD patients [11, 13]. These numbers will further increase in the future as more genes associated with TAAD development will be discovered using whole exome or whole genome sequencing. This genetic confirmation is of utmost importance for best possible patient management. When deciding on surgery, the aortic diameter is the gold standard with a diameter reaching 5 cm being recommended for surgery. The aortic growth is another determinant for aortic surgery, enlargements of >5mm annually are indications for surgery. There is increasing evidence that decisions on prophylactic surgery are also determined by the underlying gene [75]. Furthermore, the nature of the underlying variant (e.g. dominant negative versus haplo-insufficiency) in a certain gene will also determine the disease management applied. Moreover, the underlying gene variant will also drive the location and the frequency of non-invasive cardiovascular imaging [88]. For e.g. aneurysm development in LDS patients is

commonly not restricted to the aorta but throughout the whole body. To date gene panels have become a valuable tool in molecular diagnostics. Other important techniques for detecting novel disease-causing variants are whole exome (WES) and whole genome sequencing (WGS). In diagnostics, WES is becoming the standard to evaluate patients their genetic condition, indicating an ongoing transition from gene panels to WES to find variants of clinical significance.

## **8. Conclusion and future perspectives**

---

Taken together, aortic aneurysms remain a serious health concern with a high morbidity and mortality rate. Dissection of aortic aneurysms often happens unexpected, without any warning or associated clinical features. Even though numerous discoveries have been made regarding aneurysmal disease and underlying pathomechanisms, further elucidation of the pathomechanisms of TAAD development is necessary for an optimal risk stratification and for the design of personalized patient management and therapies. Current knowledge on TAAD implicates the involvement of specific pathways, cell types and biological processes. The increasing power of next generation sequencing techniques will provide us with more genetic knowledge and therefore a possible explanation for the observed clinical variability in TAAD patients, even within the same family, carrying the same pathogenic variants.

## 9. References

---

1. Creamer, T.J., E.E. Bramel, and E.G. MacFarlane, *Insights on the Pathogenesis of Aneurysm through the Study of Hereditary Aortopathies*. Genes (Basel), 2021. **12**(2).
2. Stenmark, K.R., et al., *The adventitia: essential regulator of vascular wall structure and function*. Annu Rev Physiol, 2013. **75**: p. 23-47.
3. Wagenseil, J.E. and R.P. Mecham, *Vascular extracellular matrix and arterial mechanics*. Physiol Rev, 2009. **89**(3): p. 957-89.
4. Sawada, H., et al., *Smooth Muscle Cells Derived From Second Heart Field and Cardiac Neural Crest Reside in Spatially Distinct Domains in the Media of the Ascending Aorta-Brief Report*. Arterioscler Thromb Vasc Biol, 2017. **37**(9): p. 1722-1726.
5. Cheng, J.K. and J.E. Wagenseil, *Extracellular matrix and the mechanics of large artery development*. Biomech Model Mechanobiol, 2012. **11**(8): p. 1169-86.
6. Criado, F.J., *Aortic dissection: a 250-year perspective*. Tex Heart Inst J, 2011. **38**(6): p. 694-700.
7. Lindsay, M.E. and H.C. Dietz, *Lessons on the pathogenesis of aneurysm from heritable conditions*. Nature, 2011. **473**(7347): p. 308-16.
8. Pinard, A., G.T. Jones, and D.M. Milewicz, *Genetics of Thoracic and Abdominal Aortic Diseases*. Circ Res, 2019. **124**(4): p. 588-606.
9. Sakalihasan, N., et al., *Abdominal aortic aneurysms*. Nat Rev Dis Primers, 2018. **4**(1): p. 34.
10. Li, X., et al., *Prevalence and trends of the abdominal aortic aneurysms epidemic in general population--a meta-analysis*. PLoS One, 2013. **8**(12): p. e81260.
11. Verstraeten, A., I. Luyckx, and B. Loeys, *Aetiology and management of hereditary aortopathy*. Nat Rev Cardiol, 2017. **14**(4): p. 197-208.
12. Rohde, S., et al., *Thoracic aortic aneurysm gene dictionary*. Asian Cardiovasc Thorac Ann, 2021. **29**(7): p. 682-696.
13. Pyeritz, R.E., *Heritable thoracic aortic disorders*. Curr Opin Cardiol, 2014. **29**(1): p. 97-102.
14. Wang, X., et al., *Germline mutations in ABL1 cause an autosomal dominant syndrome characterized by congenital heart defects and skeletal malformations*. Nat Genet, 2017. **49**(4): p. 613-617.
15. Milewicz, D.M., et al., *De novo ACTA2 mutation causes a novel syndrome of multisystemic smooth muscle dysfunction*. Am J Med Genet A, 2010. **152A**(10): p. 2437-43.

16. Albornoz, G., et al., *Familial thoracic aortic aneurysms and dissections--incidence, modes of inheritance, and phenotypic patterns*. *Ann Thorac Surg*, 2006. **82**(4): p. 1400-5.
17. Meester, J.A., et al., *Loss-of-function mutations in the X-linked biglycan gene cause a severe syndromic form of thoracic aortic aneurysms and dissections*. *Genet Med*, 2017. **19**(4): p. 386-395.
18. Malfait, F., et al., *The Ehlers-Danlos syndromes*. *Nat Rev Dis Primers*, 2020. **6**(1): p. 64.
19. Monroe, G.R., et al., *Familial Ehlers-Danlos syndrome with lethal arterial events caused by a mutation in COL5A1*. *Am J Med Genet A*, 2015. **167**(6): p. 1196-203.
20. Chou, E.L. and M.E. Lindsay, *The genetics of aortopathies: Hereditary thoracic aortic aneurysms and dissections*. *Am J Med Genet C Semin Med Genet*, 2020. **184**(1): p. 136-148.
21. Capuano, A., et al., *Diagnostic Exome Sequencing Identifies a Novel Gene, EMILIN1, Associated with Autosomal-Dominant Hereditary Connective Tissue Disease*. *Hum Mutat*, 2016. **37**(1): p. 84-97.
22. Costain, G., P. Kannu, and S. Bowdin, *Genome-wide sequencing expands the phenotypic spectrum of EP300 variants*. *Eur J Med Genet*, 2018. **61**(3): p. 125-129.
23. Luyckx, I., et al., *Aortic aneurysm: An underestimated serious finding in the EP300 mutation phenotypical spectrum*. *Eur J Med Genet*, 2019. **62**(2): p. 96.
24. Bolar, N., L. Van Laer, and B.L. Loeys, *Marfan syndrome: from gene to therapy*. *Curr Opin Pediatr*, 2012. **24**(4): p. 498-504.
25. Coelho, S.G. and A.G. Almeida, *Marfan syndrome revisited: From genetics to the clinic*. *Rev Port Cardiol (Engl Ed)*, 2020. **39**(4): p. 215-226.
26. Kuang, S.Q., et al., *FOXE3 mutations predispose to thoracic aortic aneurysms and dissections*. *J Clin Invest*, 2016. **126**(3): p. 948-61.
27. Guo, D.C., et al., *LOX Mutations Predispose to Thoracic Aortic Aneurysms and Dissections*. *Circ Res*, 2016. **118**(6): p. 928-34.
28. Zhu, G., et al., *Novel LTBP3 mutations associated with thoracic aortic aneurysms and dissections*. *Orphanet J Rare Dis*, 2021. **16**(1): p. 513.
29. Guo, D.C., et al., *MAT2A mutations predispose individuals to thoracic aortic aneurysms*. *Am J Hum Genet*, 2015. **96**(1): p. 170-7.
30. Barbier, M., et al., *MFAP5 loss-of-function mutations underscore the involvement of matrix alteration in the pathogenesis of familial thoracic aortic aneurysms and dissections*. *Am J Hum Genet*, 2014. **95**(6): p. 736-43.
31. Zhu, L., et al., *Mutations in myosin heavy chain 11 cause a syndrome associating thoracic aortic aneurysm/aortic dissection and patent ductus arteriosus*. *Nat Genet*, 2006. **38**(3): p. 343-9.
32. Wang, L., et al., *Mutations in myosin light chain kinase cause familial aortic dissections*. *Am J Hum Genet*, 2010. **87**(5): p. 701-7.

33. Garg, V., et al., *Mutations in NOTCH1 cause aortic valve disease*. Nature, 2005. **437**(7056): p. 270-4.
34. Yeowell, H.N. and B. Steinmann, *PLOD1-Related Kyphoscoliotic Ehlers-Danlos Syndrome*, in *GeneReviews((R))*, M.P. Adam, et al., Editors. 1993: Seattle (WA).
35. Doyle, A.J., et al., *Mutations in the TGF-beta repressor SKI cause Shprintzen-Goldberg syndrome with aortic aneurysm*. Nat Genet, 2012. **44**(11): p. 1249-54.
36. Coucke, P.J., et al., *Mutations in the facilitative glucose transporter GLUT10 alter angiogenesis and cause arterial tortuosity syndrome*. Nat Genet, 2006. **38**(4): p. 452-7.
37. Micha, D., et al., *SMAD2 Mutations Are Associated with Arterial Aneurysms and Dissections*. Hum Mutat, 2015. **36**(12): p. 1145-9.
38. van de Laar, I.M., et al., *Mutations in SMAD3 cause a syndromic form of aortic aneurysms and dissections with early-onset osteoarthritis*. Nat Genet, 2011. **43**(2): p. 121-6.
39. Teekakirikul, P., et al., *Thoracic aortic disease in two patients with juvenile polyposis syndrome and SMAD4 mutations*. Am J Med Genet A, 2013. **161A**(1): p. 185-91.
40. Luyckx, I., et al., *Confirmation of the role of pathogenic SMAD6 variants in bicuspid aortic valve-related aortopathy*. Eur J Hum Genet, 2019. **27**(7): p. 1044-1053.
41. Gould, R.A., et al., *ROBO4 variants predispose individuals to bicuspid aortic valve and thoracic aortic aneurysm*. Nat Genet, 2019. **51**(1): p. 42-50.
42. Bertoli-Avella, A.M., et al., *Mutations in a TGF-beta ligand, TGFB3, cause syndromic aortic aneurysms and dissections*. J Am Coll Cardiol, 2015. **65**(13): p. 1324-1336.
43. Loeys, B.L., et al., *A syndrome of altered cardiovascular, craniofacial, neurocognitive and skeletal development caused by mutations in TGFBR1 or TGFBR2*. Nat Genet, 2005. **37**(3): p. 275-81.
44. Dietz, H., *Marfan Syndrome*, in *GeneReviews((R))*, M.P. Adam, et al., Editors. 1993: Seattle (WA).
45. Dietz, H.C., et al., *Marfan syndrome caused by a recurrent de novo missense mutation in the fibrillin gene*. Nature, 1991. **352**(6333): p. 337-9.
46. Loeys, B.L., et al., *The revised Ghent nosology for the Marfan syndrome*. J Med Genet, 2010. **47**(7): p. 476-85.
47. Saeyeldin, A., et al., *Natural history of aortic root aneurysms in Marfan syndrome*. Ann Cardiothorac Surg, 2017. **6**(6): p. 625-632.
48. Bossone, E. and K.A. Eagle, *Epidemiology and management of aortic disease: aortic aneurysms and acute aortic syndromes*. Nat Rev Cardiol, 2021. **18**(5): p. 331-348.

49. Loeys, B., et al., *Comprehensive molecular screening of the FBN1 gene favors locus homogeneity of classical Marfan syndrome*. Hum Mutat, 2004. **24**(2): p. 140-6.
50. Groth, K.A., et al., *Evaluating the quality of Marfan genotype-phenotype correlations in existing FBN1 databases*. Genet Med, 2017. **19**(7): p. 772-777.
51. Meester, J.A.N., et al., *Molecular characterization and investigation of the role of genetic variation in phenotypic variability and response to treatment in a large pediatric Marfan syndrome cohort*. Genet Med, 2022.
52. Arnaud, P., et al., *Clinical relevance of genotype-phenotype correlations beyond vascular events in a cohort study of 1500 Marfan syndrome patients with FBN1 pathogenic variants*. Genet Med, 2021. **23**(7): p. 1296-1304.
53. Stengl, R., et al., *Potential predictors of severe cardiovascular involvement in Marfan syndrome: the emphasized role of genotype-phenotype correlations in improving risk stratification-a literature review*. Orphanet J Rare Dis, 2021. **16**(1): p. 245.
54. Baudhuin, L.M., K.E. Kotzer, and S.A. Lagerstedt, *Increased frequency of FBN1 truncating and splicing variants in Marfan syndrome patients with aortic events*. Genet Med, 2015. **17**(3): p. 177-87.
55. Takeda, N., et al., *Impact of Pathogenic FBN1 Variant Types on the Progression of Aortic Disease in Patients With Marfan Syndrome*. Circ Genom Precis Med, 2018. **11**(6): p. e002058.
56. Franken, R., et al., *Relationship between fibrillin-1 genotype and severity of cardiovascular involvement in Marfan syndrome*. Heart, 2017. **103**(22): p. 1795-1799.
57. Hernandez, A., et al., *Genotype FBN1/phenotype relationship in a cohort of patients with Marfan syndrome*. Clin Genet, 2021. **99**(2): p. 269-280.
58. Faivre, L., et al., *Effect of mutation type and location on clinical outcome in 1,013 probands with Marfan syndrome or related phenotypes and FBN1 mutations: an international study*. Am J Hum Genet, 2007. **81**(3): p. 454-66.
59. Franken, R., et al., *Increased aortic tortuosity indicates a more severe aortic phenotype in adults with Marfan syndrome*. Int J Cardiol, 2015. **194**: p. 7-12.
60. Heuts, S., et al., *Aortic elongation part II: the risk of acute type A aortic dissection*. Heart, 2018. **104**(21): p. 1778-1782.
61. Kruger, T., et al., *Ascending aortic elongation and the risk of dissection*. Eur J Cardiothorac Surg, 2016. **50**(2): p. 241-7.
62. Mahadevia, R., et al., *Bicuspid aortic cusp fusion morphology alters aortic three-dimensional outflow patterns, wall shear stress, and expression of aortopathy*. Circulation, 2014. **129**(6): p. 673-82.
63. Rodriguez-Palomares, J.F., et al., *Aortic flow patterns and wall shear stress maps by 4D-flow cardiovascular magnetic resonance in the assessment of aortic dilatation in bicuspid aortic valve disease*. J Cardiovasc Magn Reson, 2018. **20**(1): p. 28.

64. Marshall, L.M., et al., *Thoracic aortic aneurysm frequency and dissection are associated with fibrillin-1 fragment concentrations in circulation*. *Circ Res*, 2013. **113**(10): p. 1159-68.
65. Wanga, S., et al., *Aortic microcalcification is associated with elastin fragmentation in Marfan syndrome*. *J Pathol*, 2017. **243**(3): p. 294-306.
66. Benke, K., et al., *The role of transforming growth factor-beta in Marfan syndrome*. *Cardiol J*, 2013. **20**(3): p. 227-34.
67. Hofmann Bowman, M.A., K.A. Eagle, and D.M. Milewicz, *Update on Clinical Trials of Losartan With and Without beta-Blockers to Block Aneurysm Growth in Patients With Marfan Syndrome: A Review*. *JAMA Cardiol*, 2019. **4**(7): p. 702-707.
68. Habashi, J.P., et al., *Losartan, an AT1 antagonist, prevents aortic aneurysm in a mouse model of Marfan syndrome*. *Science*, 2006. **312**(5770): p. 117-21.
69. Quintana, R.A. and W.R. Taylor, *Cellular Mechanisms of Aortic Aneurysm Formation*. *Circ Res*, 2019. **124**(4): p. 607-618.
70. Neptune, E.R., et al., *Dysregulation of TGF-beta activation contributes to pathogenesis in Marfan syndrome*. *Nat Genet*, 2003. **33**(3): p. 407-11.
71. Jones, J.A., F.G. Spinale, and J.S. Ikonomidis, *Transforming growth factor-beta signaling in thoracic aortic aneurysm development: a paradox in pathogenesis*. *J Vasc Res*, 2009. **46**(2): p. 119-37.
72. Pepe, G., et al., *Marfan syndrome: current perspectives*. *Appl Clin Genet*, 2016. **9**: p. 55-65.
73. Loeys, B.L. and H.C. Dietz, *Loeys-Dietz Syndrome*, in *GeneReviews((R))*, M.P. Adam, et al., Editors. 1993: Seattle (WA).
74. Meester, J.A.N., et al., *Differences in manifestations of Marfan syndrome, Ehlers-Danlos syndrome, and Loeys-Dietz syndrome*. *Ann Cardiothorac Surg*, 2017. **6**(6): p. 582-594.
75. Van Laer, L., H. Dietz, and B. Loeys, *Loeys-Dietz syndrome*. *Adv Exp Med Biol*, 2014. **802**: p. 95-105.
76. Nistri, S., et al., *Differential Diagnosis between Marfan Syndrome and Loeys-Dietz Syndrome Type 4: A Novel Chromosomal Deletion Covering TGFB2*. *Genes (Basel)*, 2021. **12**(10).
77. MacFarlane, E.G., et al., *Lineage-specific events underlie aortic root aneurysm pathogenesis in Loeys-Dietz syndrome*. *J Clin Invest*, 2019. **129**(2): p. 659-675.
78. Baumgartner, H., et al., *2017 ESC/EACTS Guidelines for the Management of Valvular Heart Disease*. *Rev Esp Cardiol (Engl Ed)*, 2018. **71**(2): p. 110.
79. MacCarrick, G., et al., *Loeys-Dietz syndrome: a primer for diagnosis and management*. *Genet Med*, 2014. **16**(8): p. 576-87.
80. McBride, O.W., L.W. Fisher, and M.F. Young, *Localization of PGI (biglycan, BGN) and PGII (decorin, DCN, PG-40) genes on human chromosomes Xq13-qter and 12q, respectively*. *Genomics*, 1990. **6**(2): p. 219-25.

81. Halper, J., *Proteoglycans and diseases of soft tissues*. Adv Exp Med Biol, 2014. **802**: p. 49-58.
82. Heegaard, A.M., et al., *Biglycan deficiency causes spontaneous aortic dissection and rupture in mice*. Circulation, 2007. **115**(21): p. 2731-8.
83. Akiyoshi, S., et al., *c-Ski acts as a transcriptional co-repressor in transforming growth factor-beta signaling through interaction with smads*. J Biol Chem, 1999. **274**(49): p. 35269-77.
84. Carmignac, V., et al., *In-frame mutations in exon 1 of SKI cause dominant Shprintzen-Goldberg syndrome*. Am J Hum Genet, 2012. **91**(5): p. 950-7.
85. Greally, M.T., *Shprintzen-Goldberg Syndrome*, in *GeneReviews((R))*, M.P. Adam, et al., Editors. 2020: Seattle (WA).
86. Schepers, D., et al., *The SMAD-binding domain of SKI: a hotspot for de novo mutations causing Shprintzen-Goldberg syndrome*. Eur J Hum Genet, 2015. **23**(2): p. 224-8.
87. Arnaud, P., et al., *A new mutational hotspot in the SKI gene in the context of MFS/TAA molecular diagnosis*. Hum Genet, 2020. **139**(4): p. 461-472.
88. Verstraeten, A., et al., *Marfan Syndrome and Related Disorders: 25 Years of Gene Discovery*. Hum Mutat, 2016. **37**(6): p. 524-31.
89. Greally, M.T., *Shprintzen-Goldberg Syndrome*, in *GeneReviews((R))*, M.P. Adam, et al., Editors. 1993: Seattle (WA).
90. Shprintzen, R.J. and R.B. Goldberg, *A recurrent pattern syndrome of craniosynostosis associated with arachnodactyly and abdominal hernias*. J Craniofac Genet Dev Biol, 1982. **2**(1): p. 65-74.
91. Gillis, E., L. Van Laer, and B.L. Loeys, *Genetics of thoracic aortic aneurysm: at the crossroad of transforming growth factor-beta signaling and vascular smooth muscle cell contractility*. Circ Res, 2013. **113**(3): p. 327-40.
92. Germain, D.P., *Ehlers-Danlos syndrome type IV*. Orphanet J Rare Dis, 2007. **2**: p. 32.
93. Wenstrup, R.J., et al., *Prevalence of aortic root dilation in the Ehlers-Danlos syndrome*. Genet Med, 2002. **4**(3): p. 112-7.
94. Lin, C.J., C.Y. Lin, and N.O. Stitzel, *Genetics of the extracellular matrix in aortic aneurysmal diseases*. Matrix Biol, 2018. **71-72**: p. 128-143.
95. Frank, M., et al., *The type of variants at the COL3A1 gene associates with the phenotype and severity of vascular Ehlers-Danlos syndrome*. Eur J Hum Genet, 2015. **23**(12): p. 1657-64.
96. Guarnieri, V., et al., *Cardiac valvular Ehlers-Danlos syndrome is a well-defined condition due to recessive null variants in COL1A2*. Am J Med Genet A, 2019. **179**(5): p. 846-851.
97. Gaines, R., et al., *Spontaneous ruptured dissection of the right common iliac artery in a patient with classic Ehlers-Danlos syndrome phenotype*. Ann Vasc Surg, 2015. **29**(3): p. 595 e11-4.

98. Adham, S., et al., *Classical Ehlers-Danlos syndrome with a propensity to arterial events: A new report on a French family with a COL1A1 p.(Arg312Cys) variant*. Clin Genet, 2020. **97**(2): p. 357-361.
99. Malfait, F., et al., *Three arginine to cysteine substitutions in the pro-alpha (I)-collagen chain cause Ehlers-Danlos syndrome with a propensity to arterial rupture in early adulthood*. Hum Mutat, 2007. **28**(4): p. 387-95.
100. Germain, D.P. and Y. Herrera-Guzman, *Vascular Ehlers-Danlos syndrome*. Ann Genet, 2004. **47**(1): p. 1-9.
101. Pletcher, B.A., et al., *Four sibs with arterial tortuosity: description and review of the literature*. Am J Med Genet, 1996. **66**(2): p. 121-8.
102. Deguchi, M., et al., *Current Overview of Osteogenesis Imperfecta*. Medicina (Kaunas), 2021. **57**(5).
103. Balasubramanian, M., et al., *Aortic aneurysm/dissection and osteogenesis imperfecta: Four new families and review of the literature*. Bone, 2019. **121**: p. 191-195.
104. Steiner, R.D. and D. Basel, *COL1A1/2 Osteogenesis Imperfecta*, in *GeneReviews((R))*, M.P. Adam, et al., Editors. 1993: Seattle (WA).
105. Sillence, D.O., A. Senn, and D.M. Danks, *Genetic heterogeneity in osteogenesis imperfecta*. J Med Genet, 1979. **16**(2): p. 101-16.
106. Callewaert, B.L., et al., *Arterial tortuosity syndrome: clinical and molecular findings in 12 newly identified families*. Hum Mutat, 2008. **29**(1): p. 150-8.
107. Boel, A., et al., *Arterial Tortuosity Syndrome: An Ascorbate Compartmentalization Disorder?* Antioxid Redox Signal, 2021. **34**(11): p. 875-889.
108. Beyens, A., et al., *Correction: Arterial tortuosity syndrome: 40 new families and literature review*. Genet Med, 2019. **21**(8): p. 1894-1895.
109. Nemeth, C.E., et al., *Glucose transporter type 10-lacking in arterial tortuosity syndrome-facilitates dehydroascorbic acid transport*. FEBS Lett, 2016. **590**(11): p. 1630-40.
110. Albuisson, J., et al., *Clinical utility gene card for: Arterial tortuosity syndrome*. Eur J Hum Genet, 2015. **23**(10).
111. Cirnu, A., et al., *Novel Mutation in LOX Associates With a Complex Aneurysmal Vascular and Cardiac Phenotype*. Circ Genom Precis Med, 2021. **14**(1): p. e003217.
112. Dasouki, M., et al., *Compound heterozygous mutations in fibulin-4 causing neonatal lethal pulmonary artery occlusion, aortic aneurysm, arachnodactyly, and mild cutis laxa*. Am J Med Genet A, 2007. **143A**(22): p. 2635-41.
113. Halabi, C.M., et al., *Fibulin-4 is essential for maintaining arterial wall integrity in conduit but not muscular arteries*. Sci Adv, 2017. **3**(5): p. e1602532.
114. Chen, C.A., et al., *The expanding clinical phenotype of germline ABL1-associated congenital heart defects and skeletal malformations syndrome*. Hum Mutat, 2020. **41**(10): p. 1738-1744.

115. Hamandi, M., et al., *A Newly Discovered Genetic Disorder Associated With Life-Threatening Aortic Disease in a 6-Year-Old Boy*. J Investig Med High Impact Case Rep, 2020. **8**: p. 2324709620909234.
116. Tan, K.L., et al., *Ari-1 Regulates Myonuclear Organization Together with Parkin and Is Associated with Aortic Aneurysms*. Dev Cell, 2018. **45**(2): p. 226-244 e8.
117. Fergelot, P., et al., *Phenotype and genotype in 52 patients with Rubinstein-Taybi syndrome caused by EP300 mutations*. Am J Med Genet A, 2016. **170**(12): p. 3069-3082.
118. Bandaru, S., et al., *Filamin A Regulates Cardiovascular Remodeling*. Int J Mol Sci, 2021. **22**(12).
119. Chen, M.H., et al., *Thoracic aortic aneurysm in patients with loss of function Filamin A mutations: Clinical characterization, genetics, and recommendations*. Am J Med Genet A, 2018. **176**(2): p. 337-350.
120. Clark, A.R., et al., *Skeletal dysplasias due to filamin A mutations result from a gain-of-function mechanism distinct from allelic neurological disorders*. Hum Mol Genet, 2009. **18**(24): p. 4791-800.
121. Cripe, L., et al., *Bicuspid aortic valve is heritable*. J Am Coll Cardiol, 2004. **44**(1): p. 138-43.
122. Prakash, S.K., et al., *A roadmap to investigate the genetic basis of bicuspid aortic valve and its complications: insights from the International BAVCon (Bicuspid Aortic Valve Consortium)*. J Am Coll Cardiol, 2014. **64**(8): p. 832-9.
123. Bravo-Jaimes, K. and S.K. Prakash, *Genetics in bicuspid aortic valve disease: Where are we?* Prog Cardiovasc Dis, 2020. **63**(4): p. 398-406.
124. Longobardo, L., et al., *Bicuspid aortic valve and aortopathy: novel prognostic predictors for the identification of high-risk patients*. Eur Heart J Cardiovasc Imaging, 2021. **22**(7): p. 808-816.
125. Luyckx, I., et al., *Copy number variation analysis in bicuspid aortic valve-related aortopathy identifies TBX20 as a contributing gene*. Eur J Hum Genet, 2019. **27**(7): p. 1033-1043.
126. Park, J.E., et al., *A novel SMAD6 variant in a patient with severely calcified bicuspid aortic valve and thoracic aortic aneurysm*. Mol Genet Genomic Med, 2019. **7**(5): p. e620.
127. Ahluwalia, N. and B.D. Gelb, *A de novo pathogenic BMP2 variant-related phenotype with the novel finding of bicuspid aortic valve*. Am J Med Genet A, 2021. **185**(2): p. 575-578.
128. Lee, A., S. Wei, and A. Schwertani, *A Notch more: Molecular players in bicuspid aortic valve disease*. J Mol Cell Cardiol, 2019. **134**: p. 62-68.
129. Sticchi, E., et al., *Bicuspid Aortic Valve: Role of Multiple Gene Variants in Influencing the Clinical Phenotype*. Biomed Res Int, 2018. **2018**: p. 8386123.
130. Gomez, D., et al., *Syndromic and non-syndromic aneurysms of the human ascending aorta share activation of the Smad2 pathway*. J Pathol, 2009. **218**(1): p. 131-42.

131. Faggion Vinholo, T., et al., *Nonsyndromic Thoracic Aortic Aneurysms and Dissections-Is Screening Possible?* Semin Thorac Cardiovasc Surg, 2019. **31**(4): p. 628-634.
132. Coady, M.A., et al., *Familial patterns of thoracic aortic aneurysms.* Arch Surg, 1999. **134**(4): p. 361-7.
133. Milewicz, D.M. and E. Regalado, *Heritable Thoracic Aortic Disease Overview*, in *GeneReviews((R))*, M.P. Adam, et al., Editors. 1993: Seattle (WA).
134. Ware, S.M., et al., *Twins with progressive thoracic aortic aneurysm, recurrent dissection and ACTA2 mutation.* Pediatrics, 2014. **134**(4): p. e1218-23.
135. Guo, D.C., et al., *Mutations in smooth muscle alpha-actin (ACTA2) lead to thoracic aortic aneurysms and dissections.* Nat Genet, 2007. **39**(12): p. 1488-93.
136. Morisaki, H., et al., *Mutation of ACTA2 gene as an important cause of familial and nonfamilial nonsyndromic thoracic aortic aneurysm and/or dissection (TAAD).* Hum Mutat, 2009. **30**(10): p. 1406-11.
137. Luyckx, I., et al., *Two novel MYLK nonsense mutations causing thoracic aortic aneurysms/dissections in patients without apparent family history.* Clin Genet, 2017. **92**(4): p. 444-446.
138. Kamm, K.E. and J.T. Stull, *Dedicated myosin light chain kinases with diverse cellular functions.* J Biol Chem, 2001. **276**(7): p. 4527-30.
139. Zhang, W., et al., *Exome sequencing reveals a de novo PRKG1 mutation in a sporadic patient with aortic dissection.* BMC Med Genet, 2018. **19**(1): p. 218.
140. Guo, D.C., et al., *Recurrent gain-of-function mutation in PRKG1 causes thoracic aortic aneurysms and acute aortic dissections.* Am J Hum Genet, 2013. **93**(2): p. 398-404.
141. Ashvetiya, T., et al., *Identification of novel genetic susceptibility loci for thoracic and abdominal aortic aneurysms via genome-wide association study using the UK Biobank Cohort.* PLoS One, 2021. **16**(9): p. e0247287.
142. Roychowdhury, T., et al., *Regulatory variants in TCF7L2 are associated with thoracic aortic aneurysm.* Am J Hum Genet, 2021. **108**(9): p. 1578-1589.
143. Kuang, S.Q., et al., *Recurrent chromosome 16p13.1 duplications are a risk factor for aortic dissections.* PLoS Genet, 2011. **7**(6): p. e1002118.
144. Shen, Y.H., et al., *Unfolding the Story of Proteoglycan Accumulation in Thoracic Aortic Aneurysm and Dissection.* Arterioscler Thromb Vasc Biol, 2019. **39**(10): p. 1899-1901.
145. Jana, S., et al., *Extracellular matrix, regional heterogeneity of the aorta, and aortic aneurysm.* Exp Mol Med, 2019. **51**(12): p. 1-15.
146. Guemann, A.S., et al., *ELN gene triplication responsible for familial supraaortic aneurysm.* Cardiol Young, 2015. **25**(4): p. 712-7.
147. Frismantiene, A., et al., *Smooth muscle cell-driven vascular diseases and molecular mechanisms of VSMC plasticity.* Cell Signal, 2018. **52**: p. 48-64.

148. Wang, L., et al., *Association of smooth muscle cell phenotypes with extracellular matrix disorders in thoracic aortic dissection*. *J Vasc Surg*, 2012. **56**(6): p. 1698-709, 1709 e1.
149. Michel, J.B., G. Jondeau, and D.M. Milewicz, *From genetics to response to injury: vascular smooth muscle cells in aneurysms and dissections of the ascending aorta*. *Cardiovasc Res*, 2018. **114**(4): p. 578-589.
150. Milewicz, D.M., et al., *Altered Smooth Muscle Cell Force Generation as a Driver of Thoracic Aortic Aneurysms and Dissections*. *Arterioscler Thromb Vasc Biol*, 2017. **37**(1): p. 26-34.
151. Brozovich, F.V., et al., *Mechanisms of Vascular Smooth Muscle Contraction and the Basis for Pharmacologic Treatment of Smooth Muscle Disorders*. *Pharmacol Rev*, 2016. **68**(2): p. 476-532.
152. Thompson, R.W., *Reflections on the pathogenesis of abdominal aortic aneurysms*. *Cardiovasc Surg*, 2002. **10**(4): p. 389-94.
153. Majesky, M.W., *Developmental basis of vascular smooth muscle diversity*. *Arterioscler Thromb Vasc Biol*, 2007. **27**(6): p. 1248-58.
154. MacFarlane, E.G., et al., *TGF-beta Family Signaling in Connective Tissue and Skeletal Diseases*. *Cold Spring Harb Perspect Biol*, 2017. **9**(11).
155. Cannaerts, E., et al., *TGF-beta signalopathies as a paradigm for translational medicine*. *Eur J Med Genet*, 2015. **58**(12): p. 695-703.
156. Massague, J., *TGFbeta signalling in context*. *Nat Rev Mol Cell Biol*, 2012. **13**(10): p. 616-30.
157. Schmierer, B. and C.S. Hill, *TGFbeta-SMAD signal transduction: molecular specificity and functional flexibility*. *Nat Rev Mol Cell Biol*, 2007. **8**(12): p. 970-82.
158. Zhang, Y.E., *Non-Smad Signaling Pathways of the TGF-beta Family*. *Cold Spring Harb Perspect Biol*, 2017. **9**(2).
159. Rigelsky, C.M. and R.T. Moran, *Genetics of syndromic and nonsyndromic aortopathies*. *Curr Opin Pediatr*, 2019. **31**(6): p. 694-701.
160. de la Fuente-Alonso, A., et al., *Aortic disease in Marfan syndrome is caused by overactivation of sGC-PRKG signaling by NO*. *Nat Commun*, 2021. **12**(1): p. 2628.
161. Toral, M., et al., *The NO signalling pathway in aortic aneurysm and dissection*. *Br J Pharmacol*, 2022. **179**(7): p. 1287-1303.
162. Farah, C., L.Y.M. Michel, and J.L. Balligand, *Nitric oxide signalling in cardiovascular health and disease*. *Nat Rev Cardiol*, 2018. **15**(5): p. 292-316.
163. Larsson, N.G., et al., *Mitochondrial transcription factor A is necessary for mtDNA maintenance and embryogenesis in mice*. *Nat Genet*, 1998. **18**(3): p. 231-6.
164. Oller, J., et al., *Extracellular Tuning of Mitochondrial Respiration Leads to Aortic Aneurysm*. *Circulation*, 2021. **143**(21): p. 2091-2109.

165. Guo, G., et al., *Induction of macrophage chemotaxis by aortic extracts of the mgR Marfan mouse model and a GxxPG-containing fibrillin-1 fragment.* Circulation, 2006. **114**(17): p. 1855-62.
166. He, R., et al., *Characterization of the inflammatory and apoptotic cells in the aortas of patients with ascending thoracic aortic aneurysms and dissections.* J Thorac Cardiovasc Surg, 2006. **131**(3): p. 671-8.
167. Malecki, C., et al., *The Role of Inflammation and Myeloperoxidase-Related Oxidative Stress in the Pathogenesis of Genetically Triggered Thoracic Aortic Aneurysms.* Int J Mol Sci, 2020. **21**(20).
168. Pope, N.H., et al., *Interleukin-6 Receptor Inhibition Prevents Descending Thoracic Aortic Aneurysm Formation.* Ann Thorac Surg, 2015. **100**(5): p. 1620-6.
169. Skotsimara, G., et al., *Aortic Wall Inflammation in the Pathogenesis, Diagnosis and Treatment of Aortic Aneurysms.* Inflammation, 2022.



## **CHAPTER 2: AIMS OF THE THESIS**

---

Thoracic aortic aneurysm and dissection (TAAD) is a progressive and life-threatening disease with a **high mortality rate** of 80%. Currently, only 30% of TAAD patients received a genetic diagnosis, leaving the majority uncharted and without diagnosis. Even so, TAAD patients have **limited therapeutic options** to alter the course of TAAD. With this thesis we aim to further elucidate the **complex genetic architecture of TAAD** and to pave the way for TAA drug research and development by providing other entry points. Early detection and prevention with precise medicine potential will improve the outcomes for TAAD patients.

**Research objectives within this thesis are:**

**Unraveling the diverse phenotypic/genotypic spectrum of *LOX* patients**

Delineation and expansion of the heterozygous phenotypic profile of patients carrying pathogenic *LOX* variants contributing to TAAD.

**Cracking the genetic code: *IPO8*'s role in TAAD development**

Decrypting the mysteries of TAAD etiology by studying the clinical impact of the novel discovered TAAD gene, *IPO8*, and in depth phenotypical and molecular characterization of the C57BL/6N *Ipo8* knock-out mouse model.

**Investigating the homozygous *Ipo8*<sup>-/-</sup> embryonic lethality**

Unraveling the specific timing and cause of prenatal death, with special focus on the cardiovascular system, using timed matings with heterozygous C57BL/6N *Ipo8*<sup>+/-</sup> breeding pairs.

**Generating an *IPO8* induced pluripotent stem cell line (iPSCs)**

Harness the power of induced pluripotent stem cells (iPSCs) by creating a living genetic canvas from a patient carrying an *IPO8* recessive loss-of-function pathogenic variant to refine our understanding of TAA at the cellular level.

## CHAPTER 3

---

### **Novel *LOX* variants in five families with aortic/arterial aneurysm and dissection with variable connective tissue findings**

Ilse Van Gucht <sup>1</sup>, Alice Krebsova <sup>2</sup>, Birgitte Rode Diness <sup>3</sup>, Steven Laga <sup>4</sup>, Dave Adlam <sup>5</sup>, Marlies Kempers <sup>6</sup>, Nilesh J Samani <sup>5</sup>, Tom R Webb <sup>5</sup>, Ania A Baranowska <sup>5</sup>, Lotte Van Den Heuvel <sup>1</sup>, Melanie Perik <sup>1</sup>, Ilse Luyckx <sup>1</sup>, Nils Peeters <sup>1</sup>, Pavel Votypka <sup>7</sup>, Milan Macek <sup>7</sup>, Josephina Meester <sup>1</sup>, Lut Van Laer <sup>1</sup>, Aline Verstraeten <sup>1</sup> and Bart L. Loeys <sup>1,6,\*</sup>

<sup>1</sup>Cardiogenomics Research Group, University of Medical Genetics, University of Antwerp and Antwerp University Hospital, Antwerp, Belgium

<sup>2</sup>Department of Cardiology, IKEM, 14021 Praha 4 Prague, Czechia

<sup>3</sup>Department of Clinical Genetics, Copenhagen University Hospital, 2100 Copenhagen, Denmark

<sup>4</sup>Department of Cardiac Surgery, University of Antwerp and Antwerp University Hospital, 2650 Antwerp, Belgium

<sup>5</sup>Acute and interventional Cardiology, University of Leicester, Leicester LE3 9QP, UK

<sup>6</sup>Department of Human Genetics, Radboud University Medical Center, 6525 Nijmegen, The Netherlands

<sup>7</sup>Department of Biology and Medical Genetics, 2nd Faculty of Medicine, Charles University and Motol, University Hospital, 15006 Praha 5 Prague, Czechia

Published in International Journal of Molecular Sciences (MDPI), Int J. Mol. Sci. 2021, 22, x DOI 10.3390

## Abstract

---

Thoracic aortic aneurysm and dissection (TAAD) is a major cause of cardiovascular morbidity and mortality. Loss-of-function variants in *LOX*, encoding the extracellular matrix crosslinking enzyme lysyl oxidase, have been reported to cause familial TAAD. Using a next-generation TAAD gene panel, we identified five additional probands carrying *LOX* variants, including two missense variants affecting highly conserved amino acids in the *LOX* catalytic domain and three truncating variants. Connective tissue manifestations are apparent in a substantial fraction of the variant carriers. Some *LOX* variant carriers presented with TAAD early in life, while others had normal aortic diameters at an advanced age. Finally, we identified the first patient with spontaneous coronary artery dissection carrying a *LOX* variant. In conclusion, our data demonstrate that loss-of-function *LOX* variants cause a spectrum of aortic and arterial aneurysmal disease, often combined with connective tissue findings.

## 1 Introduction

---

Thoracic aortic aneurysm and dissection (TAAD) is characterized by a progressive dilatation of the aorta caused by wall weakness that leads to dissection or rupture. Unfortunately, aneurysms often remain unnoticed until dissection or rupture of the aortic wall occurs. TAAD affects thousands of people every year with a high mortality rate of almost 80%, making it a leading cause of death worldwide. More than 30 genes are known to be associated with TAAD, explaining less than 30% of all familial cases and thus leaving 70% of all families genetically unexplained [1, 2]. With respect to non-syndromic TAAD, mutations are typically located in genes that encode for proteins involved in vascular smooth muscle cell contractility, such as *MYH11* and *ACTA2* [3]. For syndromic TAAD forms, mutations are found in genes that encode for key players in the transforming growth factor- $\beta$  (TGF- $\beta$ ) signaling pathway and extracellular matrix components [4].

Marfan syndrome (MFS [MIM: 154700]) and Loeys-Dietz syndrome (LDS [MIM: 609192, MIM: 610168, MIM: 613795, MIM: 614816 and MIM: 615582]) are the most exhaustively studied TAAD syndromes. MFS is caused by mutations in the *FBN1* (fibrillin-1) [MIM: 134797] gene and is clinically characterized by a pleiotropy of skeletal (e.g., overgrowth), cardiovascular (e.g., TAAD and mitral valve prolapse), ocular (e.g., ectopia lentis) and skin abnormalities (e.g., striae) [5]. LDS is caused by mutations in *TGFBR1* [MIM: 190181], *TGFBR2* [MIM: 190182], *SMAD2* [MIM: 601366], *SMAD3* [MIM: 603109], *TGFB2* [MIM: 190220] or *TGFB3* [MIM: 190230] and presents with widespread arterial tortuosity and aneurysms, bifid uvula or cleft palate and hypertelorism [1,2]. The discovery of the involvement of the dysregulation of the TGF- $\beta$  signaling pathway and the genetic variants that predispose to heritable aortic disease have led to novel insights [6, 7]. Genes encoding for proteins that are involved in the assembly of the ECM also predispose to TAAD when mutated. The aortic wall must be able to withstand

a lot of pressure and shear stress and therefore consists of various structured layers that guarantee the strength and elasticity of the wall [8].

Lysyl oxidase, encoded by the *LOX* gene, is a cuproenzyme that catalyzes crosslinking of extracellular matrix proteins such as collagen and elastin [9]. The proper assembly of the latter key structural components of connective tissue matrices is crucial for the stability, elasticity and mechanical integrity of the aortic/arterial wall [10]. In 2016, two publications [11, 12] reported on the presence of heterozygous loss-of-function variants in the *LOX* gene in familial TAAAD patients. In 2019, Renner et al. described two additional patients with *LOX* variants [13]. At the beginning of 2021, Cirnu et al. identified a missense *LOX* variant in a patient displaying arterial aneurysms throughout the body [14]. Using a next-generation sequencing approach, we aimed to validate the reported contribution of pathogenic *LOX* variants to the genetic etiology of TAAAD and to further refine the associated phenotypic spectrum.

## 2 Material and methods

---

### 1. Sequencing

The cohort consists of genetically undiagnosed patients ( $n = 16$ ) with aortic or arterial aneurysm and dissection belonging to 5 families, both in the presence and absence of connective tissue findings.

Next-generation TAAAD gene panel (Table S4) sequencing was performed on DNA of probands according to previously described methods [15]. In brief, enrichment of the regions of interest was performed with a custom Haloplex enrichment kit according to the manufacturer's protocol (Agilent Technologies). The concentration of each library was measured by Qubit fluorometric quantification (Life Technologies). For generation of clusters and subsequent sequencing of the targeted DNA samples on a flow cell, a sequencing reagent kit from Illumina was used. High-throughput next generation sequencing data were generated on an Illumina platform. Analysis of the raw data was

performed using Seqpilot (JSI) or a Galaxy pipeline, followed by variant calling with the Genome Analysis Toolkit (GATK) and variant annotation using an in-house developed tool, VariantDB [16]. Identified variants were genotyped in both affected and unaffected available family members using Sanger sequencing.

## 2. Histology

Histological examination was performed on aortic wall tissue from two of our patients (Family 1 (p.(Leu18Profs\*111)), 1-III:4 and 1-III:6) and one control that was collected during surgery. The collected tissue was embedded in paraffin and sections of 5µm thick were created. Verhoeff Van Gieson (Sigma-Aldrich) staining was performed to assess elastic fiber integrity, while Trichrome Masson's (Sigma-Aldrich) staining was used to evaluate the collagen content. pSMAD2 and pERK1/2, important components of the TGF- $\beta$  signaling pathway, were visualized using immunohistochemistry. Sections were deparaffinized in toluene for 5 min and rehydrated in alcohol grades of 100%, 90%, 70% and 50%. Sections were submerged in 3% hydrogen peroxide to inhibit endogenous peroxidase, followed by 10 min in trypsin at 37 °C (Sigma-Aldrich, 93615-25G) for antigen retrieval and boiled in citrate buffer in a microwave for 3 s at 650 W and 10 min at 90 W. Sections were cooled down at room temperature for 30 min, rinsed with MiliQ and TBST and blocked for 20 min at room temperature with goat serum (Vector-lab consult). A primary antibody concentration of 1:5000 and 1:3000 for pSMAD2 (3101, Cell Signaling) and pERK1/2 (4370, Cell Signaling), respectively, was used to incubate the sections in a humid chamber at room temperature overnight. The day after, sections were rinsed in TBST followed by incubation with the secondary antibody (1:200, 30014 Vector, Sec goat anti-rabbit IgG) for 30 min at RT and with the avidin-biotinylated complex for 1h at RT (Vectastain ABC kit, Vector Laboratories). 3,3'-Diaminobenzidine tetrahydrochloride hydrate (DAB) chromogen (Sigma-Aldrich) was used as the substrate and Hematoxylin as counterstaining. An automated Nikon Ti-E inverted microscope equipped with a Nikon DS-U3 digital camera (Nikon Instruments)

was used to acquire staining images. Nikon NIS Elements AR software v4.51.01 was used for image acquisition at 10× magnification.

### 3 Results

We report on the identification of heterozygous *LOX* variants in five novel families, i.e., two frameshift, one nonsense and two missense variants (Figure 1A, B).

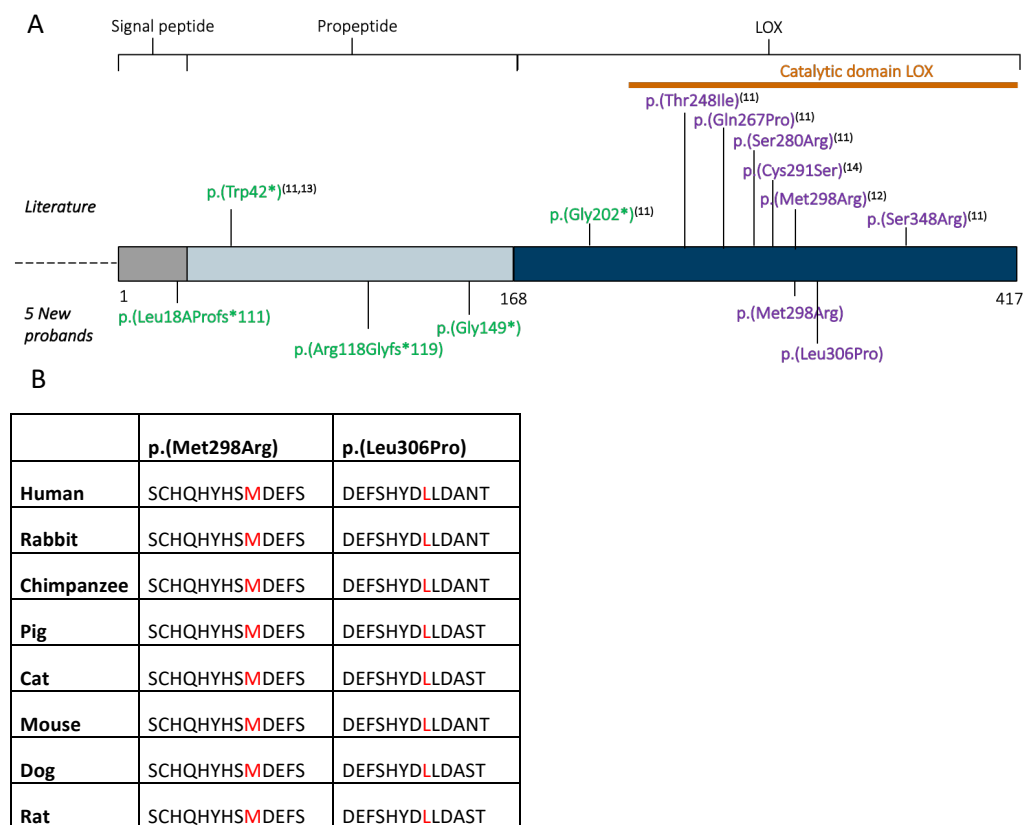


**Figure 1. Heterozygous *LOX* variants in five novel families** (A) Overview *LOX* protein and location of variants found in five new probands and literature. Variants leading to premature stop codons and missense variants are highlighted in, respectively, green and purple [11-14]. (B) Conservation of affected *LOX* amino acids.

The proband of family 1 (1-III:4; Figure 2) is a 43-year-old male who presented with a type A aortic dissection (aorta ascendens diameter: 53 mm) for which he underwent aortic root and ascendens replacement. An echocardiography one year prior showed

an aortic ascendens diameter of 46 mm. His clinical exam did not show specific connective tissue findings. The anatomopathological report of the resected aortic tissue showed aspecific cystic medial degeneration. The proband was known with arterial hypertension and was in follow-up because of a significant family history for aneurysmal disease. Two sisters (1-III:1 and 1-III:2) are both being followed because of ascending aortic dilatation (44 mm). His brother (1-III:6) had an aortic dissection at age 45 years. The ascending aorta diameter at the time of his Bentall surgery was 84 mm. The father (1-II:2) also underwent a Bentall surgery at age 60 and died at age 73 due to an acute myocardial infarction. A paternal uncle (1-II:3) of the proband died suddenly at age 50 years. No autopsy was performed. The son (1-III:10) of this paternal uncle is married to the sister of the proband (1-III:9). His MR angio screening at age 43 years showed an aortic sinus diameter of 43 mm (Z-score = 2.8; height 172 cm; weight 97 kg) with a sinotubular junction of 38 mm and an ascending aorta of 37 mm. Genetic testing of the proband revealed a 14bp deletion in *LOX* (c.53\_66delTAGTGACTGCGCC) leading to a frameshift event and, as a result, the introduction of a premature stop codon (p.(Leu18Profs\*111)). Segregation analysis demonstrated the presence of the *LOX* variant in the brother (1-III:6), brother-in-law (1-III:10) (who is also his nephew) and absence of the *LOX* variant in an unaffected brother (1-III:8). The sister (1-III:2; 56 years) with ascending aorta diameter of 44 mm and chronic hypertension did have a variant of unknown significance (VUS) in *FBN1* (c.5810 G > A; p.(Gly1937Glu)), but not the *LOX* mutation. The VUS in *FBN1* was also present in patient 1-III:6. DNA of two other sisters (1-III:1 and 1-III:3) (of which one (1-III:1) also has a dilated aorta) is not available. One of the two sons (1-IV:1; 25 years) of the proband also tested positive for the familial *LOX* variant. CT-scan of the entire aorta of this son (1-IV:1) revealed normal aortic diameters. The daughter (1-IV:7) of patient 1-III:10 was also found to carry the *LOX* variant but at age 16 years she still had normal aortic diameters.

The male proband of family 2 (2-III:1; Figure 2) is currently 40 years old but has a history of a type A dissection at age 19 for which he underwent composite graft surgery. He has a past medical history of spontaneous splenic rupture, spontaneous pneumothorax and early-onset varicose veins. Genetic testing showed a single nucleotide *LOX* deletion (c.351delC) leading to a frameshift event and the introduction of a premature stop codon (p.(Arg118Glyfs\*119)). Familial segregation analysis showed that the *LOX* variant was also present in the father (2-II:1) and in DNA extracted from a colon polyp of the paternal grandfather. The paternal grandfather (2-I:1) lived to age 73, had a diagnosis of varicose veins, cataract, ischemic heart disease (percutaneous transluminal coronary angioplasty at age 66 years), colon polyps and rheumatoid arthritis. As an infant he was operated for an incarcerated inguinal hernia. The surgery was complicated by a subsequent infection, leaving him with a limb. At age of 30 years, he had bilateral hip replacement attributed to this. At age 50 he suffered from a contralateral inguinal hernia. The father (2-II:1) has a history of arterial hypertension. His echocardiography (at age 51 years) showed a normal aortic size and dimension of all four chambers, discrete mitral and aortic valve insufficiency and no hypertrophy. At age 45 he had an inguinal hernia, mesh repaired with good results. No other connective tissue complaints. All three affected have suffered from severe eczema.

The index patient of family 3 (3-II:5; Figure 2) is a 53-years-old male presenting with a type A dissection at age 51. He underwent an aortic valve sparing procedure according to David. He had a normal tricuspid aortic valve, but mild mitral valve regurgitation. He was negative for cardiovascular risk factors. His physical exam is only significant for tall stature (191 cm), a narrow palate and flat feet (Table S1). His medical history includes an inguinal hernia surgery at age 40 and meniscal surgeries due to sport-related injuries. His father (3-I:1) died of lung cancer at age 73; his mother (3-I:2) lived up to age 81. He has four siblings (three brothers and one sister). Genetic testing of the index patient revealed a nonsense variant in *LOX* (c.445 G > T; p.(Gly149\*)). Subsequently,

two brothers (3-II:1 and 3-II:4) and a niece (3-III:1) underwent genetic testing, and all three were tested positive for the familial *LOX* variant. Cardiac CT-scan of the 56-years-old brother (3-II:4) demonstrated a borderline aortic sinus measurement of 41 mm (Z-score = 2.3; height: 199 cm; weight: 104 kg), but normal ascending aorta. From his medical history we retain an inguinal hernia surgery at age 3, a history of hypertension (treated with metoprolol), hypothyroidy (age 40 years), rupture of the supraspinatus ligament (age 41 years) and tibialis posterior neuralgia (age 42 years). The other brother (3-II:1; 59 years) also has a history of bilateral inguinal hernia, tall stature and joint hypermobility. His echocardiographic evaluation at age 59 years showed no evidence of aortic dilatation. His daughter (3-III:1; 28 years) underwent “urgent” pre-symptomatic genetic testing because of pregnancy and tested positive. She is known with joint hypermobility, arachnodactyly, flat feet, shoulder dislocations and multiple ankle distortions. Her echocardiography revealed normal aortic dimensions (sinus of Valsalva 28.6 mm; Z-score = 0.28). She is known with hypothyroidy (age 19 years), gastric sleeve surgery (25 years), cesarian section (27 years) with premature delivery (26 weeks) of male newborn who died at one week of age.

This female proband (age 50) of family 4 (4-II:1; Figure 2) has a history of posterolateral myocardial infarction due to spontaneous coronary artery dissection at age 44 and a left internal carotid artery dissection at age 46. She has a history of fibromuscular dysplasia of the renal arteries, increased skin elasticity, generalized Beighton score of 4/9, enlarged arm span (167.5 cm: ratio 1.08) and recurrent episodes of ankle dislocation (Table S1). Wound healing was normal. Echocardiography revealed a diameter of 35 mm at the level of the sinuses of Valsalva (Z-score = 0.8 for height 154.6 cm and weight 93.9 kg), 26 mm at the sinotubular junction and 30 mm for the ascending aorta. Genetic testing revealed a *LOX* missense variant (c.893T > G; p.(Met298Arg)) which was previously reported as pathogenic in an unrelated family [4]. Her family history reveals her mother (4-I:2) died at age 58 due to an intracranial bleed of a berry

aneurysm but her DNA sample is not available for testing. The father (4-I:1) and brother (4-II:2) died at, respectively, 58 and 40 years old due to acute myocardial infarction; both were known with significant cardiovascular risk factors. Another brother (4-II:3; age 54) is known with chronic obstructive pulmonary disease (COPD) and no DNA is available from him.

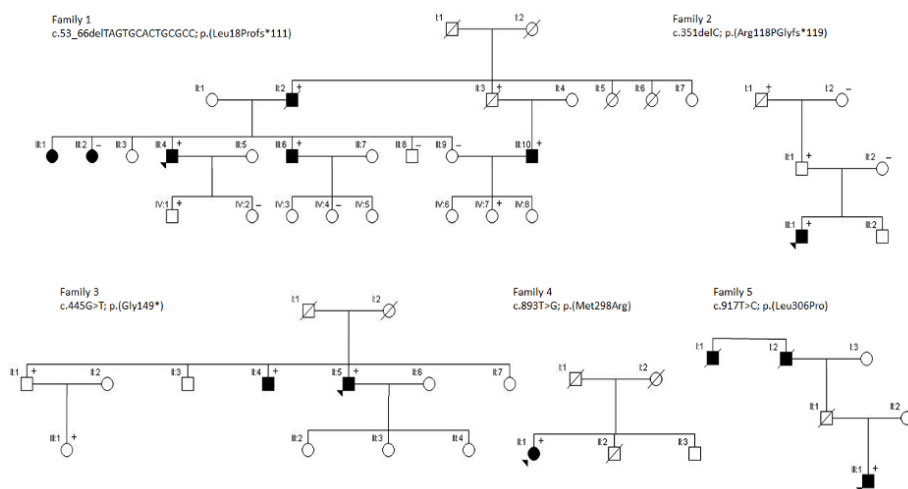


**Figure 2. Pedigrees of LOX families.** The probands are indicated with an arrow. Black symbols indicate family members that are affected with aortic/arterial aneurysm/dissection. Deceased individuals are indicated with a diagonal line. Plus and minus signs are used to indicate the presence and absence of the respective LOX variant.

The male index patient of family 5 (5-III:1; Figure 2) (21 years) was initially diagnosed with aortic dilatation (both at the level of the sinuses and even more pronounced at the ascending aorta) at the age of 6. At the age of 14, he underwent elective replacement of the ascending aorta because of fast progression (10 mm per 2 years) of its diameter to a maximum of 50 mm at the sinotubular junction and above. Microscopic findings showed an abnormal texture of the elastic component of the vascular adventitia, with suspicion of a connective tissue disorder. His height is at the 95th percentile (Table S1). There is no characteristic facial dysmorphism or joint hypermobility and his skin has normal elasticity. His father (5-II:1) committed suicide. Nonetheless, aortic dissection has been reported in the father's family, where the

paternal grandfather (5-I:2) and his brother (5-I:1) died of acute aortic dissection before the age of 50 years. The mother (5-II:2) was shown to have a normal echocardiography. Mutation analysis revealed the presence of a *LOX* missense variant (c.917T > C; p.(Leu306Pro)), which was absent from the unaffected mother.

According to the ACMG criteria, four out of five *LOX* variants are predicted to be pathogenic (Table S2), whereas variant p.(Leu306Pro) remains a variant of uncertain significance. All variants are absent from gnomAD database. Three variants create premature stop codons (c.53\_66delTAGTGCACTGCGCC; p.(Leu18Profs\*111); c.351delC; p.(Arg118Glyfs\*119) and c.445 G > T; p.(Gly149\*)), which are predicted to result in nonsense-mediated mRNA decay. The *LOX* missense variants p.(Met298Arg) and p.(Leu306Pro) are located in the catalytic domain of *LOX* (Figure 1A), located at highly conserved amino acid positions (Figure 1B) and are predicted to be disease-causing by different prediction programs (Table S2). The first one (p.(Met298Arg)) has been previously reported in a TAA family and has been proven to affect collagen-elastic crosslinking and, hence, aortic wall integrity in the respective mouse model [4]. Histological staining of aortic wall sections of *LOX* patients (1-III:4 and 1-III:6) with Verhoeff-Van Gieson staining (VVG) revealed increased elastic fiber fragmentation and disorganization in comparison to a healthy control (Figure 3). Masson's Trichrome staining to assess the collagen content in the same aortic tissue samples showed variable collagen content in the patients. To investigate the involvement of the TGF- $\beta$  signaling pathway in *LOX* deficiency and TAA development, immunohistochemistry was used to determine the levels of nuclear pSMAD2 and pERK1/2 in the aortic segments of the *LOX* patients. Compared to a control, a larger fraction of pSMAD2 and pERK1/2 positively stained nuclei can be observed in aortic tissue of both *LOX* patients (Figure 4).

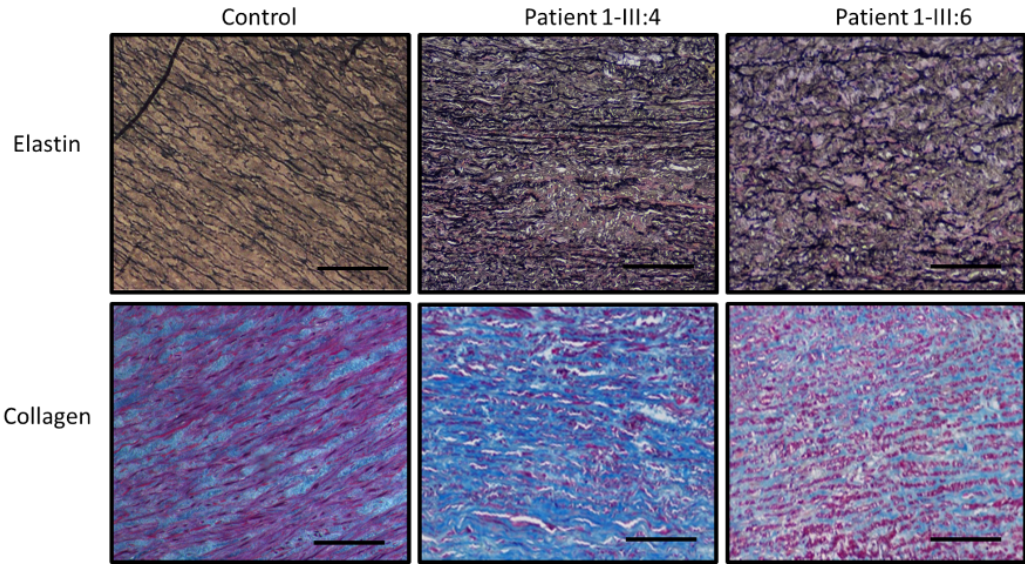


**Figure 3. Collagen and elastin histology staining.** Representative pictures of collagen and elastin stainings performed in a control and two LOX patients, respectively, patient 1-III:4 and 1-III:6. The scale bar represents 100  $\mu\text{m}$ .

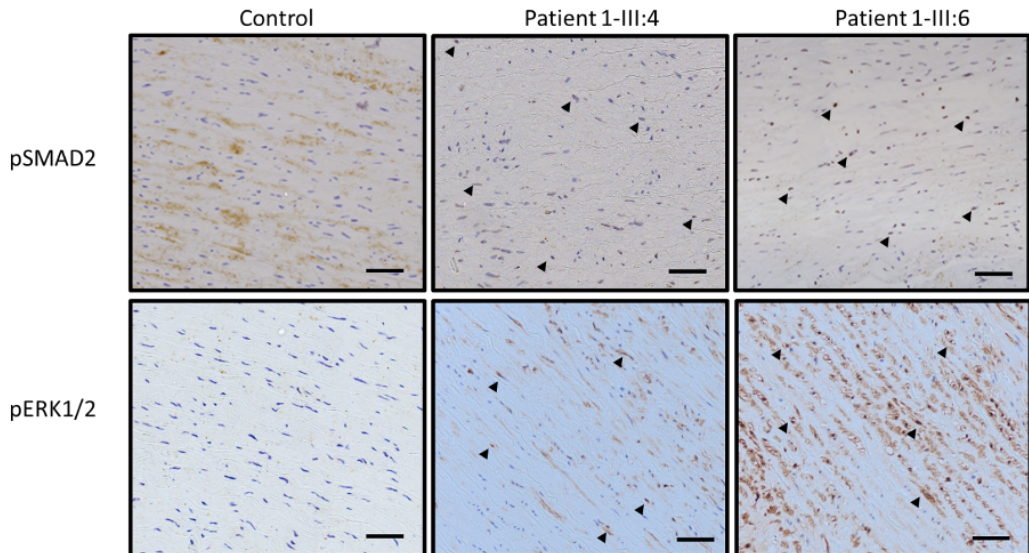


**Figure 4. pSMAD2 and pERK1/2 immunohistochemistry.** Pictures of immunohistochemistry stainings of pSMAD2 and pERK1/2 in a control and two LOX patients, respectively, 1-III:4 and 1-III:6. Black arrows indicate examples of positive stained nuclei. The scale bar represents 50  $\mu\text{m}$ .

## 4 Discussion

In 2016, (likely) pathogenic variants in *LOX* were described as a genetic cause for arterial aneurysm and dissection [11, 12]. From the nine initially described variants, three were premature stop codons (one recurrent p.(Trp42\*)) and all six missense variants were located in the *LOX* catalytic domain (Figure 1A) [11-14]. We here describe five additional variants, including three nucleotide deletions or substitutions resulting in a premature stop codon and two missense variants affecting highly conserved amino acids (Figure 1B) in the *LOX* catalytic domain. Overall, the variant pattern confirms loss-of-function as the underlying cause.

Comparison of the yet existing literature on TAAO-causing *LOX* variants with our own series of patients reveals a number of interesting observations. A summary of the clinical findings of our cohort of *LOX* patients and *LOX* patients in literature can be found in Table 1. A more detailed overview of the clinical features from literature can be found in Supplementary Table S3.

**Table 1. Summary of clinical findings of our cohort of patients with *LOX* variants compared to literature.**

Characteristics	Literature [11-14]	Our Cohort
Total number of patients	<i>n</i> = 29	<i>n</i> = 16
Male/female	20/8 (1 unknown)	13/3
Age range at diagnosis	11–73 years (median 46 years)	6–55 years (median 45 years)
Thoracic aortic dissections	<i>n</i> = 3 ascending, <i>n</i> = 1 arch	<i>n</i> = 4 ascending
Elective surgeries	<i>n</i> = 13 (age 11–70 years)	<i>n</i> = 1 (age 14 years)
BAV	<i>n</i> = 3	<i>n</i> = 0
Disease beyond ascending aorta	Aneurysm in brachiocephalicus, arteria hepatica, abdominal aorta Arterial tortuosity Coronary artery aneurysm	Coronary artery dissection
Connective tissue findings	<i>n</i> = 10	<i>n</i> = 9

First, with regard to the demographic characteristics of the patient population from literature, there is a wide range in presenting ages from 11 to 73 years (median 46

years) for cardiovascular findings. In our patient cohort, the earliest aortic aneurysm observation occurred at age 6 and the first thoracic aortic dissection occurred at age 19. In other families, we also observed non-penetrance at age 51 years (2-II:1) and 59 years (3-II:1) in family 2 and 3, respectively. As suggested in the prior *LOX* reports [11, 12, 14], there is a predilection for male gender. Overall, 77% (33/44) of the *LOX* patient population is male. The observation of male predilection with more severely dilation and more frequent dissection in males has been observed in other TAA conditions as well, both in mice and humans [17].

Second, the *LOX* variants seem to mainly cause aneurysms and dissections at the level of the thoracic aorta. Overall, eight aortic dissections that have been described, all affecting the ascending thoracic aorta, except for one that starts in the aortic arch. Thoracic aortic dissection seems to occur after significant aortic enlargement, with the largest aneurysm reaching an impressive 125 mm in the ascending aorta. So far, no type B or abdominal dissections have been described. However, a patient with abdominal aortic aneurysm has been reported [14]. Arterial disease beyond the ascending aorta seems less frequent, with an extension of thoracic aortic aneurysm into the brachiocephalic artery, one hepatic arterial aneurysm and only one patient displaying aneurysm throughout the body in literature [12, 14]. We were the first to report spontaneous coronary artery dissection as part of the *LOX* phenotype [18]. We observed no difference between premature stop codon *LOX* variants ( $n = 23$ ) and missense *LOX* variants ( $n = 22$ ) with regards to median age of diagnosis (47.5 years versus 44 years) or severity of the cardiovascular involvement.

Third, extra-aortic cardiovascular features include bicuspid aortic valve disease (3/18 in initial series [11]), as well as mitral and aortic valve insufficiency ( $n = 3$ ). Arterial tortuosity has been mentioned once but was still within the normal age-related variation. In our own patient cohort, we did not observe bicuspid aortic valve disease, whereas mitral and aortic valve insufficiency were observed once.

Fourth, several patients in the literature ( $n = 10$ ) and in our series ( $n = 9$ ) have been reported to present with other connective tissue findings. These include tall stature (7/19), pectus deformities (4/19), scoliosis (2/19), joint hypermobility with dislocation (8/19), inguinal hernia (5/19), skin striae (6/19) and dural ectasia (3/19) [11-14]. As such, there is significant clinical overlap with other syndromic aortic aneurysmal conditions such as Marfan syndrome and Loeys-Dietz syndrome [19, 20]. Remarkably, one of our patients (proband of family 2) also presented with splenic rupture, a finding also described in vascular Ehlers-Danlos syndrome and Loeys-Dietz syndrome [21]. We also for the first time describe the occurrence of spontaneous pneumothorax, a clinical complication well known to present in several connective tissue disorders [22]. Varicose veins have also been reported in at least two families (Lee et al., 2016 and family 2 in our cohort). No connective tissue findings seem specific for *LOX* mutation carriers, and it also remains unclear at present why some *LOX* mutation carriers do not seem to present with connective tissue findings at all.

Fifth, histopathological findings of the aorta seem rather aspecific, with elastic fiber fragmentation and cystic medial degeneration. These anatomopathological observations are a common theme in aortic aneurysmal walls of patients with diverse connective tissue disorders, but do not allow prediction of the underlying gene defect. Immunohistological stainings of TGF- $\beta$  pathway key effectors, pSMAD2 and pERK1/2, revealed an increase of positively stained nuclei, an indication for increased TGF- $\beta$  signaling, in aortic tissue sections from *LOX* patients. Our observations confirm prior hypothesis that enhanced TGF- $\beta$  signaling can contribute to TAA development caused by *LOX* deficiency [23-25].

## 5 Conclusion

---

Taken together, our data suggest that loss-of-function *LOX* variants cause a wide spectrum of aortic and arterial aneurysmal disease, combined with connective tissue

findings such as inguinal hernia, pneumothorax, varices, joint dislocations and splenic rupture. The time of onset of aortic aneurysm seems variable but can be as early as 6 years of age. We also report the occurrence of coronary artery dissection as part of the LOX phenotype.

## 6 References

---

1. Verstraeten, A., I. Luyckx, and B. Loeys, *Aetiology and management of hereditary aortopathy*. Nat Rev Cardiol, 2017. **14**(4): p. 197-208.
2. Lindsay, M.E. and H.C. Dietz, *Lessons on the pathogenesis of aneurysm from heritable conditions*. Nature, 2011. **473**(7347): p. 308-16.
3. Cao, G., et al., *How vascular smooth muscle cell phenotype switching contributes to vascular disease*. Cell Commun Signal, 2022. **20**(1): p. 180.
4. Pinard, A., G.T. Jones, and D.M. Milewicz, *Genetics of Thoracic and Abdominal Aortic Diseases*. Circ Res, 2019. **124**(4): p. 588-606.
5. Dietz, H.C., et al., *Marfan syndrome caused by a recurrent de novo missense mutation in the fibrillin gene*. Nature, 1991. **352**(6333): p. 337-9.
6. Takeda, N., et al., *TGF-beta Signaling-Related Genes and Thoracic Aortic Aneurysms and Dissections*. Int J Mol Sci, 2018. **19**(7).
7. Verstraeten, A., et al., *Marfan Syndrome and Related Disorders: 25 Years of Gene Discovery*. Hum Mutat, 2016. **37**(6): p. 524-31.
8. Cabral-Pacheco, G.A., et al., *The Roles of Matrix Metalloproteinases and Their Inhibitors in Human Diseases*. Int J Mol Sci, 2020. **21**(24).
9. Lucero, H.A. and H.M. Kagan, *Lysyl oxidase: an oxidative enzyme and effector of cell function*. Cell Mol Life Sci, 2006. **63**(19-20): p. 2304-16.
10. Rodriguez, C. and J. Martinez-Gonzalez, *The Role of Lysyl Oxidase Enzymes in Cardiac Function and Remodeling*. Cells, 2019. **8**(12).
11. Guo, D.C., et al., *LOX Mutations Predispose to Thoracic Aortic Aneurysms and Dissections*. Circ Res, 2016. **118**(6): p. 928-34.
12. Lee, V.S., et al., *Loss of function mutation in LOX causes thoracic aortic aneurysm and dissection in humans*. Proc Natl Acad Sci U S A, 2016. **113**(31): p. 8759-64.
13. Renner, S., et al., *Next-generation sequencing of 32 genes associated with hereditary aortopathies and related disorders of connective tissue in a cohort of 199 patients*. Genet Med, 2019. **21**(8): p. 1832-1841.

14. Cirnu, A., et al., *Novel Mutation in LOX Associates With a Complex Aneurysmal Vascular and Cardiac Phenotype*. *Circ Genom Precis Med*, 2021. **14**(1): p. e003217.
15. Proost, D., et al., *Performant Mutation Identification Using Targeted Next-Generation Sequencing of 14 Thoracic Aortic Aneurysm Genes*. *Hum Mutat*, 2015. **36**(8): p. 808-14.
16. Vandeweyer, G., et al., *VariantDB: a flexible annotation and filtering portal for next generation sequencing data*. *Genome Med*, 2014. **6**(10): p. 74.
17. Anderson, N.K., E.E. Juzwiak, and H.C. Dietz, *A sex(X/Y) Article on Marfan Syndrome*. *J Am Heart Assoc*, 2020. **9**(20): p. e018814.
18. Verstraeten, A., et al., *Enrichment of Rare Variants in Loeys-Dietz Syndrome Genes in Spontaneous Coronary Artery Dissection but Not in Severe Fibromuscular Dysplasia*. *Circulation*, 2020. **142**(10): p. 1021-1024.
19. Callewaert, B., et al., *Ehlers-Danlos syndromes and Marfan syndrome*. *Best Pract Res Clin Rheumatol*, 2008. **22**(1): p. 165-89.
20. Van Laer, L., H. Dietz, and B. Loeys, *Loeys-Dietz syndrome*. *Adv Exp Med Biol*, 2014. **802**: p. 95-105.
21. Meester, J.A.N., et al., *Differences in manifestations of Marfan syndrome, Ehlers-Danlos syndrome, and Loeys-Dietz syndrome*. *Ann Cardiothorac Surg*, 2017. **6**(6): p. 582-594.
22. Boone, P.M., et al., *The Genetics of Pneumothorax*. *Am J Respir Crit Care Med*, 2019. **199**(11): p. 1344-1357.
23. Merico, V., et al., *Inhibition of lysyl oxidase stimulates TGF-beta signaling and metalloproteinases-2 and -9 expression and contributes to the disruption of ascending aorta in rats: protection by propylthiouracil*. *Heart Vessels*, 2021. **36**(5): p. 738-747.
24. Oleggini, R., N. Gastaldo, and A. Di Donato, *Regulation of elastin promoter by lysyl oxidase and growth factors: cross control of lysyl oxidase on TGF-beta1 effects*. *Matrix Biol*, 2007. **26**(6): p. 494-505.
25. Xie, J., et al., *TGF-beta1 induces the different expressions of lysyl oxidases and matrix metalloproteinases in anterior cruciate ligament and medial collateral ligament fibroblasts after mechanical injury*. *J Biomech*, 2013. **46**(5): p. 890-8.

## 7 Supplemental

---

Table S1: Detailed clinical features overview LOX patients in our cohort, Table S2: ACMG classification and pathogenicity predictions of *LOX* variants, Table S3 part 1 and part 2: Clinical features overview *LOX* patients' literature and Table S4: Genes included in TAAD gene panel

**Table S1: Clinical features overview LOX patients**

	Family 1 p.(Leu18Profs*111)							Family 2 p.(Arg118Glyfs*119)			Family 3 p.(Gly149*)				Family 4 p.(Met298Arg)	Family 5 p.(Leu306Pro)
Individual	II:2	II:3	III:4	III:6	III:10	IV:1	IV:7	III:1	II:1	I:1	II:4	II:5	III:1	II:1	II:1	III:1
Gender	M	M	M	M	M	M	F	M	M	M	M	M	F	M	F	M
Age (years)	60	50	43	45	43	25	16	40	53	66	56	53	28	59	50	21
Arterial anomalies	Bental surgery age 60 after dissection died 73 due to myocardia infarction	Sudden death (age 50)	Type A dissection (53mm)	Aortic dissection (age 45 84mm) and Bentall surgery	Aortic sinus diameter (43mm age 43)	Normal diameter	Normal diameter	Type A dissection at age of 19 (underwent composite graft surgery)	Discrete mitral and aortic valve insufficiency		Borderline aortic sinus (41mm)	Mild valve regurgitation			Left carotid dissection (age 46)	Dilatation of aorta sinus and ascendens (age 6)
															Coronary artery dissection (age 44)	Elective replacement of the ascending aorta (age 14)
Connective tissue anomalies								Splenic rupture	Inguinal hernia surgery	Varicose veins	Inguinal hernia surgery (age 3)	Tall stature	Joint hypermobility	Bilateral inguinal hernia	Increased skin elasticity	Tall stature
								Spontaneous pneumothorax		Cataract	Rupture of supraspinatus ligament (age 41)	Narrow palate	Arachnodactyly	Tall stature	Beighton score of 4/9	
								Varicose veins		Ischemic heart disease	Tibialis posterior	Flat feet	Flat feet	Joint hypermobility	Enlarged armspan	

									neuralgia (age 42)					
								Contra-lateral and incarcerated hernia		Inguinal hernia surgery (age 40)	Shoulder dislocations and ankle distortions		Recurrent joint dislocation	

**Table S2: ACMG classification and pathogenicity predictions of *LOX* variants**

	Gnomad	CADD	REVEL	MetaLR	PolyPhen2	Mutation-Taster	ACMG classification
<b>p.(Leu18Profs*111)</b>	Absent	-	-	-	-	Disease causing	<b>Pathogenic</b> (PVS1; PM2; PS3; PP4)
<b>p.(Arg118Glyfs*119)</b>	Absent	-	-	-	-	Disease causing	<b>Pathogenic</b> (PVS1, PS3, PM2)
<b>p.(Gly149*)</b>	Absent	34	-	-	-	Disease causing	<b>Pathogenic</b> (PVS1, PS3, PM2)
<b>p.(Met298Arg)</b>	Absent	32	0,736	0,313	Probably damaging	Disease causing	<b>Pathogenic</b> (PP3; PM1; PM2; PS1; PS3)
<b>p.(Leu306Pro)</b>	Absent	31	0,811	0,358	Probably damaging	Disease causing	<b>VUS</b> (PM1; PM2; PP3)

**Table S3 part 1: Clinical features overview *LOX* patients literature (Guo et al., Lee et al., Cirnu et al., Renner et al.)**

	Guo et al TAA-602 p.(Ser280Arg)				Guo et al TAA-111 p.(Ser348Arg)	Guo et al TAA-271 p.(Gly202*)	Guo et al TAA-703 p.(Thr248Ile)	Guo et al TAA-92291 p.(Trp42*)						Guo et al TAA-9544 p.(Gln267Pro)		
Individual	III:1	II:5	II:4	II:3	III:1	III:4	II:2	IV:2	II:3	II:4	III:1	II:1	III:2	III:6	II:1	III:3
Gender	F	M	M	F	M	M	F	M	F	M	M	M	M	M	M	M
Age (years)	37	62	60	54	41	36	40	11	54	/	59	70	/	16	51	37
Arterial anomalies	Fusiform aortic root (38mm)/ ascending aortic aneurysm (41mm)	Aortic root (52mm)/ ascending aortic aneurysm (42mm)	Type A aortic dissection (age 60)	Aortic root aneurysm (39mm)	Valve and ascending surgery (age 41); Root surgery (age 51)	Elective valve	Ascending aortic aneurysm (52mm)	Aortic root/ ascending aortic aneurysm	Thoracic aortic aneurysm and repair	Thoracic aortic aneurysm and repair	Thoracic aortic aneurysm and repair	Died after thoracic aortic surgery	Thoracic aortic aneurysm	Thoracic aortic aneurysm (Bentall surgery)	Bentall surgery	Aortic root enlargement
	Mild mitral regurgitation	Left ventricular hypertrophy (LVH)		Ectatic ascending aorta	Ascending aortic aneurysm (125mm)	Aortic root aneurysm (42mm)	Transverse aortic arch aneurysm							BAV		
		Bicuspid aortic valve (BAV)			Aortic root aneurysm	Ascending aortic aneurysm (fusiform)	BAV (age 40)									
		Three-vessel coronary artery disease (CAD)			Valve and ascending surgery (age 41); Root surgery (age 51)	Elective valve	Ascending aortic aneurysm (52mm)									

	Fusiform aortic root (38mm)/ ascending aortic aneurysm (41mm)	Aortic root (52mm)/ ascending aortic aneurysm (42mm)	Type A aortic dissection (age 60)	Aortic root aneurysm (39mm)											
Connective tissue anomalies							Dolichostenomelia						High arched palate	Dural ectasia	
							Scoliosis						Joint laxity	Pectus deformity	
							Pectus excavatum						Skin striae	Joint hypermobility	
														Skin striae	

**Table S3 part 2: Clinical features overview LOX patients literature (Guo et al., Lee et al., Cirnu et al., Renner et al.)**

	Guo et al TAA-9544 p.(Gln267Pro)		Lee et al p.(Met289Arg)					Cirnu et al p.(Cys291Ser)				Renner et al p.(Trp42*)	Renner et al p.(Tyr332Cys)
<b>Individual</b>	IV:1	I:1	III:1	II:1	II:3	III:3	III:4	II-1	II-2	II-3	I-2	Subject 188	Subject 13
<b>Gender</b>	M	M	M	F	F	M	M	M	M	F	F	/	M
<b>Age (years)</b>	14	54	35	61	73	46	41	53	36	37	74	23	48
<b>Arterial anomalies</b>	Aortic root enlargement	TAA surgery	Ascending aortic aneurysm (105mm age 19)	TAA surgery (age 52)	TAA surgery	Aortic arch dissection (age 41)	Infrarenal abdominal aneurysm	Ascending aortic aneurysm and dissection (age 29)	Aortic aneurysm and rupture (sudden death)	Cerebral hemorrhage	Bowel infarction and stroke	Aortic aneurysm and dissection (type A)	Aortic aneurysm (ascending aortic replacement)
					Arterial tortuosity	Hepatic arterial aneurysm		Infrarenal abdominal aneurysm					
								Aortic arch aneurysm (age 46)					
								Aneurysms of A. iliaca communis, A. femoralis, A poplitea, A tibialis anterior					
								Coronary aneurysm					
<b>Connective tissue anomalies</b>	Dural ectasia	Dural ectasia	Pectus excavatum		Pectus excavatum	Abdominal hernia (age 43)		Mild scoliosis					Translucent skin

	Pectus deformity	Pectus deformity	Tall stature		Tall stature	Myopia		Tall stature						Easy bruising
	Joint hypermobility	Joint hypermobility	High arched palate		High arched palate			High arched palate						Hernia
	Skin striae	Skin striae	Skin striae		Varicose veins			Ascending aortic aneurysm and dissection (age 29)						Recurrent injuries of ankle ligaments
	Dural ectasia	Dural ectasia	Venous varicosities		Skin striae									

**Table S4: Genes included in TAAD gene panel**

Gene	Reference transcript (Ensembl)	Alternative exon	Reference transcript for alternative exon (Ensembl)
<i>ABL1</i>	ENST00000372348		
<i>ACTA2</i>	ENST00000458208		
<i>ARH1</i>	ENST00000379887		
<i>BGN</i>	ENST00000331595		
<i>COL3A1</i>	ENST00000304636		
<i>EFEMP2/FBLN4</i>	ENST00000307998		
<i>ELN</i>	ENST00000358929		
<i>EMILIN1</i>	ENST00000380320		
<i>FBN1</i>	ENST00000316623		
<i>FBN2</i>	ENST00000262464		
<i>FLNA</i>	ENST00000369850		
<i>FOXE3<sup>a</sup></i>	ENST00000335071		
<i>HCN4</i>	ENST00000261917		
<i>LMOD1</i>	ENST00000367288		
<i>LOX</i>	ENST00000231004		
<i>LTBP3</i>	ENST00000301873		
<i>MAT2A</i>	ENST00000306434		
<i>MFAP5</i>	ENST00000359478		
<i>MYH11</i>	ENST00000452625	Exon 42B	ENST00000396324
<i>MYLK</i>	ENST00000360304		
<i>NOTCH1</i>	ENST00000277541		
<i>PLOD1</i>	ENST00000196061	Exon 2A	ENST00000449038
<i>PMEPA1/TMEPAI</i>	ENST00000341744		
<i>PRKG1<sup>b</sup></i>	ENST00000401604		
<i>SKI</i>	ENST00000378536		
<i>SLC2A10</i>	ENST00000359271		
<i>SMAD2</i>	ENST00000402690		
<i>SMAD3</i>	ENST00000327367	Exon 1A	ENST00000439724
<i>SMAD4</i>	ENST00000342988		
<i>SMAD6</i>	ENST00000288840		
<i>TGFB2</i>	ENST00000366929		
<i>TGFB3</i>	ENST00000238682		
<i>TGFBR1</i>	ENST00000374994		
<i>TGFBR2</i>	ENST00000359013		

<sup>a</sup>Only Forkhead domain

<sup>b</sup>Only exon 3

## CHAPTER 4

---

### **A human Importin- $\beta$ -related disorder: Syndromic thoracic aortic aneurysm caused by bi-allelic loss-of-function variants in *IPO8***

Ilse Van Gucht,<sup>1#</sup> Josephina A.N. Meester,<sup>1#</sup> Jotte Rodrigues Bento,<sup>1</sup> Maaïke Bastiaansen,<sup>1</sup> Jarl Bastianen,<sup>1</sup> Ilse Luyckx,<sup>1,2</sup> Lotte Van Den Heuvel,<sup>1</sup> Cédric H.G. Neutel,<sup>3</sup> Pieter-Jan Guns,<sup>3</sup> Mandy Vermont,<sup>3</sup> Erik Fransen,<sup>1,4</sup> Melanie H.A.M. Perik,<sup>1</sup> Joe Davis Velchev,<sup>1</sup> Maaïke Alaerts,<sup>1</sup> Dorien Schepers,<sup>1,5</sup> Silke Peeters,<sup>1</sup> Isabel Pintelon,<sup>6</sup> Abdulrahman Almesned,<sup>7</sup> Matteo P. Ferla,<sup>8</sup> Jenny C. Taylor,<sup>8</sup> Anthony R. Dallosso,<sup>9</sup> Maggie Williams,<sup>9</sup> Julie Evans,<sup>9</sup> Genomics England Research Consortium,<sup>†</sup> Jill A. Rosenfeld,<sup>10,11</sup> Thierry Sluysmans,<sup>12</sup> Desiderio Rodrigues,<sup>13</sup> Ashish Chikermane,<sup>14</sup> Gangadhara Bharmappanavara,<sup>15</sup> Kayal Vijayakumar,<sup>16</sup> Hassan Mottaghi Moghaddam Shahri,<sup>17</sup> Narges Hashemi,<sup>18</sup> Paria Najarzadeh Torbati,<sup>19</sup> Mehran B. Toosi,<sup>20</sup> Zuhair N. Al-Hassnan,<sup>21</sup> Julie Vogt,<sup>22</sup> Nicole Revencu,<sup>23</sup> Isabelle Maystadt,<sup>24</sup> Erin M. Miller,<sup>25</sup> K. Nicole Weaver,<sup>26</sup> Amber Begtrup,<sup>27</sup> Henry Houlden,<sup>28</sup> David Murphy,<sup>28</sup> Reza Maroofian,<sup>28</sup> Alistair T. Pagnamenta,<sup>8</sup> Lut Van Laer,<sup>1</sup> Bart L. Loeys,<sup>1,2#\*</sup> Aline Verstraeten<sup>1#\*</sup>

<sup>1</sup>Cardiogenomics Research Group, University of Medical Genetics, University of Antwerp and Antwerp University Hospital, Antwerp, Belgium

<sup>2</sup>Department of Human Genetics, Radboud University Nijmegen Medical Center, Nijmegen 6525 GA, The Netherlands

<sup>3</sup>Laboratory of Physiopharmacology, University of Antwerp, Antwerp 2610, Belgium

<sup>4</sup>StatUa Center for Statistics, University of Antwerp, Antwerp 2000, Belgium

<sup>5</sup>Laboratory of Molecular, Cellular and Network Excitability, Department of Biomedical Sciences, University of Antwerp, Antwerp 2610, Belgium

<sup>6</sup>Laboratory of Cell Biology & Histology, Department of Veterinary Sciences, University of Antwerp, Antwerp 2610, Belgium

<sup>7</sup>Prince Sultan Cardiac Centre, Qassim 31982, Saudi Arabia

<sup>8</sup>NIHR Oxford Biomedical Research Centre, Wellcome Centre for Human Genetics, University of Oxford, Oxford OX3 7BN, United Kingdom

<sup>9</sup>Bristol Genetics Laboratory, South West Genomic Laboratory Hub, Southmead Hospital, Bristol BS10 5NB, United Kingdom

<sup>10</sup>Department of Molecular and Human Genetics, Baylor College of Medicine, Houston, Texas 77030, United States of America

- <sup>11</sup>Baylor Genetics Laboratories, Houston 77021, Texas, United States of America
- <sup>12</sup>Department of Pediatric cardiology, Cliniques universitaires Saint-Luc, University of Louvain, Brussels 1200, Belgium
- <sup>13</sup>Birmingham Women's and Children's Hospital NHS Foundation Trust, Steelhouse Lane, Birmingham B4 6NH, United Kingdom
- <sup>14</sup>Birmingham Women & Children's Hospital, Birmingham B4 6NH, United Kingdom
- <sup>15</sup>Musgrove Park Hospital, Somerset NHS Foundation Trust, Taunton TA1 5DA, United Kingdom
- <sup>16</sup>Department of Paediatric Neurology, University Hospitals Bristol NHS Foundation Trust, Bristol BS2 8BJ, United Kingdom
- <sup>17</sup>Pediatric department, Faculty of medicine, Mashhad University of Medical Sciences, Mashhad 009851, Iran
- <sup>18</sup>Department of Pediatric Neurology, School of medicine, Mashhad University of Medical Sciences, Mashhad 009851, Iran
- <sup>19</sup>Department of Molecular Genetics, Next Generation Genetic Polyclinic, Mashhad University of Medical Sciences, Mashhad 009851, Iran
- <sup>20</sup>Department of Pediatric Neurology, Ghaem Hospital, Mashhad University of Medical Sciences, Mashhad 009851, Iran
- <sup>21</sup>Cardiovascular Genetic Program, Department of Medical Genetics, King Faisal Specialist Hospital and Research Centre, Riyadh 11564, Saudi Arabia
- <sup>22</sup>West Midlands Regional Genetics Service, Birmingham Women's and Children's Hospital, Birmingham, B15 2TG United Kingdom
- <sup>23</sup>Center for Human Genetics, Cliniques universitaires Saint-Luc, University of Louvain, Brussels 1200, Belgium
- <sup>24</sup>Centre de Génétique Humaine, Institut de Pathologie et de Génétique, Gosselies (Charleroi) 6041, Belgium
- <sup>25</sup>The Heart Institute, Department of Pediatrics, Cincinnati Children's Hospital Medical Center and University of Cincinnati College of Medicine, Cincinnati 45229, Ohio, United States of America
- <sup>26</sup>Division of Human Genetics, Department of Pediatrics, Cincinnati Children's Hospital Medical Center and University of Cincinnati College of Medicine, Cincinnati 45229, Ohio, United States of America
- <sup>27</sup>GeneDx, Gaithersburg 20877, Maryland, United States of America
- <sup>28</sup>Department of Neuromuscular Disorders, UCL Queen Square Institute of Neurology, London, WC1N 3BG, United Kingdom

†Consortium members are listed in Consortia section; #These authors contributed equally to this work; \*Correspondence: [aline.verstraeten@uantwerpen.be](mailto:aline.verstraeten@uantwerpen.be) & [bart.loeys@uantwerpen.be](mailto:bart.loeys@uantwerpen.be)

Published in American Journal of Human Genetics (2021 Jun 3;108(6):1115-1125.doi:10.1016/j.ajhg.2021.04.019)

## Abstract

---

Importin-8, encoded by *IPO8*, is a ubiquitously expressed member of the importin- $\beta$  protein family that translocates cargo molecules such as proteins, RNAs and ribonucleoprotein complexes into the nucleus in a RanGTP-dependent manner. Current knowledge of the cargoes of Importin-8 is limited, but TGF- $\beta$  signaling components such as SMAD1-4 have been suggested to be amongst them. Here, we report that bi-allelic loss-of-function variants in *IPO8* cause a syndromic form of thoracic aortic aneurysm (TAA) with clinical overlap with Loeys-Dietz and Shprintzen-Goldberg syndrome. Seven individuals from six unrelated families showed a consistent phenotype with early-onset TAA, motor developmental delay, connective tissue findings and craniofacial dysmorphic features. A C57Bl/6N *Ipo8* knock-out mouse model recapitulates TAA development from 8-12 weeks onwards in both sexes, but most prominently shows ascending aorta dilatation with a propensity for dissection in males. Compliance assays suggest augmented passive stiffness of the ascending aorta in male *Ipo8*<sup>-/-</sup> mice throughout life. Immunohistological investigation of mutant aortic walls reveals elastic fiber disorganization and fragmentation along with a signature of increased TGF- $\beta$  signaling, as evidenced by nuclear pSmad2 accumulation. RT-qPCR assays of the aortic wall in male *Ipo8*<sup>-/-</sup> mice demonstrate decreased *Smad6/7* and increased *Mmp2* and *Ccn2 (Ctgf)* expression, reinforcing a role for dysregulation of the TGF- $\beta$  signaling pathway in TAA development. As Importin-8 is the most downstream TGF- $\beta$ -related effector implicated in TAA pathogenesis so far, it offers opportunities for future mechanistic studies and represents a candidate drug target for TAA.

## 1 Introduction

---

Thoracic aortic aneurysm (TAA) refers to a pathological and progressive dilatation of the aorta which, if left untreated, imposes a risk for life-threatening aortic dissection or rupture. TAA presents either as an isolated condition (non-syndromic TAA) or as part of a multi-systemic connective tissue disorder (syndromic TAA). Most typically, the inheritance pattern is autosomal dominant, but rare X-linked or autosomal recessive families have also been reported. As pathogenic variants in the more than 30 known TAA genes explain less than 30% of probands with a positive family history [1], additional TAA genes remain to be identified. Important mechanistic insights into syndromic TAA formation have largely emanated from elucidation of the etiology of two clinically overlapping autosomal dominant TAA syndromes: Marfan syndrome (MFS [MIM: 154700]) and Loeys-Dietz syndrome (LDS [MIM: 609192, MIM: 610168, MIM: 613795, MIM: 614816 & MIM: 615582]) [2]. Besides TAA, MFS is characterized by ocular (e.g. ectopia lentis), skeletal (e.g. overgrowth, pectus deformity) and cutaneous (e.g. striae, hernia) manifestations. LDS can be distinguished from MFS by the unique presence of hypertelorism, cleft palate or bifid uvula and prominent arterial tortuosity, as well as by a more widespread and severe aneurysm phenotype. Whereas MFS is caused by dominant-negative or haplo-insufficient variants in the extracellular matrix (ECM) component fibrillin 1 [3] (*FBN1* [MIM: 134797]), LDS results from loss-of-function variants in six key components of the canonical transforming growth factor  $\beta$  (TGF- $\beta$ ) signaling pathway (i.e. *TGFBR1/2* [MIM: 190181 & MIM: 190182], *SMAD2/3* [MIM: 601366 & MIM: 603109], *TGFBR2/3* [MIM: 190220 & MIM: 190230]) (Figure S1) [4-10]. In both conditions, analysis of the aortic wall in mouse models and affected individuals shows a clear tissue signature for enhanced TGF- $\beta$  signaling, including activation of signaling intermediates and increased output of TGF- $\beta$  target genes [11]. Interestingly, a third condition with extensive phenotypic overlap with MFS and LDS but less severe cardiovascular involvement and the unique presence of neurodevelopmental delay (Shprintzen-Goldberg syndrome (SGS) [MIM: 182212]) is caused by heterozygous

missense variants located in the R-SMAD-binding domain of a negative regulator of the TGF- $\beta$  transcriptional response called SKI (*SKI* [MIM: 164780]) (Figure S1) [12, 13].`

## 2 Material and methods

---

### Ethics

The human part of the study was approved by the appropriate institutional ethics review boards and the required informed consents were obtained from all participating subjects. In frame of this manuscript, a separate informed consent for the publication of identifiable photographs was signed by the subjects' legal guardians. All mouse breedings and experiments have been done in accordance with the ethical guidelines set by the Ethical Committee of Animal Testing of the University of Antwerp and have received formal ethical clearance.

### Exome/genome sequencing

Exome and genome sequencing, data annotation and interpretation were performed in five different centers using slightly different procedures. Exome sequencing of peripheral blood-derived DNA of individuals 1-II:3 and 2-II:1 and their respective parents involved sequence capture with the Agilent SureSelect Human All Exon v5 enrichment kit (Agilent Technologies), followed by sequencing on the Illumina HiSeq platform (BGI, Copenhagen, Denmark). After BWA-based read alignment (GRCh37 reference build) and variant calling with GATK, VariantDB was used to annotate and manually curate the identified variants[14]. Individual 3-II:3 and her mother were recruited to the 100K Genomes Project (100KGP), a national genome sequencing initiative [15]. Library preparation was done using the TruSeq<sup>®</sup> DNA PCR-Free method and 150bp paired-end sequencing was performed on a HiSeqX machine (Illumina). Reads were mapped to GRCh38 and variants were called with Platypus. More information is available at [https://figshare.com/articles/GenomicEnglandProtocol\\_pdf](https://figshare.com/articles/GenomicEnglandProtocol_pdf)

[/4530893/5](#). Research-based analyses on this data were performed within the Genomics England's research environment (<https://re.extge.co.uk/ovd>). Bi-allelic variants in *IPO8* were identified using the tiering table available in the Labkey application. For a recessive mode of inheritance, variants were filtered at a 1% population allele frequency. Individual 4-II:4 underwent clinical proband-only exome sequencing as described before [16]. Proband 5-II:2 was subjected to exome sequencing as previously described [17]. Using genomic DNA from individual 6-II:1, the exonic regions and flanking splice junctions of the genome were captured using the IDT xGen Exome Research Panel v1.0 (Integrated DNA Technologies, Coralville, IA). Massive parallel paired-end sequencing was done on an Illumina system. Reads were aligned to the human genome build GRCh37/UCSC hg19, and analyzed for sequence variants using a custom-developed analysis tool[18]. The general assertion criteria for variant classification are publicly available on the GeneDx ClinVar submission page (<http://www.ncbi.nlm.nih.gov/clinvar/submitters/26957/>).

### **Sanger sequencing**

Sanger sequencing was used to validate the *IPO8* variants identified by exome/genome sequencing, to check for variant segregation in family members, look for additional variants in the 25 coding exons of *IPO8* (RefSeq transcript NM\_006390.3) in 50 genetically unsolved syndromic TAA cases, and check for nonsense-mediated mRNA decay. The PCR and sequencing primer sequences and reaction conditions are available upon request. PCR products were bi-directionally sequenced using the BigDye Terminator Cycle Sequencing kit (Applied Biosystems) and separated on an ABI 3130XL Genetic Analyzer (Applied Biosystems). Sequences were analyzed using CLC DNA Workbench 5.

### ***In silico* protein modeling**

The protein models of the p.(Lys447\_Arg476del) and p.(Thr967\_Glu1006delinsLys) variants were constructed in Pyrosetta[19] using the PDB:1WA5 [20] Swissmodel threaded structures model [21] with parts from an I-Tasser model [22] and human RAN from PDB:6TVO [23]. They were energy-minimized with FastRelax mover [24], scored using the ref2015 score function [25] and assessed for their effect on the binding energy of RAN GTPase with InterfaceAnalyser mover [26]. Further 3D protein consequences of the predicted 30 amino acid deletion were determined using Remodel mover [27]. All scripts have been deposited at [https://github.com/matteoferla/IPO8\\_analysis](https://github.com/matteoferla/IPO8_analysis) and an interactive webpage to visualize the model was made in Michelangelo[28] (<https://michelangelo.sgc.ox.ac.uk/r/ipo8>).

### **Fibroblast cultivation**

Skin fibroblasts were cultured in RPMI medium supplemented with 15% fetal bovine serum, 1% L-glutamine, 1% sodium pyruvate, 1% Penicillin/Streptomycin, and 0.1% Primocin. The fibroblasts were incubated with and without puromycin (200 µg/ml) to inhibit nonsense-mediated mRNA decay. Experiments were performed at passages 4 to 8.

### **Mice**

*Ipo8*<sup>tm1.1(KOMP)*Vl*cg</sup> C57Bl/6N knockout mice were derived from ES cell clone 14312A-C12, generated by Regeneron Pharmaceuticals and obtained from the KOMP Repository. The general methods used to create Velocigene targeted alleles have been described by Valenzuela et al [29]. Pertaining to the *Ipo8*<sup>tm1.1(KOMP)*Vl*cg</sup> model specifically, insertion of the Velocigene cassette ZEN-Ub1 resulted in a 31.512bp deletion (chr6:148.799.733-148.831.244; GRCm38/mm10), replacing the genomic sequence encoding the first 529 amino acids (exon 1-14) of murine Importin-8 (Figure A). Mice that contained the reporter-tagged null allele (tm1) were subsequently bred to Cre-expressing mice,

resulting in removal of the  $\beta$ -actin promoter and the Neomycin gene it activated. The tm1.1 allele remains a lacZ reporter and is a non-conditional knockout of the gene.

In order to proof this  $lpo8^{tm1.1(KOMP)VICg}$  model is a true  $lpo8$  knock out model, an additional RT-qPCR and regular PCR with agarose gel electrophoresis were performed. RT-qPCR experiment on cDNA samples extracted from  $lpo8^{-/-}$  mouse aortas demonstrated that exon 23-24 is not expressed (Figure B). Additionally, no amplification of  $lpo8$  was observed in cDNA samples of  $lpo8^{-/-}$  mouse aortas using regular PCR and agarose gel electrophoresis (exon 23-24), whereas  $lpo8$  amplification could be observed in aortic cDNA of wild type animals (Figure C). The unequivocally demonstrates that this mouse model is a true  $lpo8$  knock-out model. The mice were housed, maintained and bred on a C57Bl/6N background at the animal facility of the University of Antwerp.

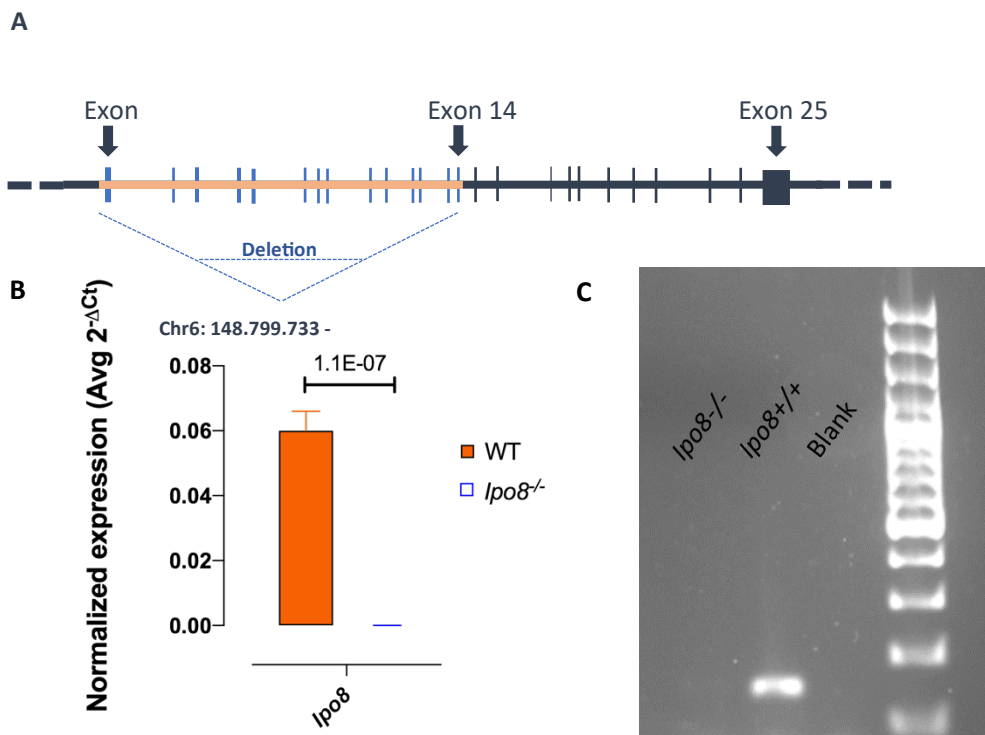


**Figure A. Schematic representation of *Ipo8* deletion (exon 1-14) in *Ipo8*<sup>tm1.1(KOMP)Vlcg</sup> model; B-C. Demonstration of *Ipo8* mRNA expression in the aorta of wild type mice and absence of *Ipo8* mRNA expression in the aorta of homozygous knock-out mice. B. RT-qPCR results (mixed model analysis,  $p=1.1E-7$ , error bars depict SEM, WT: wild type). C. Regular PCR and agarose gel electrophoresis.**

### **Transthoracic echocardiography**

TAA development was monthly investigated at the level of the sinuses of Valsalva and distal ascending aorta from the age of 4 weeks until 32 weeks of age. To visualize the aorta, the hairs of conscious mice were removed with “Veet sensitive skin” cream, followed by echocardiography using a VisualSonics Vevo 2100 imaging system and a 30 MHz transducer. Parasternal long-axis view recordings were taken and three independent measurements from the maximal internal aortic dimensions were averaged and weight-corrected. All data acquisition and measurements were performed blinded to genotype.

### **Quantification of mouse kyphosis**

For kyphosis quantification in the *Ipo8*<sup>-/-</sup> mice, we applied the method described by Laws et al [30]. We compared the severity of kyphosis of 8 *Ipo8*<sup>-/-</sup> mice to that of 8 gender-matched wild type mice using online available lateral total body X-rays (International Mouse Phenotyping Consortium; [https://www.mousephenotype.org/data/imageComparator?&parameter\\_stable\\_id=I MPC\\_XRY\\_048\\_001&acc=MGI:2444611](https://www.mousephenotype.org/data/imageComparator?&parameter_stable_id=I MPC_XRY_048_001&acc=MGI:2444611)).

### **Rodent Oscillatory Tension Set-up to study Arterial Compliance (ROTSAC)**

The ROTSA assay was used to determine the *ex vivo* ascending aorta stiffness[31]. In brief, ascending aorta vessel segments were mounted between two wire hooks and continuously stretched between alternating preloads corresponding to the systolic and diastolic transmural pressures at a physiological frequency of 10 Hz (600 beats/min).

The diameter of the ascending aorta segment was determined over different pressure ranges (80-120 mmHg to 120-160 mmHg) allowing for measuring arterial stiffness expressed as the Peterson modulus ( $E_p$ ). The  $E_p$  is defined as the pulse pressure (difference in pressure ( $\Delta P$ )), multiplied by the diastolic diameter ( $D_0$ ), and divided by the diameter change ( $\Delta D$ ) between diastolic and systolic pressure ( $E_p = D_0 * \Delta P / \Delta D$ ). Arterial stiffness was evaluated under different experimental conditions. Contraction of the aortic segments was mediated through the addition of 2  $\mu\text{M}$  of phenylephrine (PE). To discriminate interference of basal nitric oxide (NO) release from the effects of PE, the experiment was repeated after addition of 2  $\mu\text{M}$  PE along with 300  $\mu\text{M}$  N( $\Omega$ )-nitro-L-arginine methyl ester (L-NAME) (i.e. an inhibitor of endothelial nitric oxide synthase (eNOS)). To evaluate the role of basal vascular smooth muscle cell tonus, complete relaxation was achieved through stimulation with 2  $\mu\text{M}$  diethylamine NONOate (DEANO) (i.e. an exogenous NO donor).

### **Histology and immunohistochemistry**

Mice were euthanized using 100 mg/kg pentobarbital (Nembutal®). Ascending aortic tissue was collected, fixed in 4% para-formaldehyde (PFA) solution in phosphate-buffered saline (PBS) for 24 hours and transferred to 60% isopropanol. Tissue segments were paraffin embedded and 5  $\mu\text{m}$  sections were created for staining. Trichrome Masson's (Sigma-Aldrich) staining was performed to evaluate the collagen content, while Weigert-Van Gieson (Sigma-Aldrich) staining was used to assess elastic fiber integrity. Elastic fiber abnormalities were objectified using a grading system, with grade 1 sections presenting with continuous and well-organized elastic bundles and grade 4 sections displaying vastly disorganized fibers, marked fiber fragmentation and a thickened aortic wall (grade 4). Grading was done blinded to genotype by three independent researchers and the results were averaged out. pSmad2 levels were visualized using immunostaining. Aortic sections were deparaffinized in toluene (5 min) and rehydrated in graded alcohol (90, 70 and 50% ethanol). Endogenous peroxidase

was inhibited with 3 % hydrogen peroxide. Sections were submerged in trypsin at 37°C for 10 min (29 mg trypsin powder (Sigma-Aldrich, 93615-25G) in 169mL milliQ) for antigen retrieval and boiled in citrate buffer (0.154g citric acid.1H<sub>2</sub>O, 1.235g trisodium citrate.5H<sub>2</sub>O, 500 mL MilliQ, pH 6) in a microwave for 5 sec at 650 W and 10 min at 90 W. They were cooled down to room temperature for 30 min, rinsed in MilliQ and TBST and blocked with goat serum (1:10, S-1012-50, Vector-labconsult) for 20 min at room temperature (RT). Primary antibody (pSmad2 (3101, Cell Signaling; 1:5000)) incubation was performed overnight in a humid chamber at room temperature. Afterwards, the sections were washed in TBST and incubated with a secondary antibody (1:200, 30014 Vector, Sec goat anti-rabbit IgG) for 30 min at RT and with the avidin-biotinylated complex for 1 hour at RT (Vectastain ABC kit, Vector Laboratories). 3,3'-Diaminobenzidine tetrahydrochloride hydrate (DAB) chromogen (Sigma-Aldrich) was used as a substrate and slides were counterstained with Hematoxylin. Images were acquired using an automated Nikon Ti-E inverted microscope equipped with a Nikon DS-U3 digital camera (Nikon Instruments). Nikon NIS Elements AR software v4.51.01 was used for image acquisition at 20x magnification. Again, grading was done blinded to genotype by three independent researchers and averaged out to objectify differences in pSmad2 staining. Grade 1, 2, 3 and 4 denoted sections in which respectively <25%, 25-50%, 50-75% and 75-100% of nuclei stained positive.

### **Quantitative reverse transcription PCR (RT-qPCR)**

Mice were euthanized using CO<sub>2</sub>-inhalation. Ascending aortic tissue was collected, of which RNA was isolated with the RNeasy mini kit (Qiagen). Subsequent cDNA synthesis was done using the SuperScript III First-Strand Synthesis kit. Alterations in gene expression levels of nine target genes (*Tgfb1*, *Tgfb2*, *Smad4*, *Smad6*, *Smad7*, *Mmp2*, *Eln*, *Ccn2* (*Ctgf*) and *Serpine1* (*Pai1*)) were studied using SYBR green (SYBR Green no ROX mix, Eurogentec) chemistry on a Bio-Rad CFX\_384 system. Two reference genes (*Rpl4* and *Rpl32*) were used for normalization. Primers were designed with Primer3, after

which amplification efficiency and primer specificity were verified based on the determination coefficient  $R^2$ , Ct range and melting curve. An amplification efficiency between 85% and 110% was reached for all primer sets. Primer sequences are listed in the table below:

**Table: SYBR green primer sequences**

Target genes	Forward primer sequence (5'→3')	Reverse primer sequence (5'→3')
<i>Tgfb1</i>	CGCAACAACGCCATCTATGA	GGCACTGCTTCCCGAATG
<i>Tgfb2</i>	AGGCAGAGTTCAGGGTCTTC	CGCTGGGTGGGAGATGTTAA
<i>Smad4</i>	CCACAGGACAGAAGCGATTG	CTAAGGCACCTGACCCAAAC
<i>Smad6</i>	GTCTCCTCCTGACCAGTACAA	ACCCGGAGCAGTGATGAG
<i>Smad7</i>	GGCTGTGTTGCTGTGAATCT	GCCTGCAGTTGGTTTGAGAA
<i>Mmp2</i>	ACTCCGGAGATCTGCAAACA	GTGTCAGTCCGCCAAATA
<i>Eln</i>	GTTATCCCATCAAAGCACAAAG	CAGCTACTCCATAGGGCAATTT
<i>Ccn2</i>	TCCACCCGAGTTACCAATGA	ACAGGCTTGCGGATTTTAGG
<i>Serpine1</i>	GTCTTTCCGACCAAGAGCAG	GTCTTTCCGACCAAGAGCAG
Reference genes		
<i>Rpl4</i>	CCGGAAGTTGGATGAGCTGTA	TCGGAGGGCTCTTTGGATTT
<i>Rpl32</i>	GTGAAGCCCAAGATCGTCAAA	TCTGGCCCTTGAACCTTCTC

cDNA samples were diluted 1:30 in TE-4 buffer (Tris, EDTA, pH8). Each sample was measured *in triplo* under the following RT-qPCR settings: 50°C for 2min, 95°C for 10min and 40 cycles of 95°C for 15sec and 60°C for 1min. The experiment was repeated three times and the results were analyzed using the Bio-Rad CFX Maestro and qBase+ software packages. Stability of the reference genes was verified and a cut-off value of 0.50 for the M-value and 0.20 for the CV-value was maintained. To calculate normalized gene expression levels the following formulas were used,  $\Delta Ct = Ct[\text{Target gene}] - Ct[\text{Avg Reference genes}]$  and  $2^{-\Delta Ct}$ . The average of  $2^{-\Delta Ct}$  is plotted on the bar chart.

## **Western blotting**

Skin fibroblasts were collected using TrypLE Express, after which total protein was isolated using RIPA<sup>+</sup> buffer (10 mL RIPA, protease and phosphatase inhibitors, 10 uL benzoase). Mice were euthanized by CO<sub>2</sub>-inhalation, followed by isolation of the thoracic ascending aorta. Total mouse ascending aortic protein was extracted using a TissueRuptor II (Qiagen) and RIPA<sup>+</sup> buffer. Protein concentrations were measured with the Pierce BCA Protein Assay kit. Subsequently, the lysates were incubated with NuPage LDS sample buffer and NuPage Reducing agent for 10 min at 70°C. Equal amounts of human or mouse protein were subjected to gel electrophoresis using a Tris-Acetate 3-8% mini gel, together with a PageRuler Plus Prestained Protein Ladder. Proteins were then transferred to a polyvinylidene difluoride (PVDF) membrane (Millipore) and blocked in 5% milk (Nestlé, dissolved in TBST buffer) for 2 hours. Primary antibody incubation (IPO8-N (398854, Santa-Cruz), 1:100) was done overnight at 4°C. Next, the membranes were washed with TBST and incubated with a secondary antibody for 2 hours at RT (Goat anti-rabbit IgG, 1:10.000, 1706515, BioRad). Pierce<sup>™</sup> ECL Western Blotting reagent was used as a detection substrate and images were acquired using a LAS 400 mini imager (Cytiva). Ponceau staining was used as a loading control. Analysis and quantification of the protein signals was performed with Image J.

## **Statistics**

All data are expressed as mean ± SEM with N representing the number of mice. Mixed model analyses were performed on echocardiography measurements and RT-qPCR data using JMP Pro 15 Software (SAS Institute) entering the weight-corrected aortic diameters as dependent variable, the genotype, the time point and their interaction as fixed effects, accounting for the non-independence between observations from the same mouse through a random intercept. In the aforementioned regression models, the outcome variable was log transformed to obtain homoscedasticity and normality of the residuals. Two-way ANOVA analyses were performed using SPSS Statistics (IBM SPSS Statistics for Windows, Version 27.0. Armonk, NY: IBM Corp.) on ROTSAC data and

histology/immunohistochemistry scorings. If a significant time effect was detected with the two-way ANOVA analysis, a post-hoc analysis with sidak correction was carried out to compare the different time points. Furthermore, a comparison between the genotypes at the different time points of the ROTSAC assay and between the genotypes for kyphosis quantification was conducted using a non-parametric Mann-Whitney U test in SPSS statistics.  $p < 0.05$  was considered to be statistically significant.

### 3 Results

---

Using exome or genome sequencing in six unrelated probands presenting with an LDS/SGS-like phenotype (for details see supplemental materials and methods), we identified bi-allelic loss-of-function variants in *IPO8* [MIM: 605600; GenBank: NM\_006390.3], encoding the nuclear import protein Importin-8 (Figure 1A, Figure S2). None of the probands carried a likely pathogenic variant in any of the known TAA genes. Except for p.(Leu866Profs\*12) (c.2597\_2601delTTTTC) (1/250920 alleles), all identified variants are absent from the Genome Aggregation Database (gnomAD v2.1.1). Causality is further supported by segregation analysis, which demonstrated heterozygosity in the unaffected parents and siblings (Figure 1A) as well as homozygosity in one additional affected brother (individual 4-II:3; Figure 1A). Subsequent Sanger sequencing of the coding regions of *IPO8* in 50 other genetically unsolved MFS-, LDS- or SGS-like probands did not reveal additional individuals with homozygous or compound heterozygous variants.

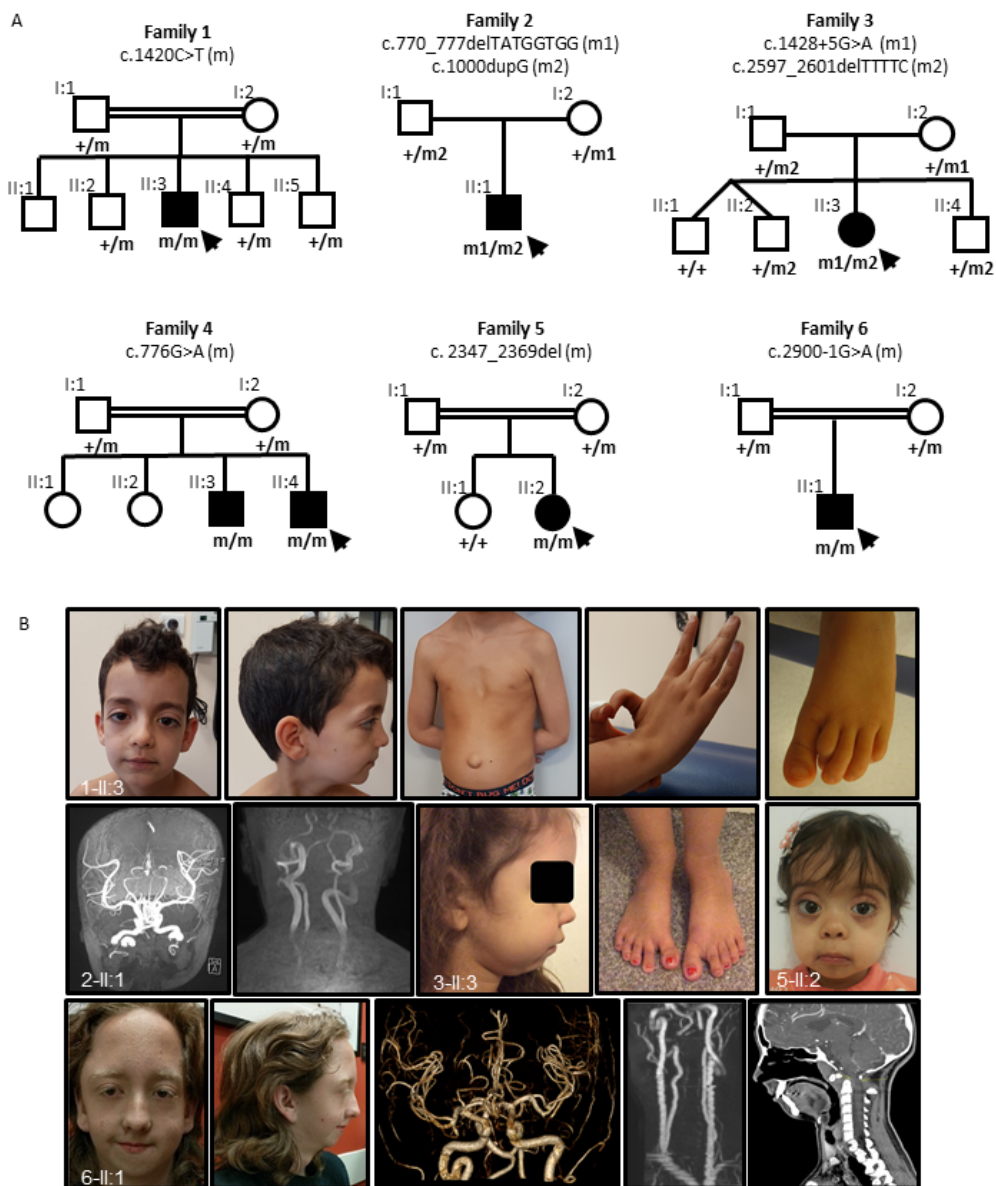


**Figure 1. Familial screening and clinical characterization of individuals with bi-allelic *IPO8* variants.** A) Pedigrees of the families with their respective pathogenic variants. Squares represent males while circles represent females, filled symbols denote affected individuals, a double line connecting spouses symbolizes consanguinity and a - or + sign denotes presence or absence of the respective *IPO8* variant. Variants are annotated against NM\_006390.3. B) Clinical phenotyping. Proband 1-II:3 showing prominent forehead, hypertelorism, mild ptosis left eye, retrognathia, pectus excavatum, umbilical hernia, joint hypermobility with thumb abduction and

*camptodactyly of the second toe. CT angiography of proband 2-II:1 demonstrating dilatation of the common carotid arteries along with marked tortuosity of the common carotid and internal carotid artery, mild tortuosity of the vertebral arteries, enlargement of the anterior and middle cerebral arteries bilaterally. Proband 3-II:3 presenting with frontal bossing with bitemporal flattening, retrognathia, downturned corners of the mouth and flat feet. Proband 5-II:2 showing prominent forehead, significant hypertelorism with flat nasal bridge, mild ptosis of left eye and retrognathia. Proband 6-II:1 demonstrating dolichocephaly, retrognathia, malar flattening, downslanting palpebral fissures and hypertelorism. MRA revealing tortuous intracranial and extracranial arterial vessels, most prominently involving the superior cervical internal carotid arteries with dilation of the left internal carotid artery at the carotid bifurcation. CT-scan (pre-surgical) showing os odontoideum with cervical spinal canal stenosis (arrows).*

Recurrent phenotypic manifestations in our series of cases with bi-allelic *IPO8* variants include facial dysmorphism with dolichocephaly (5/7), frontal bossing (6/7), hypertelorism (6/7), eyelid ptosis (4/7), retrognathia (6/7) and a high arched (6/7) or cleft palate/bifid uvula (3/7); skeletal findings with arachnodactyly (6/7), joint hypermobility (7/7), pectus excavatum (7/7), foot deformity (5/7) and scoliosis (3/7); neuromuscular features including hypotonia (7/7) and developmental delay (7/7); cardiovascular abnormalities with aortic root and/or ascending aortic aneurysm (6/7), structural heart disease (atrial or ventricular septal defect (ASD, VSD) and patent ductus arteriosus (PDA), 7/7); and finally, umbilical and/or inguinal hernia (5/7) (Figure 1B, Table 1). No disproportionate body growth was observed (Figure S3). Of note, despite the severe aneurysm phenotype, none of the affected individuals experienced an arterial or aortic dissection, but this may be due to their young age. Additionally, marked arterial tortuosity, a typical LDS feature, was reported in two cases (2-II:1 and 6-II:1), but might have been overlooked in the others as they have not yet undergone head-to-pelvis arterial imaging. Overall, the phenotype fits in the spectrum of LDS/SGS-like disorders (Table 2).

**Table 1. Detailed overview of the clinical characteristics of individuals with bi-allelic *IPO8* variants**

<b>Table 1 Part A: Family 1-3</b>			
	<b>Family 1 1-II:3</b>	<b>Family 2 2-II:1</b>	<b>Family 3 3-II:3</b>
Variant c. annotation	c.1420C>T homz	c.770_777delTATGGTGG; c.1000dupG	c.1428+5G>A; c.2597_2601delTTTTTC
Variant p. annotation	p.(Arg474*) homz	p.(Val257Glufs*3); p.(Val334Glyfs*19)	p.(Lys447_Arg476del); p.(Leu866Profs*12)
Sex	M	M	F
Current age	10 yrs	8 yrs	8 yrs
<b>Growth</b>	(7yrs 11mo)	(8 yrs)	(7yrs 4mo)
Height	124 cm (P10-25)	127 cm (P25)	118.7 cm (P10-25)
Weight	21 kg (P3-5)	19.9 kg (P1)	22 kg (P25-50)
OFC	55 cm (P97)	?	53.5 cm (P50-75)
<b>Facial features</b>			
Dolichocephaly	+	+	- (prominent sutures)
Frontal bossing	+	+	+
Hypertelorism	+	+	-
Ptosis	+ (L>R)	+ (L>R)	-
Retrognathia	+	+	+
Submucous cleft palate	-	+ & broad uvula	-
High arched palate	+	+	+
<b>Skeletal findings</b>			
Arachnodactyly	+	+	-
Joint hypermobility	+	+	+
Pectus excavatum	+	+	+
Pes planum	+	+	+
Cervical spine anomalies	ND	+	-
Scoliosis	-	+	-
Other	2nd toes camptodactyly	Kyphosis	Recurrent hip, ankle dislocation

<b>Table 1 Part A: Family 1-3 continued</b>			
<b>Neurological findings</b>			
Hypotonia	+	+	+
Developmental delay	+ (mild)	+	+ (motor)
Intellectual disability	-	-	-
<b>Cardiovascular findings</b>	(10yrs 8mo)	(8yrs)	(7yrs 5mo)
ASD	+	+	+
VSD	-	-	+ (membr & muscular)
PDA	-	+	+ (surgical repair)
Aortic root	26 mm (Z=3.5)	35 mm (Z=10)	25 mm (Z=3.58)
Ascending aorta	28 mm (Z=5.7)	28 mm (Z=8.7)	21 mm (Z=2.68)
Sinotubular junction		25 mm (Z=5.4)	23 mm (Z=4.99)
Other aneurysms	ND	Com/int carotid, cerebral arteries	ND
Arterial/aortic tortuosity		+	
<b>Other findings</b>			
Hernia	Umbilical	Umb/bilat inguinal	-
Easy bruising	+	+	-

<b>Table 1 Part B: Family 4-5</b>				
	<b>Family 4 4-II:4</b>	<b>Family 4 4-II:3</b>	<b>Family 5 5-II:2</b>	<b>Family 6 6-II:1</b>
Variant c. annotation	c.776G>A homz	c.776G>A homz	c. 2347_2369del homz	c.2900-1G>A homz
Variant p. annotation	p.(Trp259*) homz	p.(Trp259*) homz	p.(Leu783Valfs*5) homz	p.(Thr967_Glu1006 delinsLys) homz
Sex	M	M	F	M
Current age	6 yrs	10 yrs	3 yrs 9m	19 yrs

<b>Table 1 Part B: Family 4-5 continued</b>				
<b>Growth</b>	(6yrs)	(9 yrs)	(3yrs9m)	(19 years)
Height	121 cm (P75)	126 cm (P10-25)	92 cm (P3)	175 cm (P25-50)
Weight	18.3 kg (P25-50)	17.6 kg (P0.3)	11 kg (P0.5)	63 kg (P25)
OFC			47 cm (P10)	
<b>Facial features</b>				
Dolichocephaly	+	+	-	+
Frontal bossing	+	+	+	-
Hypertelorism	+	+	+	+
Ptosis	-	-	+ (L>R)	+
Retrognathia	-	-	+	+
Submucous cleft palate	-	-	+ (bifid uvula)	+ (bifid uvula)
High arched palate	+	+	-	+
<b>Skeletal findings</b>				
Arachnodactyly	+	+	+	+
Joint hypermobility	+	+	+	+
Pectus excavatum	+	+	+	+
Pes planum	+	+	-	-
Cervical spine anomalies	ND	-	-	+
Scoliosis	-	+	-	+
Other	Talipes equinovarus (L) Vertical talus (R)	Sagittal clefts of midthoracic vertebrae Talipes equino varus (R)	?	Long toes
<b>Neurological findings</b>				
Hypotonia	+	+	+	+
Developmental delay	+ (motor)	+ (motor)	+ (motor)	+
Intellectual disability	-	-	mild	+ <sup>s</sup>

<b>Table 1 Part B: Family 4-5 continued</b>				
<b>Cardiovascular findings</b>	(1yr 8mo)	(9 yrs)	(42 months)	(19 years)
ASD	-	-	+	+ (aneurysmal)
VSD	+ (membraneous)	+	+ (membraneous)	-
PDA	+	-	-	-
Aortic root	25 mm (Z=5.7)	38 mm (Z=6.0)	15 mm (Z=0,5)	41 mm (Z=6.9)
Ascending aorta	17 mm (Z=3.9)	23 mm (Z=2.7)		31 mm (Z=3.8)
Sinotubular junction		25mm (Z=3.8)	12 mm (Z=0.18)	23 mm (Z=1.2)
Other aneurysms	ND	ND	pulmonary artery, coronary sinus	ND
Arterial/aortic tortuosity				+
<b>Other findings</b>				
Hernia	-	Umbilical	Umbilical	Umb/inguinal
Easy bruising	-	-	-	-

**Table 2. Comparison of Marfan, Loews-Dietz, Shprintzen-Goldberg and IPO8 phenotypical characteristics**

	<b>MFS</b>	<b>LDS</b>	<b>SGS</b>	<b>IPO8</b>
Gene	<i>FBN1</i>	<i>TGFBR1/2</i> <i>SMAD2/3</i> <i>TGFB2/3</i>	<i>SKI</i>	<i>IPO8</i>
Inheritance	AD	AD	AD – <i>de novo</i>	AR
Ectopia lentis	+++	-	-	-
Cleft palate/bifid uvula	-	++	+	+
Hypertelorism	-	++	++	++
Proptosis	-	+	++	++
Craniosynostosis	-	+	+++	-
Arachnodactyly	+++	++	++	++
Tall stature	+++	+	++	-
Pectus deformity	++	++	++	++
Club foot	-	++	+	+
Joint hypermobility	+	++	++	+++
Cervical spine instability	-	++	+	+
Osteo-arthritis	+	++	+	?
Hernia (umbilical, inguinal,...)	+	+	+	+
Aortic root aneurysm	+++	+++	+	+++
Ascending aneurysm	+	++	+	++
Arterial aneurysm	-/+	+++	+	+
Arterial tortuosity	-	+++	+	+
Early aortic dissection	+	++	-	-
BAV/ASD/VSD/PDA	-	+	-	++
Motor developmental delay	-	-	++	++
Intellectual disability	-	-	++	-

-: absent, +: occasional, ++: common, +++: typical clinical feature, MFS: Marfan syndrome, LDS: Loews-Dietz syndrome, SGS, Shprintzen-Goldberg syndrome, TAA: thoracic aortic aneurysm; AD: autosomal dominant, AR: autosomal recessive, BAV: bicuspid aortic valve, ASD: atrial septal defect, VSD: ventricular septal defect, PDA: patent ductus arteriosus.

Six out of eight *IPO8* variants are predicted to result in a premature termination codon and, as a result, to induce nonsense-mediated mRNA decay (NMD). Indeed, in fibroblast cDNA of individual 3-II:3 c.2597\_2601delTTTTC was only observed upon puromycin treatment (Figure S4A). In blood-derived cDNA of the same child, c.1428+5G>A was found to result in exon 13 skipping (Figure S5A-B). *In silico* protein modeling of its predicted resultant in-frame deletion p.(Lys447\_Arg476del) (c.1428+5G>A) suggests abnormal folding due to removal of a single helix (Figure S5C). In fibroblast cDNA of case 1-II:3, the variant allele was seen even in the absence of inhibition of NMD with puromycin, revealing surprising escape from NMD (Figure S4B). Western blotting on fibroblast lysates of individuals 1-II:3 and 3-II:3 using an N-terminal Importin-8 antibody did not show protein presence, in keeping with a loss-of-function mechanism (Figure S4C). In proband 1-II:3, the lack of Importin-8 protein is possibly attributed to translational repression, which previously has been described in other conditions [32], or significant protein instability. For individual 6-II:1 fibroblasts are not available, but *in silico* modeling of the predicted resultant deletion-insertion p.(Thr967\_Glu1006delinsLys) (c.2900-1G>A) suggests removal of the last structured part of the protein (Figure S6), which, based on this region's role in controlling the protein conformation in some other  $\beta$ -importins, may significantly affect protein stability [33-35].

Murine Importin-8 is 92% identical and 95% similar to its human orthologue, rendering mouse a suitable animal model to pursue supportive *in vivo* evidence for a causal relationship between *IPO8* deficiency and TAA. We used a C57Bl/6N *Ipo8*<sup>-/-</sup> model that was previously only known to present with reduced grip strength and diminished vertical activity, suggesting muscle weakness as well as decreased locomotor exploration, respectively [36], and thus corroborating with the observed hypotonia and (possibly associated) motor delay in individuals with *IPO8* bi-allelic variants. Serial transthoracic echocardiography (age 4-32 weeks) of the aortic root at the level of the sinuses of Valsalva and distal ascending aorta in *Ipo8*<sup>-/-</sup> mice and their wild type (WT)

littermates (N=17/group) revealed statistically significant progressive dilatation in mutant mice at both anatomical locations, with aneurysms of the distal ascending aorta already becoming visible at the age of 8-12 weeks ( $p_{\text{root}}=1.3\text{E-}3$  (Figure 2A);  $p_{\text{asc}}=8.4\text{E-}9$  (Figure 2B)). Intriguingly, sex-stratified analyses demonstrated aortic root enlargement in both mutant females (7 *Ipo8*<sup>-/-</sup> vs 8 WT;  $p_{\text{root}_f}=2.3\text{E-}3$  (Figure S7A)) and males (10 *Ipo8*<sup>-/-</sup> vs 9 WT;  $p_{\text{root}_m}=2.3\text{E-}2$  (Figure S7B)), whereas the ascending aortic aneurysm phenotype is very pronounced and only statistically significant in the male *Ipo8*<sup>-/-</sup> animals ( $p_{\text{asc}_f}=6.5\text{E-}2$  (Figure S7C) vs  $p_{\text{asc}_m}=8.4\text{E-}10$  (Figure 2C)). After the last echo at 32 weeks, 14 *Ipo8*<sup>-/-</sup> and 17 WT animals were kept alive until the age of 48 weeks. Of these, three homozygous mutant males (3/9, 33.3%) died from an aortic rupture at the age of 32, 36 and 46 weeks, respectively, while no aortic rupture-related mortality was seen in the homozygous females (0/5, 0%) or WT animals (0/17, 0%).

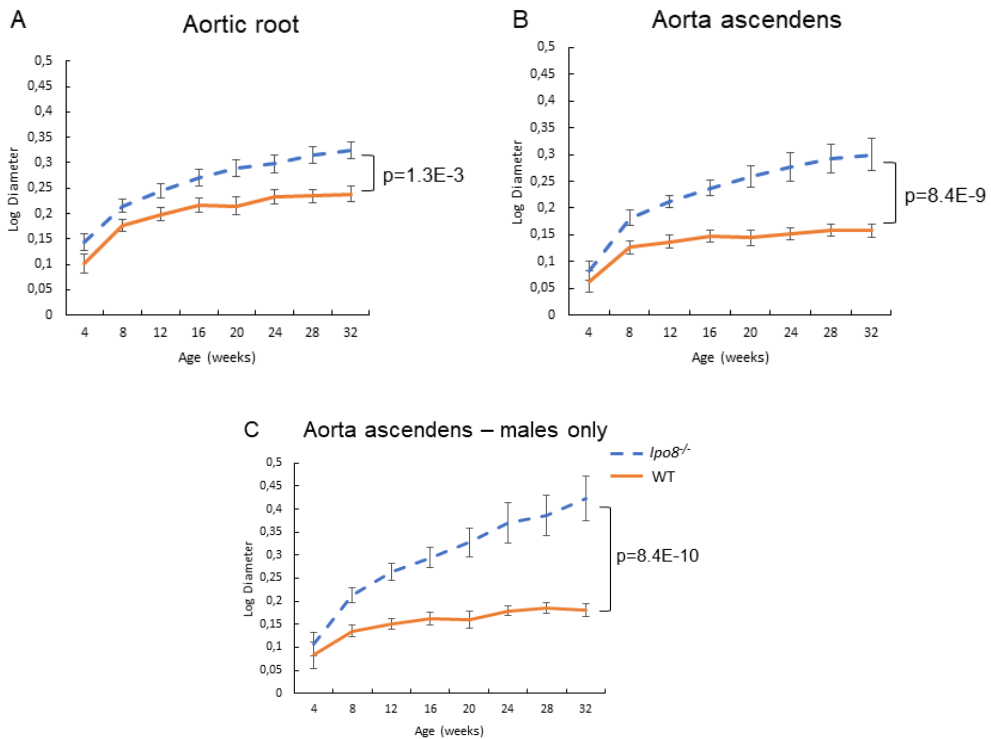


**Figure 2. Progressive TAA development in *Ipo8<sup>-/-</sup>* mice.** A) Log of weight-corrected aortic root diameters in male and female mice combined (N=17/group). B) Log of weight-corrected ascending aortic diameters in male and female mice combined (N=17/group). C) Log of weight-corrected ascending aortic diameters in male mice only (10 *Ipo8<sup>-/-</sup>* vs 9 WT). The error bars show the standard error of the mean (SEM). P-values were calculated using mixed model analysis, which represent the interaction term between genotype and age. WT: wild type.

Sex differences in syndromic TAA penetrance and severity have been reported before, both in mice and humans [37, 38]. Generally, males are more severely affected, exhibiting larger aortas and experiencing dissection and/or rupture more frequently [39, 40]. Several studies in TAA mouse models have attempted to define the basis for the observed sex differences, revealing a context-dependent role for female and male hormone signaling, hypertension and/or exacerbated ERK activation, but no predominant mechanism has been identified [38]. The C57Bl/6N *Ipo8*<sup>-/-</sup> mouse model represents a promising tool to further investigate the TAA sexual dimorphism. Of note, during our echocardiography studies we did not observe severe structural outflow tract defects. Evaluation of lateral and dorsoventral total body X-rays, which are publicly available through the International Mouse Phenotyping Consortium (IMPC) portal, did not show evidence for scoliosis (visual inspection) or increased kyphosis (quantitative evaluation;  $p=2.8E-1$ ) in *Ipo8*<sup>-/-</sup> mice as compared to wild type animals.

Given the fact that the aneurysmal phenotype is most pronounced in males at the level of the distal ascending aorta, we performed further experiments in male mice only. To study the biomechanical properties of distal ascending aortic rings, the 'rodent oscillatory tension set-up to study arterial compliance' (ROTSAC) assay was used [31]. More precisely, *ex vivo* aortic stiffness was assessed at 12 (5 *Ipo8*<sup>-/-</sup> vs 4 WT), 24 (4 *Ipo8*<sup>-/-</sup> vs 4 WT) and 52 (4 *Ipo8*<sup>-/-</sup> vs 2 WT) weeks of age. Different experimental conditions were used to evaluate the involvement of vascular smooth muscle cells (VSMCs) and/or endothelial cells. The Peterson modulus ( $E_p$ ) was first determined in Krebs-Ringer solution at a distention pressure of 80-120 mmHg and 120-160 mmHg, revealing a trend towards higher  $E_p$  values and, thus, stiffer ascending aortas at 120-160 mmHg in 12, 24 and 52 week old *Ipo8*<sup>-/-</sup> male animals as compared to controls (Figure 3, Figure S8). As complete VSMC relaxation by diethylamine NONOate (DEANO) addition or VSMC stimulation with phenylephrine (PE), even upon nitric oxide synthase (NOS) inhibition through N( $\Omega$ )-nitro-L-arginine methyl ester (L-NAME) addition, did not considerably alter the  $E_p$  increase in *Ipo8* null males (Figure 3), increased basal tone nor sustained

VSMC contraction seem to contribute to the increased aortic stiffness. Our data rather point towards an increased passive stiffness of the ascending aorta in male *Ipo8*<sup>-/-</sup> mice throughout life.

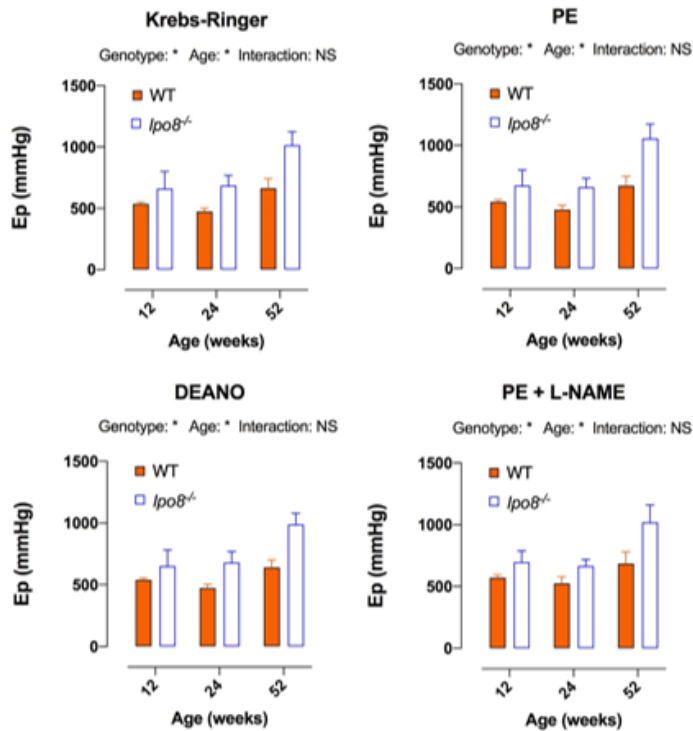


**Figure 3. Trend towards increased ascending aortic passive stiffness in *Ipo8*<sup>-/-</sup> mice at a distention pressure of 120-160 mmHg. Age- and genotype-dependency of the Peterson modulus (*Ep*) of ascending aortic segments of male *Ipo8*<sup>-/-</sup> and wild type mice under control (Krebs-Ringer), maximally relaxed (DEANO) and contracted (PE or PE + L-NAME) conditions at 12 (5 *Ipo8*<sup>-/-</sup> vs 4 WT), 24 (4 *Ipo8*<sup>-/-</sup> vs 4 WT) and 52 (4 *Ipo8*<sup>-/-</sup> vs 2 WT) weeks of age. The error bars show the SEM. Two-way ANOVA *p*-values are shown (\**p* < 0.05). Sidak post-hoc testing did not reveal statistically significant genotype-based differences in *Ep*. PE: Phenylephrine, DEANO: diethylamine NONOate, L-NAME: N(Ω)-nitro-L-arginine methyl ester, *Ep*: Peterson modulus, WT: wild type, NS: non-significant.**

Increased arterial stiffness, an important marker for cardiovascular disease, has previously been observed in genetic TAA mouse models[41] and affected individuals[42]. In an established MFS mouse model, i.e. *Fbn1*<sup>mgR/mgR</sup>, stiffness was

augmented in mutant non-aneurysmal (circa 3-fold) and aneurysmal (circa 4-fold) ascending aortas, which upon histological analysis was shown to correlate with a diffuse loss in elastic fiber integrity[41]. Compared to age-matched controls, TAA cases exhibit a stiffer mechanical response with aortic biomechanical properties resembling those of a significantly older (‘aged’) non-aneurysmal cohort [43]. Given the observed trend towards stiffer ascending aortas in *Ipo8*<sup>-/-</sup> mice (Figure 3) and recurrent prior associations between aortic ECM deterioration and TAA [2], we evaluated the structural ECM integrity using histological elastin and collagen staining in ascending aortic sections of 12- (3 *Ipo8*<sup>-/-</sup> vs 3 WT), 24- (3 *Ipo8*<sup>-/-</sup> vs 3 WT) and 52-week (3 *Ipo8*<sup>-/-</sup> vs 2 WT) old mice. Whereas the collagen content did not differ noticeably (Figure S9A), the elastic fibers were more disorganized and fragmented in mutant males of all age groups as compared to their WT counterparts ( $p_{\text{age-combined}}=5.2\text{E-}4$ ) (Figure 4A-B, Figure S9B).

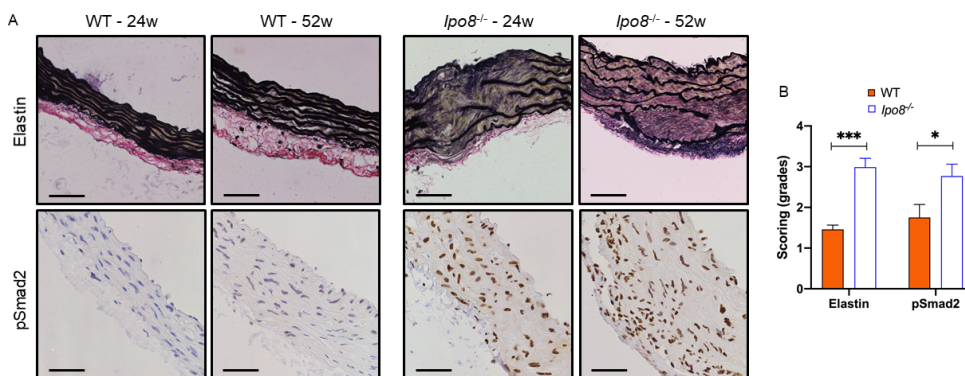


**Figure 4. Elastic fiber deterioration and nuclear pSmad2 accumulation in the ascending aorta of *Ipo8*<sup>-/-</sup> mice.** A) Histological and immunohistochemistry images demonstrating marked elastin disorganization and fragmentation as well as prominent nuclear pSmad2 accumulation in *Ipo8*<sup>-/-</sup> mice. Scale bar = 50 $\mu$ m. B) Elastic fiber integrity scores and nuclear pSmad2 grades of the ascending aorta of all ages combined (12- (3 *Ipo8*<sup>-/-</sup> vs 3 WT), 24- (3 *Ipo8*<sup>-/-</sup> vs 3 WT) and 52-weeks (3 *Ipo8*<sup>-/-</sup> vs 2 WT)). Elastin grades can range from 1 to 4, with grade 1 sections presenting with continuous and well-organized elastic bundles and grade 4 sections displaying vastly disorganized fibers, marked fiber fragmentation and a thickened aortic wall. For pSmad2, grade 1, 2, 3 and 4 denote sections in which respectively <25%, 25-50%, 50-75% and 75-100% of nuclei stained positive. Averaged age-combined scores of blinded observations of three independent

researchers are shown. The error bars depict the SEM. P-values were calculated using two-way ANOVA statistics (\* $p < 0.05$ , \*\*\* $p < 0.001$ ). WT: wild type

Importin 8 is a nuclear transport receptor belonging to the importin- $\beta$  protein family, which has not been linked to human diseases before. It is ubiquitously expressed and becomes upregulated upon TGF- $\beta$ 1 stimulation [44].  $\beta$ -importins translocate cargo molecules such as proteins, RNAs and ribonucleoprotein complexes to the nucleus in a RanGTP-dependent manner. While a specific cargo can be shuttled by multiple  $\beta$ -importins, superior affinity to one of them is often observed. The most established cargoes for human Importin-8 are phosphorylated SMADs 2-3 (pSMAD2-3), SMAD1 and SMAD4 [45], AGO2 [46], mature miRNAs [47], EIF4E [48] and SRP19 [49]. Apart from being a nuclear transport receptor, Importin-8 has been implicated in miRNA-guided gene silencing [46]. Given that individuals with bi-allelic *IPO8* variants phenotypically resemble individuals with TGF- $\beta$ -related aortopathy syndromes such as LDS and SGS and key effectors of the canonical TGF- $\beta$  pathway (i.e. pSMAD2-3, SMAD4) have been reported to be shuttled by Importin-8 [45], a plausible hypothesis is that dysregulated TGF- $\beta$  signaling is involved in the pathogenesis of *IPO8*-related disease (Figure S1). We determined the levels of nuclear pSmad2, an effector of canonical TGF- $\beta$  signaling, in ascending aortic sections of 12- (3 *Ipo8*<sup>-/-</sup> vs 3 WT), 24- (3 *Ipo8*<sup>-/-</sup> vs 3 WT) and 52-week (3 *Ipo8*<sup>-/-</sup> vs 2 WT) old mice. A larger fraction of nuclei stained positive for pSmad2 in *Ipo8*<sup>-/-</sup> mice as compared to WT animals ( $p_{\text{age-combined}}=3.4E-2$ ), suggesting a role for dysregulated TGF- $\beta$  signaling in the pathogenesis of *IPO8*-related TAA (Figure 4A-B, Figure S9C).

Subsequent RT-qPCR analysis for nine TGF- $\beta$  superfamily-related genes (i.e. *Tgfb1*, *Tgfb2*, *Smad4*, *Smad6*, *Smad7*, *Mmp2*, *Ccn2* (*Ctgf*), *Eln* and *Serpine1* (*Pai1*)) in ascending aortic samples of 16-week old *Ipo8*<sup>-/-</sup> and WT males (N=12/group) revealed significantly reduced *Smad6* ( $p=6.0E-3$ ) and *Smad7* ( $p=3.6E-2$ ) mRNA expression in the mutant

animals, along with a significant increase in *Mmp2* ( $p=4.2E-3$ ) and *Ccn2* (*Ctgf*) ( $p=7.8E-3$ ) (Figure 5).

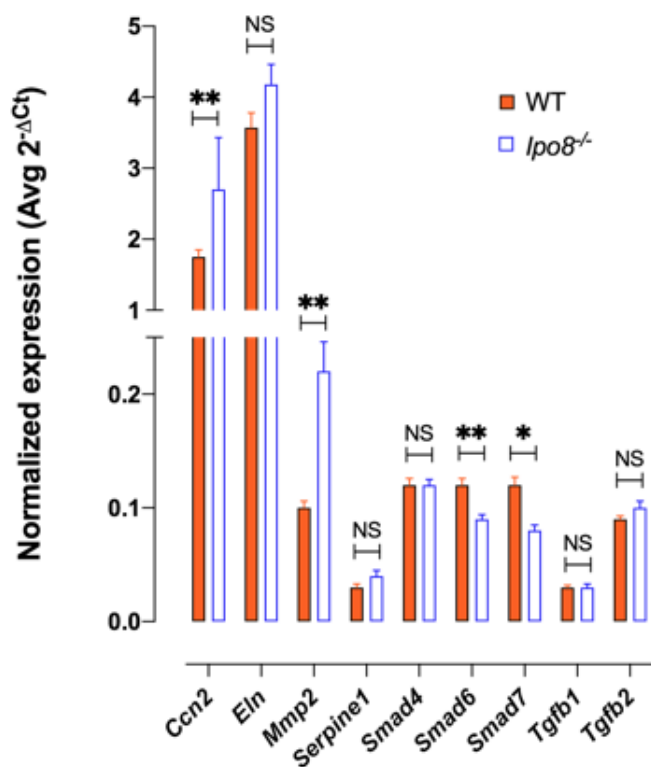


**Figure 5.** mRNA expression analysis of TGF- $\beta$ -related genes reveals decreased *Smad6* and *Smad7* levels as well as increased *Mmp2* and *Ccn2* (*Ctgf*) levels in the ascending aorta of *lpo8*<sup>-/-</sup> mice. Ascending aortic samples of 16-weeks old *lpo8*<sup>-/-</sup> and WT males were used ( $N=12$ /group). The error bars depict the SEM.  $P$ -values were calculated using mixed model statistics (\* $p < 0.05$ , \*\* $p < 0.01$ ). WT: wild type, NS: non-significant

SMAD6 and 7 inhibit SMAD-dependent and -independent TGF- $\beta$  family signaling through various mechanisms [50]. Whereas SMAD6 preferentially inhibits bone morphogenetic protein (BMP)-related signaling [51], SMAD7 impedes both TGF- $\beta$ - and BMP-induced signaling [52]. In the absence of SMAD7, TGF- $\beta$  receptor activation is

augmented, resulting in excessive SMAD2/3 phosphorylation. The detected decrease in *Smad7* mRNA levels in the *Ipo8*<sup>-/-</sup> aortic walls might thus be directly linked to the observed increase in nuclear pSmad2 levels. SMAD6, on the other hand, has mostly been linked to BMP signaling, which is less well studied in the context of TAA development. Nonetheless, our group identified loss-of-function *SMAD6* variants as a cause of bicuspid aortic valve-related TAA [53, 54], demonstrating a mechanistic link between SMAD6 deficiency and TAA development. *MMP2* and *CCN2 (CTGF)* are prototypical downstream transcriptional targets of the TGF- $\beta$  signaling pathway [55]. *MMP2* belongs to the family of matrix metalloproteinases, which mediate the physiological turnover of the aortic ECM by degrading structural ECM proteins, including collagen and elastin [56]. In TAA cases and mouse models, *MMP2* levels and/or activity are strongly increased [57-59]. Moreover, *Mmp2* deletion in *Fbn1*<sup>mgR/mgR</sup> mice inhibited TGF- $\beta$  activation and subsequent Smad2 and Erk1/2 phosphorylation [60], which significantly prolonged the lifespan of the MFS *Fbn1*<sup>mgR/mgR</sup> mice [60]. As such, increased *Mmp2* expression might connect increased TGF- $\beta$  signaling and impaired elastic fiber integrity in our *Ipo8*<sup>-/-</sup> mouse model. *CCN2 (CTGF)* is a multifunctional protein that is involved in ECM remodeling [55]. Overexpression of *CCN2 (CTGF)* has been proven to be associated with TAA development [61] and was previously been shown to be upregulated in the aortic walls of individuals with LDS [4, 7]. Interestingly, elastic fiber fragmentation but normal collagen content, as well as reduced *Smad6* and *Smad7* mRNA expression levels and higher *Mmp* activity were also described in aneurysmal aortic tissue specimens and/or VSMCs of *Smad3*<sup>-/-</sup> mice, an established LDS model that presents with TAA already at the age of 6 weeks [62]. Together, our histological, immunohistochemistry and RT-qPCR findings suggest a link between *IPO8* deficiency and dysregulated TGF- $\beta$  signaling. Moreover, they recapitulate prior observations in an established LDS mouse model, further relating *IPO8*-related TAA to the LDS disease spectrum.

## 4 Conclusion

---

In conclusion, we describe a syndrome caused by bi-allelic loss-of-function variants in *IPO8*. The human and mouse phenotypes caused by Importin-8 loss-of-function are characterized by severe early-onset TAA development. Our immunohistochemistry and RT-qPCR studies of murine *Ipo8*-deficient aortic tissue reveal pathophysiological mechanisms that have previously been described in clinically overlapping TGF- $\beta$ -related signalopathies. Further research is warranted to obtain more in-depth insight into the disease's clinical course and mechanisms. First, identification of additional individuals with bi-allelic *IPO8* variants will shed better light on the variability with respect to disease expressivity and penetrance. Moreover, longitudinal follow-up of affected individuals will provide information on aortic/arterial dissection or rupture risk. Interestingly, our clinical findings are corroborated by the observations of Ziegler et al, this issue<sup>47</sup> who describe aortic dilatation in 11 out of 12 individuals with bi-allelic *IPO8* variants. Second, it remains to be determined if and how abnormal cytosol-to-nucleus shuttling elicits *IPO8*-related disease and dysregulated TGF- $\beta$  signaling in aneurysmal aortic walls. Finally, as we predominantly focused on the TAA phenotype, it would be interesting to have a closer look at the mechanisms involved in the other affected organ systems, especially the neuromuscular system in order to explain the motor developmental delay that was observed in individuals with *IPO8* bi-allelic variants.

## 5 References

---

1. Faggion Vinholo, T., et al., *Genes Associated with Thoracic Aortic Aneurysm and Dissection: 2019 Update and Clinical Implications*. Aorta (Stamford), 2019. **7**(4): p. 99-107.
2. Verstraeten, A., I. Luyckx, and B. Loeys, *Aetiology and management of hereditary aortopathy*. Nat Rev Cardiol, 2017.
3. Dietz, H.C., et al., *Marfan syndrome caused by a recurrent de novo missense mutation in the fibrillin gene*. Nature, 1991. **352**(6333): p. 337-9.

4. Loeys, B.L., et al., *A syndrome of altered cardiovascular, craniofacial, neurocognitive and skeletal development caused by mutations in TGFBR1 or TGFBR2*. *Nat Genet*, 2005. **37**(3): p. 275-81.
5. Cannaeerts, E., et al., *Novel pathogenic SMAD2 variants in five families with arterial aneurysm and dissection: further delineation of the phenotype*. *J Med Genet*, 2019. **56**(4): p. 220-227.
6. Micha, D., et al., *SMAD2 Mutations Are Associated with Arterial Aneurysms and Dissections*. *Hum Mutat*, 2015. **36**(12): p. 1145-9.
7. van de Laar, I.M., et al., *Mutations in SMAD3 cause a syndromic form of aortic aneurysms and dissections with early-onset osteoarthritis*. *Nat Genet*, 2011. **43**(2): p. 121-6.
8. Boileau, C., et al., *TGFBR2 mutations cause familial thoracic aortic aneurysms and dissections associated with mild systemic features of Marfan syndrome*. *Nat Genet*, 2012.
9. Lindsay, M.E., et al., *Loss-of-function mutations in TGFBR2 cause a syndromic presentation of thoracic aortic aneurysm*. *Nat Genet*, 2012. **44**(8): p. 922-7.
10. Bertoli-Avella, A.M., et al., *Mutations in a TGF-beta ligand, TGFBR3, cause syndromic aortic aneurysms and dissections*. *J Am Coll Cardiol*, 2015. **65**(13): p. 1324-36.
11. Cannaeerts, E., et al., *TGF-beta signalopathies as a paradigm for translational medicine*. *Eur J Med Genet*, 2015. **58**(12): p. 695-703.
12. Doyle, A.J., et al., *Mutations in the TGF-beta repressor SKI cause Shprintzen-Goldberg syndrome with aortic aneurysm*. *Nat Genet*, 2012.
13. Schepers, D., et al., *The SMAD-binding domain of SKI: a hotspot for de novo mutations causing Shprintzen-Goldberg syndrome*. *Eur J Hum Genet*, 2015. **23**(2): p. 224-8.
14. Vandeweyer, G., et al., *VariantDB: a flexible annotation and filtering portal for next generation sequencing data*. *Genome Med*, 2014. **6**(10): p. 74.
15. Turnbull, C., et al., *The 100 000 Genomes Project: bringing whole genome sequencing to the NHS*. *BMJ*, 2018. **361**: p. k1687.
16. Yang, Y., et al., *Molecular findings among patients referred for clinical whole-exome sequencing*. *JAMA*, 2014. **312**(18): p. 1870-9.
17. Makrythanasis, P., et al., *Biallelic variants in KIF14 cause intellectual disability with microcephaly*. *Eur J Hum Genet*, 2018. **26**(3): p. 330-339.
18. Retterer, K., et al., *Clinical application of whole-exome sequencing across clinical indications*. *Genet Med*, 2016. **18**(7): p. 696-704.
19. Chaudhury, S., S. Lyskov, and J.J. Gray, *PyRosetta: a script-based interface for implementing molecular modeling algorithms using Rosetta*. *Bioinformatics*, 2010. **26**(5): p. 689-91.
20. Matsuura, Y. and M. Stewart, *Structural basis for the assembly of a nuclear export complex*. *Nature*, 2004. **432**(7019): p. 872-7.

21. Bienert, S., et al., *The SWISS-MODEL Repository-new features and functionality*. Nucleic Acids Res, 2017. **45**(D1): p. D313-D319.
22. Yang, J., et al., *The I-TASSER Suite: protein structure and function prediction*. Nat Methods, 2015. **12**(1): p. 7-8.
23. Shaikhqasem, A., et al., *Characterization of Inhibition Reveals Distinctive Properties for Human and Saccharomyces cerevisiae CRM1*. J Med Chem, 2020. **63**(14): p. 7545-7558.
24. Conway, P., et al., *Relaxation of backbone bond geometry improves protein energy landscape modeling*. Protein Sci, 2014. **23**(1): p. 47-55.
25. Alford, R.F., et al., *The Rosetta All-Atom Energy Function for Macromolecular Modeling and Design*. J Chem Theory Comput, 2017. **13**(6): p. 3031-3048.
26. Stranges, P.B. and B. Kuhlman, *A comparison of successful and failed protein interface designs highlights the challenges of designing buried hydrogen bonds*. Protein Sci, 2013. **22**(1): p. 74-82.
27. Huang, P.S., et al., *RosettaRemodel: a generalized framework for flexible backbone protein design*. PLoS One, 2011. **6**(8): p. e24109.
28. Ferla, M.P., et al., *MichelaNglo: sculpting protein views on web pages without coding*. Bioinformatics, 2020. **36**(10): p. 3268-3270.
29. Valenzuela, D.M., et al., *High-throughput engineering of the mouse genome coupled with high-resolution expression analysis*. Nat Biotechnol, 2003. **21**(6): p. 652-9.
30. Laws, N. and A. Hoey, *Progression of kyphosis in mdx mice*. J Appl Physiol (1985), 2004. **97**(5): p. 1970-7.
31. Leloup, A.J., et al., *A novel set-up for the ex vivo analysis of mechanical properties of mouse aortic segments stretched at physiological pressure and frequency*. J Physiol, 2016. **594**(21): p. 6105-6115.
32. You, K.T., et al., *Selective translational repression of truncated proteins from frameshift mutation-derived mRNAs in tumors*. PLoS Biol, 2007. **5**(5): p. e109.
33. Zachariae, U. and H. Grubmuller, *A highly strained nuclear conformation of the exportin Cse1p revealed by molecular dynamics simulations*. Structure, 2006. **14**(9): p. 1469-78.
34. Yamazawa, R., et al., *Structural Basis for Selective Binding of Export Cargoes by Exportin-5*. Structure, 2018. **26**(10): p. 1393-1398 e2.
35. Koyama, M., N. Shirai, and Y. Matsuura, *Structural insights into how Yrb2p accelerates the assembly of the Xpo1p nuclear export complex*. Cell Rep, 2014. **9**(3): p. 983-95.
36. Dickinson, M.E., et al., *High-throughput discovery of novel developmental phenotypes*. Nature, 2016. **537**(7621): p. 508-514.
37. Robinet, P., et al., *Consideration of Sex Differences in Design and Reporting of Experimental Arterial Pathology Studies-Statement From ATVB Council*. Arterioscler Thromb Vasc Biol, 2018. **38**(2): p. 292-303.

38. Anderson, N.K., E.E. Juzwiak, and H.C. Dietz, *A seX(X/Y) Article on Marfan Syndrome*. J Am Heart Assoc, 2020. **9**(20): p. e018814.
39. Roman, M.J., et al., *Associations of Age and Sex With Marfan Phenotype: The National Heart, Lung, and Blood Institute GenTAC (Genetically Triggered Thoracic Aortic Aneurysms and Cardiovascular Conditions) Registry*. Circ Cardiovasc Genet, 2017. **10**(3).
40. Renard, M., et al., *Sex, pregnancy and aortic disease in Marfan syndrome*. PLoS One, 2017. **12**(7): p. e0181166.
41. Bellini, C., et al., *Differential ascending and descending aortic mechanics parallel aneurysmal propensity in a mouse model of Marfan syndrome*. J Biomech, 2016. **49**(12): p. 2383-2389.
42. Humphrey, J.D. and G. Tellides, *Central artery stiffness and thoracic aortopathy*. Am J Physiol Heart Circ Physiol, 2019. **316**(1): p. H169-H182.
43. Sulejmani, F., et al., *Biomechanical properties of the thoracic aorta in Marfan patients*. Ann Cardiothorac Surg, 2017. **6**(6): p. 610-624.
44. Hu, X., et al., *Mitogen-activated protein kinase inhibitors reduce the nuclear accumulation of phosphorylated Smads by inhibiting Imp 7 or Imp 8 in HepG2 cells*. Oncol Lett, 2018. **15**(4): p. 4867-4872.
45. Yao, X., et al., *Preferential utilization of Imp7/8 in nuclear import of Smads*. J Biol Chem, 2008. **283**(33): p. 22867-74.
46. Weinmann, L., et al., *Importin 8 is a gene silencing factor that targets argonaute proteins to distinct mRNAs*. Cell, 2009. **136**(3): p. 496-507.
47. Wei, Y., et al., *Importin 8 regulates the transport of mature microRNAs into the cell nucleus*. J Biol Chem, 2014. **289**(15): p. 10270-5.
48. Volpon, L., et al., *Importin 8 mediates m7G cap-sensitive nuclear import of the eukaryotic translation initiation factor eIF4E*. Proc Natl Acad Sci U S A, 2016. **113**(19): p. 5263-8.
49. Dean, K.A., et al., *Signal recognition particle protein 19 is imported into the nucleus by importin 8 (RanBP8) and transportin*. J Cell Sci, 2001. **114**(Pt 19): p. 3479-85.
50. Miyazawa, K. and K. Miyazono, *Regulation of TGF-beta Family Signaling by Inhibitory Smads*. Cold Spring Harb Perspect Biol, 2017. **9**(3).
51. Goto, K., et al., *Selective inhibitory effects of Smad6 on bone morphogenetic protein type I receptors*. J Biol Chem, 2007. **282**(28): p. 20603-11.
52. Hanyu, A., et al., *The N domain of Smad7 is essential for specific inhibition of transforming growth factor-beta signaling*. J Cell Biol, 2001. **155**(6): p. 1017-27.
53. Gillis, E., et al., *Candidate Gene Resequencing in a Large Bicuspid Aortic Valve-Associated Thoracic Aortic Aneurysm Cohort: SMAD6 as an Important Contributor*. Front Physiol, 2017. **8**: p. 400.

54. Luyckx, I., et al., *Confirmation of the role of pathogenic SMAD6 variants in bicuspid aortic valve-related aortopathy*. Eur J Hum Genet, 2019. **27**(7): p. 1044-1053.
55. Lipson, K.E., et al., *CTGF is a central mediator of tissue remodeling and fibrosis and its inhibition can reverse the process of fibrosis*. Fibrogenesis Tissue Repair, 2012. **5**(Suppl 1): p. S24.
56. Van Doren, S.R., *Matrix metalloproteinase interactions with collagen and elastin*. Matrix Biol, 2015. **44-46**: p. 224-31.
57. Meffert, P., et al., *Characterization of serum matrix metalloproteinase 2/9 levels in patients with ascending aortic aneurysms*. Interact Cardiovasc Thorac Surg, 2017. **24**(1): p. 20-26.
58. Wang, C., et al., *Angiotensin II Induces an Increase in Matrix Metalloproteinase 2 Expression in Aortic Smooth Muscle Cells of Ascending Thoracic Aortic Aneurysms Through JNK, ERK1/2, and p38 MAPK Activation*. J Cardiovasc Pharmacol, 2015. **66**(3): p. 285-93.
59. Chung, A.W., et al., *Loss of elastic fiber integrity and reduction of vascular smooth muscle contraction resulting from the upregulated activities of matrix metalloproteinase-2 and -9 in the thoracic aortic aneurysm in Marfan syndrome*. Circ Res., 2007. **101**(5): p. 512-22. Epub 2007 Jul 19.
60. Xiong, W., et al., *MMP-2 regulates Erk1/2 phosphorylation and aortic dilatation in Marfan syndrome*. Circ Res, 2012. **110**(12): p. e92-e101.
61. Branchetti, E., et al., *Oxidative stress modulates vascular smooth muscle cell phenotype via CTGF in thoracic aortic aneurysm*. Cardiovasc Res, 2013. **100**(2): p. 316-24.
62. van der Pluijm, I., et al., *Defective Connective Tissue Remodeling in Smad3 Mice Leads to Accelerated Aneurysmal Growth Through Disturbed Downstream TGF-beta Signaling*. EBioMedicine, 2016. **12**: p. 280-294.

## 6 Supplemental

---

### 6.1 Supplemental case reports

Proband 1-II:3 is a 10-years old boy clinically diagnosed with Shprintzen-Goldberg syndrome (SGS) and born as the third child from healthy consanguineous parents. Four male siblings are in good health. Growth parameters at age 7 years 11 months: 124 cm (P10-P25), weight 21 kg (P3-P5), head circumference 55 cm (P97). He has severe dolichocephaly with bilateral parietal bossing, hypertelorism, eye proptosis and eyelid ptosis (left>right), and a high arched palate but normal uvula. With respect to the

musculoskeletal system, arachnodactyly, 2<sup>nd</sup> toe camptodactyly, pes planum, joint hyperlaxity (Beighton 9/9) are apparent. He presents with bell-shaped thorax and pectus excavatum. In addition, his medical history is significant for neonatal hypotonia, mild developmental delay (independent walk at 17 months, no speech delay) and an umbilical hernia. He has normal cognitive functions and no learning difficulties. From a cardiovascular point of view, he presents with an atrial septal defect (ASD, type II) as well as severe dilatation of the aortic root (Z=3.5) and ascending aorta (Z=5.7) (last echocardiography at 10 years 8 months). The aortic dilatation remains stable under losartan treatment.

Proband 2-II:1 is an 8-years old boy with a suspected clinical diagnosis of Loeys-Dietz syndrome (LDS). He is the only child of unrelated, healthy parents. Mother had two unexplained miscarriages at respectively 8 and 20 weeks. Growth parameters at age 8 years are: height 127 cm (P24), weight 19.96 kg (P1). Facial characteristics include dolichocephaly and frontal bossing, hypertelorism, eyelid ptosis (left>right), a slightly broader and flat nasal bridge, a tubular shape nose, malar hypoplasia, retrognathia and a small mouth with tented upper lip. He has a slightly arched palate with submucous cleft palate and a broad uvula. Arachnodactyly, joint hypermobility, pectus excavatum, pes planum, scoliosis and a kyphotic posture are the most apparent musculoskeletal manifestations. Cervical spine anomalies include dysplastic left occipital condyle and C1 vertebral body with abnormal articulation, and minimal widening of the left atlantoaxial joint and mild malalignment of the right occipital condyle and right lateral mass of C1. The body of C2 is also dysplastic and the odontoid peg lies to the left of the midline and points posteriorly. His skin is soft but translucent, with a large, depigmented patch on the abdomen, and he bruises easily. Additional manifestations include hypotonia, developmental delay, delayed secondary dentition, rectal prolapse and umbilical and bilateral inguinal hernias. At age 6 years and 5 months, he presented with possible transient ischemic attacks which were treated with aspirin. Brain MRI revealed moderate-sized middle cranial fossa arachnoid cysts, right slightly larger than the left.

His last echocardiographic evaluation at age 8 showed aneurysm at the level of the aortic root (Z=10), sinotubular junction (Z=5.4) and ascending aorta (Z=8.7) with mild aortic valve insufficiency and mild mitral valve prolapse with mild insufficiency. More extended imaging with CT angiography demonstrated dilatation of the common carotid arteries and aortic arch, along with marked tortuosity of the aorta, the common carotid and internal carotid artery and mild tortuosity of the vertebral arteries. There is also enlargement of the anterior and middle cerebral arteries bilaterally. The basilar artery is tortuous but otherwise unremarkable. No aneurysms are associated with the circle of Willis or its major branches. Additional cardiac manifestations include patent ductus arteriosus (PDA), a small ASD, mitral valve prolapse as well as mild mitral and aortic regurgitation. Finally, kidney ultrasound revealed multiple small cysts in the left kidney.

Proband 3-II:3 is born as the fourth child of healthy non-consanguineous parents. In the neonatal period she underwent surgery for ventricular septal defect (VSD), ASD and PDA. She presented with significant axial and peripheral hypotonia with poor swallowing necessitating naso-gastric tube feeding. She experienced significant motor developmental delay and joint laxity with multiple joint dislocations of hips and ankles. In addition, she presents with pes planum. She had an extensive neurological work-up with EEG, EMG and brain MRI (which showed aspecific patchy hyperintensities within the white matter and striatum). A muscle biopsy showed small fiber size but no other significant features of myopathy. Craniofacial features encompass frontal bossing with bitemporal flattening, downturned corners of the mouth with a high arched palate. Ophthalmological features include bluish sclerae, megalocornea and cupped optic disc, but a normal vision. Skeletal findings are prominent pectus excavatum as well as prominent metopic and cranial sutures. Most recent echocardiographic evaluation at age 7 years 5 months revealed aortic dilatation at the level of the sinuses (Z=3.58), sinotubular junction (Z=4.99) and ascending aorta (Z=2.68).

Individuals 4-II:3 and 4-II:4 are two brothers of respectively 6 and 10 years old, born to consanguineous parents of Saudi-Arabian descent. Both are followed because of suspected LDS-like connective tissue disorders. Both present with similar craniofacial features including dolichocephaly, frontal bossing with hypertelorism and high arched palate. In addition to joint hypermobility and pes equinovarus, they have arachnodactyly and pectus excavatum. The eldest brother has developed scoliosis and X-ray revealed sagittal clefts of the midthoracic vertebrae. He also has a history of umbilical hernia. Both present with delayed motor development but no intellectual disability. Cardiovascular evaluation has revealed VSD and significant aortic dilatation, mostly affecting the aortic root in both brothers (Z-score = 5.7 and 6). The youngest brother has a history of PDA.

Proband 5-II:2 was born as the second daughter of healthy consanguineous Iranian parents (first cousins). At birth, she was diagnosed with bilateral club feet for which she underwent surgery, knee joint hypermobility, arachnodactyly, pectus excavatum, umbilical hernia and dysmorphic facies, including frontal bossing, eye proptosis (L>R), hypertelorism, downslanting palpebral fissures, retrognathia and cleft palate with a bifid uvula. Karyotyping was normal (46 XX). Echocardiography at 42 months revealed a bicuspid aortic valve (BAV), dilated coronary sinus, patent foramen ovale (PFO), small aneurysmal membranous VSD and dilated pulmonary artery. Aortic measurements were in normal range: aortic root 15 mm (Z=0.5) and 12 mm (Z=0.18). Growth parameters at 3 yrs 9 months: height 92 cm (P3), weight 11kg (<P3), head circumference 47.5 cm. Mild development delay was observed, i.e. mostly motor development, with walking at 2.5 years old. She is speaking four-word sentences.

Proband 6-II:1 (19 yrs old) was born as the first child of consanguineous parents (first cousins). He was born at term and diagnosed with severe hypotonia in infancy, with global developmental delays noted in childhood. He received occupational, physical, and speech therapies as a young child and required special education in school.

Umbilical and inguinal hernias required surgical repair. He began having severe headaches around age 8 and brain MRI identified cervical spine instability (cervical stenosis and os odontoideum) and arterial tortuosity. Cervical spine anomalies were treated with cervical laminectomy with occipital cervical fusion at age 15. He was genetically evaluated and had his first echocardiogram at age 16, which identified aortic root dilation (3.8 cm, Z score 4.4). Subsequent MRAngio at age 16yrs9mo demonstrated intra and extracranial arterial tortuosity (most prominently involving the superior cervical internal carotid arteries, with dilation of the left internal carotid artery at the carotid bifurcation), as well as dural ectasia. His physical exam was notable for arachnodactyly with positive wrist and thumb sign, scoliosis, dolichocephaly, micrognathia, malar flattening, hypertelorism, downslanting palpebral fissures, bifid uvula, and a mild asymmetric pectus excavatum. His mother and younger maternal half-brother both presented with learning disability. Importantly, clinical genetic testing included a microarray which identified a duplication of uncertain significance (1.779 Mb gain of 19q13.41) and multiple regions of homozygosity (5%). Unfortunately, segregation analysis of this duplication was not possible.

## 6.2 Supplemental Figures

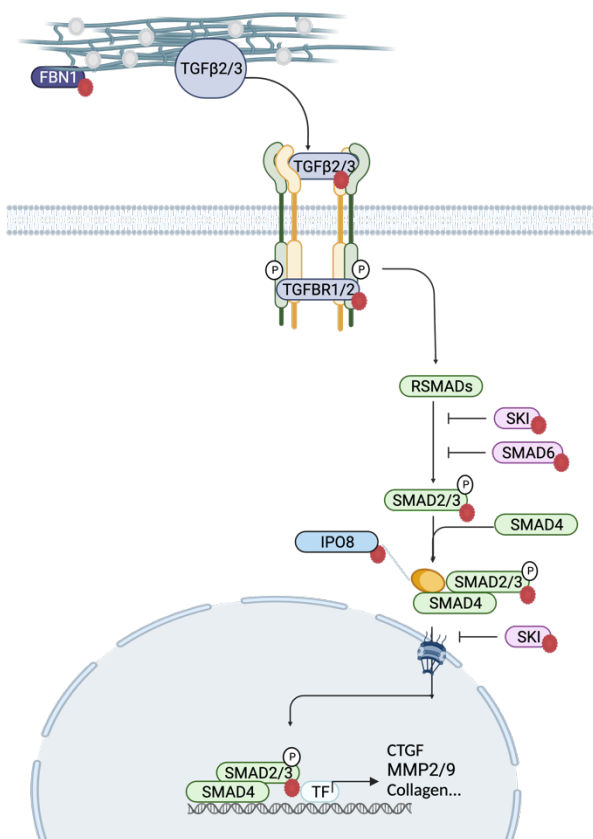


**Figure S1. Genetic defects in components of the extracellular matrix and TGF-β signaling pathway cause syndromic TAA.** In Marfan syndrome individuals, *FBN1* mutations lead to an uncontrolled release of TGF-β ligands, resulting in downstream overexpression of TGF-β target genes. Loeys-Dietz syndrome results from loss-of-function mutations in important ligands from the canonical transforming growth factor β (TGF-β) signaling pathway (i.e. *TGFBR1/2*, *SMAD2/3*, *TGFBR2/3*), yet also leading to a paradoxical increase in TGF-β signaling. Shprintzen-Goldberg syndrome is caused by inactivation of *SKI*, a proto-oncogene that activates a negative feedback loop preventing translocation of the *SMAD2/3*-*SMAD4* complex to the nucleus. Importin-8 translocates cargoes from the cytosol to the nucleus in a RanGTP-dependent manner. We hypothesize that *IPO8* deficiency leads to miss-shuttling of TGF-β related cargoes, leading to aortopathy, comparable to Marfan syndrome, Loeys-Dietz syndrome and Shprintzen-Goldberg syndrome. *MFS*: Marfan syndrome, *LDS*: Loeys-Dietz syndrome, *SGS*: Shprintzen-Goldberg syndrome.

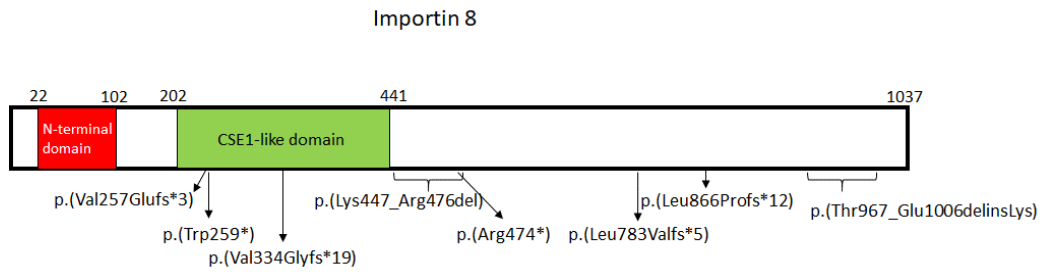


**Figure S2. Schematic protein representation of the identified bi-allelic Importin-8 variants.**



**Figure S3. Proportionate growth in individuals with bi-allelic *IPO8* variants.**

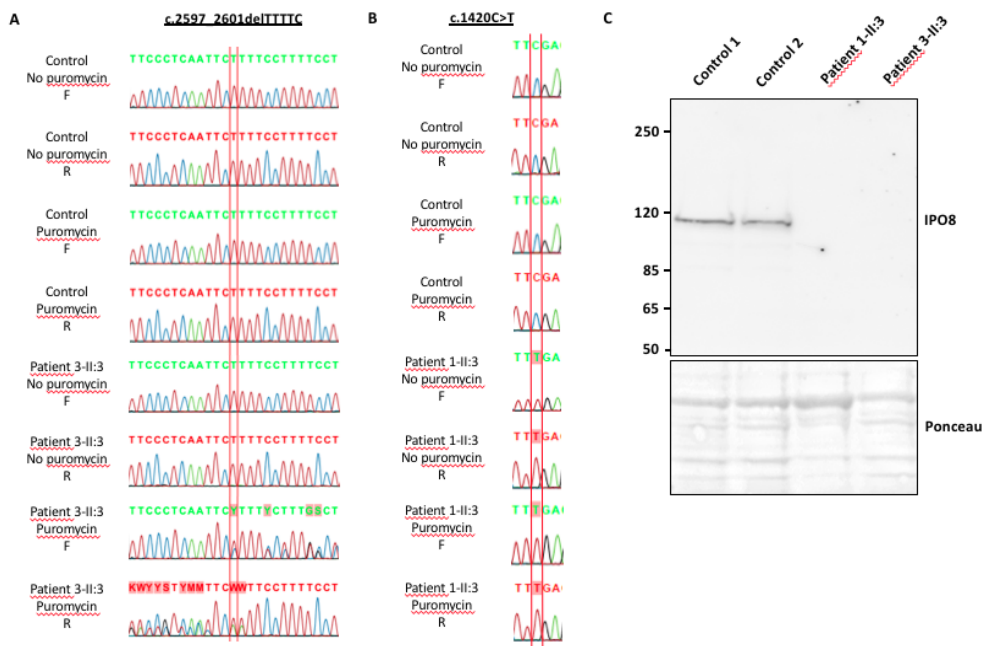


**Figure S4. Complete lack of Importin-8 in mutant fibroblasts despite opposing evidence for nonsense-mediated mRNA decay.** A) cDNA sequencing of *c.2597\_2601delTTTTTC* in puromycin-treated and non-treated fibroblasts of individual 3-II:3 and a healthy control. The mutant allele is only observed in the presence of puromycin, being consistent with nonsense-mediated mRNA decay. B) cDNA sequencing of *c.1420C>T* in puromycin-treated and non-treated fibroblasts of individual 1-II:3 and a healthy control. The mutant allele is observed both in the presence and absence of puromycin, indicating escape from nonsense-mediated mRNA decay. C) Western blotting for Importin-8 using an N-terminal antibody, revealing absence of protein in fibroblasts of individuals 1-II:3 and 3-II:3.

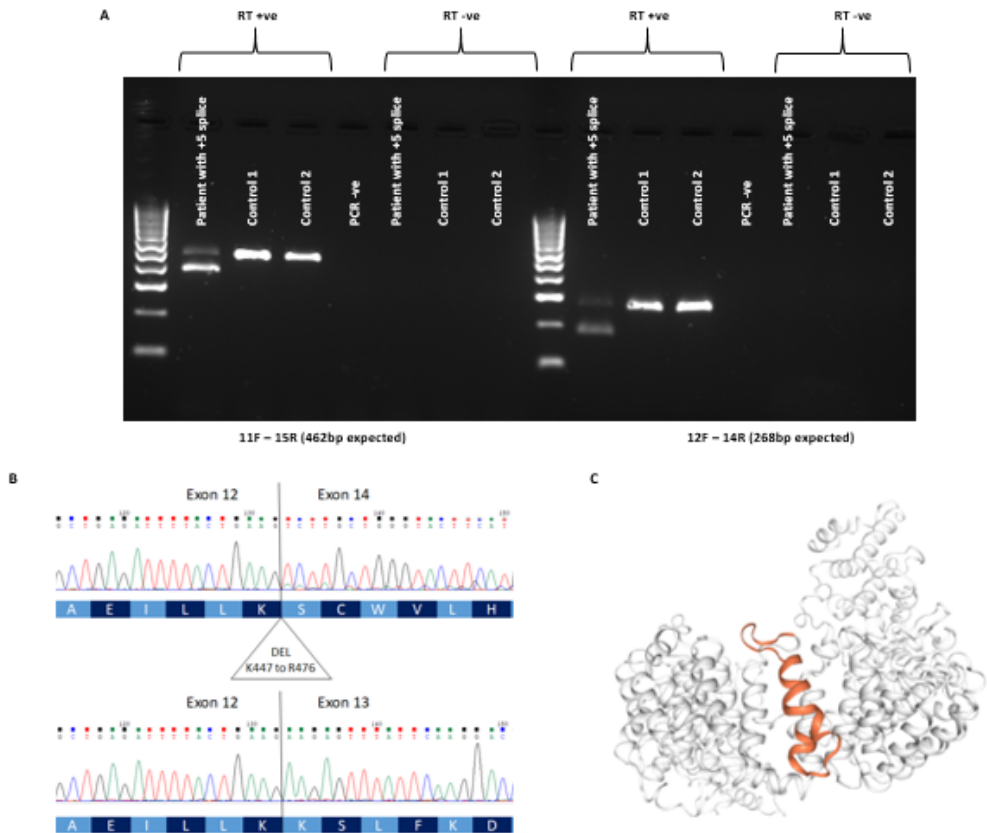


**Figure S5. c.1428+5G>A in individual 3-II:3 leads to exon 13 skipping and a predicted in-frame deletion of 30 amino acids (p.(Lys447\_Arg476del)).** A) PCR analysis of blood-derived cDNA of individual 3-II:3 using two different primer pairs demonstrates the presence of a shorter transcript, whereas only the wild type transcript is present in control samples. B) Sanger sequencing of the RT-PCR product confirms in-frame skipping of exon 13. The representative sequencing electropherograms that are shown are from a forward primer in exon 11. C) In silico protein modeling of the predicted p.(Lys447\_Arg476del) allele suggests abnormal protein folding due to loss of a single helix (indicated in orange).

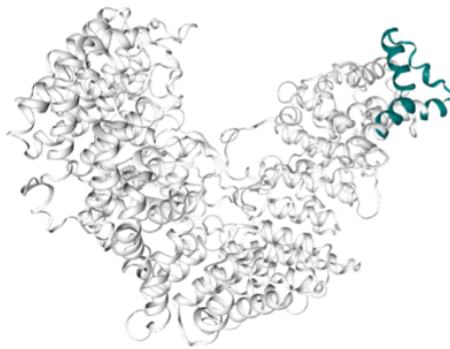


**Figure S6.** *In silico* protein modeling of the predicted p.(Thr967\_Glu1006delinsLys) allele suggests abnormal protein folding due to loss of the last structured part of the protein (indicated in green).

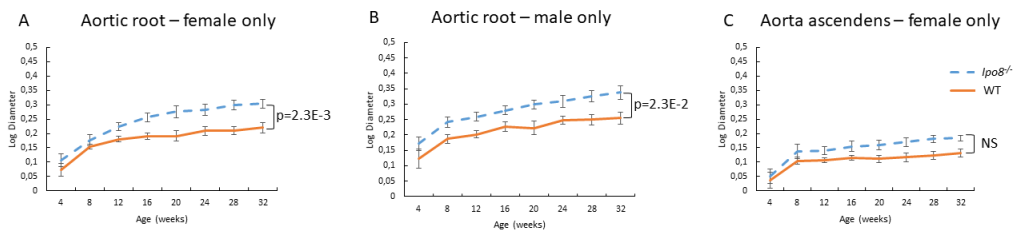


**Figure S7.** Sex-tailored echocardiography analyses reveal significant TAA formation in both male and female *Ipo8*<sup>-/-</sup> mice at the level of the Sinuses of Valsalva, whereas the ascending aortic aneurysm phenotype is largely restricted to *Ipo8*<sup>-/-</sup> males. A) Log of weight-corrected aortic root diameters in female mice only (7 *Ipo8*<sup>-/-</sup> vs 8 WT). B) Log of weight-corrected aortic root diameters in male mice only (10 *Ipo8*<sup>-/-</sup> vs 9 WT). C) Log of weight-corrected ascending aortic diameters in female mice only (7 *Ipo8*<sup>-/-</sup> vs 8 WT). The error bars show the standard error of the mean (SEM). P-values were calculated using mixed model analysis, which represent the interaction term between genotype and age. NS: non-significant, WT: wild type.

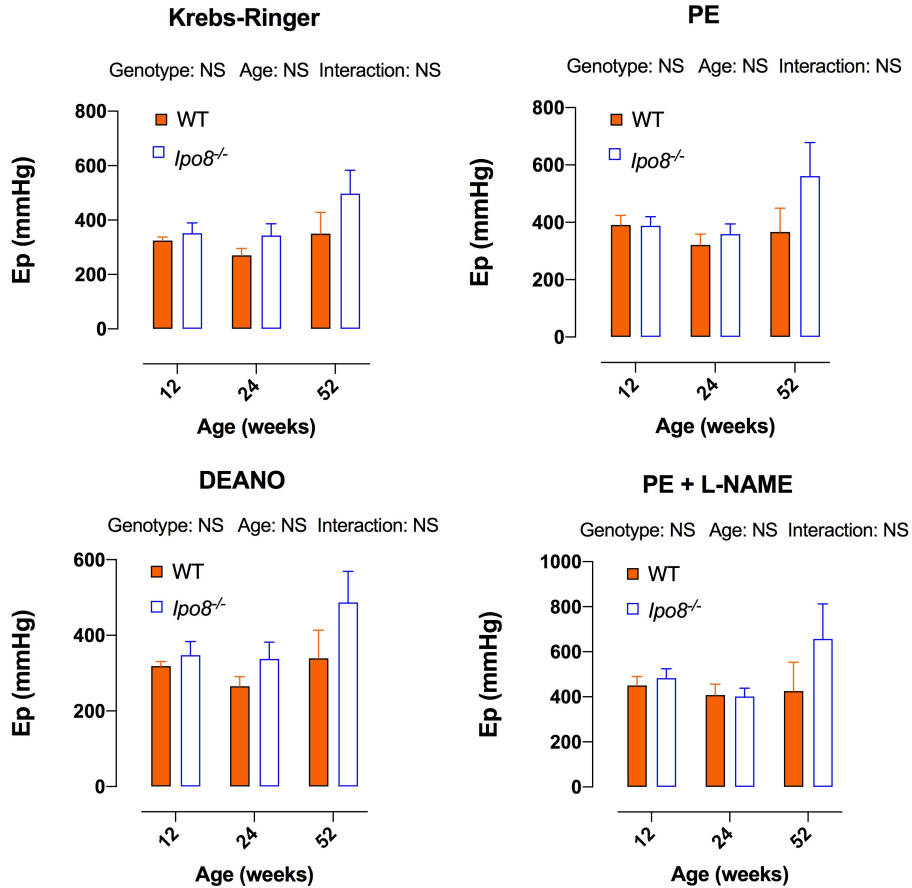


**Figure S8. Normal ascending aorta stiffness in *Ipo8*<sup>-/-</sup> mice at a distention pressure of 80-120 mmHg.** Age- and genotype-dependency of the Peterson modulus (*Ep*) of ascending aortic segments of male *Ipo8*<sup>-/-</sup> and WT mice under control (Krebs-Ringer), maximally relaxed (DEANO), partially contracted (PE) and completely contracted (PE + L-NAME) conditions at 12 (5 *Ipo8*<sup>-/-</sup> vs 4 WT), 24 (4 *Ipo8*<sup>-/-</sup> vs 4 WT) and 52 (4 *Ipo8*<sup>-/-</sup> vs 2 WT) weeks of age. The error bars show SEM. No statistical significance was reached using Two-way ANOVA testing. PE: Phenylephrine, DEANO: diethylamine NONOate, L-NAME: N(Ω)-nitro-L-arginine methyl ester, *Ep*: Peterson modulus, WT: wild type, NS: non-significant.

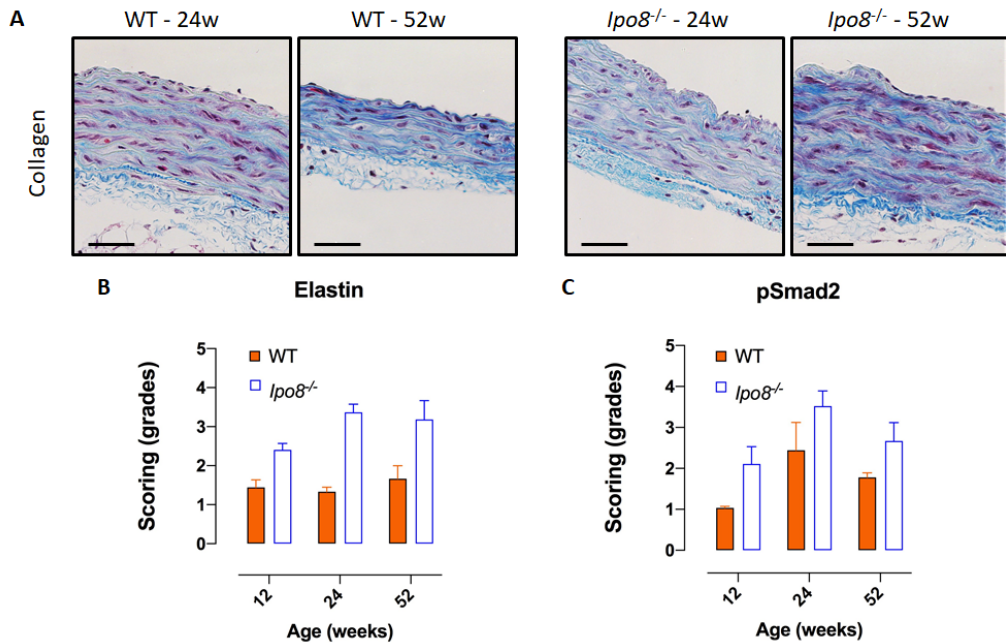


**Figure S9. Normal collagen levels despite elastic fiber deterioration and nuclear pSmad2 accumulation in the ascending aorta of *lpo8*<sup>-/-</sup> mice amongst all age groups.** A) Histological images for collagen. B) Age-tailored elastic fiber integrity scores of the ascending aorta of 12- (3 *lpo8*<sup>-/-</sup> vs 3 WT), 24- (3 *lpo8*<sup>-/-</sup> vs 3 WT) and 52-week (3 *lpo8*<sup>-/-</sup> vs 2 WT) old mice. Elastin grades can range from 1 to 4, with grade 1 sections presenting with continuous and well-organized elastic bundles and grade 4 sections displaying vastly disorganized fibers, marked fiber fragmentation and a thickened aortic wall. C) Age-tailored nuclear pSmad2 grades of the ascending aorta of 12- (3 *lpo8*<sup>-/-</sup> vs 3 WT), 24- (3 *lpo8*<sup>-/-</sup> vs 3 WT) and 52-week (3 *lpo8*<sup>-/-</sup> vs 2 WT) old mice. Grade 1, 2, 3 and 4 denote sections in which respectively <25%, 25-50%, 50-75% and 75-100% of nuclei stained positive. Averaged scores of blinded observations of three independent researchers are shown. The error bars depict SEM. WT: wild type.

## CHAPTER 5

---

### **Remarkable alleviation of ascending aortic aneurysm phenotype in 129/Sv *Ipo8*<sup>-/-</sup> mice as compared to their C57BL/6N *Ipo8*<sup>-/-</sup> counterparts**

Ilse Van Gucht<sup>1</sup>, Josephina A.N. Meester<sup>1</sup>, Ilse Luyckx<sup>1,2</sup>, Mandy Vermont<sup>3</sup>, Jarl Bastianen<sup>1</sup>, Maaïke Bastiaansen<sup>1</sup>, Pieter-Jan Guns<sup>3</sup>, Lut Van Laer<sup>1</sup>, Bart L. Loeys<sup>1,2</sup> and Aline Verstraeten<sup>1</sup>

<sup>1</sup>Cardiogenomics Research Group, University of Medical Genetics, University of Antwerp and Antwerp University Hospital, Antwerp, Belgium

<sup>2</sup>Department of Human Genetics, Radboud University Medical Center, Nijmegen, The Netherlands

<sup>3</sup>Laboratory of Physio Pharmacology, University of Antwerp, Antwerp, Belgium

## Abstract

---

Thoracic aortic aneurysm and/or dissection is a common and important clinical feature of genetic diseases such as Loeys-Dietz syndrome or Marfan syndrome. Bi-allelic loss-of-function variants in *IPO8*, a ubiquitously expressed nucleocytoplasmic transport receptor of the TGF- $\beta$  signaling pathway, cause thoracic aortic aneurysm in humans and mice. Interestingly, the progressive aneurysmal phenotype with aortic dissection described in C57BL/6N *Ipo8*<sup>-/-</sup> mice is absent in the congenic 129/Sv *Ipo8*<sup>-/-</sup> mice. Moreover, elastic fibers breaks and their disorganization are not present in 129/Sv *Ipo8*<sup>-/-</sup> mice in contrast to their C57BL/6N *Ipo8*<sup>-/-</sup> counterparts. Here, we report that *Ipo8* deficiency on different genetic backgrounds leads to a different phenotype.

## 1 Introduction

---

Thoracic aortic aneurysm (TAA) is a progressive widening of the thoracic aorta caused by wall weakness and leading to life-threatening aortic dissections and/or ruptures. TAA development is gradual, painless and often remains unnoticed until dissection occurs, making TAA/TAD a silent killer [1]. TAA presents either as a manifestation of rare heritable connective tissue diseases such as Marfan syndrome (MFS) and Loeys-Dietz syndrome (LDS), or as an isolated symptom. Over the past 20 years, pathogenic variants in more than 35 genes have been described to be associated with TAA [2, 3]. One of these genes, *IPO8*, was recently identified as a culprit gene for TAA by Ziegler et al and Van Gucht et al [4, 5]. *IPO8* encodes Importin-8, which is a nucleocytoplasmic transport receptor that mediates cargo shuttling towards the nucleus in a RanGTP-dependent manner [6, 7]. Smad proteins have been suggested as cargoes to be shuttled towards the nucleus by Importin-8 [8, 9]. Bi-allelic loss-of-function *IPO8* variant carriers present with a connective tissue disease resembling MFS and LDS, which is characterized by early-onset aortic aneurysm at the level of the aortic root and/or ascending aorta, motor developmental delay, skeletal findings such as pectus excavatum and joint hypermobility, and craniofacial dysmorphism [4].

The extension of the TAA landscape with this gene provides us with novel therapeutic entry points, since current medications such as  $\beta$ -blockers and angiotensin receptor blockers can slow down aortic dilation to some extent but are not able of preventing or reversing the aneurysmal phenotype [10]. Prophylactic surgery is still the most often used in preventing aortic catastrophes such as dissection/rupture but despite major improvements over the past decades, surgical intervention is not without risks and reintervention can be necessary [11, 12]. Acquisition of improved insights into the pathophysiology of TAA is warranted to develop novel, and especially more effective, drug therapies. Moreover, personalized medicine or patient-specific therapies are becoming of great importance and are based on differences in patient's genetic content.

Not only in humans but also in mouse models, the genetic background can influence a strain's phenotype significantly [13].

To investigate the disease mechanisms underlying *IPO8*-related TAA in an *in vivo* setting, we previously used an *Ipo8* knock-out mouse model (*Ipo8*<sup>-/-</sup>) on a C57BL/6N genetic background, which we demonstrated to present with TAA starting from the age of eight weeks onwards. Furthermore, in aneurysmal aortic tissue samples, an upregulation of the TGF-β pathway was demonstrated, evidenced by an increase in pSmad2 positive nuclei and elevated mRNA levels of *Ccn2* and *Mmp2*, two downstream targets of the TGF-β signaling pathway [14, 15]. On the other hand, a downregulation of *Smad6* and *Smad7* was observed, indicating a lack of negative feedback on TGF-β signaling [16]. Additionally, severe elastic fiber fragmentation and disorganization was shown [4].

Several mouse models have been developed to investigate the molecular events that take place in aneurysmal aortic tissue and study the pathological process that causes the aorta to dilate and eventually rupture [17]. Nevertheless, it was reported before that the genetic background of the TAA mouse strains can affect the penetrance of the phenotype, even within substrains. So was stated previously that MFS *Fbn1*<sup>mgΔloxPneo</sup> mice with a 129/Sv background showed an earlier onset of aortic aneurysm compared to mice with a C57BL/6 background [18].

In this study, we investigated the hypothesis that *Ipo8*<sup>-/-</sup> mice on a 129/Sv genetic background also develop a TAA phenotype comparable or more severe than their C57BL/6N counterparts. To assess whether *Ipo8* deficiency on a different genetic background, also leads to TAA development, a 129/Sv *Ipo8*<sup>-/-</sup> knock-out mouse model was backcrossed and bred, followed by aortic phenotyping.

## 2 Materials and methods

---

### 2.1 Ethics

The experimental set-up to conduct this research was approved by the Ethical Committee of Animal Testing of the University of Antwerp (ECD application number 2019-15). Experiments were applied in good practice and in accordance with prescribed and approved protocols, with respect to animal welfare at all times. The mice were bred, housed and taken care of at the animal facility of the University of Antwerp.

### 2.2 Creation of the 129/Sv *Ipo8*<sup>-/-</sup> back crossed strain

A C57BL/6N *Ipo8*<sup>tm1.1(KOMP)Vlcg</sup> knockout mouse line derived from embryonic stem (ES) cell clone 14312A-C12 from KOMP (<https://www.komp.org/redirect.html?geneid=64935>) was purchased, bred, housed and maintained at the Animal Facility of the University of Antwerp. C57BL/6N *Ipo8*<sup>+/-</sup> mice were crossed with 129/Sv wild type mice (Charles River) for eight generations. Ear punch DNA of the offspring was subjected to a 384-single nucleotide polymorphism panel (7Mbp spacing, Charles River) and compared to the genotype profile of a 129S2/SvPasCrl reference animal to prove successful creation of a 129/Sv congenic strain (129/Sv-*Ipo8*<sup>tm1.1(KOMP)Vlcg</sup>). In this report the congenic mouse strain will be referred to as 129/Sv *Ipo8*. A profile match between 99.3 and 99.6% was obtained. The heterozygous animal with the highest allelic profile Percent Match was used for further breedings and creating of the experimental mice cohort, making these mice the 10<sup>th</sup> generation of a 129/Sv *Ipo8*<sup>+/-</sup> x Sv129 *Ipo8*<sup>+/-</sup> breeding. All mouse strains were housed, bred and maintained at the animal facility of the University of Antwerp in accordance with protocols approved by the Ethical Committee of Animal Testing of the University of Antwerp.

### **2.3 Transthoracic echocardiography**

The thoracic aorta was visualized using transthoracic echocardiography with the Visual Sonics Vevo-2100 Ultrasound imaging system and a 30MHz transducer. For clear visualization of the aorta, a hair removal cream (Veet sensitive skin) was utilized. Starting from the age of four weeks until 32 weeks, mice were monthly monitored with transthoracic echocardiographic to investigate TAA development. The diameter of two anatomical locations of the thoracic aorta was assessed, including the aortic root at the level of the sinuses of Valsalva and the aorta ascendens. To warrant reliability, three independent measurements at each anatomical location for each mouse were performed and used for mean calculations. For every group (129/Sv *Ipo8*<sup>-/-</sup> mice and wild type littermates) and time point (4-8-12-16-20-24-28-32 weeks of age), at least 20 animals (10 per gender) were included.

### **2.4 Histological stainings and immunohistochemistry**

129/Sv *Ipo8*<sup>-/-</sup> and their littermate wild type mice were sacrificed at age 24 weeks using a gradual fill CO<sub>2</sub>-inhalation (N=7 per group, five males and two females), after which aortic tissue was isolated. Histological assessment was performed on the aorta ascendens part of the thoracic aorta tissue samples. The aortic tissue samples were kept in 4% formaldehyde in PBS for 24 hours, after which they were stored in 60% isopropanol at 4°C for several days. Tissue samples were paraffin embedded before cutting them into 5µm sections that were placed on microscopic slides coated with gelatin/APES (amiopropylthiethoxysaline). The tissue slides were emerged in 100% xylene to deparaffinize the slides, followed by a series of different alcohol grades (100%-90%-70%-50%) for 5 minutes to dehydrate the tissue samples. A Weigert-Van Gieson staining was performed to evaluate the elastic fibers present in the aortic wall. Elastic fibers integrity was scored using a range from one to four, with one representing healthy, no elastic fiber breaks containing aortic tissue and, with four representing diseased, disorganized elastic fibers and marked fiber fragmentation in the aortic wall.

Three representative sections per animal were selected and each section was scored by three independent observers blinded for genotype.

## 2.5 Statistical analyses

Transthoracic echocardiographic data is expressed as mean  $\pm$  SD with N representing the number of mice. Mixed model analyses were performed on the echocardiographic data using JMP Pro 15 Software (SAS institute). With weight corrected aortic diameters as dependent variable, with genotype, time point and interaction as fixed values. Two-way ANOVA was used to assess the statistical significance of the elastin staining.

## 3 Results

---

### 3.1 Transthoracic echocardiographic results show absence of an aneurysmal aortic phenotype in 129/Sv *Ipo8*<sup>-/-</sup> mice

Transthoracic echocardiographic measurements of the 129/Sv *Ipo8*<sup>-/-</sup> mice and wild type littermates were conducted starting from the age of four weeks until 32 weeks. Images were analyzed and on both investigated anatomical locations, i.e. the aortic root ( $p = 0.05$ ) and aorta ascendens ( $p = 0.4$ ), normal diameters were observed. The non-significant p-values for both, aortic root and aorta ascendens, confirm the absence of TAA development in 129/Sv *Ipo8*<sup>-/-</sup> mice. A representation of the weight-corrected aortic root and aorta ascendens diameters in both genders (*Ipo8*<sup>-/-</sup> N = 23 vs WT N = 21) can be found in Figure 1.

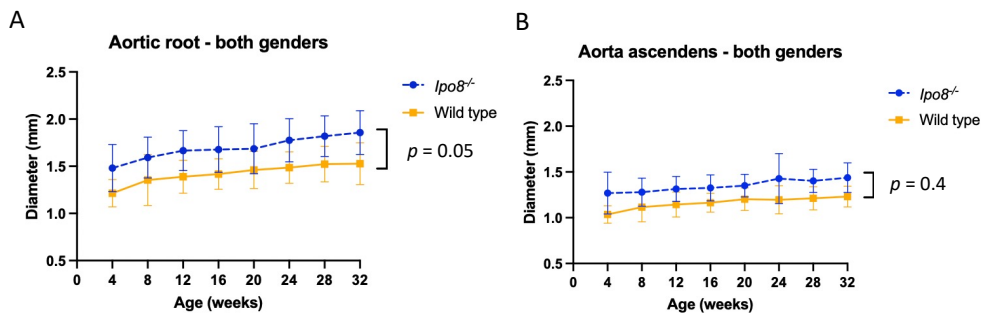


**Figure 1. Absence of aortic root and ascending aorta dilatation in 129/Sv *Ipo8*<sup>-/-</sup> mice over time.** Weight-corrected diameters (mm) are displayed on the y-axis and age in weeks is displayed on the x-axis. 129/Sv *Ipo8*<sup>-/-</sup> mice (n23) are indicated in blue dotted line, wild type mice (n=21) are indicated in orange full line. (A) Aortic root both genders, (B) Aorta ascendens both genders. The error bars depict SD. P-values were calculated using a mixed model analysis presenting the interaction term between genotype and age.

A gender-tailored analysis was performed as well and did not reveal any sexual dysmorphism. There were no differences observed in aortic root (AR) or aorta ascendens (AA) weight-corrected diameters for 129/Sv *Ipo8*<sup>-/-</sup> males only (AR  $p = 0.08$  and AA  $p = 0.3$ ) and females only (AR  $p = 0.1$  and AA  $p = 0.6$ ). The weight-corrected aortic root and aorta ascendens diameters in female mice only (*Ipo8*<sup>-/-</sup> N = 11 vs WT N = 10) and male mice only (*Ipo8*<sup>-/-</sup> N = 12 vs WT N = 11) are displayed in Supplementary Figure S1.

Taken together, no significant progressive dilatation of the aortic root nor aorta ascendens could be observed until the age of 32 weeks. Furthermore, necropsies of four mutant animals that deceased during experimental progress before the age of 32 weeks, did not reveal dissection or rupture of the aortic wall as a cause of death. No other obvious explanation for the mortality could be determined.

### 3.2 Absence of statistically significant elastic fiber breaks in aortic tissue from 129/Sv *Ipo8*<sup>-/-</sup> mice

Aortic tissue from 129/Sv *Ipo8*<sup>-/-</sup> mice was histologically investigated. The extracellular matrix (ECM) integrity was evaluated with elastin stainings. Each group (*Ipo8*<sup>-/-</sup> and wild type mice) contains 24-weeks old animals, consisting of five males and two females.

Minimal elastic fiber breaks seem to be present in some 129/Sv *Ipo8*<sup>-/-</sup> mice as well as in wild type mice, indicating no significant difference in elastic integrity between both groups ( $p = 0.78$ ). Furthermore, no distinction between the genders based on prevalence of the breaks or disorganization can be made. The elastic fiber breaks and disorganization are distributed heterogeneously throughout the aortic wall. A representative example of the Weigert-Van Gieson elastin staining of aortic ascendens tissue samples can be found in Figure 2A and B whereas the elastic fiber integrity scores can be found in Figure 2C.

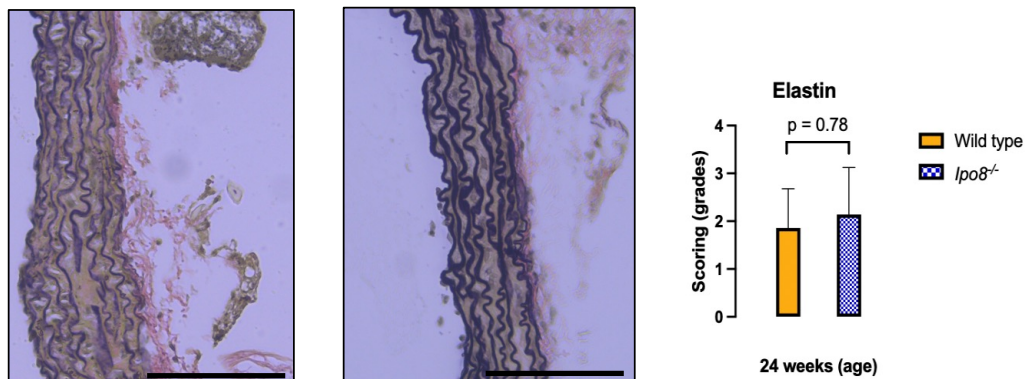


**Figure 2. Elastic fiber staining with Weigert-Van Gieson staining of thoracic aortic tissue.** (A) 129/Sv *Ipo8*<sup>-/-</sup> mice, (B) Wild type mice, (C) elastic fiber integrity scores in graphs; Animals are 24 weeks old mice (7 *Ipo8*<sup>-/-</sup> mice vs 7 wild type mice). Scale bars are 100  $\mu\text{m}$ . P-value was calculated using a two-way ANOVA statistical test and error bars depict SD.

#### 4. Discussion

---

Here, we demonstrate that thoracic aortic aneurysm development is absent in 129/Sv *Ipo8*<sup>-/-</sup> mice. In our study, transthoracic echocardiography was performed on *Ipo8*<sup>-/-</sup> mice on a 129/Sv genetic background to look at the aortic phenotype. Surprisingly, the diameter of the aortic root as well as the aorta ascendens falls within normal diameter ranges, proving the absence of an aortic aneurysmal phenotype. Furthermore, the assessment of ECM integrity and the aortic wall maintenance of 129/Sv *Ipo8*<sup>-/-</sup> mice, using Weigert-Van Gieson staining for elastic fibers, showed the absence of severe elastic fiber breaks and/or disorganized elastic fibers. Lastly, no sexual dysmorphism was observed in the 129/Sv *Ipo8*<sup>-/-</sup> mouse model for elastic fiber fragmentation.

Interestingly, C57BL/6N *Ipo8*<sup>-/-</sup> mice have been phenotypically characterized by early onset progressive TAA followed by dissection in a subset of male mice only [4] and reduced grip strength previously determined by IMPC (International Mouse Phenotyping Consortium). Moreover, severe elastic fiber breaks were present in C57BL/6N *Ipo8*<sup>-/-</sup> mice.

Taken our data together, our findings nicely fit within ongoing research into genetic background issues of mouse models [19, 20]. In line with recent TAA mouse models studies, evidence is accumulating on a causative role for genetic modifiers explaining the differences in aneurysmal phenotype of the same knock-out mice on different genetic backgrounds [21]. Consequently, choosing a genetic background for a knock-out mouse model is of great importance. Multiple studies on TAAD have been published highlighting this phenomenon [19]. As an example, TAAD causing gene, *BGN* (biglycan), has been modeled in mice on two different genetic background, i.e. BALB/cA, exhibiting sudden death from aortic rupture, and C57BL/6, missing the aortic phenotype. The precise molecular mechanism for these differences remains unknown [22]. A seconds

example, is the knock-out mouse model of another TAA(D) gene, *Smad3*, an intracellular effector of the TGF- $\beta$  signaling pathway, presented with an aortic phenotype on a BALB/c genetic background, whereas the phenotype was not reproduced in C57BL/6 mice [23].

Recent data indicate that there is no specific or consistent genetic background on which the aneurysmal phenotype is more severe, as this appears to be different for the different TAA(D) genes. An illustrative example of this phenomenon is the phenotype related to *Fbn1*<sup>+/-</sup> mice and *Ipo8*<sup>-/-</sup> mice. Whilst *Fbn1*<sup>+/-</sup> mice are more protected from aneurysmal development when bred on a C57BL/6 genetic background instead of 129/Sv (unpublished data), this is the other way around for our *Ipo8*<sup>-/-</sup> mice. Similarly, a previously reported MFS mouse model (*mg* $\Delta^{\text{loxPneo}}$ ) showed earlier onset of the disease in mice on a 129/Sv genetic background in comparison to mice on a BL6 genetic background [18].

Based on our data, it seems that C57BL/6N is an aggravating genetic background for *Ipo8* knock-out and that 129/Sv is a protecting genetic background for TAA(D) development. However, the underlying pathophysiological mechanism remains unknown. An explanation for the phenomenon observed in our study may be found in the presence of a dominant genetic modifier that rescues or aggravates the *Ipo8* induced TAA(D) phenotype in 129/Sv *Ipo8*<sup>-/-</sup> or C57BL/6N *Ipo8*<sup>-/-</sup> mice, respectively. Since C57BL/6N *Ipo8*<sup>-/-</sup> mice have a baseline dysregulated TGF- $\beta$  signaling [4] and in view of the involvement of the TGF- $\beta$  signaling pathway in TAA(D) development and, one might hypothesize the genetic or epigenetic modifier influences this pathway. Besides genetic differences, one must consider environmental influences which can also have an impact on incomplete penetrance and variable expressivity of a phenotype [13]. However, in our case, 129/Sv *Ipo8*<sup>-/-</sup> mice were bred, housed and fed in exactly the same circumstances than their C57BL/6N *Ipo8*<sup>-/-</sup> counterparts.

## 5. Conclusion

---

In conclusion, we found that the progressive aortic aneurysmal phenotype previously observed in C57BL/6N *Ipo8*<sup>-/-</sup> is not present in the 129/Sv *Ipo8*<sup>-/-</sup> mice. This supports the finding that the choice of a genetic background for generating a knock-out mouse model is of utmost importance, as it may influence the development of an aortic phenotype. To reveal the underlying cause of the observed phenotypical differences between different genetic strains carrying the same pathogenic variants, genetic and epigenetic modifier studies should be performed. Although more research is needed on the underlying mechanisms involved, it is clear that our study expands the knowledge about TAAD modeling in mouse models.

## 6. References

---

1. De Cario, R., et al., *Tracking an Elusive Killer: State of the Art of Molecular-Genetic Knowledge and Laboratory Role in Diagnosis and Risk Stratification of Thoracic Aortic Aneurysm and Dissection*. Diagnostics (Basel), 2022. **12**(8).
2. Luyckx, I., et al., *Update on the molecular landscape of thoracic aortic aneurysmal disease*. Curr Opin Cardiol, 2022. **37**(3): p. 201-211.
3. Faggion Vinholo, T., et al., *Genes Associated with Thoracic Aortic Aneurysm and Dissection: 2019 Update and Clinical Implications*. Aorta (Stamford), 2019. **7**(4): p. 99-107.
4. Van Gucht, I., et al., *A human importin-beta-related disorder: Syndromic thoracic aortic aneurysm caused by bi-allelic loss-of-function variants in IPO8*. Am J Hum Genet, 2021. **108**(6): p. 1115-1125.
5. Ziegler, A., et al., *Bi-allelic variants in IPO8 cause a connective tissue disorder associated with cardiovascular defects, skeletal abnormalities, and immune dysregulation*. Am J Hum Genet, 2021. **108**(6): p. 1126-1137.
6. Volpon, L., et al., *Importin 8 mediates m7G cap-sensitive nuclear import of the eukaryotic translation initiation factor eIF4E*. Proc Natl Acad Sci U S A, 2016. **113**(19): p. 5263-8.
7. Weinmann, L., et al., *Importin 8 is a gene silencing factor that targets argonaute proteins to distinct mRNAs*. Cell, 2009. **136**(3): p. 496-507.
8. Yao, X., et al., *Preferential utilization of Imp7/8 in nuclear import of Smads*. J Biol Chem, 2008. **283**(33): p. 22867-74.

9. Hu, X., et al., *Mitogen-activated protein kinase inhibitors reduce the nuclear accumulation of phosphorylated Smads by inhibiting Imp 7 or Imp 8 in HepG2 cells*. *Oncol Lett*, 2018. **15**(4): p. 4867-4872.
10. Forteza, A., et al., *Efficacy of losartan vs. atenolol for the prevention of aortic dilation in Marfan syndrome: a randomized clinical trial*. *Eur Heart J*, 2016. **37**(12): p. 978-85.
11. Lacro, R.V., H.C. Dietz, and L. Mahony, *Atenolol versus Losartan in Marfan's Syndrome*. *N Engl J Med*, 2015. **372**(10): p. 980-1.
12. Teixido-Tura, G., et al., *Losartan Versus Atenolol for Prevention of Aortic Dilation in Patients With Marfan Syndrome*. *J Am Coll Cardiol*, 2018. **72**(14): p. 1613-1618.
13. Doetschman, T., *Influence of genetic background on genetically engineered mouse phenotypes*. *Methods Mol Biol*, 2009. **530**: p. 423-33.
14. Lipson, K.E., et al., *CTGF is a central mediator of tissue remodeling and fibrosis and its inhibition can reverse the process of fibrosis*. *Fibrogenesis Tissue Repair*, 2012. **5**(Suppl 1): p. S24.
15. Van Doren, S.R., *Matrix metalloproteinase interactions with collagen and elastin*. *Matrix Biol*, 2015. **44-46**: p. 224-31.
16. Hanyu, A., et al., *The N domain of Smad7 is essential for specific inhibition of transforming growth factor-beta signaling*. *J Cell Biol*, 2001. **155**(6): p. 1017-27.
17. Seong, E., et al., *To knockout in 129 or in C57BL/6: that is the question*. *Trends Genet*, 2004. **20**(2): p. 59-62.
18. Lima, B.L., et al., *A new mouse model for marfan syndrome presents phenotypic variability associated with the genetic background and overall levels of Fbn1 expression*. *PLoS One*, 2010. **5**(11): p. e14136.
19. Sanford, L.P., et al., *Influence of genetic background on knockout mouse phenotypes*. *Methods Mol Biol*, 2001. **158**: p. 217-25.
20. Hay, A.M., et al., *Mouse background genetics in biomedical research: The devil's in the details*. *Transfusion*, 2021. **61**(10): p. 3017-3025.
21. Ren, W., et al., *beta-Aminopropionitrile monofumarate induces thoracic aortic dissection in C57BL/6 mice*. *Sci Rep*, 2016. **6**: p. 28149.
22. Meester, J.A., et al., *Loss-of-function mutations in the X-linked biglycan gene cause a severe syndromic form of thoracic aortic aneurysms and dissections*. *Genet Med*, 2017. **19**(4): p. 386-395.
23. Kashyap, S., et al., *Cardiovascular phenotype in Smad3 deficient mice with renovascular hypertension*. *PLoS One*, 2017. **12**(10): p. e0187062.

## 7. Supplementary

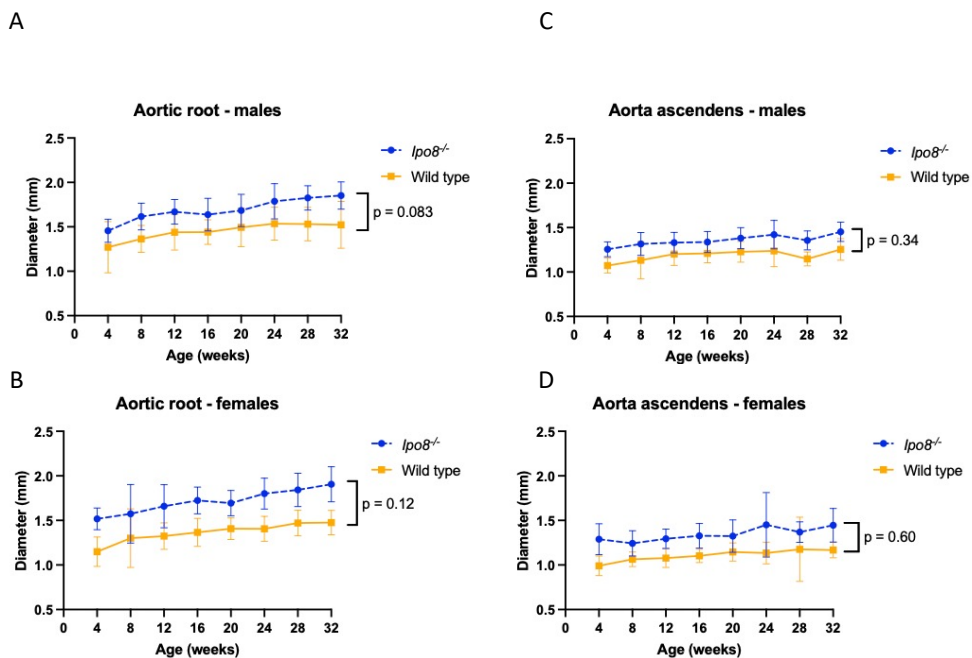


**Figure S1. Gender-tailored representation of the diameter of the aortic root and aorta ascendens over time.** Log of weight-corrected diameters is displayed on the y-axis and age in weeks is displayed on the x-axis. *Ipo8<sup>-/-</sup>* mice are indicated in blue dotted line, wild types are indicated in an orange full line. (A) Aortic root males, (B) Aortic root females, (C) Aorta ascendens males and (D) Aorta ascendens females. The error bars depict SD. P-values were calculated using a mixed model analysis presenting the interaction term between genotype and age. N *Ipo8<sup>-/-</sup>* = 10 females and 10 males, N Wild type = 10 females and 10 males.

## CHAPTER 6

---

### **Embryonic lethality in homozygous *Ipo8*<sup>-/-</sup> mice on a C57BL/6N genetic background**

Ilse Van Gucht<sup>1</sup>, Ilse Luyckx<sup>1,2</sup>, Mandy Vermont<sup>3</sup>, Jarl Bastianen<sup>1</sup>, Maaïke Bastiaansen<sup>1</sup>, Isabel Pintelon<sup>4</sup>, Sofie Thys<sup>4</sup>, Josephina A.N. Meester<sup>1</sup>, Pieter-Jan Guns<sup>3</sup>, Marco C. DeRuiter<sup>5</sup>, Lambertus J. Wisse<sup>5</sup>, Lut Van Laer<sup>1</sup>, Aline Verstraeten<sup>1</sup> and Bart L. Loeys<sup>1,2</sup>

<sup>1</sup>Cardiogenomics Research Group, University of Medical Genetics, University of Antwerp and Antwerp University Hospital, Antwerp, Belgium

<sup>2</sup>Department of Human Genetics, Radboud University, Nijmegen Medical Center, Nijmegen 6525, GA, The Netherlands

<sup>3</sup>Laboratory of Physiopharmacology, University of Antwerp, 2610 Wilrijk, Belgium

<sup>4</sup>Laboratory of Cell Biology & Histology, Antwerp Centre for Advanced Microscopy (ACAM), Department of Veterinary Sciences, University of Antwerp, Antwerp 2610, Belgium

<sup>5</sup>Department of Anatomy and Embryology, Leiden University Medical Center, Leiden, The Netherlands.

## Abstract

---

Bi-allelic loss-of-function variants in *IPO8*, encoding the cytoplasm-to-nucleus transport receptor Importin-8, have recently been described to cause an early-onset aortopathy syndrome. A C57BL/6N *Ipo8* knock-out (*Ipo8*<sup>-/-</sup>) mouse model was shown to carefully replicate the thoracic aortic aneurysm (TAA) phenotype. Interestingly, 50% embryonic lethality of C57BL/6N *Ipo8*<sup>-/-</sup> pups born out of C57BL/6N *Ipo8*<sup>+/-</sup> x C57BL/6N *Ipo8*<sup>+/-</sup> breedings was also observed, suggesting a role for Importin-8 in normal embryonic development. Timed matings and investigation of embryos at E13.5-E14.5, an important timepoint in cardiovascular development, were performed to further investigate the cause of death. At E13.5-14.5 several main events in embryonic development take place including septation of the outflow tract and ventricles, atrioventricular cushion remodeling and aortic arch development. At this phase, a mendelian distribution of genotypes was observed. Macroscopically, E13.5-E14.5 C57BL/6N *Ipo8*<sup>-/-</sup> animals presented with paleness caused by decreased cardiac output or lack of vasculature, hemorrhages and/or a bulging neck (edema) and, microscopically, a decrease in left ventricle lumen with endothelial cell layer detachment from the endocardium, likely leading to left ventricle function impairment and, hence, lethality. Remarkably, no embryonic was observed in 129/Sv *Ipo8*<sup>-/-</sup> mice, demonstrating the major influence the genetic background has on mouse phenotypes.

## 1 Introduction

---

Thoracic aortic aneurysm (TAA) is a pathological dilatation of the aorta caused by degenerative changes in the aortic wall affecting proper integrity [1]. TAAs are extremely life-threatening due to their high risk of rupture/dissection, representing an important cause of sudden death. The genetic landscape of TAA contains more than 40 causal genes, nevertheless, for the majority of TAA patients no genetic diagnosis can be provided [2]. TAA is a part of the clinical profile of several genetic diseases such as Marfan syndrome, Loeys-Dietz syndrome and Shprintzen-Goldberg syndrome [3]. In 2021, bi-allelic loss-of-function variants in *IPO8* were first described in Loeys-Dietz syndrome-resembling patients. Pathogenic variant carriers have a highly consistent phenotype and are characterized by severe, early-onset TAA, global developmental delay, hypertelorism, joint hypermobility, hernia, pectus deformities and hypotonia [4]. *IPO8* encodes for the transport receptor Importin-8, which is a member of the Importin- $\beta$  family and is involved in the translocation of cargoes from the cytosol into the nucleus in a RanGTP-dependent manner. As it is ubiquitously expressed throughout the body, tissue specificity of the cargoes might explain why certain organ systems are affected and others are not [5]. A C57BL/6N *Ipo8* knock-out (*Ipo8*<sup>-/-</sup>) mouse model, previously known to suffer from reduced grip strength, was shown to recapitulate the human TAA phenotype [4], delivering a novel pre-clinical model that can be used to gain further insights into the pathogenesis of syndromic TAA.

The structural similarities between the human and mouse heart make mouse models appropriate animal models for cardiovascular investigation. Nevertheless, there are some differences in embryonic development between the human and mouse heart. The most important difference can be found in the venous structures entering the atria. In a human heart there is only one vena cava superior that regulates the venous return from the upper body towards the right atrium, whilst in mice there is a left superior vena cava persisting and draining into the coronary sinus [6]. Another remarkable

difference is the presence of four pulmonary openings in the left atrium in humans, while in contrast to mice there is only one [7]. A well-organized cardiogenesis is an important but very complicated process and is crucial for the survival of the embryo, with failure giving cause to embryonic or prenatal lethality [6, 8].

An important event that can occur during breeding of transgenic mice is embryonic/prenatal lethality. It is estimated that about 30% of knock-out strains present with embryonic lethality [9]. In-depth investigation of this lethality phenotype is of great importance since it may lead to a better understanding of gene function and pathway dysregulation early in life, paving the way for the discovery of novel drug targets or intervention strategies for congenital phenotypes.

Here, we report and characterize embryonic lethality in *Ipo8*<sup>-/-</sup> mice on a C57BL/6N genetic background. Timed matings with *Ipo8*<sup>+/-</sup> mice were performed, the offspring were genotyped and morphologically checked to determine the time of death and cause of lethality. Given the key cardiovascular events taking place at E13.5-E14.5, we first checked this time window for anomalies in heart development.

## **2 Materials and methods**

---

### **2.1 Ethics**

Ethics approval for the described experiments was granted by the Ethical Committee of Animal Testing of the University of Antwerp (2021-32). Animals were bred, housed and taken care of by trained personnel of the University of Antwerp according to the European animal welfare guidelines [10].

## 2.2 Mice

*Ipo8*<sup>tm1.1(KOMP)Vl<sub>cg</sub></sup> mice on a C57BL/6N genetic background were obtained from the KOMP (Knockout Mouse Project) repository. Initially, these mice were derived from an embryonic stem (ES) cell clone 14312A-C12 generated by Regeneron Pharmaceuticals. Insertion of the VelociGene cassette ZEN-Ub1 resulted in a deletion of 31.512bp located at chr6:148.799.733-148.831.244; (GRCm38/mm10), removing the first 529 amino acids (exon 1-14) of Importin-8. In a next step, Cre-expressing mice were bred to mice that contained the reporter-tagged null allele (tm1), leading to activation of the Neomycin gene and removal of the  $\beta$ -actin promoter. The tm1.1 allele remains a lacZ reporter and is a non-conditional knockout of the gene [4]. To generate the 129/Sv *Ipo8*<sup>tm1.1(KOMP)Vl<sub>cg</sub></sup> mouse model, heterozygous C57BL/6N *Ipo8*<sup>tm1.1(KOMP)Vl<sub>cg</sub></sup> mice were backcrossed to a 129/Sv genetic background for eight generations. To achieve this, wild type 129/Sv animals were purchased at Charles River Laboratory and used for breeding with C57BL/6N *Ipo8*<sup>+/-</sup> mice. A genetic testing service was applied to generate an allelic profile of the backcrossed C57BL/6N *Ipo8*<sup>tm1.1(KOMP)Vl<sub>cg</sub></sup> mice strain. DNA from the offspring was collected and subjected to a 384-single nucleotide polymorphism panel (7Mbp spacing, Charles River). Their genotype profile was compared to a 129S2SvPasCrl reference animal profile confirming the generation of a 129/Sv mouse strain with a profile match between 99.3% and 99.6%. At this point the 129/Sv animals with the best profile match were used for further breedings. The offspring of this last breeding were used to set-up a cohort of 129/Sv mice, delivering the 10<sup>th</sup> generation of backcrossed animals.

### 2.3 Timed matings

An adapted version of the timed mating protocol from The Jackson Laboratory was used (<https://www.jax.org/news-and-insights/jax-blog/2014/september/six-steps-for-setting-up-timed-pregnant-mice>). In short, fertile males of 12 weeks of age and females of 14-16 weeks of age were used for mating. To ensure fertility, only the breeding pairs who had previously been shown to generate at least one offspring were included. Prior to mating, the female C57BL/6N *Ipo8*<sup>+/-</sup> mice were housed with eight in one cage for minimally one week to ensure them to become anestrus or to have a suppression or prolongation of the estrus cycle (Lee-Boot effect). The male C57BL/6N *Ipo8*<sup>+/-</sup> mice were housed by two for one week to warrant sperm recovery. The estimated time needed for sperm recovery of a C57BL/6N strain is about 4 days [11]. Three days prior to mating, the females received male pheromones via dirty bedding of males to synchronize their estrus cycle (Whitten effect). The proestrus and estrus phases were visually checked to increase the chance of a successful mating. On the evening of mating, two females were put together with one male for 36 hours to increase the likelihood of pregnancy, after which the vaginal plug was checked and the mice were separated again. Since the mice are spending two nights together, it should be considered that matings can occur during the first night or later resulting in embryos having a maximum age difference of one day. Day E0.5 or E1.5, also known as 0.5- or 1.5-days post-conception, depending on the moment of copulation within these 36 hours, is referred to as the morning on which the males are separated from the females. 13 days later (E13.5 or E14.5), pregnant females were dissected when they appeared pregnant. The set-up of this protocol and timeline are shown in Figure 1.

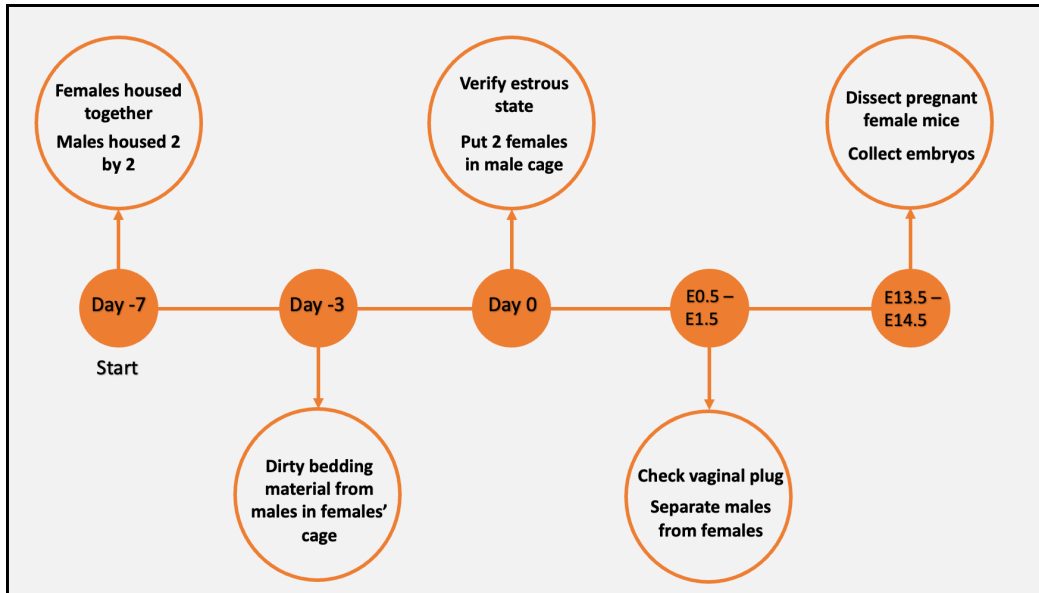


**Figure 1. Timeline of timed matings set-up.** *E* = embryonic day. *E0.5/E1.5* stands for the time point on which pups were conceived, during the first/second night, respectively.

## 2.4 Embryo collection

At embryonic stage E13.5-E14.5 (13.5-14.5 days after gestation), the pregnant females were sacrificed (by CO<sub>2</sub> gradual fill) and the embryos were isolated and fixed in 4% paraformaldehyde (PFA) in phosphate-buffered saline (PBS) for 24 hours, after which they were stored in 60% iso-propanol. The embryos (both genders) were entirely embedded in paraffin and cut into 5µm transverse sections with a rotary microtome (Leica RM2135 with foot switch; 14050238257) connected to a pedal for automatization and pasted onto microscopic slides for staining. The whole embryo was prepared for further histological investigation.

## 2.5 Histological staining

The embryonic tissue slides were stained with hematoxylin and eosin (HE) to assess the embryos' general architecture. Whole embryo sections were deparaffinized in toluene

for 5 minutes and a series of different graded alcohol solutions (90 %, 70 % and 50 % of ethanol) to rehydrate the tissue. Next, the Abcam HE staining kit was used (ab245880). An incubation time of 5 minutes with hematoxylin (Merck Hematoxylin To gill III pH2.5 Hx99385674- 1024390500) was applied. In a second step the slides were immersed with Bouin's solution, followed by addition of 100% ethanol. Eosin was added to the slides for 3 minutes (Merck Eosin Y-solution 0.5% alcoholic Hx90162739 – 1024390500), followed by dehydration with graded ethanol solutions (70% and 100%) and immersion in toluene for 2 times 5 minutes. Coverslips were mounted on the stained sections with HistoMount™ Mounting Solution (Invitrogen). All embryos were sectioned serially in transverse plane.

Immunohistochemistry was performed for PECAM-1 (M-20)-R (CD31) (AB0962-Santa Cruz) with Alexa Fluor 555-Donkey Anti-Rabbit IgG (H+L) (AB1127-Life Technologies) as a secondary antibody and PCNA (proliferating cell nuclear antigen) (AB1962-Sigma-Aldrich) with an Alexa Fluor 488-donkey anti-mouse IgG secondary antibody (AB0980-Invitrogen). Deparaffinization of the embryo sections was performed in xylene for 2x5 minutes followed by a series of different graded alcohol solutions (100%, 90 %, 80%, 70 % and 50 % of ethanol) to rehydrate the tissue. Slides were heated at 97°C for 12minutes in 0.01M citric buffer of pH 6.0. Primary and secondary antibodies were applied with several PBS rinsing steps in between. DAPI was used as nuclei stain and slides were mounted with Prolong gold (P36930-ThermoFisher).

## **2.6 Scanning**

Stained slides were mounted and visualized using an automated ZEISS AxioScan Z1 and ZEISS AxioScan 7 slide scanner at 10x magnification.

## **2.7 Statistical analysis**

A Chi-Square Goodness Fit test was used to assess differences between the expected and observed genotype frequencies and differences in gender. For the macroscopic aberrations, a Fisher's exact statistical test was done. An unpaired t-test was performed on the litter size of pre- and post-natal.

### 3 Results

#### 3.1 Embryonic lethality of 50% in C57BL/6N *Ipo8*<sup>-/-</sup> mice

Table 1. Expected and observed genotypes at birth after breeding of *Ipo8*<sup>+/-</sup> animals.

EXPECTED	<i>Ipo8</i> <sup>+/+</sup>	<i>Ipo8</i> <sup>+/-</sup>	<i>Ipo8</i> <sup>-/-</sup>	Total
Males and females	25%	50%	25%	100%
Males	50%	50%	50%	50%
Females	50%	50%	50%	50%
OBSERVED	<i>Ipo8</i> <sup>+/+</sup>	<i>Ipo8</i> <sup>+/-</sup>	<i>Ipo8</i> <sup>-/-</sup>	Total
Males and females	142 (32.6%)	237 (54.5%)	<b>56 (12.9%) ***</b>	435 (100%)
Males	79 (55.6%)	129 (54.4%)	35 (62.5%)	243 (55.9%)
Females	63 (44.4%)	108 (45.6%)	21 (37.5%)	192 (44.1%)

*Ipo8*<sup>+/+</sup>: wild types, *Ipo8*<sup>+/-</sup>: heterozygotes, *Ipo8*<sup>-/-</sup>: homozygotes. \*\*\* indicates *p*-value < 0.00001

C57BL/6N *Ipo8*<sup>+/-</sup> x C57BL/6N *Ipo8*<sup>+/-</sup> breedings with 34 different females and six males were set up and yielded 435 mice from 108 litters. Embryonic lethality of 50% of *Ipo8*<sup>-/-</sup> offspring was observed (Table 1). Instead of the expected 25% of *Ipo8*<sup>-/-</sup> mice, only 12.9% were born alive (*p* < 0.00001). A non-significant (*p* = 0.18) increase in live-born *Ipo8*<sup>-/-</sup> male (62.5%) as compared to female (37.5%) mice was observed. Supporting evidence for embryonic lethality is the smaller size (4.85 vs 6 to 8; *p* < 0.0001) of the litters

stemming from C57BL/6N *Ipo8*<sup>+/-</sup> x C57BL/6N *Ipo8*<sup>+/-</sup> breedings as compared to C57BL/6N wild type x wild type C57BL/6N breedings (literature data) [12, 13]. Surviving *Ipo8*<sup>-/-</sup> embryos reach adulthood but develop a TAA phenotype, in a fraction of animals followed by aortic dissection from 32 weeks of age onwards.

The International Mouse Phenotyping Consortium (IMPC) is a global consortium of different research centers working on the identification of protein-coding genes in the mouse genome by generating and phenotyping knock-out mouse models. The C57BL/6N *Ipo8*<sup>tm1.1(KOMP)Vicz</sup> knock-out mouse model used in this study and purchased from KOMP was also phenotyped by IMPC. C57BL/6N *Ipo8*<sup>+/-</sup> x C57BL/6N *Ipo8*<sup>+/-</sup> breedings yielded 189 pups, i.e. 55 wild types (29.1%), 107 heterozygotes (56.6%) and 27 homozygotes (14.3%) ( $p = 0.009$ , Supplementary Table 1), also indicating embryonic lethality of C57BL/6N *Ipo8*<sup>-/-</sup> mice and thus confirming our in-house data. Again, a non-significant trend ( $p = 0.42$ ) in gender distribution among *Ipo8*<sup>-/-</sup> mice was observed (Supplementary Table 1).

In conclusion, there is a significant negative correlation between the *Ipo8*<sup>-/-</sup> genotype and neonatal survival, with only about half of the expected number of homozygous animals being born alive (12.9 and 14.3% instead of 25%).

### **3.2 Expected mendelian distribution in the offspring of C57BL/6N *Ipo8*<sup>+/-</sup> x C57BL/6N *Ipo8*<sup>+/-</sup> breedings at embryonic stage E13.5-E14.5**

E13.5-E14.5 was chosen as a starting point for embryonic investigation as it is a critical time point for development of the cardiovascular system [14]. Three key events occur at E13.5-E14.5. First, by E13.5 the outflow tract and ventricles should be completely septated whereas atrial and atrioventricular septation is developing. Second, the atrioventricular cushions are being remodeled to form the atrioventricular valve leaflets. Finally, the aortic arch and its branches develop [8, 15, 16].

In total, 120 E13.5-E14.5 embryos were collected from 16 litters of 16 different *Ipo8<sup>+/-</sup>* females. *Ipo8<sup>+/+</sup>*, *Ipo8<sup>+/-</sup>* and *Ipo8<sup>-/-</sup>* embryos were observed at expected frequencies, 20%, 54.2% and 25.8% respectively ((25.8% vs 25%)  $p = 0.35$ ). Statistical analyses of the size of the litters emanating from the C57BL/6N *Ipo8<sup>+/-</sup>* x C57BL/6N *Ipo8<sup>+/-</sup>* breeding couples revealed a mean litter size of 7.87 embryos prenatally versus 4.85 pups postnatally ( $p < 0.0001$ ). No deviation from the expected gender distribution was seen (Table 2). Our data suggest no embryonic lethality of *Ipo8<sup>-/-</sup>* embryos before E13.5-E14.5.

**Table 2. Observed genotypes of embryos collected at E13.5-E14.5 from C57BL/6N *Ipo8<sup>+/-</sup>* x C57BL/6N *Ipo8<sup>+/-</sup>* breedings.**

<b>OBSERVED E13.5 – E14.5</b>	<i>Ipo8<sup>+/+</sup></i>	<i>Ipo8<sup>+/-</sup></i>	<i>Ipo8<sup>-/-</sup></i>	<b>Total</b>
<b>Males and females</b>	24 (20%)	65 (54.2%)	31 (25.8%)	120 (100%)
<b>Males</b>	9 (37.5%)	33 (50.8%)	17 (54.8%)	59 (49.2%)
<b>Females</b>	15 (62.5%)	32 (49.2%)	14 (45.2%)	61 (50.8%)

*Ipo8<sup>+/+</sup>*: wild types, *Ipo8<sup>+/-</sup>*: heterozygotes, *Ipo8<sup>-/-</sup>*: homozygotes

### 3.3 No evidence for embryonic lethality in 129/Sv *Ipo8<sup>-/-</sup>* mice

The offspring genotype distribution of 129/Sv *Ipo8<sup>+/-</sup>* x 129/Sv *Ipo8<sup>+/-</sup>* breedings (26 breeding females, 42 litters) was normal (Table 3), with a mean litter size of 7.92. Gender distribution was also as expected (Table 3).

**Table 3. Expected and observed genotypes at birth after 129/Sv *Ipo8*<sup>+/-</sup> x *Ipo8*<sup>+/-</sup> breedings.**

Observed at birth	<i>Ipo8</i> <sup>+/+</sup>	<i>Ipo8</i> <sup>+/-</sup>	<i>Ipo8</i> <sup>-/-</sup>	Total
<b>Males and females</b>	72 (29.1%)	115 (46.6%)	60 (24.3%)	247 (100%)
<b>Males</b>	36 (50%)	64 (55.7%)	29 (48.3%)	129 (52.2%)
<b>Females</b>	36 (50%)	51 (44.3%)	31 (51.7%)	118 (47.8%)

*Ipo8*<sup>+/+</sup>: wild types, *Ipo8*<sup>+/-</sup>: heterozygotes, *Ipo8*<sup>-/-</sup>: homozygotes.

Absence of embryonic lethality in 129/Sv *Ipo8*<sup>-/-</sup> mice highlights the influence of the genetic background on phenotypic expression. *Ipo8* deficiency-related embryonic lethality appears to be prone to aggravating and/or protective genetic modifiers.

### **3.4 Macroscopic examination of E13.5-E14.5 C57BL/6N *Ipo8*<sup>-/-</sup> embryos revealed abnormal appearance in 58% of *Ipo8*<sup>-/-</sup> animals**

Next, a gross morphological exam of the E13.5-E14.5 embryos was done. The embryos were morphologically studied, and several common features were observed, including a pale appearance, due to minor vascularization or decreased blood flow, head/neck bulging (edema), presence of hemorrhages and underdeveloped limbs and digits (Table 4).

**Table 4. Overview morphological observations in *Ipo8*<sup>-/-</sup> embryos and *Ipo8*<sup>+/-</sup> embryos.**

<i>Ipo8</i> <sup>-/-</sup> animals	Total	Males	Females
<b>Normal appearance</b>	13/31 (41.9%)	5/17 (29.4%)	8/14 (57.1%)
<b>Hemorrhages</b>	5/31 (16.1%)	3/17 (17.6%)	2/14 (14.3%)
<b>Pale</b>	14/31 (45.2%)	11/17 (64.7%)	3/14 (21.4%)
<b>Bulging neck/head (edema)</b>	3/31 (9.7%)	1/17 (5.9%)	2/14 (14.3%)

<b>Underdeveloped limbs</b>	2/31 (6.5%)	1/17 (5.9%)	1/14 (7.1%)
<b><i>Ipo8<sup>+/-</sup></i> animals</b>	<b>Total</b>	<b>Males</b>	<b>Females</b>
<b>Normal appearance</b>	21/24 (87.5%)	8/9 (88.9%)	13/15 (86.7%)
<b>Hemorrhages</b>	0/24	0/9	0/15
<b>Pale</b>	3/24 (12.5%)	1/9 (11.1%)	2/15 (13.3%)
<b>Bulging neck/head (edema)</b>	0/24	0/9	0/15
<b>Underdeveloped limbs</b>	0/24	0/9	0/15

58% of *Ipo8<sup>-/-</sup>* mice have gross morphological abnormalities (18/31), whereas 23% (15/65) of *Ipo8<sup>+/-</sup>* (Table S2) and only 13% (3/24) of *Ipo8<sup>+/+</sup>* mice present with macroscopic anomalies (Figure 2). Statistical analysis showed that more abnormalities were present in *Ipo8<sup>-/-</sup>* mice than in *Ipo8<sup>+/+</sup>* mice ( $p = 0.0007$ ), especially with respect to the pale appearance due to the lack of normal vasculature or decreased blood volume ( $p = 0.0089$ ). A pale appearance seems to be more common in male *Ipo8<sup>-/-</sup>* mice (11/17) than in female *Ipo8<sup>-/-</sup>* mice (3/14) ( $p = 0.016$ ).

Although several findings such as hemorrhages and a pale skin were also observed in heterozygous animals (despite the fact that adult *Ipo8<sup>+/-</sup>* mice are not known to present with a disease phenotype), statistical analysis showed that more abnormalities were present in *Ipo8<sup>-/-</sup>* mice than in *Ipo8<sup>+/-</sup>* mice ( $p = 0.014$ ), especially with respect to the lack of normal vasculature or decreased blood volume ( $p = 0.0052$ ) and the bulging neck (edema) ( $p = 0.032$ ). For wild type animals, only a pale appearance could be observed, no other abnormalities. More detailed data can be found in supplementary Table 2.

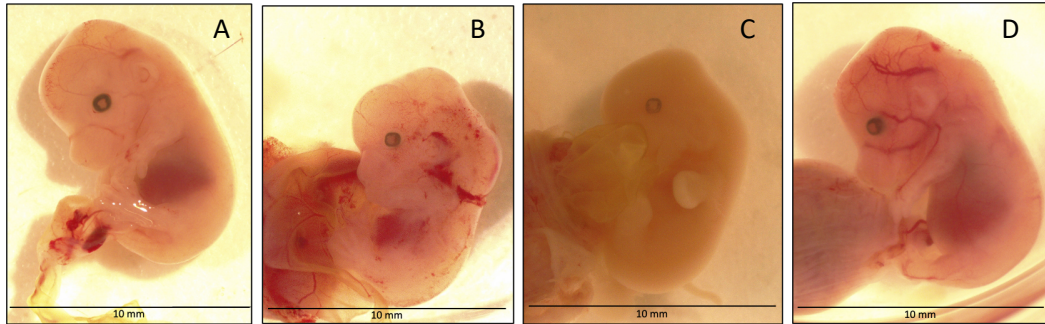


**Figure 2. Examples of homozygous mutant embryos with different morphological characteristics.** (A) *Ipo8*<sup>-/-</sup> embryo lacking vasculature or have decreased circulation (looking pale) (B) *Ipo8*<sup>-/-</sup> embryo looking pale, hemorrhages widespread throughout the body and a bulging neck (edema). (C) *Ipo8*<sup>-/-</sup> embryo looking pale, with underdeveloped vasculature, and underdeveloped limbs and digits. (D) *Ipo8*<sup>+/+</sup> (wild type) embryo looking healthy.

### **3.5 Histological examination reveals excessive trabeculation in left ventricle with endothelial cell layer detachment from endocardium**

To identify the cause of embryological death, C57BL/6N *Ipo8*<sup>-/-</sup> embryos were microscopically evaluated after embedding, transversal sectioning and HE staining. Specific attention was given to the cardiovascular embryonic processes that are supposed to be completed by E13-E14.5. The latter include the septation of the outflow tract and ventricles, remodeling of the atrioventricular cushion and development of the aortic arch with its branches [8, 9].

In total three *Ipo8*<sup>-/-</sup> females, four *Ipo8*<sup>-/-</sup> males and three *Ipo8*<sup>+/+</sup> embryos (two males and one female) were analyzed for HE staining and IHC. A distinction between E13.5 and E14.5 embryos, based on the presence/absence of the interventricular foramen and atrioventricular valve development, revealed that three *Ipo8*<sup>-/-</sup> embryos were of age E14.5, whilst the other *Ipo8*<sup>-/-</sup> embryos were of age E13.5. Two wild types were of ages E14.5 and one was E13.5. Based on the observed 50% embryonic lethality in *Ipo8*<sup>-/-</sup> mice, we anticipated to find anomalies in about half of the homozygotes and in none of the wild type embryos. These anomalies should be severe enough to cause late gestational death.

After analysis of the HE histological slides, we observed a pronounced pathological cardiovascular phenotype in three (two males and one female, all E14.5) out of seven investigated *lpo8<sup>-/-</sup>* mice. Remarkably, the three affected embryos with excessive trabeculation were all age E14.5. In those three affected mice, we identified a near-absence of, or a decrease in, left ventricular lumen (obliteration) (3/3), as well as a slightly dilated pulmonary artery (3/3) and a thinner aortic wall in comparison to the pulmonary artery wall (3/3), an increase in thickness of the right ventricular wall (1/3) and thickening of the interventricular septum (2/3) (Figure 3). These findings indicate obliteration of the left ventricle, where the right part of the heart tries to compensate for the malfunctioning of the left ventricle. Subsequently, a thinner aortic wall is probably due to the decrease in aortic blood flow, lowering cardiac output and pressure on the aortic wall.

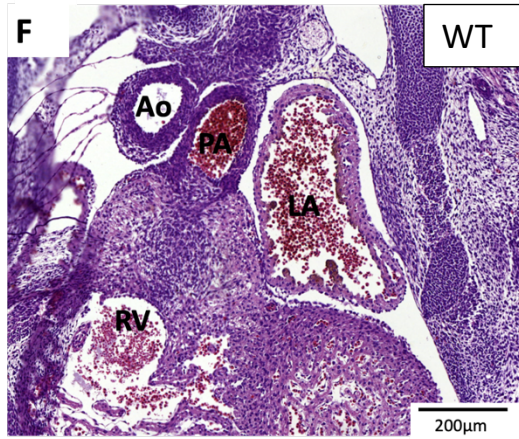
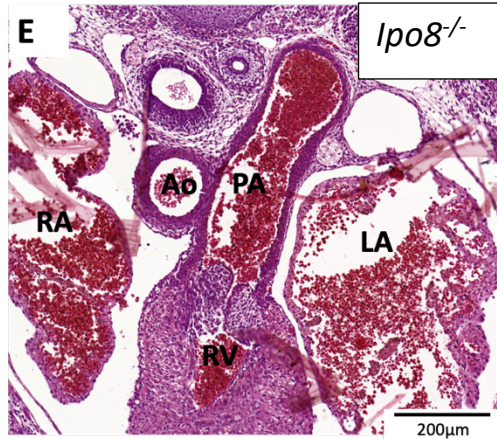
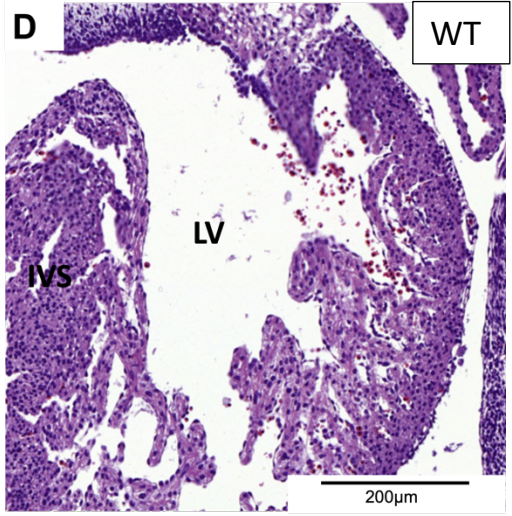
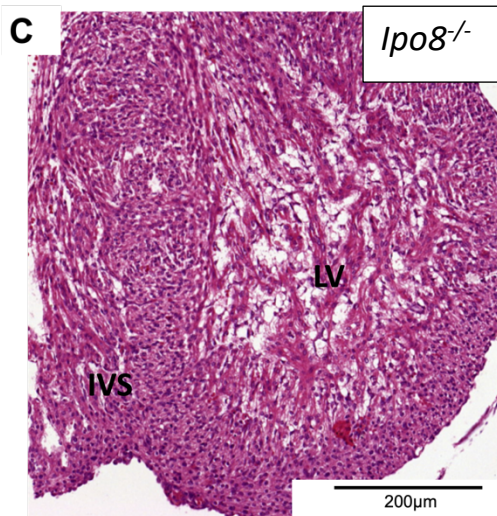
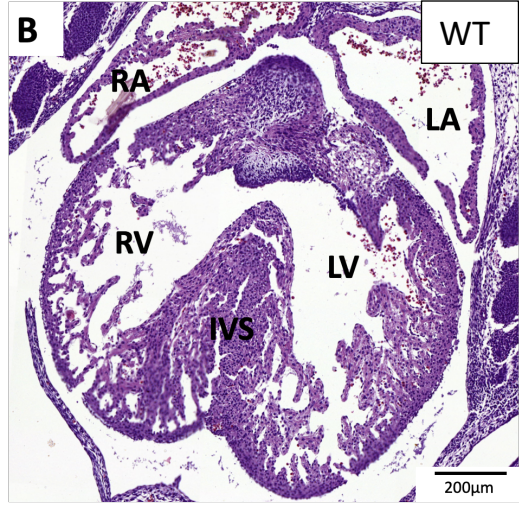
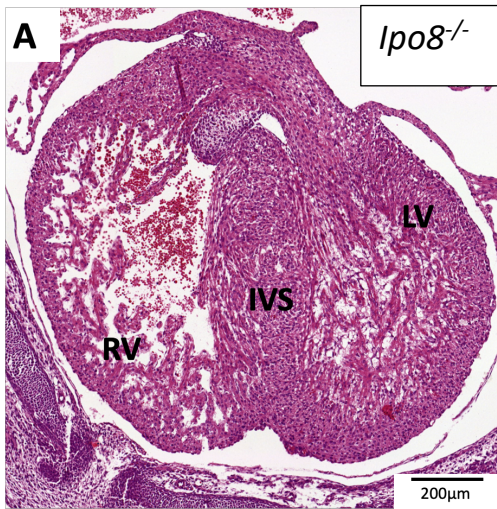


**Figure 3. Histological Hematoxylin-Eosin staining (HE) on embryonic sections.** A representation of (A) *Ipo8*<sup>-/-</sup> heart with left ventricle obliteration (B) Wild type heart with normal left ventricle (C) Close-up of *Ipo8*<sup>-/-</sup> with left ventricle obliteration (D) Close-up of wild type left ventricle (E) *Ipo8*<sup>-/-</sup> with increased pulmonary artery diameter (F) Wild type with normal pulmonary artery diameter LV: left ventricle, RV: right ventricle, RA: right atrium, LA: left atrium, Ao: aorta, PA: pulmonary artery, IVS: interventricular septum.

Strictly controlled cell proliferation is an essential process during embryonic cardiovascular development. We hypothesized that an increase in proliferative capacity could be the cause of the observed obliteration of the left ventricular lumen. However, regarding the immunostaining with proliferation marker PCNA no major conclusions on excessive proliferation in the affected mutants can be made (Supplementary Figure 1). Next, we investigated the abundance and localization of left ventricular endothelial cells using immunostaining for the endothelial cell marker CD31. Detachment of the endocardium's inner endothelial cell layer was observed in 3/3 affected *Ipo8*<sup>-/-</sup> mice (Figure 4A-C), along with edema-like filling in-between the detached endothelial cell layer and the subendocardial connective tissue. It remains to be determined what exactly fills the newly developed voids. Additionally, a thinner compact myocardium zone in the left ventricle was seen (Figure 4A).

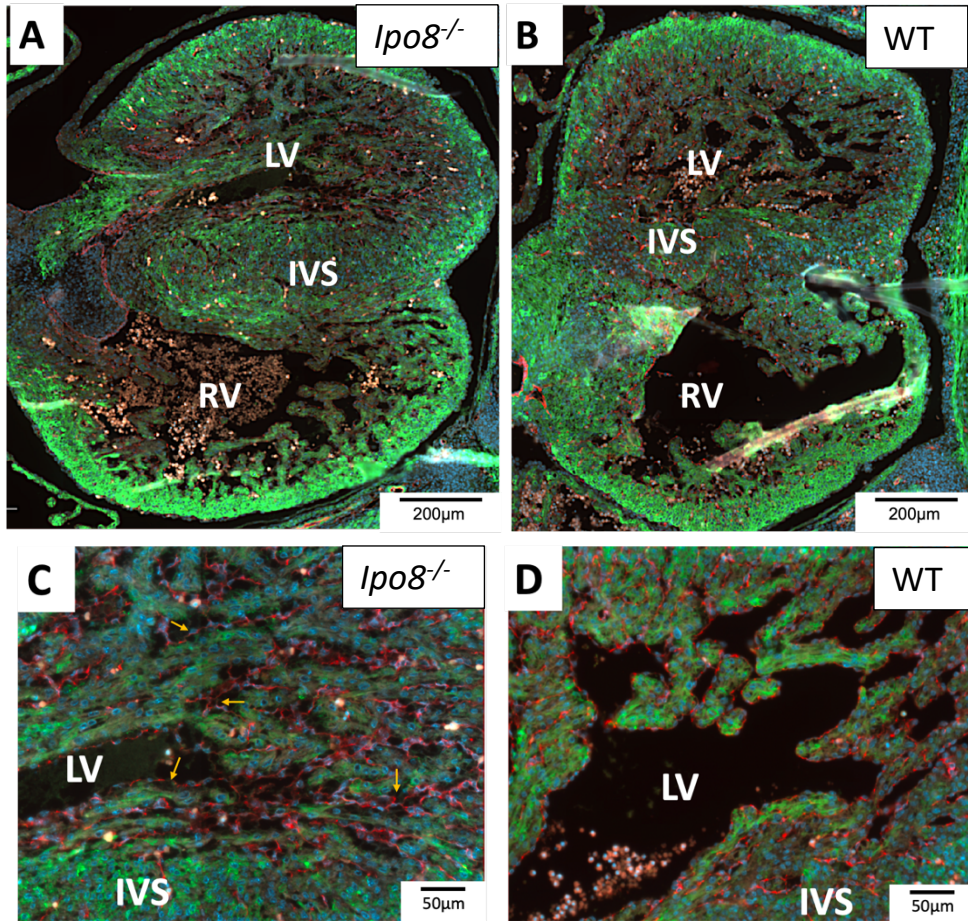


**Figure 4. Immunohistochemistry staining on embryonic sections.** *CD31* in red, *1A4* smooth muscle actin in green and *DAPI* in blue. A representation of (A) *Ipo8*<sup>-/-</sup> heart with left ventricle obliteration (B) Wild type heart (C) A close-up of *Ipo8*<sup>-/-</sup> left ventricle with endothelial cell layer detachment (D) A close-up of *Ipo8*<sup>+/+</sup> left ventricle. Several detachment regions have been indicated with a yellow arrow. LV: left ventricle, RV: right ventricle, IVS: interventricular septum

One might expect that the *Ipo8*<sup>-/-</sup> embryos with severe macroscopic abnormalities would be the same as those with microscopic defects. To our surprise, however, no correlation was seen between the presence of macroscopic and microscopic defects. More precisely, one out of the three mice exhibiting severe microscopic defects was macroscopically normal. The other two severely affected *Ipo8*<sup>-/-</sup> embryos were

macroscopically pale, but the relevance is unclear as paleness was also observed in *Ipo8*<sup>+/+</sup> animals.

Besides the cardiovascular system also the respiratory system was briefly examined, but it did not show abnormalities. At E13.5-14.5, the lungs are in a pseudoglandular stage, where the fluid-filled respiratory tree is too primitive and immature to support gas exchange efficiently [17]. Since no microscopic abnormalities of the respiratory system were observed and the proper lung function is only of importance postnatally, it is unlikely that abnormal respiratory tree development is the cause of embryonic lethality in *Ipo8*<sup>-/-</sup> mice.

#### 4 Discussion

---

Here we report and investigate 50% embryonic lethality in C57BL/6N *Ipo8*<sup>-/-</sup> mice, occurring between E13.5-E14.5 and birth, likely due to severe defects in cardiovascular development. Importin-8 has previously been demonstrated to function as a nucleocytoplasmic transport receptor, transporting cargoes from the cytosol to the nucleus in a RanGTP dependent manner [5]. Its role during embryonic development specifically has not been studied before.

Initial IMPC phenotyping of the KOMP C57BL/6N *Ipo8*<sup>-/-</sup> mouse model revealed loss of grip strength as the only significant observation. This phenotype correlates well with the hypotonia seen in *IPO8* patients (<https://phenome.jax.org/komp/genotypes/2660002?study=EAP>). Subsequently, we further phenotyped the C57BL/6N *Ipo8*<sup>-/-</sup> mouse model in light of our TAA research [4]. During our studies, we noticed that upon C57BL/6N *Ipo8*<sup>+/-</sup> x C57BL/6N *Ipo8*<sup>+/-</sup> breeding, 50% of *Ipo8*<sup>-/-</sup> mice die during embryonic development. Timed matings revealed a normal genotypic distribution at age E13.5-E14.5, suggesting that death occurs between E13.5-E14.5 and birth. The 50% of *Ipo8*<sup>-/-</sup> mice that are born alive develop progressive TAA with possible dissection from eight weeks onwards [4].

In 58% of *Ipo8*<sup>-/-</sup> embryos gross anatomical abnormalities were seen, including lack of vasculature/decreased cardiac output leading to a pale appearance (14/31), a bulging head or neck with possible edema (3/31), underdeveloped limbs (2/31) and hemorrhages throughout the whole body (5/31). Several of these morphological abnormalities can also be found in *Ipo8*<sup>+/-</sup> and even *Ipo8*<sup>+/+</sup> mice, but to a much lesser extent. In literature, it has been stated that these macroscopic findings represent normal anatomical variations occurring during murine pregnancy. They can be a harbinger for cardiovascular embryonic lethality but are not an exclusive or decisive factor [18-20]. Of note, macroscopic evaluation cannot distinguish between a decrease in blood flow due to insufficient cardiac output, what we would expect based on our microscopic results, or impaired vascularization. A whole embryonic body immunostaining for vascular smooth muscle cells, could provide us with more information on the degree of vascularization.

Immunohistological examination of *Ipo8*<sup>-/-</sup> embryos revealed an abnormally filled left ventricular lumen with endocardial-myocardial cell layer detachment as well as a dilated pulmonary artery and a thinner aortic wall compared to the pulmonary artery wall. Three out of seven *Ipo8*<sup>-/-</sup> embryos were found to exhibit a decreased left ventricular lumen volume with endocardial cell layer detachment, lowering cardiac output and resulting in inadequate blood and oxygen supply throughout the body. Abnormal heart development thus seems to contribute to the lethality seen in *Ipo8*<sup>-/-</sup> embryos. The fact that both genders were found to have these structural abnormalities, indicates the absence of a gender-specific effect and corroborates with the observed gender ratios of live-born *Ipo8*<sup>-/-</sup> mice. The 50% embryonic survival rate can probably be explained by the severity of left ventricle impairment: the size of the remaining lumen will most probably determine whether the embryo survives or not. Several causes of a filled left ventricular lumen exist. The most likely one involves the presence of left ventricle non-compaction (LVNC) [21], recently renamed as excessive trabeculation

[22]. Trabeculation is the consequence of abnormal muscle cell extension into the left ventricular lumen, with the formation of deep endomyocardial spaces called sinusoids. Excessive trabeculation can coexist with other cardiac abnormalities, often leading to systolic impairment [23]. Determinants of excessive trabeculation include mutations in genes coding for proteins of myofibril structures and sarcomeres [24, 25], such as  $\beta$ -myosin heavy chain (MYH7), cardiac troponin T and I (TNNT2 and TNNI3) [26] and myosin light chains (MYL2 and MYL3), which are often also associated with cardiomyopathies and/or congenital malformations [27]. Other genes involved in excessive trabeculation are *SCN5A* and *HCN4*, both encoding for cardiac ion-channels [28]. However, the genetic landscape is likely to be much more extensive, with more than 25 knock-out mouse models being yet described to present with an excessive trabeculation phenotype. In these models, excessive trabeculation has been causally linked to prenatal lethality, with the degree of trabeculation correlating to the percentage of embryonic death [26, 29-31]. The endothelial cell layer detachment that we observed in our *Ipo8*<sup>-/-</sup> pups has not been observed in any of the aforementioned models, suggesting that excessive trabeculation is sufficient to induce embryonic lethality, and that the endothelial detachment could be a consequence or bystander effect.

Molecularly, we hypothesize the involvement of abnormal TGF- $\beta$  signaling in impaired cardiogenesis, including excessive trabeculation leading to embryonic lethality in C57BL/6N *Ipo8*<sup>-/-</sup> mice. Our hypothesis is based on several findings described in literature. First, Kodo et al delivered evidence on the central role of TGF- $\beta$  in the pathogenesis of exaggerated left ventricle trabeculation [32]. Additionally, evidence for a relationship between TGF- $\beta$  dysregulation and embryonic lethality comes from vascular-specific overexpression of TGFB1 in transgenic mice (C57BL/6JxSJL), which results in 100% lethality before age E10.5 [33]. Furthermore, FKBP12-deficient mice (C57BL/6J/129SvEv), who also exhibit excessive trabeculation, die between embryonic

day E14.5 and birth, similarly to our *Ipo8*<sup>-/-</sup> mice. FKBP12 functions as a subunit of the TGF-β1 receptor and acts as an inhibitor for TGF-β signaling via the Smad7-Smurf1 complex [34, 35]. Additionally, FKBP12-deficient mice showed an upregulation of *Bmp10*, a key member of the TGF-β superfamily and expressed in the developing heart, which led to increased cardiomyocyte proliferation, differentiation and maturation as well as excessive trabeculation. Given the normal proliferation rates seen in the left ventricle of *Ipo8*<sup>-/-</sup> embryos, we hypothesize that abnormal differentiation and/or immaturity of cardiomyocytes during ventricular wall formation are a cause of left ventricle obliteration, corroborating with the observed left ventricle lumen obliteration in the absence of excessive cell proliferation. Research in *Smad7* knock-out embryos (C57BL/6), lacking the TGF-β inhibitor Smad7, confirms that lethal (E14.5-E16.E) excessive trabeculation can occur without increased cell proliferation [36].

Besides Importin-8 another Importin member of the karyopherin family, i.e. Importin-11 (*IPO11*), has been linked to embryonic lethality. The *Ipo11*<sup>-/-</sup> mouse model on a C57BL/6J genetic background shows a 100% embryonic lethal phenotype by age E11.5. Important findings were a reduced body size at embryonic day E10.5 in comparison to their wild type counterparts. Morphological examination showed no difference between the *Ipo11*<sup>-/-</sup> and *Ipo11*<sup>+/+</sup> mice at E9.5. Whereas it seems that Importin-11 is involved in the early embryonic stage, Importin-8 could be involved in the mid-or-late embryonic stages [37].

In contrast to the C57BL/6N *Ipo8*<sup>-/-</sup> embryos, 129/Sv *Ipo8*<sup>-/-</sup> pups are all live-born, indicating that *Ipo8*-related embryonic lethality can be influenced by protective or aggravative genetic modifiers which are specific to certain genetic backgrounds. Embryonic death is commonly observed in transgenic mouse models and its penetrance often differs between discrete genetic background [38]. Sanford et al, for example, also reported a strain dependency of lethal phenotypes in *Tgfb1* knock-out mice. On a mixed background, 50% of mutant animals survive to birth and develop an autoimmune-like

inflammatory disorder [39]. On the contrary, only 1% of mutant animals on a C57BL/6 inbred background are born and develop an auto-immune-like inflammatory disorder [40].

## 5 Study limitations

---

While providing interesting insights, the current study has some limitations. A first one is the small size of the cohort used for microscopic evaluation as well as the one-day heterogeneity in embryonic age (E13.5 vs E14.5). A further increase in embryos subjected to microscopic evaluation at age E14.5 can provide more confident proof for our findings and preliminary conclusions. Second, as *IPO8* is ubiquitously expressed, it can play a crucial role in the development of other organ systems too. At E13.5-E14.5, *IPO8* is expressed in the heart, lung and kidney ([FANTOM5 data](#)). Additionally, kidney dysfunction has been reported as a cause for embryonic lethality occurring around E12.5 during embryogenesis [41]. We excluded lung abnormalities as a possible leading cause of embryonic lethality in *Ipo8*<sup>-/-</sup> mice but did not yet examine the kidneys. Third, no explanation has yet been found for left ventricular endothelial cell layer detachment, neither is it known which substance fills the created voids. Nonetheless, based on literature data, excessive trabeculation alone has been demonstrated to cause embryonic lethality, rendering it unclear how physiologically relevant this “edema-like” phenotype is.

## 6 Conclusions

---

In conclusion, we can say that C57BL/6N *Ipo8*<sup>-/-</sup> mice show embryonic/perinatal lethality of approximately 50% starting from the age of E13.5-E14.5 until birth. On the contrary, no embryonic lethality was reported in 129/Sv *Ipo8*<sup>-/-</sup> mice. Morphological and histological examination of C57BL/6N *Ipo8*<sup>-/-</sup> mice points towards a cardiovascular cause, i.e. impaired left ventricular function. The precise contribution of TGF-β

dysfunction to the observed embryonic death remains to be determined. Furthermore, as we hitherto only looked for aortic abnormalities in adult *Ipo8*<sup>-/-</sup> mice, it might be interesting to study the entire adult heart, both with respect to function and structure, in more depth.

## 7 References

---

1. De Cario, R., et al., *Tracking an Elusive Killer: State of the Art of Molecular-Genetic Knowledge and Laboratory Role in Diagnosis and Risk Stratification of Thoracic Aortic Aneurysm and Dissection*. Diagnostics (Basel), 2022. **12**(8).
2. Luyckx, I., et al., *Update on the molecular landscape of thoracic aortic aneurysmal disease*. Curr Opin Cardiol, 2022. **37**(3): p. 201-211.
3. Pinard, A., G.T. Jones, and D.M. Milewicz, *Genetics of Thoracic and Abdominal Aortic Diseases*. Circ Res, 2019. **124**(4): p. 588-606.
4. Van Gucht, I., et al., *A human importin-beta-related disorder: Syndromic thoracic aortic aneurysm caused by bi-allelic loss-of-function variants in IPO8*. Am J Hum Genet, 2021. **108**(6): p. 1115-1125.
5. Hu, X., et al., *Mitogen-activated protein kinase inhibitors reduce the nuclear accumulation of phosphorylated Smads by inhibiting Imp 7 or Imp 8 in HepG2 cells*. Oncol Lett, 2018. **15**(4): p. 4867-4872.
6. Graham, E., et al., *The atlas of mouse development eHistology resource*. Development, 2015. **142**(14): p. 2545.
7. Hutson, M.R. and M.L. Kirby, *Model systems for the study of heart development and disease. Cardiac neural crest and conotruncal malformations*. Semin Cell Dev Biol, 2007. **18**(1): p. 101-10.
8. Savolainen, S.M., J.F. Foley, and S.A. Elmore, *Histology atlas of the developing mouse heart with emphasis on E11.5 to E18.5*. Toxicol Pathol, 2009. **37**(4): p. 395-414.
9. Adams, D., et al., *Bloomsbury report on mouse embryo phenotyping: recommendations from the IMPC workshop on embryonic lethal screening*. Dis Model Mech, 2013. **6**(3): p. 571-9.
10. Health, E.P.o.A. and Welfare, *Guidance on Risk Assessment for Animal Welfare*. EFSA Journal, 2012. **10**(1): p. 2513.
11. Byers, S.L., et al., *Mouse estrous cycle identification tool and images*. PLoS One, 2012. **7**(4): p. e35538.
12. Flurkey, K. and J.M. Curren, *The Jackson Laboratory handbook on genetically standardized mice*. 2009: Jackson Laboratory.
13. Finlay, J.B., et al., *Maternal Weight Gain as a Predictor of Litter Size in Swiss Webster, C57BL/6J, and BALB/cJ mice*. J Am Assoc Lab Anim Sci, 2015. **54**(6): p. 694-9.

14. Ward, J.M., S.A. Elmore, and J.F. Foley, *Pathology methods for the evaluation of embryonic and perinatal developmental defects and lethality in genetically engineered mice*. Vet Pathol, 2012. **49**(1): p. 71-84.
15. Fisher, S.A., B.L. Langille, and D. Srivastava, *Apoptosis during cardiovascular development*. Circ Res, 2000. **87**(10): p. 856-64.
16. Hurle, J.M., E. Colvee, and A.M. Blanco, *Development of mouse semilunar valves*. Anat Embryol (Berl), 1980. **160**(1): p. 83-91.
17. Warburton, D., et al., *Lung organogenesis*. Curr Top Dev Biol, 2010. **90**: p. 73-158.
18. Bonney, E.A. and S.A. Brown, *To drive or be driven: the path of a mouse model of recurrent pregnancy loss*. Reproduction, 2014. **147**(5): p. R153-67.
19. Wang, W.J., et al., *Adoptive transfer of pregnancy-induced CD4+CD25+ regulatory T cells reverses the increase in abortion rate caused by interleukin 17 in the CBA/JxBALB/c mouse model*. Hum Reprod, 2014. **29**(5): p. 946-52.
20. Huo, S., et al., *Porcine soluble CD83 alleviates LPS-induced abortion in mice by promoting Th2 cytokine production, Treg cell generation and trophoblast invasion*. Theriogenology, 2020. **157**: p. 149-161.
21. Chen, H., et al., *Analysis of ventricular hypertrabeculation and noncompaction using genetically engineered mouse models*. Pediatr Cardiol, 2009. **30**(5): p. 626-34.
22. Petersen, S.E., et al., *Excessive Trabeculation of the Left Ventricle: JACC: Cardiovascular Imaging Expert Panel Paper*. JACC Cardiovasc Imaging, 2023. **16**(3): p. 408-425.
23. Abela, M. and A. D'Silva, *Left Ventricular Trabeculations in Athletes: Epiphenomenon or Phenotype of Disease?* Curr Treat Options Cardiovasc Med, 2018. **20**(12): p. 100.
24. Klaassen, S., et al., *Mutations in sarcomere protein genes in left ventricular noncompaction*. Circulation, 2008. **117**(22): p. 2893-901.
25. Xing, Y., et al., *Genetic analysis in patients with left ventricular noncompaction and evidence for genetic heterogeneity*. Mol Genet Metab, 2006. **88**(1): p. 71-7.
26. Luedde, M., et al., *Severe familial left ventricular non-compaction cardiomyopathy due to a novel troponin T (TNNT2) mutation*. Cardiovasc Res, 2010. **86**(3): p. 452-60.
27. van Waning, J.I., et al., *Systematic Review of Genotype-Phenotype Correlations in Noncompaction Cardiomyopathy*. J Am Heart Assoc, 2019. **8**(23): p. e012993.
28. Milano, A., et al., *HCN4 mutations in multiple families with bradycardia and left ventricular noncompaction cardiomyopathy*. J Am Coll Cardiol, 2014. **64**(8): p. 745-56.

29. Liu, Y., H. Chen, and W. Shou, *Potential Common Pathogenic Pathways for the Left Ventricular Noncompaction Cardiomyopathy (LVNC)*. *Pediatr Cardiol*, 2018. **39**(6): p. 1099-1106.
30. Li, D., et al., *Dishevelled-associated activator of morphogenesis 1 (Daam1) is required for heart morphogenesis*. *Development*, 2011. **138**(2): p. 303-15.
31. Lee, Y.C., et al., *Glycogen-branching enzyme deficiency leads to abnormal cardiac development: novel insights into glycogen storage disease IV*. *Hum Mol Genet*, 2011. **20**(3): p. 455-65.
32. Kodo, K., et al., *iPSC-derived cardiomyocytes reveal abnormal TGF-beta signalling in left ventricular non-compaction cardiomyopathy*. *Nat Cell Biol*, 2016. **18**(10): p. 1031-42.
33. Agah, R., et al., *Cardiovascular overexpression of transforming growth factor-beta(1) causes abnormal yolk sac vasculogenesis and early embryonic death*. *Circ Res*, 2000. **86**(10): p. 1024-30.
34. Shou, W., et al., *Cardiac defects and altered ryanodine receptor function in mice lacking FKBP12*. *Nature*, 1998. **391**(6666): p. 489-92.
35. Wang, T. and P.K. Donahoe, *The immunophilin FKBP12: a molecular guardian of the TGF-beta family type I receptors*. *Front Biosci*, 2004. **9**: p. 619-31.
36. Chen, Q., et al., *Smad7 is required for the development and function of the heart*. *J Biol Chem*, 2009. **284**(1): p. 292-300.
37. Lee, J.Y., et al., *Importin-11 is Essential for Normal Embryonic Development in Mice*. *Int J Med Sci*, 2020. **17**(6): p. 815-823.
38. Papaioannou, V.E. and R.R. Behringer, *Early embryonic lethality in genetically engineered mice: diagnosis and phenotypic analysis*. *Vet Pathol*, 2012. **49**(1): p. 64-70.
39. Kulkarni, A.B., et al., *Transforming growth factor beta 1 null mutation in mice causes excessive inflammatory response and early death*. *Proc Natl Acad Sci U S A*, 1993. **90**(2): p. 770-4.
40. Sanford, L.P., et al., *Influence of genetic background on knockout mouse phenotypes*. *Methods Mol Biol*, 2001. **158**: p. 217-25.
41. Bergmann, C., et al., *Loss of nephrocystin-3 function can cause embryonic lethality, Meckel-Gruber-like syndrome, situs inversus, and renal-hepatic-pancreatic dysplasia*. *Am J Hum Genet*, 2008. **82**(4): p. 959-70.

## Web resources

JAX phenome, <https://phenome.jax.org/komp/genotypes/2660002?study=EAP>  
 JAX, timed matings, <https://www.jax.org/news-and-insights/jax-blog/2014/september/six-steps-for-setting-up-timed-pregnant-mice>  
<https://www.mousephenotype.org/impress/ProcedureInfo?action=list&procID=707&pipeID=12>

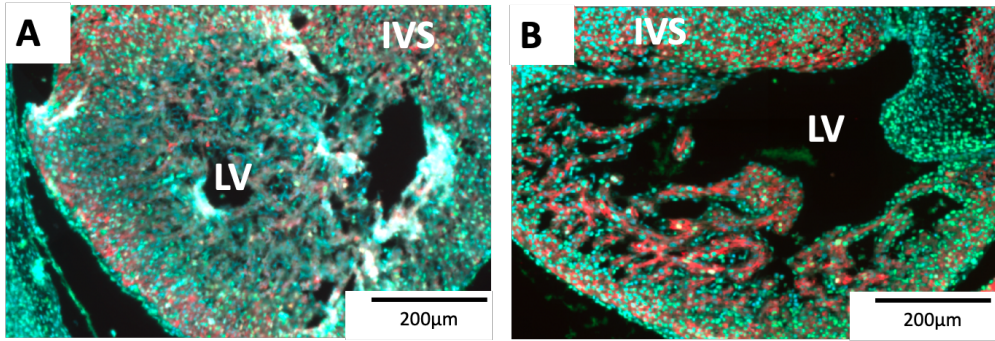
## 8 Supplementary

**Supplementary Table 1: IMPC data of observed genotypes at birth after breeding of *Ipo8*<sup>+/-</sup> animals.** *Ipo8*<sup>+/+</sup>: wild types, *Ipo8*<sup>+/-</sup>: heterozygotes, *Ipo8*<sup>-/-</sup>: homozygotes. (IMPC reference: [https://www.mousephenotype.org/data/charts?accession=MGI:2444611&parameter\\_stable\\_id=IMPC\\_VIA\\_001\\_001&parameter\\_stable\\_id=IMPC\\_VIA\\_063\\_001&parameter\\_stable\\_id=IMPC\\_VIA\\_064\\_001&parameter\\_stable\\_id=IMPC\\_VIA\\_065\\_001&parameter\\_stable\\_id=IMPC\\_VIA\\_066\\_001&parameter\\_stable\\_id=IMPC\\_VIA\\_067\\_001](https://www.mousephenotype.org/data/charts?accession=MGI:2444611&parameter_stable_id=IMPC_VIA_001_001&parameter_stable_id=IMPC_VIA_063_001&parameter_stable_id=IMPC_VIA_064_001&parameter_stable_id=IMPC_VIA_065_001&parameter_stable_id=IMPC_VIA_066_001&parameter_stable_id=IMPC_VIA_067_001))

Observed IMPC	<i>Ipo8</i> <sup>+/+</sup>	<i>Ipo8</i> <sup>+/-</sup>	<i>Ipo8</i> <sup>-/-</sup>	Total
<b>Males and females</b>	55 (29.1%)	107 (56.6%)	27 (14.3%)	189 (100%)
<b>Males</b>	27 (49.1%)	55 (51.4%)	16 (59.3%)	98 (51.9%)
<b>Females</b>	28 (50.9%)	52 (48.6%)	11 (40.7%)	91 (48.1%)

**Supplementary Table 2. Overview morphological observations in *Ipo8*<sup>+/-</sup> embryos.**

<i>Ipo8</i> <sup>+/-</sup> animals	Total	Males	Females
<b>Normal appearance</b>	50/65 (76.9%)	26/33 (78.8%)	24/32 (75%)
<b>Hemorrhages</b>	5/65 (7.7%)	2/33 (6%)	3/32 (9.4%)
<b>Pale</b>	10/65 (15.4%)	6/33 (18%)	4/32 (12.5%)
<b>Bulging neck/head (edema)</b>	1/65 (1.5%)	0/33	1/32 (3.1%)
<b>Underdeveloped</b>	0/65	0/33	0/32



**Supplementary Figure 1. Immunohistochemistry staining on embryonic sections.** *PCNA* in green, *Troponin I* in red and *DAPI* in blue. A representation of (A) *Ipo8*<sup>-/-</sup> with left ventricle obliteration (B) Wild type. LV: left ventricle, RV: right ventricle, IVS: interventricular septum, WT: wild type.

## CHAPTER 7

---

### **Generation of one induced pluripotent stem cell (iPSC) line (BBANTWi011-A) from a patient carrying an *IPO8* bi-allelic loss-of-function variant**

Ilse Van Gucht <sup>1</sup>, Lucia Buccioli <sup>1</sup>, Laura Rabaut <sup>1</sup>, Ivanna Fedoryshchenko <sup>1</sup>, Josephina Meester <sup>1</sup>, Lut Van Laer <sup>1</sup>, Bart L. Loeys <sup>1,6</sup> and Aline Verstraeten <sup>1</sup>

<sup>1</sup>Cardiogenomics Research Group, University of Medical Genetics, University of Antwerp and Antwerp University Hospital, Antwerp, Belgium

<sup>2</sup>Department of Human Genetics, Radboud University Medical Center, Nijmegen, The Netherlands

Published in Stem Cell Research, Lab Resources: Single Cell Line  
<https://doi.org/10.1016/j.scr.2023.103061>

## ABSTRACT

---

Patients carrying *IPO8* bi-allelic loss-of-function variants have a highly consistent phenotype that resembles the phenotype of Loeys-Dietz syndrome. They present with early onset thoracic aortic aneurysm (TAA) and connective tissue findings such as arachnodactyly and joint hypermobility. Other recurrent phenotypic manifestations include facial dysmorphisms, a high arched or cleft palate/bifid uvula and motor developmental delay as well. An iPSC cell line (BBANTWi011-A) was generated started from peripheral blood mononuclear cells (PBMCs) from a patient carrying a homozygous variant in the *IPO8* gene (MIM: 605600, NM\_006390.3: c.1420C>T, p.(Arg474\*)). PBMCs were reprogrammed using the Cytotune®-iPS 2.0 Sendai Reprogramming Kit (Invitrogen). The generated iPSCs are expressing pluripotency markers and able to differentiate into the three germ layers

## 1 Resource Table

Unique stem cell line identifier	BBANTWi011-A <a href="https://hpscereg.eu/cell-line/BBANTWi011-A">https://hpscereg.eu/cell-line/BBANTWi011-A</a>
Alternative name(s) of stem cell line	iPSC_PBMC_IPO8_p.(Arg474*)
Institution	University of Antwerp, Cardiogenomics research group
Contact information of distributor	Bart Loeys – bart.loeys@uantwerpen.be
Type of cell line	iPSC
Origin	Human
Additional origin info required for human ESC or iPSC	Age: 12 years old Sex: Male African
Cell Source	Peripheral blood mononuclear cells (PBMCs)
Clonality	Clonal
Method of reprogramming	Single-stranded RNA Sendai viral transfer of the 4 Yamanaka reprogramming factors including: Oct4, Sox2, c-Myc and Klf4
Genetic Modification	Yes
Type of Genetic Modification	Hereditary
Evidence of the reprogramming transgene loss (including genomic copy if applicable)	Sendai virus presence was proven negative using RT-qPCR.
Associated disease	<i>IPO8</i> related aortopathy syndrome
Gene/locus	IPO8 c.1420C>T; p.(Arg474*)
Date archived/stock date	April 2022
Cell line repository/bank	<a href="https://hpscereg.eu/cell-line/BBANTWi011-A">https://hpscereg.eu/cell-line/BBANTWi011-A</a>
Ethical approval	This study was approved by the Ethics Committee of the Antwerp University Hospital with following approval number 19/19/242.

## 2 Resource Utility

Because the invasiveness of an aortic biopsy often prohibits the use of native vascular smooth muscle cells (VSMC) to investigate the pathomechanism of thoracic aortic aneurysms, iPSC-derived VSMC provide an alternative an unlimited resource to study the underlying disease mechanisms and enable TAA drug discovery.

### 3 Resource Details

---

Thoracic aortic aneurysm (TAA) is caused by a progressive dilatation of the aortic wall, leading to possible dissection or rupture. This event is life-threatening and associated with a high mortality rate of almost 80%. 1-2% of all deaths in Western population are caused by aortic aneurysm and dissection. TAA can occur as an isolated condition or as a part of a systemic disorders affecting connective tissue as well. At present, only 20-30% of TAA patient receive a genetic diagnosis, making the discovery of novel TAA genes of great importance. Using whole exome and genome sequencing (WES/WGS), bi-allelic loss-of-function variants in *IPO8*, encoding for importin 8, a ubiquitously expressed nuclear transport receptor of the importin- $\beta$  family were shown to cause an aortic aneurysm phenotype, overlapping with Loeys-Dietz syndrome. Importin 8 transports RNAs, proteins and ribonucleoprotein complexes from the cytosol to the nucleus in a RanGTP-dependent manner [1]. In addition to TAA, patients carrying *IPO8* bi-allelic loss-of-function present also with structural heart disease including patent ductus arteriosus (PDA), connective tissue findings such as arachnodactyly, joint hypermobility, pectus excavatum, scoliosis and foot deformity. Other recurrent phenotypic manifestations are facial dysmorphisms with dolichocephaly, frontal bossing, hypertelorism, retrognathia and a high arched or cleft palate/bifid uvula. Neurological findings include hypotonia and global developmental delay [2].

At the start of this study, PBMCs from a male 12 years old *IPO8* patient carrying a bi-allelic loss-of-function variant p.(Arg474\*) were isolated and transduced with a Sendai virus containing the four Yamanaka factors more specifically, Oct3/4, Sox2, c-Myc and Klf4. iPSC colonies started to emerge around 12 days post transduction and were manually picked eight times before further expansion and freezing. An example of an iPSC colony is shown in Figure 1A. The presence of pluripotency markers, including Tra-1-60, Tra-1-81, Nanog, Sox2 and Oct3/4 was confirmed using immunocytochemistry

(ICC) (Figure 1B, Table 2) and mRNA expression levels of *NANOG*, *POU5F1*, *DNMT3B* and *SOX2* were determined using RT-qPCR (Figure 1H). Sanger sequencing results revealed the presence of the *IPO8* variant in the created iPSCs, c.1420C>T (p.(Arg474\*)) (Figure 1I). Trilineage differentiation potential was demonstrated via mRNA expression levels of several germ layer specific markers. More specifically, *PAX6*, *MAP2*, *HES5* served as ectodermal markers, whereas *FOXA2*, *SOX17* and *CXCR4*, were used as endodermal markers and *ACTA2*, *NKX2.5* and *DCN* as mesodermal markers (Figure 1F). SNP array results confirmed that the isolated PBMCs and generated iPSCs were derived from the same patient (Figure 1C). No clinically relevant deletions or duplications were detected during CNV analysis (Figure 1G). A more detailed overview of the deletions and duplications can be found in Supplementary Table 1. The Sendai vector was no longer present in the cells and a mycoplasma test was performed that confirmed the absence of the bacteria (Figure 1E).

**Table 1. Characterization and validation**

Classification	Test	Result	Data
<b>Morphology</b>	Photography Bright field	Visual records of the line: normal	Figure 1A
<b>Phenotype</b>	Qualitative analysis Immunocytochemistry	Presence of pluripotency markers Oct3/4, Sox2, Nanog, Tra-1-60, Tra1-81.	Figure 1B
	Quantitative analysis RT-qPCR	mRNA expression of <i>POU5F1</i> , <i>NANOG</i> , <i>SOX2</i> and <i>DNMT3B</i>	Figure 1H
<b>Genotype</b>	HumanCytoSNP-12 array	No clinically relevant abnormalities observed. Resolution 72kb.	Figure 1G
<b>Identity</b>	HumanCytoSNP-12 array	>99.9% of identical SNPs	Figure 1C

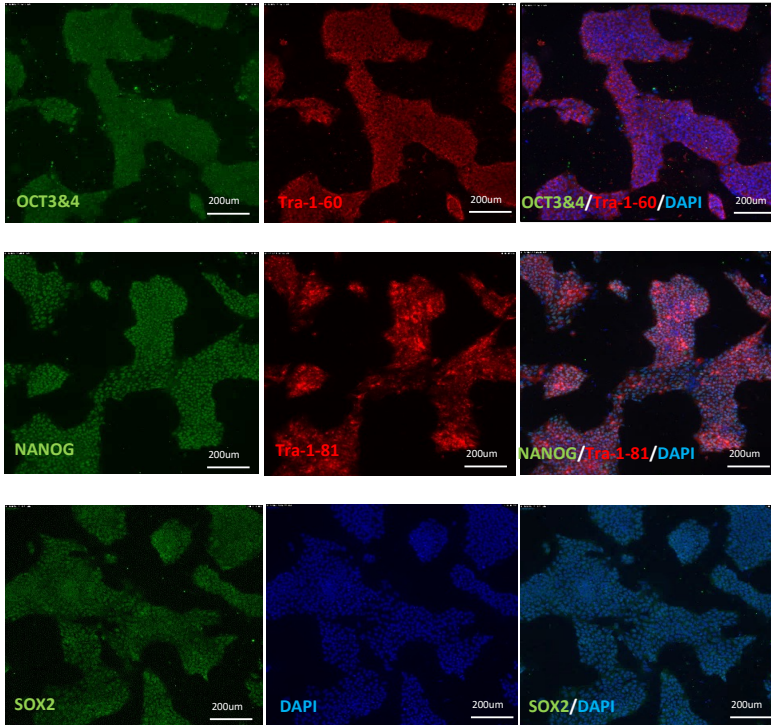
	STR analysis	N/A	N/A
<b>Mutation analysis (IF APPLICABLE)</b>	Sequencing	<i>IPO8</i> , NM_006390.3, c.1420C>T; p.(Arg474*), homozygous	Figure 1I
	Southern Blot OR WGS	N/A	N/A
<b>Microbiology and virology</b>	Mycoplasma	Mycoplasma by RT-PCR : Negative	Figure 1D
<b>Differentiation potential</b>	Directed differentiation	Ectoderm: <i>PAX6</i> , <i>MAP2</i> , <i>HES5</i> Endoderm: <i>FOXA2</i> , <i>SOX17</i> , <i>CXCR4</i> Mesoderm: <i>ACTA2</i> , <i>NKX2.5</i> , <i>DCN</i>	Figure 1F
<b>Donor screening (OPTIONAL)</b>	HIV 1 + 2 Hepatitis B, Hepatitis C	N/A	N/A
<b>Genotype additional info (OPTIONAL)</b>	Blood group genotyping	N/A	N/A
	HLA tissue typing	N/A	N/A

**Table 2. Reagents details**

<b>Antibodies used for immunocytochemistry/flow-cytometry</b>					
	<b>Antibody</b>	<b>Dilution</b>	<b>Company Cat #</b>	<b>RRID</b>	
Pluripotency Markers (Primary)	Tra1-60 Mouse Anti-Human IgM	1:200	Cell Signaling technology Cat# 4746S	AB_2119059	
	Oct 4, Rabbit Anti-human IgG	1:100	Thermo Fisher Scientific Cat# PA5-96860	AB_2808662	
	Sox2, Rabbit Anti-Human IgG	1:500	Thermo Fisher Scientific Cat# PA1-097	AB_2286686	
	Tra 1-81, Mouse Anti-Human IgM	1:200	Millipore Cat# AB5603	AB_2119060	
	Nanog, Rabbit Anti-Human IgG	1:500	Cell Signaling Technology Cat# 4745S	AB_2539867	
Pluripotency Markers (Secondary)	AF555 Goat Anti-Mouse IgM	1:500	Thermo Fisher Scientific Cat# A-21426	AB_2535847	
	AF488, Goat Anti-Rabbit	1:500	Thermo Fisher Scientific Cat# A-11034,	AB_2576217	
Pluripotency Markers (Secondary)	AF555 Goat Anti-Mouse IgM	1:500	Thermo Fisher Scientific Cat# A-21426	AB_2535847	
	AF488, Goat Anti-Rabbit	1:500	Thermo Fisher Scientific Cat# A-11034,	AB_2576217	
<b>Primers</b>					
	<b>Target</b>	<b>Size of band</b>	<b>Forward/Reverse primer (5'-3')</b>		
Targeted mutation sequencing (Sanger Sequencing)	<i>IPO8</i> , NM_006390.3, c.1420C>T; (p.(Arg474*))	502 bp	CAC GGG GCA TCT TTC AGT GG TGA GTG TGG CTT GGC TCT GG		
Pluripotency Markers (RT-qPCR)	<i>POU5F1</i>	77 bp	Hs04260367_gH		
	<i>NANOG</i>	99 bp	Hs04260366_g1		
	<i>SOX2</i>	91 bp	Hs01053049_s1		
	<i>DNMT3B</i>	55 bp	Hs00171876_m1		

Endodermal markers (qPCR)	<i>SOX17</i> <i>FOXA2</i> <i>CXCR4</i>	149 bp 66 bp 153 bp	Hs00751752_s1 Hs00232764_m1 Hs00607978_s1
Mesodermal markers (qPCR)	<i>NKX2.5</i> <i>ACTA2</i> <i>DCN</i>	64 bp 105 bp 109 bp	Hs01387463_g1 Hs00426835_g1 Hs00754870_s1
Ectodermal markers (qPCR)	<i>PAX6</i> <i>MAP2</i> <i>HES5</i>	76 bp 98 bp 62 bp	Hs00240871_m1 Hs00258900_m1 Hs01387463_g1
House-Keeping Genes (qPCR)	<i>GAPDH</i> <i>ACTB</i>	93 bp 63 bp	Hs99999905_m1 Hs01060665_g1
Sendai virus	SeV	181 bp	GGA TCA CTA GGT GAT ATC GAG C ACC AGA CAA GAG TTT AAG AGA TAT GTA TC

B



F

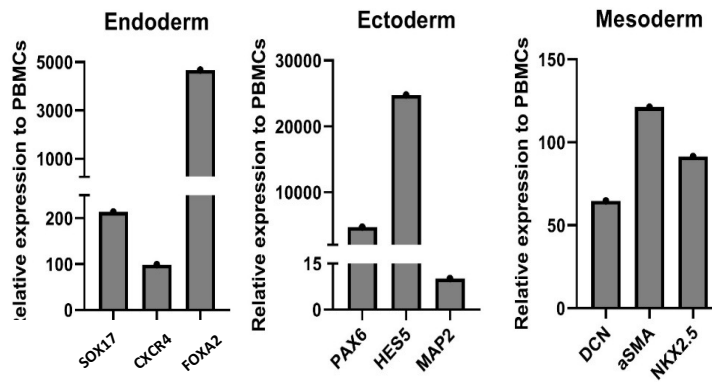


**Figure 1 (Part B and F). Characterization and validation results – (B) Immunohistochemistry (F) Differentiation potential with endodermal, ectodermal and mesodermal markers.**

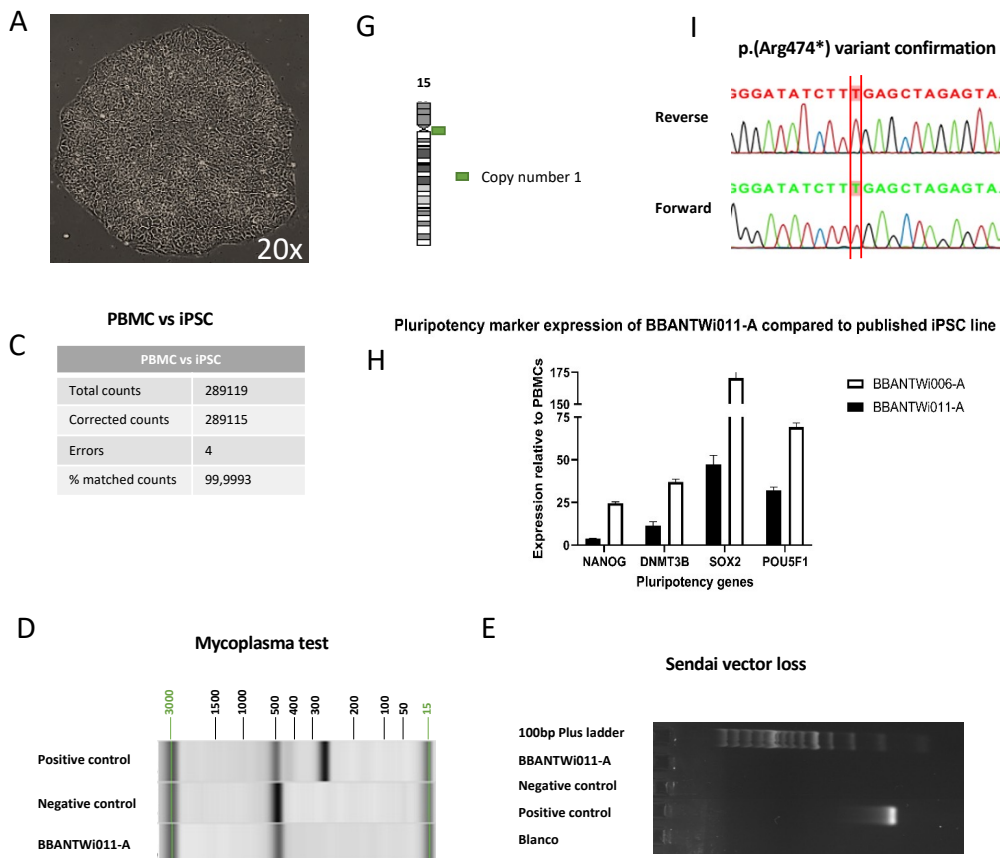


**Figure 1 (Part A-C-D-E-G-H-I). Characterization and validation results (A) Bright field morphology (C) Results from HumanCytoSNP-12 array identity check (D) Mycoplasma test (E) Results Sendai virus detection (G) Results from HumanCytoSNP-12 array genotype check (H) Quantitative analysis RT-qPCR pluripotency markers (I) Results mutation analysis with sequencing**

## 4. Materials and methods

### 1. Ethical statement

The study was approved by the appropriate institutional ethics review boards and the required informed consents were obtained from the participating subject. Approval number: 19/19/242.

## **2. PBMC culture and iPSC generation and culture**

Lymphosep Separation medium (Biowest) was used to isolate peripheral blood mononuclear cells (PBMCs) from whole blood. Before transduction, PBMCs were cultured for 12 days in StemSpan SFEM II medium (StemCell Technologies) with Erythroid expansion supplement (StemCell Technologies) at 37°C; 5% CO<sub>2</sub> and 10% O<sub>2</sub> after which they were reprogrammed. A CytoTune™-iPS 2.0 Sendai Reprogramming Kit (Life Technologies) introducing the four Yamanaka reprogramming factors (Oct3/4, Sox2, c-Myc and Klf4) was used. Three days after transduction, the cells were passaged and seeded on a Geltrex-coated plate (Life Technologies) and grown in Essential 8 Flex Medium (ThermoFisher Scientific) supplemented with Pen/Strep (Life Technologies). Appearing colonies were manually picked and passaged on a Geltrex-coated 24-well plate. After seven picking rounds, the cells were chemically passaged with 0.5mM EDTA to a 12-well plate when reaching a confluency of 85%. After every picking and passaging the medium was supplemented with ROCK inhibitor Y-27632 (Sigma-Aldrich) for 24hours for maintenance of the stem cell phenotype. Different clones were generated and frozen down in KnockOut™ Serum Replacement (Life Technologies) with 10% DMSO (Merck).

## **3. Mutation analysis**

*IPO8* exon 13 was amplified in genomic DNA obtained from iPSCs and PBMCs, by PCR (Protocol: 94°C 5 min, 35x (94°C 30", 60°C 30", 72°C 45"), 72°C 10', 15°C 1') in a Veriti Fast Thermal Cycler (Applied Biosystems). The mutation was verified with Sanger sequencing. Primers are listed in Table 2.

## **4. Immunocytochemistry**

The iPSCs (passage 15) were passaged to Geltrex-coated cover slips and fixed with ice-cold methanol for 20 minutes at -20°C. 0.1% TritonX-100 (Sigma-Aldrich) was applied to the cells for 15 at RT to induce permeabilization. The iPSCs were blocked with 5%

goat serum (Jackson ImmunoResearch) for 30 minutes and incubated overnight with primary antibodies at 4°C. The next day, the cells were washed three times with PBS followed by secondary antibodies incubation for 1 hour at RT. The nuclei were counterstained with DAPI (Life Technologies). Antibodies are listed in Table 2.

## **5. RNA extraction and RT-qPCR**

Total RNA was extracted from the iPSC (passage 15) and differentiated cells with a Quick-RNA™ Miniprep Kit (Zymo-Research) followed by cDNA synthesis using SuperScript™ III First-Strand Synthesis System (Life Technologies). RT-qPCR was performed using the CFX384 Touch Real-Time PCR detection system (Bio-Rad) with TaqMan® probes (Life Technologies) and TaqMan® gene expression mastermix (Life Technologies) following manufacturer's protocol. The TaqMan® probes used for every RT-qPCR experiment are listed in Table 2.

## **6. Trilineage differentiation potential –RT-qPCR**

The StemMACS™ Trilineage differentiation kit (Miltenyi Biotec) was used for directed differentiation of the iPSC cell line (p22) into endoderm, mesoderm and ectoderm. On day seven, the differentiated cells were dissociated with Trypsin/EDTA (0.05%), 5 min, 37 °C. 0.5 mg/mL Soybean Trypsin Inhibitor (Merck) was used to stop the reaction after which the cells were collected for gene expression analysis using RT-qPCR.

## **7. Mycoplasma detection**

The absence of mycoplasma contamination was confirmed using the LookOut Mycoplasma PCR Detection Kit (Sigma-Aldrich) following manufacturer's protocol. Cells were tested at passage15.

## **8. Sendai virus detection**

iPSCs were harvested earliest after 10 picking/passaging rounds followed by total RNA isolation using the Quick-RNA™ Miniprep Kit (Zymo-Research). cDNA was synthesized

using the Superscript<sup>TM</sup> III First-Strand Synthesis System (Life Technologies) with random hexamers. SeV genome and transgenes detection in iPSCs was performed with RT-PCR (94°C 5 min, 34x (94°C 15 s, 60°C 30 s, 72°C 45 s), 72°C 10 min, 10°C 1 min) using Sendai vector-specific primers (IDT) (Table 2) provided in the manufacturer's protocol. Sendai vector loss is shown in Figure 1 panel E.

### 9. Genomic integrity and SNP array (CNV analysis)

A detailed genomic integrity test was performed with a HumanCytoSNP-12 array (automated Infinium HD Assay Ultra) run on an iScan instrument from Illumina and results were visualized with Genome Studio (Illumina). iPSCs from passage 12 were matched with corresponding blood genotypes. The CNV analysis was performed using an in-house generated online tool, the CNV-WebStore (<http://cnv-webstore.ua.ac.be>). These results ruled out the presence of large aberrations or clinically relevant deletions or duplications. The discovered CNV is not a TAD causing gene and therefore we can conclude that no clinically relevant CNVs were introduced during the reprogramming. Important to take into account is that balanced chromosomal rearrangements and low-level mosaicism cannot be detected with a SNP array.

### 3 References

---

1. Wei, Y., et al., *Importin 8 regulates the transport of mature microRNAs into the cell nucleus*. J Biol Chem, 2014. **289**(15): p. 10270-10275.
2. Van Gucht, I., et al., *A human importin-beta-related disorder: Syndromic thoracic aortic aneurysm caused by bi-allelic loss-of-function variants in IPO8*. Am J Hum Genet, 2021. **108**(6): p. 1115-1125.

#### 4 Supplementary

**Supplementary Table 1** – Copy number variant analysis

<b>BBANTWi0011-A</b>					
<b>Chromosome</b>	<b>Location minimal region</b>	<b>Copy number</b>	<b>Minimal size</b>	<b>Variant found in</b>	<b>Genes in minimal region</b>
15	Chr15:20,558,072-22,383,292	Duplication	1,825,221	Only present in iPSC	MIR5701-3, LOC101927079, CXADRP2, MIR5701, LINC02203, MIR3118-3, OR4N3P, POTEb, OR4M2

Note: STR analysis is replaced by a SNP-array which provides higher resolution

## **CHAPTER 8: DISCUSSION**

---

Thoracic aortic aneurysm (TAA) results from dilatation of the aorta due to vessel wall weakness and is associated with a high morbidity and mortality rate due to the high risk for sudden aortic dissection (TAAD) or rupture [1]. Years of intensive research revealed that TAA(D) is a genetically and clinically heterogeneous disease [2]. It can be classified as syndromic or non-syndromic [3]. In most patients TAA(D) occurs as an isolated manifestation restricted to the aorta, referred to as non-syndromic TAA(D). However, approximately 5% of TAA(D) patients also present with systemic and dysmorphic features, referred to as syndromic TAA(D) [4]. Syndromic TAA patients present with a pleiotropy of musculoskeletal, ocular and craniofacial anomalies, on top of their cardiovascular anomalies. Marfan syndrome (MFS) and Loeys-Dietz syndrome (LDS) are the two most prevalent and best characterized TAA syndromes [3]. Other established TAA-related syndromes are Shprintzen-Goldberg syndrome (SGS) [5], Meester-Loeys syndrome (MLS) [6] and vascular Ehlers-Danlos syndrome (vEDS) [7]. In addition, an increasing number of extremely rare syndromes has been found to occasionally present with TAA as one of the clinical features, e.g. the syndromes caused by pathogenic variants in *ABL1* [8], or *KCNMA1* [9]. Nevertheless, significant overlap between syndromic and non-syndromic TAA(D) exists at the genetic, molecular and clinical level. The substantial majority of non-syndromic TAA(D) cases (80%) miss a positive family history [10]. These are also known as sporadic TAA(D) and are mainly associated with risk factors such as hypertension history, male sex, age [10, 11], obesity [12] and smoking [13]. As compared to sporadic TAA(D), familial TAA(D) is more virulent, with the first aneurysmal presentation at younger age and with faster growth rates [12]. Approximately 30% of familial TAA patients can be explained by pathogenic variants in the more than 40 TAA(D) genes that have been identified up to now. These genes encode proteins involved in extracellular matrix (ECM) remodeling, vascular smooth muscle cell (VSMC) contraction and the TGF- $\beta$  signaling pathway [14-16]. Familial TAA(D) is most often inherited in an autosomal dominant manner, but recessive and X-

linked genes have been reported as well. Moreover, reduced penetrance and variable expressivity are commonly observed in TAA(D) patients [3].

Current TAA(D) management includes administration of blood pressure and heart rate lowering agents such as  $\beta$ -blockers (e.g. propranolol) and/or Ang II receptor inhibitors (e.g. losartan) [17], serial aortic imaging, and surgical aneurysm repair to prevent dissection [18, 19]. Nevertheless, medical therapies capable of stopping the aneurysm from growing or even reversing its expansion are missing. Hence there is a desperate need for novel insights in the genetic underpinnings and in the molecular processes leading to aneurysmal disease as those will reveal new entry points for advanced therapeutic strategies and will enable optimized risk stratification.

In this thesis we aimed to further contribute to the elucidation of the etiology of syndromic TAA(D) by identifying novel syndromic TAA(D) genes, expanding syndromic TAA(D) genotype-phenotype correlations, and unraveling the molecular processes underlying syndromic TAA by generating and validating pre-clinical disease models.

## 1. The evolving genetic landscape of syndromic TAA(D): novel gene identification

---

Over the past 30 years, great research efforts have been made to find novel TAA genes and variants. So far, more than 40 TAA genes have been identified. Several diagnostic genetic centers use Next Generation Sequencing (NGS) gene panels that aim at molecularly confirming the clinical diagnosis of TAA(D) by the identification of the causal variant. If no genetic cause can be identified in a TAA patient by applying the NGS diagnostic gene panel, the patient may have a causal genetic variant in a gene that still awaits identification. Continuous improvements in NGS techniques have enabled time-efficient and cost-effective simultaneous examination of all coding and even non-coding regions of the genome. Whole exome sequencing (WES) and whole genome sequencing (WGS) are nowadays frequently used to search for novel causative variants in TAA families, which has enabled large progress in gene identification [20, 21]. This technical switch has made it possible to look exome- and genome-wide in TAA patients of even small families, or even in single patients and to identify TAA-associated mutations in novel TAA(D) genes. This approach has already led to the discovery of several TAA genes, including *SKI* [5] and *TGFB3* [22], and more recently *IPO8* [23].

In **Chapter 4** of this thesis, WES/WGS investigation led to the identification of pathogenic bi-allelic loss-of-function (LOF) variants in a novel syndromic TAA gene, i.e. *IPO8*, in six unrelated LDS- and Marfan syndrome-like probands with an early-onset TAA phenotype, motor developmental delay, connective tissue findings and craniofacial dysmorphism features [23, 24]. Worldwide, so far only a handful of *IPO8* patients have been identified through a collaboration between different research labs and genetic centers. The latter is important as collaborative efforts can provide more and stronger evidence of an association between a certain genetic disease and a possible disease-causing gene/pathogenic variant. Our fruitful collaboration with the research group of Prof. Marianna Parlato in Paris, synergistically contributed to the association between bi-allelic *IPO8* variants and TAA development [24].

Since *IPO8* obviously explains only a small percentage of TAA patients, a major portion of the genetic etiology of TAA is still missing, leaving a fair amount of TAA patients without a genetic diagnosis. When looking at the gene discovery trends for TAA over the past few years, it becomes clear that the genes explaining large percentages of TAA patients had already been discovered in the past (20%). Over the last decade, genes have been discovered that only explain a small percentage of TAA patients (<1%), including *IPO8*. Therefore, I believe that an additional perspective on gene/variant identification is needed, in which structural variation and variants in non-coding parts of the genome may become the focus of future investigations into TAA causal variants. More precisely, I propose to search for unbalanced CNVs or balanced inversions and translocations as well as single nucleotide variants in non-coding functional variants such as promotor regions, long noncoding RNAs (lncRNAs) and microRNAs (miRNAs). Within this perspective, I believe that large scale WGS investigations will contribute to the elucidation of the genetic spectrum of TAA(D), as well as the emergence of long-read sequencing (LRS), which will allow us to detect complex structural variants [25]. The inclusion of WGS will generate a huge amount of data, which needs to be stored and analyzed. Several bioinformatics pipelines, also within our research center, are being developed to facilitate this. A drawback of performing WES/WGS on a larger scale is that this may increase the risk for VUS (variant of unknown significance) identification, but I believe that also the variant interpretation pipelines will evolve fast during the coming years and will be able to follow the fast technical developments in the (next-generation) sequencing field.

## **2. Expanded TAA(D) genotype-phenotype correlations**

---

In **Chapter 3** of this thesis, we used TAAD gene panel sequencing to identify five probands carrying (likely) pathogenic *LOX* variants. These probands presented with a heterogeneous aneurysmal and connective tissue disease phenotype, which at first sight, we would not have linked with *LOX* deficiency. We identified one *LOX* patient with

a spontaneous coronary artery dissection, which had not been observed in *LOX* patients before. Furthermore, a broad spectrum of connective tissue manifestations with a significant clinical overlap with LDS and MFS was observed in a substantial fraction of *LOX* probands [26]. Reporting *LOX* variants as being responsible for a non-syndromic phenotype is the standard at present [11, 27-29], however, our findings suggests that *LOX* patients should rather be described as syndromic. With this chapter we were able to validate the contribution of pathogenic *LOX* variants to the genetic etiology of TAA and to refine the variable phenotypical spectrum of *LOX* patients. Nevertheless, it remains unexplained why some *LOX* patients do not seem to present with connective tissue findings at all [16]. We believe that carefully defining the clinical landscape of TAA genes contributes to an appropriate identification of TAA patients and therefore to personalized medical health care. Similarly, our research group has contributed previously to this important goal by the identification of *JAG1*, a gene previously known to cause Alagille syndrome, but that is now also being recognized as a TAA(D) causal gene. As such, *JAG1* is now being included in diagnostic NGS panels, hereby contributing to on-time diagnosis and intervention with an appropriate treatment for *JAG1* variant harboring patients [30].

Intriguingly, MFS and LDS patients are known to suffer from dissections of the aorta, in contrast to *IPO8* patients in whom no dissections have been observed so far. Several young *IPO8* patients already exhibit large aortic diameters, with Z-scores up to 10, in which one would expect a dissection or rupture sooner or later. Moreover, the currently known *IPO8* patients all are young people. This contrasts with other TAA associated syndromes, in which the mean age of the patients is significantly older. This has made us wonder whether adult/older *IPO8* patients do exist and whether these young *IPO8* patients will survive till older age. A natural history study would shed better light on this. Also, I believe it is crucial to keep a close eye on our *IPO8* patients with regular imaging follow-up to assure timely intervention. The decision to operate depends on different factors, including the age of the child, the rate of aneurysm

progression, the absolute and normalized size of the aneurysm and the suitable type of surgery [31, 32].

### 3. Unravelling the molecular basis of TAA(D)

---

TAA(D) is part of the clinical profile of connective tissue disorders including MFS, LDS [33], SGS [5], and MLS [6], predominantly caused by genes encoding for proteins involved in TGF- $\beta$  signaling and ECM remodeling [7, 34, 35]. Matrix deposition and degradation are strictly regulated processes, and of utmost importance to maintain structural integrity of the aortic wall for tensile strength and recoil propensity [36]. A disrupted balance of these processes is often caused by altered expression of structural integrity genes encoding for elastins, collagens, fibulins and integrins, and dysregulation of ECM-associated pathways. An association between aortic ECM deterioration and TAA development has repeatedly been reported [16, 37, 38]. Our findings in **Chapter 3** and **Chapter 4** complement ECM homeostasis involvement in TAA, with elastic fiber fragmentation and disorganization being present in aortic tissue from both *Ipo8*<sup>-/-</sup> [23] and *Lox*<sup>-/-</sup> [27] mouse models, and in human aortic samples of LOX patients [28, 39]. Predominantly, ECM homeostasis is regulated by matrix metalloproteinases (MMPs) and tissue inhibitors of metalloproteinases (TIMPs), mediating the physiological turnover of aortic ECM, by degradation of collagen and elastin [40, 41]. Increased *MMP2* and/or *MMP9* expression is a hallmark for TAA in humans and in mouse models [42, 43]. In line with these findings, RT-qPCR experiments in ascending aortic tissue from our *Ipo8*<sup>-/-</sup> mouse model, described in **Chapter 4**, revealed also increased expression of *Mmp2*. Additionally, *Ccn2* (*Ctgf*), another gene involved in ECM remodeling as well as a downstream target of the transforming growth factor- $\beta$  (TGF- $\beta$ ) signaling pathway and previously reported to be increased in the aortic wall of LDS patients [44], was found to be overexpressed in aortic tissue from our *Ipo8*<sup>-/-</sup> mice.

Another important molecular signature of syndromic TAA is the dysregulation of the TGF- $\beta$  signaling pathway [1]. In both MFS and LDS patients, dysregulation of the TGF- $\beta$  signaling pathway was reported. Investigations in MFS Fbn1<sup>C1039G/+</sup> mice revealed TGF- $\beta$  dysregulation as a molecular cause of TAA development [45]. LDS patients harboring loss-of-function variants in one of the TGF- $\beta$  pathway receptors and ligands demonstrated a paradoxical increase in TGF- $\beta$  signaling at the protein level. The latter is also known as the TGF- $\beta$  paradox [1, 46]. Several hypotheses have been proposed to explain the TGF- $\beta$  paradox, including the altered balance between canonical and non-canonical TGF- $\beta$  signaling, altered cycling of TGF- $\beta$  receptors on the cell surface, a ligand shift towards TGFB1 or differences in TGF- $\beta$  sensitivity of VSMCs depending on their embryonic origin present in different regions of the aorta [1, 47]. Whether these explanations hold true for *IPO8* patients is not clear yet and should be further studied. Single cell RNA (scRNA) sequencing of aortic samples of TAA(D) mouse models as well as TAA(D) patients, followed by pathway analysis may provide excellent tools to further unravel this paradox.

Since *IPO8* patients present with a consistent phenotype, which resembles the phenotype of patients with other TGF- $\beta$  related aortopathy syndromes such as LDS, and suggested cargoes of *IPO8* are key-effectors of the TGF- $\beta$  signaling pathway [48], we hypothesized the involvement of dysregulated TGF- $\beta$  signaling in *IPO8* associated TAA. I strongly believe in the involvement of TGF- $\beta$  in *IPO8*-related TAA and TAA in general since this hypothesis is strongly supported by our findings in **Chapter 4**. Firstly, immunohistological pSmad2 stainings in ascending aortic tissue from *Ipo8*<sup>-/-</sup> mice revealed an increase in pSmad2 positively stained nuclei. Such an increase in pSmad2 has previously been observed in several LDS types [11]. Secondly, RT-qPCR experiments for nine TGF- $\beta$  superfamily related genes revealed an increase of *Mmp2* and *Ccn2* (*Ctgf*), two downstream transcriptional targets of the TGF- $\beta$  signaling pathway, and a decrease of *Smad6* and *Smad7*, two TGF- $\beta$  pathway inhibitors. The increase in *Mmp2* and *Ccn2*

could be explained by the upregulation of the TGF- $\beta$  signaling pathway, affecting both downstream targets leading to increased transcription. *Smad6* is associated with BMP-related signaling [49], while *Smad7* seems to be essential for specific inhibition of TGF- $\beta$  and BMP-induced signaling [50]. These data support our hypothesis regarding the pathomechanism of *IPO8*-related disease and provide additional evidence for the dysregulation of TGF- $\beta$  signaling in TAA in general.

Our data suggest a role for *IPO8* as a transport-receptor in the TGF- $\beta$  signaling pathway, thus being the most downstream effector known to be associated with TAA(D) so far. This novel TGF- $\beta$  signaling effector will provide us with a new entry point for the development of novel promising therapies. However, the exact role of TGF- $\beta$  in TAA(D) is still being discussed as other signaling pathways may be involved as well. In the past decade, additional pathways have been linked to TAA, A putative association between TAA(D) and the BMP signaling pathway has been proposed, but this association has not yet been extensively studied. Other possible contributing pathways include inflammatory pathways [51] and the NO signaling pathway [52, 53]. As such, the full pathomechanism of TAA(D) remains to be elucidated.

As mentioned above, our working hypothesis was that *IPO8* functions as an Importin involved in the TGF- $\beta$  signaling pathway, making it the most downstream gene of the TGF- $\beta$  signaling pathway. Our data strongly point in this direction, but to fully confirm our hypothesis, further studies are needed to find out which cargoes are shuttled by *IPO8* and more importantly, which ones are miss-shuttled in *IPO8* deficiency. Previously suggested cargoes are SMAD2, SMAD3 and SMAD4 [48], but many more are likely to exist. These cargoes can be identified using a cell fractionation/protein isolation protocol in combination with western blot, but also by more up-to-date techniques such as spatial proteomics. The latter could be a valuable tool since it preserves the protein subcellular localization and this will enable us to exactly locate the proteins that

are being shuttled by IPO8 and compare the abundance of suggested cargoes on specific locations between an *IPO8* patient and a healthy control.

In summary, the TGF- $\beta$  paradox in TAA development remains to be further unraveled, as should the molecular mechanisms and consequences of IPO8-mediated TAA and its cargoes.

#### **4. Pre-clinical TAA(D) disease models**

---

Pre-clinical disease models have been used for decades and have led to groundbreaking discoveries with respect to elucidation of disease mechanisms and identification of novel therapies, leaving them indispensable in genetic research [45, 54]. Mouse models, zebrafish models [24], and human induced pluripotent stem cell (hiPSC) derived cell models are currently used in TAA research. The most commonly used models for TAA are mouse models, of which dozens have already been created and functionally studied on numerous different genetic backgrounds [54]. The most important advantages of a mouse TAA model are the similarities in anatomy, genetics and physiology between mice and humans and the possibility to make genetically engineered mice that mimic human aortic diseases. A drawback of mouse models in TAA studies is the fact that the phenotypical expression and severity of the disease is highly dependent on the genetic background [55]. For several years, people have gained interest in using zebrafish as TAA models, since they are inexpensive, easy to house, have a physical transparency during early stages which makes them ideal for direct microscopic assessment of the aorta and have a high spawning ratio. Recently, they are being promoted as a tool for rapid assessment of VUSs, often identified as a result of WES [56, 57].

#### 4.1 hiPSCs as a TAA(D) model

The main advantage of hiPSC-derived cell models is that they are patient specific and thus carry the genetic background of the patient in question, whereas their disadvantage is the cellular heterogeneity and immaturity [58].

Patient-derived hiPSC models [59] can be retrieved from somatic cells such as skin fibroblasts or peripheral blood mononuclear cells (PBMCs), preventing invasive interventions for tissue/cell collection [60]. Indeed, the collection of aortic tissue samples is often limited and can only be done during surgery. The information gathered from these surgical tissues is per definition hampered to late-stage events, and therefore missing out on early-stage or even pre-TAA mechanisms. Understanding the driver processes is most valuable to develop TAA-preventing therapies and to identify early biomarkers [61]. Although iPSC reprogramming is time-consuming and labor intensive, iPSC models are precious tools as they can be further differentiated in any cell type as desired, such as VSMCs or endothelial cells (ECs) [62-66]. In **Chapter 7**, I took the first steps towards developing an *IPO8*-specific hiPSC-VSMC derived cell line by creating and validating an *IPO8* patient-derived hiPSC line starting from PBMCs [67]. This hiPSC line is registered in 'Biobank Antwerpen' as well as the European Human Pluripotent Stem Cell Registry database and is made available for other research labs and pharmaceutical companies interested in drug research and development.

Historically, VSMCs are considered the most important cell type contributing to the pathogenesis of TAA(D). Dysregulation of the switch between the contractile and synthetic VSMC state and apoptosis are well-studied events in aneurysmal disease [68, 69]. Therefore, we hypothesize the involvement of VSMCs in *IPO8*-related TAA. Already a fair amount of research has been published on the use of hiPSC-VSMCs to study MFS [70, 71], with protocols for hiPSCs-VSMC generation and validation, along with functional testing experiments, being broadly available [72] even for lineage-specific VSMCs (lateral plate mesoderm, neural crest and paraxial mesoderm) [73]. ECs, which

can be found as a single layer lining the tunica intima of the aortic wall, represent another functionally important cell type in aortic tissue, EC dysfunction has been repeatedly reported to contribute to TAA as well [74]. Fibroblasts are considered the third group of most important cells present in the aortic wall. However, recent studies have drawn attention towards other cell types as crucial players in conserving aortic wall integrity, such as immune cells, pericytes and mesenchymal stem cells (MSC) [75]. It might be a future plan to establish EC differentiation and validation protocols, followed by functional studies in an *IPO8*-specific hiPSC-VSMC derived cell line. In this way, the generated *IPO8* patient-specific hiPSC-derived VSMCs or ECs might serve for *in vitro* drug screening assays, in this way contributing to personalized medicine.

Additionally, the *IPO8* patient-derived hiPSC model is a promising tool that can be used in the creation of micro-tissues and organoids [76, 77]. These models allow us to design a 3D high-throughput method to study biological processes and the interplay between cells, cytokines, growth factors and other biological factors, in a more suitable and representative microenvironment for aortic cells as compared to VSMC or EC monolayers [78].

#### **4.2 Mouse as a model for TAA(D)**

In my *IPO8* research I chose to work with a mouse model because of its biological and physiological similarity to humans, which allows representative investigations of the cardiovascular system. Furthermore, genetic manipulation is relatively easy, which allows the study of specific gene mutations or complete knockouts. The cardiovascular physiology, including that of the aorta, of murine models is often similar and closely related to humans, making the transition towards the clinic more straightforward [79, 80]. Moreover, modifier genes and the effect of the genetic background can be studied as well. Another advantage is that they reproduce relatively fast and thus large numbers, genetically identical animals can be generated. A final big advantage is their accelerated lifespan: one mouse year equals 30 years in men. Since TAA is a progressive

disease that develops throughout life and can be expressed at any age, using a mouse model that recapitulates the disease development in as little as 1-2 years is time-saving [81].

Although *in vitro* cell models are widespread used pre-clinical models, mouse models remain the gold standard for studying syndromic and non-syndromic TAA [82]. In this particular case, murine Importin-8 is reported to be identical and similar to its human orthologue for 92% and 95%, respectively, rendering the mouse suitable for pre-clinical TAA assessment of *IPO8*-related disease (<http://www.ncbi.nlm.nih.gov/homologene/>). The functional characterization of TAA mouse models, described in **Chapter 4** and **Chapter 5**, contributes to the molecular landscape of TAA. With the aortic characterization of the *Ipo8*<sup>-/-</sup> mouse model, we have provided evidence for a novel aortopathy syndrome caused by bi-allelic LOF variants in *IPO8*, characterized by progressive early-onset TAA development and the involvement of TGF- $\beta$  dysregulation. Although mouse models remain the gold standard, the 3 R's principle of animal research: substitution (replacing animals with other models if possible), reduction (using as few animals as possible) and refinement (minimizing animal discomfort), must certainly be considered. These ethical considerations are very important to adhere to when starting animal research and must be safeguarded at all times.

Another advantage of mouse models over hiPSC-derived cells is the fact that they allow us to study embryonic developmental defects, possibly causing embryonic lethality. Embryonic or perinatal lethality is a common phenotype observed in genetically engineered knock-out mice, presenting in 30% of knock-out strains [83]. The cause of lethality can often be found in vasculogenesis or angiogenesis leading to cardiovascular insufficiency or hematopoietic defects [84]. In **Chapter 6** we describe embryonic lethality in the C57Bl/6N *Ipo8*<sup>-/-</sup> TAA mouse model. Timed matings were performed followed by morphological and histological examination revealing an embryonic lethality of 50% in *Ipo8*<sup>-/-</sup> mice between E13.5-14.5 and birth, with possible lethal

defects in the cardiovascular system [85]. Interestingly, an *Ipo11*<sup>-/-</sup> mouse model, a knock-out for Importin-11, another member of the karyopherin family, is reported to present with embryonic lethality of 100% at E11.5 due to abrupt morphological changes [86]. These observations might indicate a role for at least some Importins in embryonic development.

The implementation of high-resolution imaging techniques to reconstruct 3D-models of collected mouse embryos [87] is facilitating embryonic developmental research. This technique allows us to generate images of embryos without microtome-based embryo sectioning, reducing the risk of losing parts of tissue or information during the process [88]. More in-depth histological analysis with specific stainings should be conducted on a larger cohort of *Ipo8*<sup>-/-</sup> embryos.

## 5. Importance of genetic background and genetic modifiers in TAA(D)

---

It is important to note that familial or syndromic TAA patients often display noticeable inter- and intrafamilial phenotypic variability, even when carrying the same specific mutation, which makes prediction of disease severity and progression rather difficult [89]. Variation can be observed with respect to age of onset, severity degree and progressiveness of the aneurysm as well as absence/presence of aortic dissection. This phenotypically heterogeneous profile of TAA(D) seems, at least in part, to be influenced by genetic modifiers with an either aggravating or rather protective effect [90-93].

Importantly, the genetic background of a mouse model can also influence the phenotypic outcome, highlighting the importance of the genetic background choice [94]. To anticipate on the possible differences in phenotypical outcome of TAA(D) due to the genetic background, we have backcrossed our C57Bl/6N *Ipo8* mice from **Chapter 4** onto a 129/Sv genetic background, with C57Bl/6 and 129/Sv being the most commonly used strains in TAA research. Rather unexpectedly, in **Chapter 5**, the congenic 129/Sv *Ipo8*<sup>-/-</sup> mice, did not present with early-onset progressive TAA or

dissection. Moreover, in **Chapter 6**, embryonic lethality was not observed in 129/Sv *Ipo8*<sup>-/-</sup> mice either. These findings might indicate that although *Ipo8* deficiency can be a cause of TAA and embryonic lethality, these phenotypic aspects can be influenced by protective or aggravative genetic modifiers which are genetic background dependent [84]. Further identification of the responsible genetic modifiers should be performed as well as the investigation of their associated molecular mechanisms and consequences.

## **6. Challenges and future perspectives in TAA(D)**

---

Although major efforts have been made using plenty of different approaches, techniques, hypotheses and *in vitro* and *in vivo* models, declaring the remaining unknown genetic parts of TAA(D) remains challenging. On the one hand, the replacement of the currently used diagnostic TAAD gene panels with a broader WES/WGS approach, will enable a more complete molecular conceptualization of the disease. On the other hand, WGS will provide us with several intronic or intergenic genetic variants, which will often not be interpretable. As syndromic TAA(D) has already been largely mapped, the challenge will especially be to resolve the genetic basis underlying non-syndromic TAA(D), which remains elusive in 70-80% of cases [11]. Especially for non-syndromic TAA, somatic coding or non-coding mutations might also be putative disease culprits.

scRNA sequencing is a promising tool to study molecular and genetic TAA(D) heterogeneity. With scRNA sequencing we can compare the transcriptome profile of the diseased aortic wall to that of control tissue in a cell-specific manner. Moreover, scRNA sequencing can reveal whether certain cell populations are enriched or depleted in the disease context. As mentioned earlier, various cell types and subtypes of these cells are present in the aorta and can thus contribute to TAA(D) development including VSMC, ECs, fibroblasts, pericytes, MSCs and possibly immune cells [95]. Based on differential expression patterns and/or specific genes and markers present in different subtypes of cells, scRNA sequencing can be used to distinguish phenotypes of VSMCs

undergoing the 'phenotypic switch' [96] and look at the maturation or stressed state of cells [97]. For MFS, such scRNA sequencing studies have been conducted, both on human and murine aortic tissue samples, leading to novel insights in MFS TAA(D) [68, 98]. The phenotypic switch of VSMCs previously was believed to shift between two phenotypes only, contractile and synthetic VSMCs, with the synthetic form more abundant in MFS patient's aortic tissue. However, scRNA sequencing studies have shown a phenotype continuum/spectrum rather than two discrete stages [98]. I believe that this approach may provide us with a better understanding of the factors and aortic cell types driving TAA in *IPO8* patients. We might be able to identify cell types and their subtypes, possible novel key pathways via pathway analysis or elucidate the contribution of already TAA(D) associated pathways. With these data we also might be able to untangle (a part of) the TGF- $\beta$  paradox and eventually describe other interesting entry points for therapy. An obstacle might be the advanced stages of aneurysmal growth at which tissue is collected since surgery often is performed on TAA(D) patients only in a rather critical aneurysmal growth stage.

It would be beneficial to also study the course of the disease, by looking at changes in expression patterns of certain cell types present in the aortic material at different time points, as this would allow us, eventually, to intervene therapeutically to prevent the aneurysm from forming. Of course, in patients this is only possible if we would be able to collect aortic material at different time points throughout TAA(D) development, which is obviously invasive and not routinely done. Nevertheless, looking at changes in gene expression levels before the start of aneurysm formation and throughout the process of TAA(D) development, is a study that can be performed in TAA(D) mouse models.

A drawback of scRNA sequencing is the loss of spatial information, which can be sustained using spatial transcriptomics, to evaluate gene expression levels across tissue spaces [99]. Using this technique, the transcriptome of the different layers in the aorta

can be investigated in intact tissue specimens. The expression patterns of receptors and their ligands can be determined, to possibly detect miscommunication and contribution to TAA(D) [100]. I also believe that other pathways, including inflammatory (e.g. macrophages), oxidative stress (ROS), apoptotic and miRNA guided regulatory pathways, although less studied, may turn out to be valuable contributors to TAA(D) and should be investigated in more detail.

Currently, evidence on the role of microRNAs (miRNAs) in the development of TAA(D) is rapidly accumulating. miRNAs are gene-expression-regulating, small non-coding RNAs, several of which have already been identified as critical regulators for TAA(D) [95, 101, 102]. Moreover, miRNAs have been reported to rescue aortic dissection [103]. Yang et al recently described a specific miRNA (miR-26b), that could suppress the development of aortic dissection by regulating the *HMGA2* gene and the TGF- $\beta$  signaling pathway [104]. Interestingly, IPO8 is predicted to be required for cytoplasmic miRNA guided gene silencing and nuclear localization of miRNA-Ago protein complexes [105], possibly implicating IPO8 as component of miRNA-guided regulatory pathways [106]. Taken this, together with the fact that miRNAs are detectable and stable in plasma and serum, miRNAs are potential therapeutic targets and diagnostic biomarkers. However, as their drawbacks include off-targets and unknown possible side-effects, the regulatory function and working mechanisms of miRNAs, certainly need further investigations.

TAA(D) patient management is another challenging aspect. Prophylactic surgery often remains the only effective intervention to prevent TAA from dissecting, an intervention that does not go without risk. Another part of TAA(D) therapy consists of decreasing blood pressure with  $\beta$ -blockers (propranolol) or angiotensin II receptor antagonist (Losartan). Still, no curative medications are available [107]. With IPO8 as the most downstream key effector of the TGF- $\beta$  pathway, we hope to be able to contribute to the development of therapies capable of stopping or even reversing TAA growth. The

beneficiary positioning of IPO8 will serve as a starting point for novel TAA(D)-therapeutic development. Other pathways that are (being) discovered must be taken into account as possible drug/therapy targets as well, including the promising regulatory miRNA-guided pathways.

## 7. In conclusion

---

The complex genetic architecture and underlying molecular pathomechanisms of TAA(D) remain partially unexplained and require more in-depth research. Risk stratification and disease severity prediction methods and therefore proper patient risk stratification is currently lacking. Specific biomarkers that can be used to predict or monitor disease progression are missing and should be focused on in the future. TAA(D) patient management with personalized medicine is a major goal. That goal will be reached by studying pre-clinical models, such as mouse or cell models, which can be used for drug library screenings and contribute to the development of personalized aneurysm preventing therapeutics. Novel approaches and emerging techniques, including proteomics and single cell-RNA sequencing, have gained a lot of interest in enhancing the TAA(D) genetic dictionary.

## 8. References

---

1. Lindsay, M.E. and H.C. Dietz, *Lessons on the pathogenesis of aneurysm from heritable conditions*. Nature, 2011. **473**(7347): p. 308-16.
2. Montgomery, R.A., et al., *Multiple molecular mechanisms underlying subdiagnostic variants of Marfan syndrome*. Am J Hum Genet, 1998. **63**(6): p. 1703-11.
3. Verstraeten, A., I. Luyckx, and B. Loeys, *Aetiology and management of hereditary aortopathy*. Nat Rev Cardiol, 2017. **14**(4): p. 197-208.
4. Takeda, N. and I. Komuro, *Genetic basis of hereditary thoracic aortic aneurysms and dissections*. J Cardiol, 2019. **74**(2): p. 136-143.
5. Doyle, A.J., et al., *Mutations in the TGF-beta repressor SKI cause Shprintzen-Goldberg syndrome with aortic aneurysm*. Nat Genet, 2012. **44**(11): p. 1249-54.
6. Meester, J.A.N., et al., *Meester-Loeys Syndrome*. Adv Exp Med Biol, 2021. **1348**: p. 265-272.

7. Callewaert, B., et al., *Ehlers-Danlos syndromes and Marfan syndrome*. Best Pract Res Clin Rheumatol, 2008. **22**(1): p. 165-89.
8. Wang, X., et al., *Germline mutations in ABL1 cause an autosomal dominant syndrome characterized by congenital heart defects and skeletal malformations*. Nat Genet, 2017. **49**(4): p. 613-617.
9. Liang, L., et al., *De novo loss-of-function KCNMA1 variants are associated with a new multiple malformation syndrome and a broad spectrum of developmental and neurological phenotypes*. Hum Mol Genet, 2019. **28**(17): p. 2937-2951.
10. Ostberg, N.P., et al., *The Genetics of Thoracic Aortic Aneurysms and Dissection: A Clinical Perspective*. Biomolecules, 2020. **10**(2).
11. Luyckx, I., et al., *Update on the molecular landscape of thoracic aortic aneurysmal disease*. Curr Opin Cardiol, 2022. **37**(3): p. 201-211.
12. Pinard, A., G.T. Jones, and D.M. Milewicz, *Genetics of Thoracic and Abdominal Aortic Diseases*. Circ Res, 2019. **124**(4): p. 588-606.
13. Lederle, F.A., D.B. Nelson, and A.M. Joseph, *Smokers' relative risk for aortic aneurysm compared with other smoking-related diseases: a systematic review*. J Vasc Surg, 2003. **38**(2): p. 329-34.
14. Neptune, E.R., et al., *Dysregulation of TGF-beta activation contributes to pathogenesis in Marfan syndrome*. Nat Genet, 2003. **33**(3): p. 407-11.
15. Verstraeten, A., et al., *Marfan Syndrome and Related Disorders: 25 Years of Gene Discovery*. Hum Mutat, 2016. **37**(6): p. 524-31.
16. Cheuk, B.L. and S.W. Cheng, *Differential expression of elastin assembly genes in patients with Stanford Type A aortic dissection using microarray analysis*. J Vasc Surg, 2011. **53**(4): p. 1071-1078 e2.
17. Gao, L., et al., *The effect of losartan on progressive aortic dilatation in patients with Marfan's syndrome: a meta-analysis of prospective randomized clinical trials*. Int J Cardiol, 2016. **217**: p. 190-4.
18. Milewicz, D.M. and F. Ramirez, *Therapies for Thoracic Aortic Aneurysms and Acute Aortic Dissections*. Arterioscler Thromb Vasc Biol, 2019. **39**(2): p. 126-136.
19. Hofmann Bowman, M.A., K.A. Eagle, and D.M. Milewicz, *Update on Clinical Trials of Losartan With and Without beta-Blockers to Block Aneurysm Growth in Patients With Marfan Syndrome: A Review*. JAMA Cardiol, 2019. **4**(7): p. 702-707.
20. Regalado, E.S., et al., *Exome sequencing identifies SMAD3 mutations as a cause of familial thoracic aortic aneurysm and dissection with intracranial and other arterial aneurysms*. Circ Res, 2011. **109**(6): p. 680-6.
21. Capuano, A., et al., *Diagnostic Exome Sequencing Identifies a Novel Gene, EMILIN1, Associated with Autosomal-Dominant Hereditary Connective Tissue Disease*. Hum Mutat, 2016. **37**(1): p. 84-97.

22. Bertoli-Avella, A.M., et al., *Mutations in a TGF-beta ligand, TGF $\beta$ 3, cause syndromic aortic aneurysms and dissections*. J Am Coll Cardiol, 2015. **65**(13): p. 1324-1336.
23. Van Gucht, I., et al., *A human importin-beta-related disorder: Syndromic thoracic aortic aneurysm caused by bi-allelic loss-of-function variants in IPO8*. Am J Hum Genet, 2021. **108**(6): p. 1115-1125.
24. Ziegler, A., et al., *Bi-allelic variants in IPO8 cause a connective tissue disorder associated with cardiovascular defects, skeletal abnormalities, and immune dysregulation*. Am J Hum Genet, 2021. **108**(6): p. 1126-1137.
25. Mantere, T., S. Kersten, and A. Hoischen, *Long-Read Sequencing Emerging in Medical Genetics*. Front Genet, 2019. **10**: p. 426.
26. Verstraeten, A., et al., *Enrichment of Rare Variants in Loeys-Dietz Syndrome Genes in Spontaneous Coronary Artery Dissection but Not in Severe Fibromuscular Dysplasia*. Circulation, 2020. **142**(10): p. 1021-1024.
27. Guo, D.C., et al., *LOX Mutations Predispose to Thoracic Aortic Aneurysms and Dissections*. Circ Res, 2016. **118**(6): p. 928-34.
28. Cirnu, A., et al., *Novel Mutation in LOX Associates With a Complex Aneurysmal Vascular and Cardiac Phenotype*. Circ Genom Precis Med, 2021. **14**(1): p. e003217.
29. Lee, V.S., et al., *Loss of function mutation in LOX causes thoracic aortic aneurysm and dissection in humans*. Proc Natl Acad Sci U S A, 2016. **113**(31): p. 8759-64.
30. Rodrigues Bento, J., et al., *Isolated aneurysmal disease as an underestimated finding in individuals with JAG1 pathogenic variants*. Hum Mutat, 2022. **43**(12): p. 1824-1828.
31. Hetzer, R., et al., *Isolated giant aortic aneurysm in an infant: Ehlers-Danlos syndrome type IV*. Ann Thorac Surg, 2008. **86**(2): p. 632-4.
32. Cattaneo, S.M., et al., *Surgery for aortic root aneurysm in children: a 21-year experience in 50 patients*. Ann Thorac Surg, 2004. **77**(1): p. 168-76.
33. Loeys, B.L. and H.C. Dietz, *Loeys-Dietz Syndrome*, in *GeneReviews((R))*, M.P. Adam, et al., Editors. 1993: Seattle (WA).
34. Faggion Vinholo, T., et al., *Genes Associated with Thoracic Aortic Aneurysm and Dissection: 2019 Update and Clinical Implications*. Aorta (Stamford), 2019. **7**(4): p. 99-107.
35. Velchev, J.D., et al., *Loeys-Dietz Syndrome*. Adv Exp Med Biol, 2021. **1348**: p. 251-264.
36. Creamer, T.J., E.E. Bramel, and E.G. MacFarlane, *Insights on the Pathogenesis of Aneurysm through the Study of Hereditary Aortopathies*. Genes (Basel), 2021. **12**(2).
37. Sulkava, M., et al., *Differentially expressed genes and canonical pathways in the ascending thoracic aortic aneurysm - The Tampere Vascular Study*. Sci Rep, 2017. **7**(1): p. 12127.

38. Lin, C.J., C.Y. Lin, and N.O. Stitzel, *Genetics of the extracellular matrix in aortic aneurysmal diseases*. *Matrix Biol*, 2018. **71-72**: p. 128-143.
39. Van Gucht, I., et al., *Novel LOX Variants in Five Families with Aortic/Arterial Aneurysm and Dissection with Variable Connective Tissue Findings*. *Int J Mol Sci*, 2021. **22**(13).
40. Cabral-Pacheco, G.A., et al., *The Roles of Matrix Metalloproteinases and Their Inhibitors in Human Diseases*. *Int J Mol Sci*, 2020. **21**(24).
41. Van Doren, S.R., *Matrix metalloproteinase interactions with collagen and elastin*. *Matrix Biol*, 2015. **44-46**: p. 224-31.
42. Koullias, G.J., et al., *Increased tissue microarray matrix metalloproteinase expression favors proteolysis in thoracic aortic aneurysms and dissections*. *Ann Thorac Surg*, 2004. **78**(6): p. 2106-10; discussion 2110-1.
43. Rabkin, S.W., *Differential expression of MMP-2, MMP-9 and TIMP proteins in thoracic aortic aneurysm - comparison with and without bicuspid aortic valve: a meta-analysis*. *Vasa*, 2014. **43**(6): p. 433-42.
44. Loeys, B.L., et al., *A syndrome of altered cardiovascular, craniofacial, neurocognitive and skeletal development caused by mutations in TGFBR1 or TGFBR2*. *Nat Genet*, 2005. **37**(3): p. 275-81.
45. Habashi, J.P., et al., *Losartan, an AT1 antagonist, prevents aortic aneurysm in a mouse model of Marfan syndrome*. *Science*, 2006. **312**(5770): p. 117-21.
46. Takeda, N., et al., *TGF-beta Signaling-Related Genes and Thoracic Aortic Aneurysms and Dissections*. *Int J Mol Sci*, 2018. **19**(7).
47. MacFarlane, E.G., et al., *Lineage-specific events underlie aortic root aneurysm pathogenesis in Loeys-Dietz syndrome*. *J Clin Invest*, 2019. **129**(2): p. 659-675.
48. Yao, X., et al., *Preferential utilization of Imp7/8 in nuclear import of Smads*. *J Biol Chem*, 2008. **283**(33): p. 22867-74.
49. Goto, K., et al., *Selective inhibitory effects of Smad6 on bone morphogenetic protein type I receptors*. *J Biol Chem*, 2007. **282**(28): p. 20603-11.
50. Hanyu, A., et al., *The N domain of Smad7 is essential for specific inhibition of transforming growth factor-beta signaling*. *J Cell Biol*, 2001. **155**(6): p. 1017-27.
51. Chen, F., J. Han, and B. Tang, *Patterns of Immune Infiltration and the Key Immune-Related Genes in Acute Type A Aortic Dissection in Bioinformatics Analyses*. *Int J Gen Med*, 2021. **14**: p. 2857-2869.
52. Bhushan, R., et al., *An integrative systems approach identifies novel candidates in Marfan syndrome-related pathophysiology*. *J Cell Mol Med*, 2019. **23**(4): p. 2526-2535.
53. Luyckx, I., et al., *Confirmation of the role of pathogenic SMAD6 variants in bicuspid aortic valve-related aortopathy*. *Eur J Hum Genet*, 2019. **27**(7): p. 1044-1053.

54. Bellini, C., et al., *Comparison of 10 murine models reveals a distinct biomechanical phenotype in thoracic aortic aneurysms*. J R Soc Interface, 2017. **14**(130).
55. Hay, A.M., et al., *Mouse background genetics in biomedical research: The devil's in the details*. Transfusion, 2021. **61**(10): p. 3017-3025.
56. Prendergast, A., et al., *Phenotyping Zebrafish Mutant Models to Assess Candidate Genes Associated with Aortic Aneurysm*. Genes (Basel), 2022. **13**(1).
57. Gould, R.A., et al., *ROBO4 variants predispose individuals to bicuspid aortic valve and thoracic aortic aneurysm*. Nat Genet, 2019. **51**(1): p. 42-50.
58. Shen, M., et al., *Generation of Vascular Smooth Muscle Cells From Induced Pluripotent Stem Cells: Methods, Applications, and Considerations*. Circ Res, 2021. **128**(5): p. 670-686.
59. Takahashi, K. and S. Yamanaka, *Induction of pluripotent stem cells from mouse embryonic and adult fibroblast cultures by defined factors*. Cell, 2006. **126**(4): p. 663-76.
60. Yu, J., et al., *Induced pluripotent stem cell lines derived from human somatic cells*. Science, 2007. **318**(5858): p. 1917-20.
61. Davaapil, H., D.K. Shetty, and S. Sinha, *Aortic "Disease-in-a-Dish": Mechanistic Insights and Drug Development Using iPSC-Based Disease Modeling*. Front Cell Dev Biol, 2020. **8**: p. 550504.
62. Nijak, A., et al., *Morpho-functional comparison of differentiation protocols to create iPSC-derived cardiomyocytes*. Biol Open, 2022. **11**(2).
63. Cheung, C., et al., *Generation of human vascular smooth muscle subtypes provides insight into embryological origin-dependent disease susceptibility*. Nat Biotechnol, 2012. **30**(2): p. 165-73.
64. Dolmetsch, R. and D.H. Geschwind, *The human brain in a dish: the promise of iPSC-derived neurons*. Cell, 2011. **145**(6): p. 831-4.
65. Voulgaris, D., P. Nikolakopoulou, and A. Herland, *Generation of Human iPSC-Derived Astrocytes with a mature star-shaped phenotype for CNS modeling*. Stem Cell Rev Rep, 2022. **18**(7): p. 2494-2512.
66. Wu, Q., et al., *Deriving Osteogenic Cells from Induced Pluripotent Stem Cells for Bone Tissue Engineering*. Tissue Eng Part B Rev, 2017. **23**(1): p. 1-8.
67. Van Gucht, I., et al., *Generation of one induced pluripotent cell (iPSC) line (BBANTWi011-A) from a patient carrying an IPO8 bi-allelic loss-of-function mutation*. Stem Cell Res, 2023. **69**: p. 103061.
68. Pedroza, A.J., et al., *Single-Cell Transcriptomic Profiling of Vascular Smooth Muscle Cell Phenotype Modulation in Marfan Syndrome Aortic Aneurysm*. Arterioscler Thromb Vasc Biol, 2020. **40**(9): p. 2195-2211.
69. Ignatieva, E., et al., *Mechanisms of Smooth Muscle Cell Differentiation Are Distinctly Altered in Thoracic Aortic Aneurysms Associated with Bicuspid or Tricuspid Aortic Valves*. Front Physiol, 2017. **8**: p. 536.

70. Crosas-Molist, E., et al., *Vascular smooth muscle cell phenotypic changes in patients with Marfan syndrome*. *Arterioscler Thromb Vasc Biol*, 2015. **35**(4): p. 960-72.
71. Perrucci, G.L., et al., *Vascular smooth muscle cells in Marfan syndrome aneurysm: the broken bricks in the aortic wall*. *Cell Mol Life Sci*, 2017. **74**(2): p. 267-277.
72. Granata, A., et al., *An iPSC-derived vascular model of Marfan syndrome identifies key mediators of smooth muscle cell death*. *Nat Genet*, 2017. **49**(1): p. 97-109.
73. Majesky, M.W., *Developmental basis of vascular smooth muscle diversity*. *Arterioscler Thromb Vasc Biol*, 2007. **27**(6): p. 1248-58.
74. Fan, L.M., et al., *Endothelial cell-specific reactive oxygen species production increases susceptibility to aortic dissection*. *Circulation*, 2014. **129**(25): p. 2661-72.
75. Li, Y., et al., *Single-Cell Transcriptome Analysis Reveals Dynamic Cell Populations and Differential Gene Expression Patterns in Control and Aneurysmal Human Aortic Tissue*. *Circulation*, 2020. **142**(14): p. 1374-1388.
76. Salewskij, K. and J.M. Penninger, *Blood Vessel Organoids for Development and Disease*. *Circ Res*, 2023. **132**(4): p. 498-510.
77. Archer, C.R., et al., *Characterization and Validation of a Human 3D Cardiac Microtissue for the Assessment of Changes in Cardiac Pathology*. *Sci Rep*, 2018. **8**(1): p. 10160.
78. Kurokawa, Y.K. and S.C. George, *Tissue engineering the cardiac microenvironment: Multicellular microphysiological systems for drug screening*. *Adv Drug Deliv Rev*, 2016. **96**: p. 225-33.
79. Krishnan, A., et al., *A detailed comparison of mouse and human cardiac development*. *Pediatr Res*, 2014. **76**(6): p. 500-7.
80. Wessels, A. and D. Sedmera, *Developmental anatomy of the heart: a tale of mice and man*. *Physiol Genomics*, 2003. **15**(3): p. 165-76.
81. Jonas, A.M., *The mouse in biomedical research*. *Physiologist*, 1984. **27**(5): p. 330-46.
82. Wenstrup, R.J., et al., *Murine model of the Ehlers-Danlos syndrome. col5a1 haploinsufficiency disrupts collagen fibril assembly at multiple stages*. *J Biol Chem*, 2006. **281**(18): p. 12888-95.
83. Adams, D., et al., *Bloomsbury report on mouse embryo phenotyping: recommendations from the IMPC workshop on embryonic lethal screening*. *Dis Model Mech*, 2013. **6**(3): p. 571-9.
84. Papaioannou, V.E. and R.R. Behringer, *Early embryonic lethality in genetically engineered mice: diagnosis and phenotypic analysis*. *Vet Pathol*, 2012. **49**(1): p. 64-70.

85. Savolainen, S.M., J.F. Foley, and S.A. Elmore, *Histology atlas of the developing mouse heart with emphasis on E11.5 to E18.5*. *Toxicol Pathol*, 2009. **37**(4): p. 395-414.
86. Lee, J.Y., et al., *Importin-11 is Essential for Normal Embryonic Development in Mice*. *Int J Med Sci*, 2020. **17**(6): p. 815-823.
87. Ward, J.M., S.A. Elmore, and J.F. Foley, *Pathology methods for the evaluation of embryonic and perinatal developmental defects and lethality in genetically engineered mice*. *Vet Pathol*, 2012. **49**(1): p. 71-84.
88. Waddingham, M.T., et al., *Using Synchrotron Radiation Imaging Techniques to Elucidate the Actions of Hexarelin in the Heart of Small Animal Models*. *Front Physiol*, 2021. **12**: p. 766818.
89. Dietz, H.C., et al., *Marfan syndrome caused by a recurrent de novo missense mutation in the fibrillin gene*. *Nature*, 1991. **352**(6333): p. 337-9.
90. Aubart, M., et al., *Association of modifiers and other genetic factors explain Marfan syndrome clinical variability*. *Eur J Hum Genet*, 2018. **26**(12): p. 1759-1772.
91. Kashyap, S., et al., *Cardiovascular phenotype in Smad3 deficient mice with renovascular hypertension*. *PLoS One*, 2017. **12**(10): p. e0187062.
92. Ashvetiya, T., et al., *Identification of novel genetic susceptibility loci for thoracic and abdominal aortic aneurysms via genome-wide association study using the UK Biobank Cohort*. *PLoS One*, 2021. **16**(9): p. e0247287.
93. Pirruccello, J.P., et al., *Deep learning enables genetic analysis of the human thoracic aorta*. *Nat Genet*, 2022. **54**(1): p. 40-51.
94. Doetschman, T., *Influence of genetic background on genetically engineered mouse phenotypes*. *Methods Mol Biol*, 2009. **530**: p. 423-33.
95. De Cario, R., et al., *Tracking an Elusive Killer: State of the Art of Molecular-Genetic Knowledge and Laboratory Role in Diagnosis and Risk Stratification of Thoracic Aortic Aneurysm and Dissection*. *Diagnostics (Basel)*, 2022. **12**(8).
96. Cao, G., et al., *How vascular smooth muscle cell phenotype switching contributes to vascular disease*. *Cell Commun Signal*, 2022. **20**(1): p. 180.
97. Dawson, A., et al., *Single-Cell Analysis of Aneurysmal Aortic Tissue in Patients with Marfan Syndrome Reveals Dysfunctional TGF-beta Signaling*. *Genes (Basel)*, 2021. **13**(1).
98. Wirka, R.C., et al., *Atheroprotective roles of smooth muscle cell phenotypic modulation and the TCF21 disease gene as revealed by single-cell analysis*. *Nat Med*, 2019. **25**(8): p. 1280-1289.
99. Mizrak, D., H. Feng, and B. Yang, *Dissecting the Heterogeneity of Human Thoracic Aortic Aneurysms Using Single-Cell Transcriptomics*. *Arterioscler Thromb Vasc Biol*, 2022. **42**(8): p. 919-930.
100. Stahl, P.L., et al., *Visualization and analysis of gene expression in tissue sections by spatial transcriptomics*. *Science*, 2016. **353**(6294): p. 78-82.

101. Cheng, M., et al., *Non-coding RNAs in aortic dissection: From biomarkers to therapeutic targets*. J Cell Mol Med, 2020. **24**(20): p. 11622-11637.
102. Hu, Y.Y., et al., *Non-coding RNAs Regulate the Pathogenesis of Aortic Dissection*. Front Cardiovasc Med, 2022. **9**: p. 890607.
103. Sun, Y., et al., *miR-27a regulates vascular remodeling by targeting endothelial cells' apoptosis and interaction with vascular smooth muscle cells in aortic dissection*. Theranostics, 2019. **9**(25): p. 7961-7975.
104. Yang, P., et al., *MiR-26b Suppresses the Development of Stanford Type A Aortic Dissection by Regulating HMGA2 and TGF-beta/Smad3 Signaling Pathway*. Ann Thorac Cardiovasc Surg, 2020. **26**(3): p. 140-150.
105. Wei, Y., et al., *Importin 8 regulates the transport of mature microRNAs into the cell nucleus*. J Biol Chem, 2014. **289**(15): p. 10270-10275.
106. Weinmann, L., et al., *Importin 8 is a gene silencing factor that targets argonaute proteins to distinct mRNAs*. Cell, 2009. **136**(3): p. 496-507.
107. Gao, J., et al., *The mechanism and therapy of aortic aneurysms*. Signal Transduct Target Ther, 2023. **8**(1): p. 55.



## **LIST OF ABBREVIATIONS**

---

AA	Aortic aneurysm
AAA	Abdominal aortic aneurysm
ACE	Angiotensin-converting-enzyme
ACMG	American College of Medical Genetics
ACTA2	Actin alpha 2
AD	Autosomal dominant
AR	Autosomal recessive
ASD	Atrial septal defect
ATS	Arterial tortuosity syndrome
AV	Aortic valve
BAV	Bicuspid aortic valve
BGN	Biglycan
BMP	Bone morphogenic protein
Bp	Baise pair
CAD	Coronary artery disease
cDNA	Copy DNA
CNV	Copy number variation
CoA	Coarctation of the aorta
CT	Computed tomography
CTGF/CCN2	Connective tissue growth factor

DAB	Diaminobenzidine tetrahydrochloride hydrate
DEANO	Diethylamine NONOate
ECM	Extracellular matrix
EDS	Ehlers-Danlos syndrome
FTAA	Familial thoracic aortic aneurysm
FTAAD	Familial thoracic aortic aneurysm and dissection
GATK	Genome Analysis Toolkit
gDNA	Genomic DNA
gnomAD	Genome Aggregation Database
HE	Hematoxylin-eosin
HRP	Horse radish peroxidase
IHC	Immunohistochemistry
IMPC	International Mouse Phenotyping Consortium
IPO8	Importin-8
iPSCs	Induced pluripotent stem cells
JAG	Jagged
KO	Knock-out
KOMP	Knock-out mouse project
LAP	Latency-associated protein
LDS	Loeys-Dietz syndrome

LNAME	N-nitro-L-arginine methyl ester
LOX	Lysyl oxidase
LTBP	Latent TGFbeta binding protein
MFS	Marfan syndrome
MMP	Matrix metalloprotease
MRA	Magnetic resonance angiography
MRLS	Meester-Loeys syndrome
MYH11	Myosin heavy chain 11
NLS	Nuclear localisation signal
NMD	Nonsense mediated mRNA decay
NS	Non-significant
OFT	Outflow tract
OI	Osteogenesis imperfecta
OMIM	Online Mendelian Inheritance in Man
PBMCs	Peripheral blood mononuclear cells
PDA	Patent ductus arteriosus
PE	Phenylephrine
qPCR	Quantitative polychain reaction
Rsmad	Receptor SMAD
SEM	Standard error of the mean

SeV	Sendai virus
SGS	Shprintzen-Goldberg syndrome
SHF	Secondary heart field
TAA	Thoracic aortic aneurysm
TAAD	Thoracic aortic aneurysm and dissection
TGFbeta	Transforming growth factor beta
TGFBRII	Transforming growth factor beta receptor subunit type I
TGFBRII	Transforming growth factor beta receptor subunit type II
TIMP	Tissue inhibitor metalloproteinase
VSD	Ventricular septal defect
VSMCs	Vascular smooth muscle cells
VUS	Variant of unknown significance
WES	Whole exome sequencing
WGS	Whole genome sequencing
WT	Wild type



# CURRICULUM VITAE

---

## Personal data

---

Name: Ilse Van Gucht  
Date of birth: 6/08/1994  
Nationality: Belgian  
E-mail: [ivangucht@hotmail.com](mailto:ivangucht@hotmail.com)

## Education

---

August 2018 - Present **PhD in Cardiogenomic research**  
*Center of Medical Genetics in Antwerp -  
University of Antwerp*

2021 - Present **Bachelor in Medicine**  
*University of Antwerp, FGG faculty*

2016 - 2018 **Master in Biomedical Sciences: Molecular and  
Cellular Biomedical Sciences**  
*University of Antwerp, FBD faculty*

2013 - 2016 **Bachelor in Biomedical Sciences**  
*University of Antwerp, FBD faculty*

## Student job – Internships

---

April 2023 - Present **Lab Technician (workstudent)**  
*CPU Janssen - Jan Palfijn - Merksem - Antwerpen*

October 2022 **Nursing internship (2weeks)**  
*AZ Klina, Brasschaat*

November 2017 - June 2018 **Internship, Cardiogenomics Research Group**  
*Center of Medical Genetics – University of Antwerp*

September 2016 **Internship, Laboratory for Molecular Biophysics,  
Physiology and Pharmacology**  
*University of Antwerp*

2012 - 2014 **Catering industry**  
*Restaurant Hong Kong, Brasschaat*

## Certificates

---

2022	<b>ICH Good Clinical Practice E6 (R2)</b> <i>The Global Health Network</i>
2022	<b>Basic Life Support – BLS P certificate</b> <i>European Resuscitation Council - University of Antwerp</i>
2020	<b>The Interuniversity Certificate in Human Genetics</b> <i>BeSHG, UA, KUL, IPG, ULB, VUB, ULiège and Ugent</i>
2017	<b>FELASA Certificate Category C</b> <i>University of Antwerp</i>

## Publications

---

1. **Ilse Van Gucht**, Josephina A.N. Meester, Jotte Rodrigues Bento, Maaïke Bastiaansen, Jarl Bastianen, Ilse Luyckx, Lotte Van Den Heuvel, Cédric H.G. Neutel, Pieter-Jan Guns, Mandy Vermont, Erik Fransen, Melanie H.A.M. Perik, Joe Davis Velchev, Maaïke Alaerts, Dorien Schepers, Silke Peeters, Isabel Pintelon, Abdulrahman Almesned, Matteo P. Ferla, Jenny C. Taylor, Anthony R. Dallosso, Maggie Williams, Julie Evans, Genomics England Research Consortium,<sup>†</sup> Jill A. Rosenfeld, Thierry Sluysmans, Desiderio Rodrigues, Ashish Chikermane, Gangadhara Bharmappanavara, Kayal Vijayakumar, Hassan Mottaghi Moghaddam Shahri, Narges Hashemi, Paria Najarzadeh Torbati, Mehran B. Toosi, Zuhair N. Al-Hassnan, Julie Vogt, Nicole Revencu, Isabelle Maystadt, Erin M. Miller, K. Nicole Weaver, Amber Begtrup, Henry Houlden, David Murphy, Reza Maroofian, Alistair T. Pagnamenta, Lut Van Laer, Bart L. Loeys and Aline Verstraeten, *A human importin- $\beta$ -related disorder: Syndromic thoracic aortic aneurysm caused by bi-allelic loss-of-function variants in IPO8*, June 3, 2021, *American Journal of Human genetics*
2. **Ilse Van Gucht**, Alice Krebsová, Birgitte Rode Diness, Steven Laga, Dave Adlam, Marlies Kempers, Nilesh J Samani, Tom R Webb, Ania A Baranowska, Lotte Van Den Heuvel, Melanie Perik, Ilse Luyckx, Nils Peeters, Pavel Votypka, Milan Macek, Josephina Meester, Lut Van Laer, Aline Verstraeten and Bart L. Loeys, *Novel LOX Variants in Five Families with Aortic/Arterial Aneurysm and Dissection with Variable Connective Tissue Findings*, July 1, 2021, *International Journal of Molecular Sciences*
3. Jotte Rodrigues Bento, Alice Krebsová, **Ilse Van Gucht**, Irene Valdivia Callejon, An Van Berendoncks, Pavel Votypka, Ilse Luyckx, Petra Peldova, Steven Laga, Marek Havelka, Lut Van Laer, Pavel Trunecka, Nele Boeckx, Aline Verstraeten, Milan Macek,

Josephina Meester and Bart Loeys, *Isolated aneurysmal disease as an underestimated finding in individuals with JAG1 pathogenic variants*, February 2, 2022, under review in Human Mutation

4. Aleksandra Nijak, Eline Simons, Bert Vandendriessche, Dieter Van de Sande, Erik Fransen, Ewa Sieliwończyk, **Ilse Van Gucht**, Emeline Van Craenenbroeck, Johan Saenen, Hein Heidbuchel, Peter Ponsaerts, Alain J. Labro, Dirk Snyders, Winnok De Vos, Dorien Schepers, Maaïke Alaerts and Bart L. Loeys, *Morpho-functional comparison of differentiation protocols to create iPSC-derived cardiomyocytes*, February 23, 2022, The Company of Biologists
5. **Ilse Van Gucht**, Lut Van Laer, Aline Verstraeten and Bart L. Loeys, *The Genomic and Molecular Cardiovascular Medicine*, Elsevier, Book Chapter, *Chapter 12: Aortopathy*, submitted
6. **Ilse Van Gucht**, Lucia Buccioli, Laura Rabaut, Ivanna Fedoryshchenko, Josephina Meester, Lut Van Laer, Bart L. Loeys and Aline Verstraeten, *Stem Cells research, Generation of one induced pluripotent cell (iPSC) line (BBANTWi011-A) from a patient carrying an IPO8 bi-allelic loss-of-function mutation*, 2023 Mar 9;69:103061, doi: 10.1016/j.scr.2023.103061
7. **Ilse Van Gucht**, Ilse Luyckx, Jarl Bastianen, Mandy Vermont, Josephina Meester, Lut Van Laer, Aline Verstraeten and Bart L. Loeys. *Embryonic lethality in C57Bl/6N Ipo8 knock out mice*. Submission planned 2024, journal TBD.

## Conferences

---

### 1 Oral presentations

1. Lightning talk at Genomics of Rare Disease 2019, 27-29 March, 2019, Wellcome Genome Campus in Hinxton, Cambridge, UK: *'Novel LOX mutations in five probands with thoracic aortic/arterial aneurysm and dissection with variable connective tissue findings'*
2. Annual Meeting of the Belgian Working Group of Basic Research in Cardiology, BWG-BRC, June 9, 2021, virtual meeting: *'The first human importin-beta-related disorder: syndromic thoracic aortic aneurysm caused by bi-allelic loss-of-function variants in IPO8'*
3. Progress report presentation Ilse Van Gucht, April 1<sup>st</sup>, 2021, Center of Medical Genetics Antwerp, University Hospital Antwerp, University of Antwerp: *'Functional assessment and therapeutic targeting of a novel aortopathy syndrome cause by recessive IPO8 mutations'*

4. European Society of Human Genetics 2021, August 28-31, 2021, Virtual Conference: *'The first human importin-beta-related disorder: syndromic thoracic aortic aneurysm caused by bi-allelic loss-of-function variants in IPO8'*
5. BeSHG - Belgian Society of Human Genetics 2021, 17 September 2021, Crowne Plaza Brussels Airport, *'The first human importin-beta-related disorder: syndromic thoracic aortic aneurysm caused by biallelic loss-of-function variants in IPO8'*
6. Princess Lilian Visiting Professorship 2022, 30 April 2022, Antwerp University Hospital Research Club Auditorium Kinsbergen, - Antwerp University Hospital, *'Importin-8: a novel player in syndromic aortopathy'*

## **2 Poster presentations**

1. Genomics of Rare Disease 2019, Wellcome Genome Campus in Hinxton, 27-29 March, 2019, Cambridge, UK: *'Novel LOX mutations in five probands with thoracic aortic/arterial aneurysm and dissection with variable connective tissue findings'*
2. 19th annual meeting of the Belgian Society of Human Genetics, March 15, 2019, in Liège: *'Novel LOX mutations in five probands with thoracic aortic/arterial aneurysm and dissection with variable connective tissue findings'*
3. FASEB science research conference, TGF $\beta$  superfamily conference 2021: signaling in development and disease, July 20-21, 2021, *'The first human importin-beta-related disorder: syndromic thoracic aortic aneurysm caused by bi-allelic loss-of-function variants in IPO8'*
4. European Society of Human Genetics 2020, June 6-9, 2020, Virtual Conference: *'Aortic aneurysm and dissection, an underestimated finding in JAG1 mutation carriers'*
5. 22nd annual meeting of the Belgian Society of Human Genetics, April 21-22, 2021, in Bruges: *'Striking phenotypical differences between Ipo8 knock-out mouse models on different genetic backgrounds'*
6. BeSHG - Belgian Society of Human Genetics 2022, 20-21-22 April 2022, Joint BeSHG/NVHG meeting and genetic retreat, Bruges, Belgium, *'Striking phenotypical differences between Ipo8 knock-out mouse models on a different genetic background'*.

## Research grants and prizes

---

1. Registration Bursary, Genomics of Rare Disease 2019, Wellcome Genome Campus in Hinxton, 27-29 March, 2019, Cambridge, UK
2. Fonds Wetenschappelijk Onderzoek, FWO-Flanders, January 2019-December 2022, PhD fellowship for PhD-student Ilse Van Gucht: '*Functional assessment and therapeutic targeting of a novel aortopathy syndrome cause by recessive IPO8 mutations*'

## Courses and educational activities

---

1. Image Processing workshop, Introduction to Image Processing, December 10-12, 2018, VIB training, Leuven
2. European Society Human Genetics, Cardiogenetics course Antwerp, April 27-30, 2019, University Hospital Antwerp, University of Antwerp, Belgium
3. The interuniversity Certificate in Human Genetics course, June 5, 2020, Universiteit Gent, Université de Liège, Université Libre de Bruxelles, Katholieke Universiteit Leuven, Université Catholique de Louvain, Institute de Pathologie et de Genetique Gosselies, Universiteit Antwerpen, Vrije Universiteit Brussel and Belgian Society of Human Genetics.
4. Master Dissertation Mentor, Karo De Rycke: 'Oxidative stress in Marfan syndrome: repositioning of allopurinol for the prevention of aortic aneurysm development', Master in Biomedical Sciences, University of Antwerp, 2019-2020, Mentor
5. E-learning course ICH, good clinical practice E6 (R2), 3 December 2022, The Global Health Network

## **DANKWOORD**

---

YES, I MADE IT!!!!

Mijn eerste dank gaat uit naar mijn promotoren, **Bart Loeyts**, **Aline Verstraeten** en **Lut Van Laer**. Ik wil jullie van harte bedanken voor de kans die ik van jullie gekregen heb, een kans die ik nooit zal vergeten. Bedankt voor al jullie tijd, de soms lange *IPO8* meetings, (last minute) vragen maar vooral ook de kans om fouten te maken en hieruit te leren. Het was een geweldige ervaring, dank jullie wel.

Als masterstudent in 2018 kwam ik solliciteren op 1 van de stageplekken in de aortagroep. Ik kwam onder de supervisie van **Maaïke A** en **Ola** terecht in de PED-groep en werd meteen met open armen ontvangen. Een ongelooflijk toffe groep, goede begeleiding en een interessant onderwerp, wat heeft een masterstudent nog meer nodig? De interesse en motivatie werd groter en groter, tot op de dag dat ik mijn masterdiploma behaalde en ik de kans kreeg om een doctoraat te starten in de cardiogenetica groep. Uiteraard was hier geen twijfel mogelijk, gebeten door de onderzoeksmicrobe en de ongelooflijke sfeer binnen de cardiogenetica groep, was dit de uitgesproken opportuniteit. Ik startte in de TAAD-groep op het *IPO8* project. De eerste maanden waren vrijwel erg hard doorwerken, om het project te schrijven, me in te lezen en voor te bereiden op een FWO-verdediging, alsook zoveel mogelijk preliminaire data proberen te verzamelen. Op 26 november 2018 mocht ik mijn project gaan verdedigen in Brussel bij het FWO. Later in december kreeg ik te horen dat ik geslaagd was en een FWO-fellowship zou mogen ontvangen, joepieeee! Het doctoraat was nu echt gestart.

Doorheen mijn doctoraat heb ik mezelf kunnen ontplooiën en verder ontwikkelen tot de persoon die ik nu geworden ben. Op mijn pad ben ik veel mensen tegengekomen die me veel hebben bijgebracht, daarom volgt nu een dankwoord aan al diegenen die deze mijlpaal in mijn leven mogelijk maakten. **Jeannette**, bedankt om mijn mentor te zijn en me altijd in de juiste richting op pad te sturen. Niet alleen op wetenschappelijk vlak maar ook op andere vlakken heb ik mijn hart altijd bij jou kunnen luchten, bedankt om altijd met raad en daad klaar te staan. **Ilse L**, wat was het een eer om jouw naamgenoot te mogen zijn in de cardiogenetica groep. Bedankt om al je kennis over het muizenwerk, echoën, coupes snijden en kleuren, embryonale ontwikkeling en nog veel andere zaken met me te delen. Onze trip naar Zwitserland was een ervaring, hard werken maar ook wel genieten, zelfs even de tijd genomen om een sneeuwman te maken :p. **Maaïke A**, bedankt voor je altijd vrolijke aanwezigheid en steeds jouw kennis te delen en al mijn hiPSC-gerelateerde vragen te beantwoorden. **Dorien S**, bedankt om een luisterend oor te zijn wanneer ik het nodig had, ook jouw opgewekte zelve bracht voor mij altijd kleur

op het CMG. **Silke**, bedankt voor jou bezorgdheid en het altijd tijd hebben om iemand met vragen of bedenkingen te woord te staan. De simpele vraag 'hoe gaat het met jou?' werd me door jou regelmatig gesteld waardoor ik niet enkel kon ventileren maar me ook begrepen voelde, heel erg bedankt.

Wat zouden we zijn zonder onze laboranten, **Maaïke B, Jarl, Laura, Jolien** en **Sofie**, niet veel denk ik. Daarom wil ik jullie ook enorm hard bedanken voor jullie ondersteuning en inzet. **Jarl**, heel erg bedankt voor al het muizenwerk. Al het spenen, genotyperen, transporteren, echoën... noem maar op! **Maaïke B**, wat hebben we gevloekt op die cell fractionations en al die western blots. Bedankt voor al je harde werk, flexibiliteit en doorzettingsvermogen. **Laura**, bedankt voor al het celwerk dat je verricht hebt, alsook alle collecties, extracties, syntheses en qPCRs, of om gewoon een babbeltje te slaan en even de mislukte experimenten te vergeten :p. **Jolien**, jij ook bedankt voor al het celwerk en de toffe babbeltjes! **Sofie**, ik wens jou heel veel succes en plezier in de cardiogenetica groep, vanuit het beste plekje op heel het CMG ;).

Bedankt aan onze collaborators. **Prof Marco Deruiter** en **Bert Wisse** om al jullie kunnen en kennen in verband met embryonale letaliteit in muismodellen met ons te delen. Prof **Pieter-Jan Guns** van physio-pharmacology bedankt om uw labo open te stellen zodat ik met mijn muizenexperimenten bij jullie terecht kon. **Cedric Neutel**, bedankt om me alles te leren over de ROTSAC-assay en voor de fijne begeleiding. Allerliefste **Mandy**, wat begon met een korte opleiding in jouw labo eindigde in een vriendschap gebaseerd op liefde voor eten, veel eten! :p Ook qua muziekstijl konden we elkaar vinden (lang leve de Electric Callboys en Elton John!). Heel erg bedankt voor de vele gezellige dagen bij jou in het labo, zonder jou hadden deze dagen er waarschijnlijk heel anders uitgezien. **Abi**, jou wil ik ook bedanken voor jouw enthousiasme in het labo op T2 en jouw hulp tijdens het inbedden, wat toch niet zo vanzelfsprekend was aangezien je er zelf nog maar net mee gestart was. Desondanks hebben we het wel tot een goed einde gebracht! Liefste, **Jente**, samen gestart aan biomedische wetenschappen en beiden een doctoraat gestart. Af en toe dezelfde smart met elkaar kunnen delen wat het wel draaglijker maakte. Bedankt voor wie je bent en om er altijd te zijn.

Many thanks to **Elineke, Melanie, Jolien, Ewa** en **Ola**, aka the anciens. Dear **Ola**, the perseverance and determination you have, not only during your PhD thesis, but also in life, is something I really envy. Thank you for being my supervisor during my master thesis, you inspired me to pursue a PhD and I am really happy I did. **Ewa**, mijn bureaubuur, twee smossers bij elkaar, dat schept een band eh. Net zoals onze gedeelde liefde voor kazen en Poolse worst (door jou ontdekt uiteraard ;)). Voor mij ben je echt een bron van inspiratie, zowel vanwege hoe je in het leven staat maar ook als de wetenschapper en dokter die je bent. Je realistische kijk op de dingen kon me vaak een

ander inzicht geven in bepaalde situatie of gebeurtenissen. Bedankt om er steeds te zijn wanneer ik het nodig had. **Elineke**, feestbeest numero uno. Wat begon met een goede plaat op hemato vloeide al snel over in een vriendschap vol toffe en zotte belevenissen. Onze reis naar Turkije was zalig, ik denk dat ik op 1 week tijd nog nooit zoveel gelachen heb als toen. Bedankt dat ik met om het even wat bij jou terecht kan en mag ventileren :p Wat ben ik blij dat ik jou heb leren kennen, op nog vele pizza-tv-avonden, loco contigo's, wijntjes, dansfeestjes en plezier. **Melanie**, bedankt voor alle lieve zorgen, de survival box om moeilijke periodes door te komen, of de kleine geschreven attenties. Jouw bezorgdheid en meelevendheid zorgde voor een huiselijk sfeer op het CMG. Af en toe samen wat traantjes laten kon al eens deugd doen, heel erg bedankt. **Jolien**, jouw humor en aanstekelijke lach zullen me altijd bijblijven. De brunches, lunches en spelletjesavonden waren altijd super gezellig met jou erbij. Bedankt om altijd jou enthousiaste zelve te zijn. **Lotte**, Lotje, onze Ca-experimenten op T1 waren een fijne ervaring, zeker onze lunches in het UZA die daar gepaard mee gingen. Ik wens je nog ongelooflijk veel succes met je PhD, je gaat dat knallen. **Jotte**, bedankt voor de kletsuurtjes (voor en na de uren, soms ook tijdens :p) en de gin-tonics. Het HipHop feestje in Mechelen ga ik nooit meer vergeten, wat een zalige avond. **Pauline**, bedankt voor de fijne lunches en jouw gezellige aanwezigheid. Ik wens je nog ongelooflijk veel succes toe met je doctoraat. **Joe D**, thank you for your enthusiasm, not only in the lab but also at the CMG parties. And for taking care of my cells when I couldn't. **Lucia** and **Irene**, thank you for the happy vibes you bring to CMG. I wish you all the best during your PhDs! **Ivanna** and **Anne**, I wish you both a great PhD experience, with a lot of successful experiments. Verder wil ik iedereen van de cardiogenetica groep heel erg bedanken voor de toffe jaren, de zalige sfeer, de samenhang en ondersteuning.

Een grote danku aan mijn bureaumatjes, **Yentl**, **Ellen E**, **Evelien**, **Dogan**, **Merlijn**, **Bert** en **Ewa**, om altijd voor een toffe sfeer te zorgen in onze bureau. Ondanks de extreme temperatuurschommelingen in onze bureau, bleef de sfeer toch altijd op niveau ;). Special thanks to **Yentl**, ik denk niet dat ik mijn PhD overleefd had mocht jij er niet geweest zijn haha. De overheerlijke lachbuien, maar ook de zwarte bananen, de intense tennislessen, de onvergetelijke reis naar Vigueron, onze paarden ervaring in Durbuy, of het uitproberen van je net nieuwe auto op de puttenparking aan de voetbalkantine, de vele wandelingen, de niet open te krijgen oesters op oudjaar, en zo kan ik nog wel even doorgaan. Kortom, bedankt voor al deze memorabele momenten, hop naar meer. **Ellen E**, voor mij was jij een beetje de mama van onze bureau, bezorgd over ieders welzijn en steeds klaarstaan om iemand op te peppen of een hart onder de riem te steken. Bedankt om te zijn wie je bent. **Merlijn**, bedankt voor de rijsttaartjes en de Star Bucks koffie, de beste pauzes! Ook bedankt om steeds te geloven dat alles altijd goed komt. Ik wens je nog heel veel succes met doctoraat. **Bert**, over de visjes heb ik nooit veel

kunnen meepraten, maar ik wens je nog heel veel succes met je doctoraat! **Dogan**, al snel kwamen we achter onze gemeenschappelijke interesses; gym en cappuccino. Het was fijn om jou als bureaumaatje te hebben, zowel voor de wetenschappelijke gesprekken als de gesprekken over squatten en benchen :p. Never forget, de beste baklava die je regelmatig meebracht als er iets te vieren viel of gewoon omdat het kon. Succes met je doctoraat! **Evelien**, eindelijk onze eigen koelkast! Eindelijk een gekoelde plek waar we al onze Cola zero konden stockeren. **Sara D**, jij was al aan je PhD bezig toen ik aan de mijne begon. Van jouw manier van onderzoek doen en presentaties geven kon ik wel wat leren. Als groentje vond ik het fijn jou om advies of raad te vragen tijdens mijn PhD. Maar ook buiten de CMGmuren was het heel fijn om met jou ergens heen te gaan of je ergens tegen te komen. Bedankt om een voorbeeld te zijn.

Graag zou ik iedereen van het CMG, research en diagnostiek, willen bedanken voor de fijne jaren, de ontstane vriendschappen, gezellige afterworks, aangename werksfeer en zoveel meer. Bedankt, **Hanne, Joe I, Farhan, Dale, Kirsten, Claudio, Janah, Isabelle, Ana Regina, Liene, Mathijs, Frank, Guy, Wim, Erik, Arvid, Ken, Gerarda, Lisse, Laura M., Kathleen, Thomas, Marc, Eef, Nele, Ellen S., Tammy, Charlotte C., Ligia, Tycho en Anne S.**

Een Dikke merci aan mijn 2 grootste fans, **Xena** en **Eline**. Bedankt voor jullie steun en toeverlaat, de vele zoo-bezoeken, Mexicaanse diners, culturele uitstappen en de befaamde puzzel- en spelletjesavonden. Na een vriendschap van al meer dan 25jaar kan dat ook gewoon niet verkeerd gaan he. Ik wens het iedereen toe om zo'n vriendinnen als jullie te hebben, effenaf. Lieve **Nathalie**, bedankt om altijd die straffe opgewekte en gemotiveerde madam te zijn. Vroeger samen opstap, goeiemorgen Dixieees! Nu breekdeweek'jes die ons even doen ontsnappen aan de stevige werkweek. Van serieuze gesprekken tot zotte dansavonden, u vraagt wij draaien. Liefste **Amber**, jou leerde ik kennen tijdens mijn PhD op het CMG. Al snel sprak jouw sociale zelve mij aan en enkele weken later waren we samen terug te vinden in de fitness. Onze reis naar Tenerife was er eentje in een miljoen en zal ik nooit vergeten. Ook een grote danku aan de ladies, **Veroniek, Magali, Anouk** en **Ellen**, voor jullie begrip als ik weer eens een deadline had, en iets moest afzeggen of te laat aankwam. Hopelijk mogen er nog veel thema-diners, pyjama avonden en topfeestjes volgen. **Dieter**, onze eerste ontmoeting dateert al van 2016, tijdens de vrijwillige stage die ik in 3<sup>e</sup> bachelor deed bij jou op het labo en leerde hoe de mooie techniek 'patchclamp' in zijn werk gaat. Naast collega's zijn we ondertussen ook goede vrienden geworden. Je bent er altijd voor me geweest tijdens moeilijkere periodes, zowel PhD gerelateerd als daarbuiten. Daar ben ik je ongelooflijk dankbaar voor.

**Moemoe'ke**, wat ben ik blij dat jij hierbij bent. Jouw grote interesse in mijn studies heeft mij altijd gemotiveerd om te blijven doorzetten. Ik hoop dat ik je trots maak. Mijn allerliefste nichtje, **Sofie**, we go way back, van barbiepoppen en K3 tot verjaardagsfeesten in't kot vanachter en diners met Nieuwjaar. Doorheen de jaren ben jij heel vaak een lichtpuntje geweest. Al onze lunchkes, pannenkoekendates, mosseltjessoupés, familiefeestjes, verkleedfeestjes, 80ies parties, knutsels, kooksels, en nog te veel om allemaal op te noemen zijn dingen die ik voor altijd zal koesteren. Merci om er altijd te zijn! Bedankt aan al mijn neven en nichten, **Tim, Karel, Myriam, Siemen, Eva, Tiemen, Isabel, Bart, Elise, Jeroen, Sofie, Sam, An, Emiel** en **Aaron**. Special thanks to **Karel**, om mijn de cover van mijn thesis te ontwerpen, het is een prachtig land'schaap' geworden! **Nonkel Peter** en **Tante Esmi**, **Nonkel Dirk** en **Tante Kris**, **Nonkel Wouter** en **Tin**, **Nonkel Herman**, **Tante Dina** en **Nonkel Jan**. Bedankt aan de familie Van Gucht om regelmatig te vragen hoe het met mij en mijn doctoraat ging en me te blijven motiveren verder te doen.

Mijn favoriete broer, **Anton**, bedankt om een voorbeeld te zijn. Als kleine zus is het fijn om iemand te hebben waar je naar kan opkijken en op kan terugvallen.

**Mama** en **papa**, alles begint bij jullie. Ook al is het niet altijd even gemakkelijk en vanzelfsprekend, ik weet dat wanneer het moeilijk wordt jullie er voor mij zullen zijn. Bedankt dat ik mijn dromen mag en kan waarmaken.

Bedankt iedereen. Wat is het fijn om omringd te zijn door zoveel fantastische mensen.